MEDICAL DEVICES
INNOVATION FOR AFRICA

Enabling Industrialisation

Edited by
SUDESH SIVARASU

FOREWORD

It is with great pleasure to recognise all our partners in the merSETA Viro-Vent Innovation Skills Challenge who contributed to this publication: University of Cape Town, Cape Peninsula University of Technology, University KwaZulu Natal, University of Witwatersrand and National Technologies Implementation Platform.

Thank you, Professor Sivarasu, for your leadership of the University of Cape Town for supporting these efforts to find new forms of collaboration that focus on *"Skills for localisation"* and *"Skills for re-industrialisation".*

This publication comes at a time when South Africa and the world are still recovering from the devastating effects of the covid-19 pandemic complicated by an emerging war in Ukraine. This is expected to continue disrupting social and economic activities, including education, training, and work. The merSETA and its stakeholders are working tirelessly to ensure that training and other skills development activities continue despite these challenges.

This innovation project, among others at the merSETA, utilises existing research and Higher Education Institution (HEI) Infrastructure to stimulate rapid response technology innovation aimed at the development, design and prototype production of a medical device in response not only to the COVID-19 pandemic, but also to an economic sector dominated by imports.

To serve the skills development mandate of the merSETA, the project investigates the technology management capabilities or future skills required to accelerate South Africa's post-covid recovery. The concept of innovation, as vested in this program, is aligned to the merSETA's strategic intentions, that include:

i.   Supporting skills for Economic Reconstruction, Recovery and Growth,
ii. Supporting skills for the changing world of work,
iii. Supporting skills for the growth and sustainability of the green and circular economies and
iv. Exploring and supporting the role of the mer-sector in the digital economy, as well as
v.   Continuing to strengthen the role of the SETA as an intermediary body

Making informed sector skills planning decisions is the objective of this program. – that is, to understand those future jobs that would drive the localisation of components in a model that could stimulate expanded manufacturing opportunities through relevant skills supply. The merSETA's Viro-Vent Innovation Skills Challenge anticipates a contribution towards closing the skills gap through a job generation model.

The merSETA remains committed and is looking forward to engaging on how this initiative sees a pipeline of new product innovations expanding the manufacturing sector. We owe it to the citizens of South Africa to find innovative ways of harnessing our young talent into industrial expansion.

<div style="text-align:right">

Ms Sebolelo Mokhobo-Nomvete
Acting Chief Operations Officer, merSETA
March 2022

</div>

CHAPTER 1:
OVERVIEW OF THE MEDIVENTORS CHALLENGE

Sudesh Sivarasu, Harry Teifel
ORCID ID: 0000-0002-0812-568x, 0000-0002-6144-0275

ABSTRACT

With the SA outbreak of COVID in 2020 it was decided that the country needed to develop skills for medical device innovation – while using COVID as backdrop to learn about satisfying real-world medical industrialisation demands. Various parties including the National Ventilator Project (NVP), MerSETA and others initiated the challenge. A tender process was instituted for applicants to be selected. Various parties got together under the lead of UCT, namely UKZN, WITS, CPUT and NTIP, and successfully applied for grant funding in terms of Challenge. Collectively, the consortium is called as "MediVentors". MerSETA is the Manufacturing, Engineering and Related Services Sector Training Authority. MerSETA is both funding and overseeing the challenge. MerSETA is funded by levies collected from people being employed in various industries. This means that levies collected from the current generation of employees is deployed to fund the next generation of medical device engineers and innovators. The goal of this challenge was to:

- *Build competencies related to the conversion of innovations from post- school learning institutions to manufacturing and engineering companies;.*
- *Establish relationships between universities – and between universities and industry, to facilitate future industrialisation of innovation and employment; and*
- *Encourage Higher Education Institutions towards the supply of skills equipped for a new collaborative manufacturing- and 4th Industrial Revolution paradigm.*

THE INTEGRATED SKILLS DEVELOPMENT PROGRAMME

The Integrated Skills Development Programme (ISDP**)** was the learning strategy adopted as part of the challenge to achieve optimal outcomes. It is based on international best practice by integrating different pedagogical instrument for optimal outcomes, namely:

i.   Project Activity

Project activity by the students focuses on a real-life medical device challenge as a core context. Every student, from each university, worked on a medical device project as part of their academic studies. After each student had progressed significantly in their projects, they completed an abstract submission which is consolidated within this book.

Each abstract was independently reviewed by two sets of reviewers knowledgeable within the Biomedical Engineering field. If the abstract scored poorly against the set of criteria, then the submission was rejected. The set of abstracts that were not rejected by the reviewers were sent back to the authors for revisions. Thereafter, the abstracts were checked by a copyeditor and then finally formatted according to the UCT library approved format.

ii.   Skills Development

Focused skills development through three courses, which support vital industrialisation competencies currently not forming part of the curriculum. The three courses that the students have participated in are:

- Medical Device Sector Essentials (MDSE) Course

Understanding the production and commercialisation of a medical device, the working of critical standards such as ISO 13485, ISO 27001 and ISO 62366, regulatory compliance and usability engineering and testing.

- Tooling, Manufacturing and Industralisation (TMI) Course

Understanding the progressive development and transformation of manufacturing a tool to industrialised competence, applying the industrialisation anatomy considering of the implications of the 4th industrial revolution, tooling design, life-cycle optimisation, service integration and supply chains.

- Introduction to Systems Engineering and Product LifeCycle Management (SEPLM) Course

Basic understanding of key systems engineering, and product life cycle processes and activities performed during the design, development, industrialisation, and production phases.

iii.   Definition of User's Needs

Placing oneself in the shoes of others by defining needs from the perspective of the customers. The students were required to complete the Lions' Den Project Proposal document which was the primary input to determine the participants who will be selected to present at the MediVentors Lions' Den Event. This document was marked by a MediVentor selection committee. The purpose of this document is to approach the project work from a customer / patient perspective and train students in convincing other parties to back their industrialisation efforts.

iv.   Participation in MediVentors Lions' Den Event

Participation in a simulated real-world competition ("MediVentors Lions' Den Conference") to develop skills in promoting and communicating one's solution to garner support or funding for realisation. The goal of the conference was to simulate

a real-life challenge of any innovator, namely, to convince other parties to support their industrialisation proposal and provide funding.

The conference also detailed the courses that the students participated in and how they applied their skills to their individual projects. Finalists were selected prior to the conference who submitted the best project proposal. These finalists presented their solution to garner support or funding for realisation to a panel of esteemed jurors.

MEDIVENTORS LIONS' DEN EVENT

On Wednesday the 2nd of March, some of the most innovative minds in biomedical engineering gathered to celebrate the conclusion of the first MerSETA Virovent Innovation Skills Challenge. This challenge saw participants from various institutions across the country collaborate toward one common goal: to develop skills for medical device innovation in South Africa.

The challenge ended with a MediVentors Lions' Den Event. The competition was inspired by the television series "Shark Tank." The event provided the platform for the MediVentors to engage with other role-players in the MedTech space by presenting innovative ideas. This served to convince the industry to support their industrialisation proposal and, among other things, make funding available for product realisation.

The goal of this event was to:
  i.   Witness the potential of innovations coming out of ViroVent to support an emerging SA Medical Device Manufacturing sector;
 ii.   Showcase the integrated Systems Thinking-based solution as instrument for 4th Industrial Revolution (4IR) Skills Development;
iii.   Showcase the top ranked MedTech student projects and select/recognise winners;
iv.   Provide a student-centric perspective to learning and challenges faced in a post-Covid world;
 v.   Offer a platform for representatives of the SA MedTech eco-system to reflect on synchronized industrialisation for optimal outcomes; and
vi.   Contribute towards bridge-building between key parties in the MedTech industrialisation value chain.

The jury constituted various stakeholders in the MedTech innovation value chain, with a total prize value of R110 000 being awarded across the board following the Lion's Den pitching event. The Lions' Den Event also included two panellist discussions namely: Innovation conversion: The skills and learner perspective and Industrialisation: Putting the pieces of the chain together. The participants and panellists actively engaged in these discussions highlighting the current gaps within the context of the South African MedTech space, specifically the current difficulty in medical device product realisation and industrialisation.

There was a total of nine finalists from across the four institutions (UKZN, CPUT, UCT and WITs) that battled it out in front of the esteemed lions. Every finalist did a commendable job with convincing the lions to support their medical device proposal. Several awards were distributed according to the participants unique proposals. Lan Xu (WITs) was awarded the WCMDC Most Promising MedTech Award (R5000), Joel Philpott was awarded the MDMSA Most Promising MedTech Award (R5000), the MediVentors Best in Action Award (R1000) was awarded to Mikhail Solomons (CPUT) and the People's Choice MedTech Award (R1000) was awarded to Pragesh Govender (UKZN).

Third place was awarded to Uchenna Okwuosa from CPUT, receiving R20 000 towards further development of the PEEP Valve, CAPTUL. Joel Philpott from UCT came second overall and was awarded R30 000 for further development of his medical device. First place for the MediVentors Lions' Den Event was awarded to UCT's Kerstin Lisa Hall and her novel design of the auto-injector. The device is called the OptiJect. Hall walks away with a prize of R50 000 to be used toward MedTech device development.

CHAPTER 2
ESTABLISHING ECO-SYSTEMS IN SUPPORT OF MEDICAL DEVICES INDUSTRIALISATION

Harry Teifel
ORCID ID: 0000-0002-6144-0275

ABSTRACT

Africa is set to become the most populous continent in the decades to come. In contrast to this – and with minor exceptions – only a small fraction of the Medical Devices deployed here are sourced from Africa. This anomaly is not sustainable in the medium term and begs several questions:

i. *How does one create an eco-system that is conducive to localisation in South Africa and other African countries?*

ii. *What are the specific challenges that often lead to the non-conversion of ideas to viable products – and how can wasteful industrialisation be avoided?*

iii. *Looking into the future, what is the nature of Systems Thinking solutions required to support optimal collaborative industrialisation in a 4th Industrial Revolution (4IR) environment?*

The purpose of this write-up is to offer a high-level glimpse into these three issues with a view to defining the requirements for sustainable and future-orientated Medical Devices industrialisation in Africa.

ESTABLISHMENT OF MEDICAL DEVICES ECO-SYSTEMS FOR EFFECTIVE INDUSTRIALISATION

How does a country in Africa establish an eco-system, which supports the establishment of a vibrant and sustainable Medical Devices industry? Building on Michael Porter's "Porter Diamond" (Porter, 1998), competitive advantage can be derived and improved by the optimal alignment of various aspects related to value creation, such as technology industry, skilled labour, and government support for a country's economy.

2.1 Establishment of an overarching Industrialisation Eco-system Framework

Applying competitiveness enablement principles at a very practical level means dealing with two dimensions:

i. Definition and establishment of a Medical Devices Value Chain, to outline the respective stages that play a critical role in end-to-end and successful product industrialisation and deployment; and

ii. Focus areas for the effective enablement of the respective stages in the Value Chain.

The proposed solution model sees the application of three primary industrialisation enablement focus areas overlayed with eight customized Medical Devices Value Chain stages:

i. Policy, intelligence, regulations and investment planning / funding;
ii. Market demand / orders, tariffs, designation and partnering;
iii. Ideation, Research and Product Development;
iv. Prototyping, base product testing, 1st level regulatory solution and venture funding;
v. Regulatory compliance preparations incl. manufacturing site certification;
vi. Sourcing, sub-assemblies, final assembly and regulatory compliance;
vii. Distribution / market segment penetration: Local and international; and Business Development, sales, device deployment and post-sales.

In combination, this leads to the so-called "Medical Devices Industrialisation Eco-system establishment Matrix", Figure 1, where the shaded areas indicate which industrialisation enablement area applies to which stage in the Medical Devices Value Chain:

Medical Devices Industrialization Eco-system establishment Matrix			Value Chain stages							
			a	b	c	d	e	f	g	h
			Policy, intelligence, regulations and investment planning / funding	Market demand / orders, tariffs, designation and partnering	Ideation, Research and Product Development	Prototyping, base product testing, 1st level regulatory solution and venture funding	Regulatory compliance preparations incl. manufacturing site certification	Sourcing, sub-assemblies, final assembly and regulatory compliance	Distribution / market segment penetration: Local and international	Business Development, sales, device deployment and Post-sales
Eco-system enablement focus areas	1	Policy, legislative, local socio-economic imperatives, procurement et al								
	2	Research & Development, product industrialization, regulatory compliance and industrialization skills								
	3	Sourcing, manufacturing, in-country operational challenges and satisfaction of market needs								

Figure 1: Medical Devices Industrialisation Eco-system establishment Matrix

2.2 Enablement focus area: Research & Development, Skills Development, industrialisation, regulatory compliance and similar

The next level of industrialisation eco-system development relates to the detailing of the three focus areas as outlined in section 2.1. For obvious reasons, the

6

focus area to be detailed relates to "Research & Development, product industrialisation, regulatory compliance and industrialisation skills". The following enablers are believed to be critical for enablement:

i. Use of academia and publicly funded institutions as extended R&D workbench of industry;

ii. Use of public funded IP development and alignment with industry;

iii. Testing and prototyping facilities incl. Technology stations;

iv. Regulatory measures - Local and export focused ("Extensive" such as FDA and CE Mark) and Local-only ("Lite" such as SAHPRA as regional body);

v. Securing and channeling various sources of funding and investments in capacity building and eco-system enablement;

vi. Use of public and private sector resources (funding, support, facilities etc.) for optimal eco-system enablement;

vii. Inspection authorities- and enablement support;

viii. Support programs to curb illegal or illicit activities;

ix. Critical number of ISO 13485 companies and optimal use of multi-national registration for activities in-country and overseas; and

x. Skills Development and on-going industrialisation training.

When the critical enablers of this focus area are aligned with a Value Chain perspective, this leads to the so-called "Medical Devices focus area 2 Enablement Matrix", Figure 2, where the shaded areas indicate which industrialisation enabler applies to which stage in the Medical Devices Value Chain:

Medical Devices focus area 2 Enablement matrix: Research & Development, Skills Development, industrialization, regulatory compliance and similar		Value Chain stages							
		a	b	c	d	e	f	g	g
		Policy, intelligence, regulations and investment planning / funding	Market demand / orders, tariffs, designation and partnering	Ideation, Research and Product Development	Prototyping, base product testing, 1st level regulatory solution and venture funding	Regulatory compliance preparations incl. manufacturing	Sourcing, sub-assemblies, final assembly and regulatory compliance	Distribution / market segments: Local and international	Business Development, sales, device deployment and Post-sales
Critical enablers	1	Use of academia and publically funded institutions as extended R&D work-bench of industry							
	2	Use of public funded IP development and alignment with industry							
	3	Testing and prototyping facilities incl. Technology stations							
	4	Regulatory measures - Local and export focused ("Extensive") and Local-only ("Lite")							
	5	Securing and channelling various sources of funding and investments in capacity building and eco-system enablement							
	6	Use of public and private sector resources (funding, support, facilities etc.) for optimal eco-system enablement							
	7	Inspection authorities- and enablement support							
	8	Support programs to curb illegal or illicit activities							
	9	Critical number of ISO 13485 companies and optimal use of multi-national registration for activities in-country and overseas							
	10	Skills Development and on-going industrialization training							

Figure 2: Medical Devices focus area 2 Enablement Matrix

The establishment of a localisation-friendly Medical Devices eco-system is not a haphazard and laissez-faire occurrence, but instead requires multi-party buy-in, value chain thinking and the alignment of various measures for success.

INDUSTRIALISATION CHALLENGES RELATED TO THE "VALLEY OF DEATH"

One could be tempted to assume that industrialisation is largely a technocratic and mechanistic process, where an optimal "sausage machine" assures a constantly pipeline of successful Medical Devices. This is not the case! Instead, a variety of factors are at work and involving people – with their inherent strengths and weaknesses. Outcomes are much more difficult to predict, than one would imagine. Also, not all stages of the value chain are equally prone to failure with certain specific hand-over stages being particularly susceptible to ineffectiveness and problems. Welcome to the phenomenon called the "Valley of Death".

3.1 The "Valley of Death" phenomenon plaguing Product Development

There is an extensive body of knowledge dealing with the so-called "Valley of Death", as the gap between invention and (implemented) innovation or the challenge of accelerating an innovation after proof of concept has been given.

The Valley of Death, as described in Markham, Ward, Aiman-Smith, & Kingon (2010) is defined as the space between opportunity discovery and product development as shown in Figure 3. It occurs between the Product life-cycle stages of pre-New Product Development (pre-NPD) and completed Development:
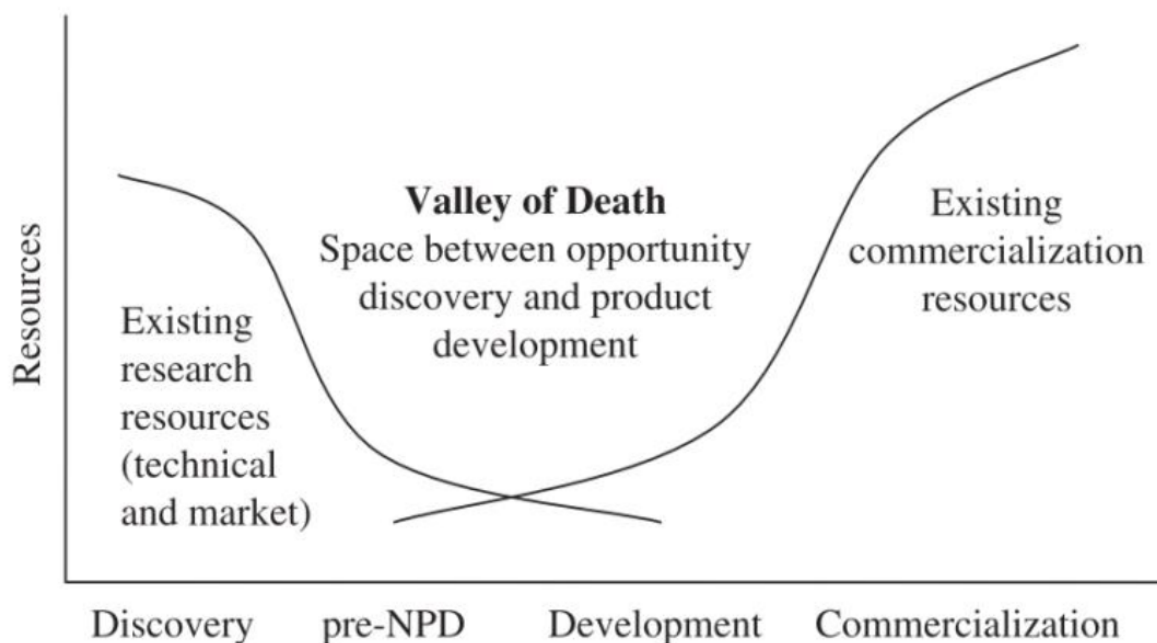

Figure 3: Valley of Death (Klitsie, Price & de Lille, 2018)

Sandberg & Aarikka-Stenroos (2014) further assert that the Valley of Death phenomenon is most likely to occur in the following Technical Readiness Levels (TRLs):

8

- TRL 4: Technology validation in lab;
- TRL 5: Technology validation in operation;
- TRL 6: Technology demonstration in operation; and
- TRL 7: System demonstration in real world.

This, in turn, leads to affected parties being confronted by the following type of challenges inhibiting successful industrialisation:
- Product challenges (Quality, performance, sustainability etc.);
- Business challenges (Costs, production efficiency, profitability etc.);
- Innovation challenges (Commercial success, market attractiveness, customer feedback etc.); and
- Process challenges (Expertise, relationships, diverse goals etc.).

3.2 Understanding contributors to the Valley of Death phenomenon

To illustrate the challenges of industrialisation, it is apt to create an analogy between Product Development and rugby with a multitude of "passes" between parties being necessary to achieve winning results. Simplistically put, the current game is characterized by undefined teams, poor passes and the ball often being dropped.

After extensive exposure to the phenomenon during Covid 19 and the personal involvement in a number of Medical Devices industrialisation projects, a list of the most prominent Valley of Death contributors has been created, Table 1:

Table 1: Most Prominent Valley of Death contributors

Nr	Valley of Death contributor	Description
1	Parties operating in silos	• The parties along the value chain (e.g. academia, manufacturers, funders etc.) mostly only understand their siloed perspective - and not the other stages and perspectives required for success. • *Silo-based perspectives pose challenges for collaborative multi-stage product development.*
2	Long learning cycles to gain necessary expertise	• Industries like Medical Devices are very complex and require a long learning period for parties to get their own and extended domain knowledge to function optimally. • All people in the value chain (e.g. innovator, manufacturer, patent lawyer etc.) constantly need to upskill given the pace of change - with learning only being topical when the issue actually occurs and relative to the role played in the industrialisation eco-system. • There is a shortage of "integrative" skills development solutions, that allow for accelerated- and multi-

		perspective learning and Systems Thinking enablement.
3	Lacking Product Life-cycle Management expertise	• The parties don't have a common industrialisation process or understanding of milestones (from different role-player perspectives) to work off and have a problem of communicating what they need from each other - and why this is important for the achievement of goals. • *Effective collaboration is hampered by parties first needing to agree on "basics", which should form part of their sector "general knowledge" portfolio.*
4	Challenges with inter-party communica-tion in terms of information needs	• The sectors are highly data-intensive (e.g. Data on markets, trends, products, competitors etc.) with parties not knowing where to find the right information or what information is required to satisfy the requirements of other value chain role-players (e.g. market size, feasibility etc.) • *Communication between parties is often in-effective with the needs of the other party not being clearly understood and the messages being conveyed, not satisfying the needs of the receiving party.*
5	Use of common reference framework between eco-system role-players	• Parties don't have a common "language" or reference framework to optimally govern the handovers between each other and uniquely describe the basis of their interaction. • *The use of different and potentially confusing terms by different parties as synonyms (e.g. "Ventilator", "Non-invasive ventilator, "BPAP" etc.) when interacting, contributes to significant confusion but also limits the effective deployment of digitalisation technologies for value addition.*
6	Alignment between innovation and demand-side triggers and role-players	• Value chains typically require sound and timeous inter-linkages between "demand" and "supply" in order for innovation activities to be off take orientated and fundable. • *There is a need to establish better connections between the major role-players along the value chain such as innovators, manufacturers, and Medical Devices buyers – and use "push" or "pull" triggers to initiate collaborative interactions between parties.*

3.3 Active avoidance and countering of the Valley of Death phenomenon

Equal emphasis should be given to both Valleys of Death, which are arguably equal in their negative effect on successful product industrialisation:

- Valley of Death 1: Space between opportunity discovery and product development, i.e. between "idea" and "product"; and
- Valley of Death 2: Space between successful product development and commercial success, i.e. "product" and "market".

The following checklist, Figure 4, has been created to avoid the Valley of Death phenomenon from negatively affecting Product Industrialisation outcomes of Medical Devices:

Valley of Death Avoidance *Checklist*

Sufficient key skills and competencies to execute key tasks to deal with Valley of Death hand-overs?	Sufficient commercial demand-side orientation and optimal use of public innovation funding?	Sufficient attention placed on viability of products and related ability to secure commercial funding?
Deployment of complementary pan-industry strengths and areas of differentiation?	Mechanisms in place to connect complementary partners together to create competitive value chains?	Access to information about opportunities and timeous partnering with complementary role-players?
Aligned understanding of end-to-end product life-cycles and roles played by each party?	Existence of a shared context of product life-cycle stages and Medical Device related aspects?	Access to funding and support mechanisms specific to TRL stages and reflective of Valley of Death challenges?

Figure 4: Valley of Death Avoidance Checklist

Similar to the establishment of localisation-friendly eco-systems being strategic and deliberate, so too is there a need for concerted Systems Thinking solutions to effectively counter-act and avoid the Valley of Death phenomenon from negatively inhibiting national and regional Medical Devices industrialisation.

INDUSTRIALISATION IN A DIGITALLY ENABLED COLLABORATIVE 4IR ENVIRONMENT

Is it possible to deal with the significant challenges of industrialisation, as outlined in the previous chapters, without significantly altering the make-up of the industrialisation "system"? The author believes that product industrialisation value chains will increasingly experience seismic change through 4th Industrial Revolution (4IR) factors. This will necessitate a fundamental re-invention as to how parties

collaborate to create value around new products. Current outcomes are simply not good enough – and "tweaking" existing industrialisation systems will not lead to the desired results.

4.1 Imagining a new industrialisation paradigm for Medical Devices

As the world becomes increasingly globalized and competitive, people and organisations are challenged in the following areas, as shown in Figure 5:

i. Dramatic increase in the amount of data and information needing to be processed;
ii. Dramatic increase in competitive pressures and client expectations;
iii. Dramatic increase in the reach and spread of localized competition; and
iv. Dramatic increase in the number of relationships and networks to be maintained.

In contrast to this, however, the there is a reduction in the available resources to deal with these increases, as shown in Figure 5, namely:

i. A reduction in the time available to perform tasks;
ii. A reduction in resources and an expectation for costs to be reduced; and
iii. A change in people, who are increasingly impatient to do perform activities deemed to be time-wasting in nature; and
iv. A reduction in the time-scale that learned knowledge is relevant and topical:
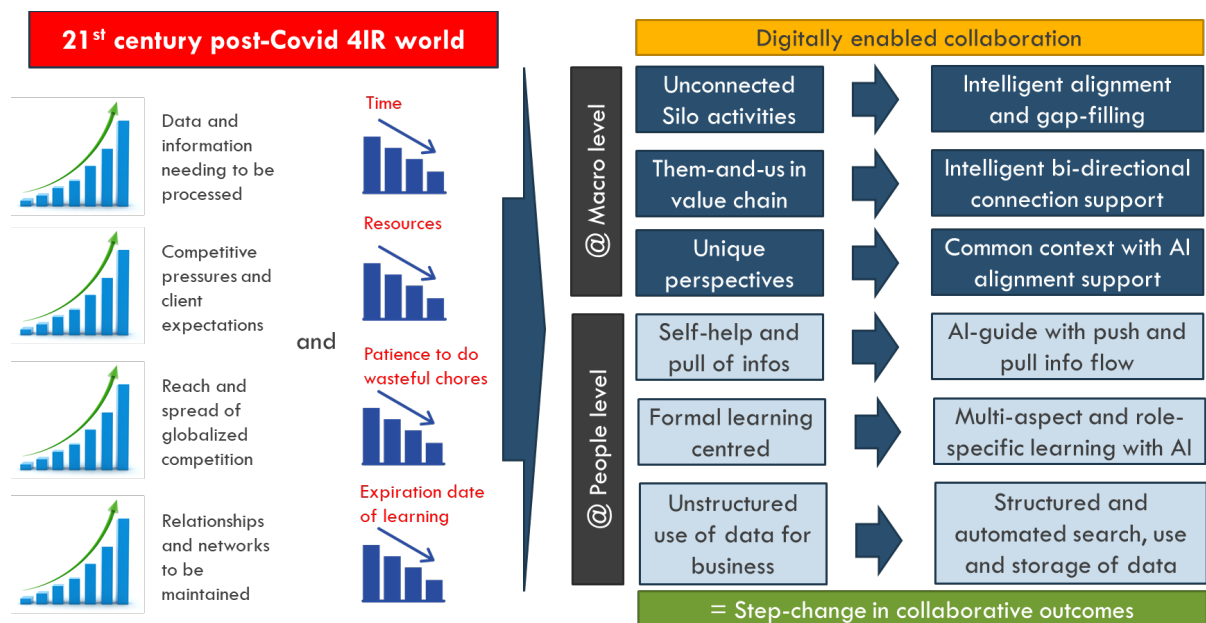

Figure 5: Industrialisation paradigm for Medical Devices

It is argued that the ever-increasing "imbalance" created will drive new forms of collaboration, both at a macro- as well as people level. This will herald a fundamental shift to digitally enabled collaboration, as the only way for the increased demands to be accommodated, as shown in Table 2:

Table 2: Implications and benefits of digitally enabled collaboration

Nr	Future state collaboration base-line	Implications and benefits:
1	Intelligent alignment and gap-filling	• Definition of role-specific partnering profile • Selection of best partners on the basis of dynamic data, various decision aspects and Machine Learning • *Benefit: Support for best role-player specific value chain for optimal competitiveness*
2	Intelligent bi-directional connection support	• Intelligent identification and notification of cooperation opportunities along value chain • Support for better fit of partnering activities (e.g. cooperation of academia and manufacturer around R&D project) with use of common nomenclature • *Benefit: Dynamic, ongoing and "push-driven" notification to all parties of parties as soon as opportunities are identified*
3	Common context with AI alignment support	• Use of common product life-cycle management processes and templates for referencing and mapping of stakeholder activities • *Benefit: Use of digital tools including AI to intelligently monitor collaborative processes, identify gaps and support remediating actions – with massive benefits for users*
4	AI-guide with push and pull info flow	• Support for the industrialisation eco-system participants in the form of a personalized and role-specific "AI-guide" to assist • Intelligent AI-enabled identification of aspects of importance and actions required – and notification of the user to act or take a decision (referred to as "push" process) • *Benefit: Significant saving of time and effectiveness improvements for the user through the "filtering" out of irrelevant information and notifying the user to act*
5	Multi-aspect and role-specific learning	• Definition of competency requirements for different roles performed in the industrialisation eco-system • Ability of technology to identify learning aspects based on defined profiles and dynamically adjust skill level requirements • Intelligent AI-enabled identification of aspects to be

		learned and insights to be acquired – and notification of the user to be trained and monitor learning progress
		• _Benefit_: *Dramatic shortening of customary periods to gain the necessary knowledge combined, ongoing dynamic skills development as well as the ongoing customisation of learning content around the value chain role fulfilled and personal learner preferences*
6	Structured and automated search, use and storage of data	• Use of sector-related nomenclature (e.g. General Medical Devices Nomenclature or GMDN) for the systematic identification, sourcing, notification, storage of relevant data
		• Deployment of value chain context (Refer to number 3) to create a link between the information and relevant operational implications and deployment areas
		• Intelligent AI-enabled identification of data / information to be collected and leveraged for differentiation and value-add, with the notification of the user to take cognizance
		• _Benefit_: *Dramatic reduction in time to stay abreast of relevant developments, satisfy key information requirements and support differentiation through insights.*

It is envisaged that the future state collaboration baseline, as described in the table above, will become an indispensable enabler to achieve the necessary level of competitiveness required for success in a 4IR environment.

4.2 The need for digital platforms to enable future state eco-system collaboration in the Medical Devices sector

Can future state industrialisation be achieved without technology? The author is of the belief that this is not possible, and that the improvement potential of existing multi-party industrialisation activities is limited.

Inherently, the limitation is human in nature and the ability of people to deal with the enormous and ever-growing challenges associated with industrialisation. Effectively the work requirements of people operating along the industrialisation value chain are so complex, specialized, time intensive and silo-specialized that a dramatic improvement is ONLY possible through the effective deployment of technology to support value creation of the individual parties - as well as their collaborative efforts.

People need support from technology for industrialisation outcomes to be dramatically improved!

It is not possible to train every party along the value chain up to be a Systems Engineer, who understands all interactions. Neither is it possible nor feasible to try and upskill an innovator to also be an expert on patent law - and vice versa.

It is argued that substantial improvements to industrialisation outcomes are only possible through the application of digital platforms or eco-systems, which allow parties to work together in a cloud environment and where is technology is systematically deployed to support people. The envisaged platform solution:

i. Supports each of the parties in better performing the role that they play (e.g. innovator, testing laboratory, manufacturer etc.) - while supporting with the best "interface" or "translation" when dealing with other parties;
ii. Creates a common "game-plan" or reference framework for industrialisation for all parties to alleviate current communication and position themselves in terms of TRLs and other parameters;
iii. Uses sector-specific "language" to facilitate communication and process flow along the industrialisation value chain and between parties;
iv. Builds on standard human phenomena, which is one of making acquaintances, establishing relationships / trust and seeing a track-record when partnering; and
v. Leverages the "system framework" created by the measures above to enable digitalisation as the critical instrument to enable improvements for people, organisations, collaborating partners and sector eco-systems.

Industrialisation in the future is likely to be very different to today's relatively ineffective and hit-and-mis practices. Continuous improvement of current industrialisation systems is unlikely to lead to breakthrough results. It is argued that dramatic improvements in industrialisation outcomes are only possible through the intelligent application of technology to deal with current systematic shortcomings and play a key enabling role in maximizing the ability of people to add value.

Implications for Medical Devices Industrialisation in Africa

Africa needs to industrialize more Medical Devices and reduce its dependency on import. This process will not be easy – nor will it happen overnight. However, there are certain guidelines that the continent can draw from in charting its Medical Devices Industrialisation Roadmap:

i. Medical Devices Eco-systems can be established for sustainability, provided that these are well designed and based on Systems Thinking design principles;

ii. Universal phenomena such as the Industrialisation "Valleys of Death" are reasonably well understood, and measures can be undertaken to counteract their debilitating impact – provided that this is done systematically;

iii. Industrialisation is set to change in an emerging 4IR world and Africa would be well advised not to emulate current ineffective practices and systems – which are set for a fundamental overhaul in the years to come. Instead, platform solutions offer significant potential to leapfrog African Medical Devices industrialisation to global levels of competitiveness.

It is hoped that the consideration of the pointers provided will in some way contribute to the development of a sustainable and future-orientated Medical Devices industrialisation in Africa.

REFERENCES

Klitsie, J.B, Price, R.A., & de Lille, C. (2018). Overcoming the Valley of Death: A Design Innovation Perspective. In *Next Wave: The 21st dmi: Academic Design Management Conference Proceedings* (pp. 958-972). Design Management Institute.

Markham, S.K., Ward, S.J., Aiman-Smith, L. and Kingon, A.I. (2010), The Valley of Death as Context for Role Theory in Product Innovation. Journal of Product Innovation Management, 27: 402-417. https://doi.org/10.1111/j.1540-5885.2010.00724.x

Porter, M. E. (1998). *The competitive advantage of nations: With a new introduction*. New York: Free Press.

Sandberg, B., & Aarikka-Stenroos, L. (2014). What makes it so difficult? A systematic review on barriers to radical innovation. *Industrial Marketing Management, 43*, 1293-1305.

CHAPTER 3
MEDICAL MONITORING WEARABLE TECHNOLOGY

Riaan Stopforth
ORCID ID: 0000-0002-8878-2232
Stopforth Mechatronics
Robotics and Research Lab
University of KwaZulu-Natal
Durban
South Africa

ABSTRACT

A medical wearable technology was designed with all the electronic devices needed for the smartwatch to perform medical monitoring functions such as body temperature sensing and heart rate sensing. The medical smartwatch requires an enclosure for the electronic devices and a mechanism that would be worn on a human wrist. The medical smartwatch was designed to have electronic devices such as an electrocardiography (ECG) sensor, impulse and oximeter sensor, light emitting diode (LED) light, a battery, Bluetooth module, humidity and temperature sensors, flame sensor, vibrator, electromyography (EMG) sensor, Infrared (IR) LED sensor, transistor, and a Arduino board and manymore. The focus was designing an enclosure that will interface between these electronic devices and the user. This paper shows the design that was considered for the enclosure, and the effect a casing has on the temperature and ECG sensors.

Keywords: medical, monitoring, wearable technology

INTRODUCTION

Smartwatches or wearable technology are multifunctional wrist-worn devices that can constantly monitor the user's physiological data. Smartwatches have applications like maps, music players and schedulers installed in them (Dehghani & Kim, 2019). There are different wearable technologies that are multifunctional, with some using technologies like biosensors and wireless data communication that allow the user to access and transmit their physiological data (Lu, Fu, Ma, Fang & Turner, 2016). Smartwatches can support health in everyday living since they monitor personal activity and obtain feedback based on these measures (Reeder & David, 2016).

Constant skin contact is one of the most important features that the enclosure must have to ensure that the sensors have enough contact with the relevant part of the patient's body. Constant skin contact in smartwatches allows easy recording of heart rate, heart rate variability, blood oxygen and galvanic skin response. Smartwatches that estimate heart rate are gaining popularity and are becoming

useful in medical tools in many ways. Although many smartwatches are not marketed for medical use, these devices have proven to be useful in patients with arrhythmias. There has been an increasing number of visits to medical rooms due to heart rate abnormalities detected by smartwatches (Koshy et al., 2017).

The use of wearable medical devices helps reduce hospital visits and admissions because of improperly managed personal health. Medical smartwatch users agreed that the wearable technology help them engage with their health. Companies worldwide are looking at the benefits that could come from the use of medical smartwatches by their employees. Medical smartwatches enable customers to have wearable pressure monitors and electrocardiography (ECG) sensors (Phaneuf, 2021).

There are mandatory quality management systems for medical devices to ensure that all medical devices adhere to all regulations before entering the markets. There are two regulations for medical device manufactures, these are ISO 13485 and 21 CFR 820. These regulations ensure that the medical devices are efficient and safe to use. ISO 13485 is focused on certificates based on the quality management system, management responsibility, resource management, product realisation and measurement, analysis, and improvement (Ramakrishna, Tian, Wang, Liao & Teo, 2015).

The research contributions presented in this paper are:
- The design of a wearable technology casing that will be in contact with a person's skin.
- Identifying if the casing has any effect in the reading comparison of the temperature and pulse rate sensors.

DESIGN AND METHODS
The following design and methods were utilised for the developed wearable technology.

i.   Materials

The design as shown in Figure 1 was developed. It must be noted that this wearable device, also referred to as a smartwatch, does not display any information but integrates to the linked smartphone. The ECG was connected using wired electrodes that are attached to the forearm for sensing.
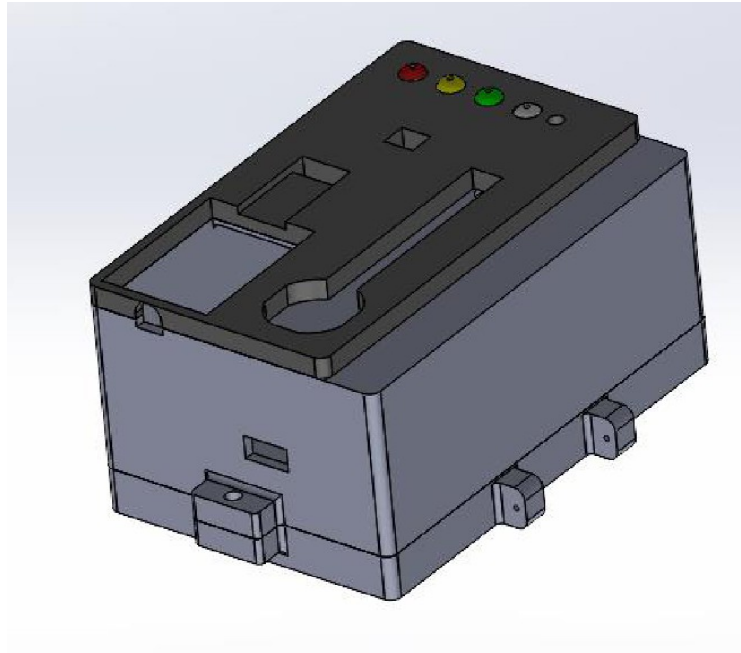
Figure 1: The enclosure of the wearable technology where sensors were placed

The advantages of this design concept are:
- The absence of a display screen reduces the number of electronic devices and therefore reduces the size and weight of the smartwatch.
- Increased accuracy of the sensor readings as they are in direct contact with the person's skin.

The disadvantage of this design is:
- The sensors are exposed to the environment, such as water. This means there is a need to identify a watertight system that will minimise any influence on the readings.

ii. Methods

Tests were conducted for the different sensors to test the accuracy of the reading obtained by the sensor when they operate without the enclosure and inside the enclosure. These tests are performed to determine the deviations caused by the integration of the electronics with the enclosure.

The sensors that were tested were the LM35 temperature sensor and the Key studio AD8232 electrocardiography (ECG) sensor. With the temperature sensor, it is possible to measure the temperatures at the same time with two different sensors, one attached to the enclosure, and the other placed in contact with the person's skin. With the ECG comparison, it is possible to take readings with two different ECG sensors, one attached to the enclosure, while the other was placed in contact with the person's skin without the enclosure.

RESULTS AND DISCUSSION

The temperature test results are shown in Figure 2. It is evident that the temperature sensor with the enclosure was consistent. The sensor that was not covered by the enclosure, shows in increase in temperature over time. The reason for the initial lower temperature was that the sensor exposed to the surrounding environment allows it to cool down by the moving air around it, and the temperature sensor had to stabilise with the transfer of heat from the person's body to the sensor.
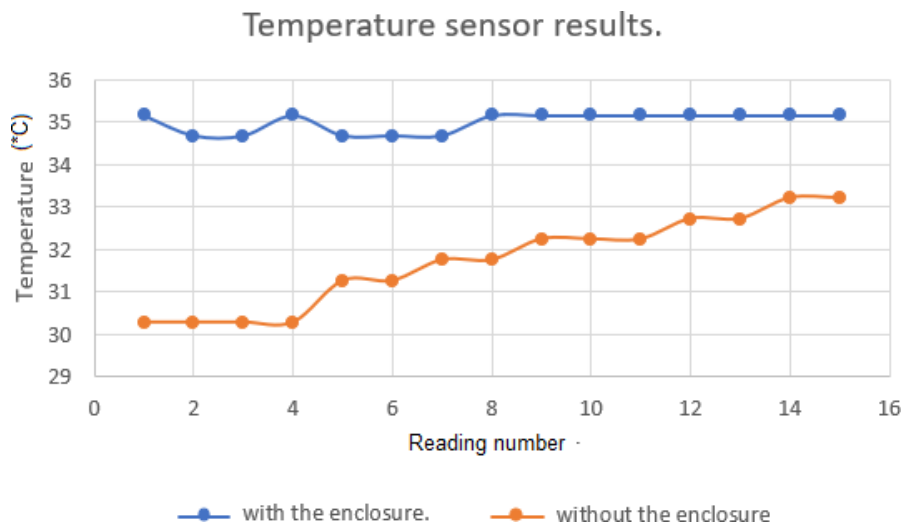
Figure 2: The comparison of the temperature sensors with and without the enclosure

The pulse rate sensor results are seen in Figure 3. The ECG sensor outside the enclosure was stable after two seconds, fluctuating with an increase or decrease of two bpm. The ECG sensor in the enclosure shows a decrease in the pulse rate over time, with a larger fluctuation of17 bpm. These tests prove that the enclosure and electronics within the enclosure, has an impact on the readings. It is recommended that future work requires a means to prevent interference from other electronics with the ECG sensor.
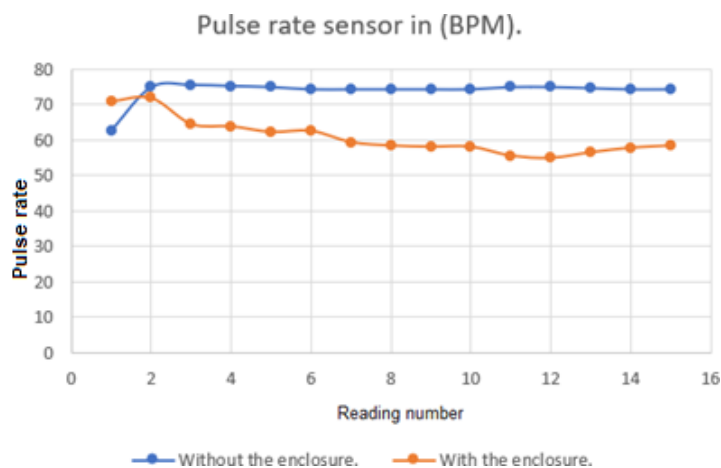

Figure 3: The comparison of the temperature sensors with and without the enclosure

20

CONCLUSION

An enclosure was designed and tested to be used for a wearable device or a smartwatch technology. The effect that the enclosure has on the sensors were of interest, to identify if the sensors would need to be calibrated accordingly. The research contributions presented in this paper were achieved. The design of a wearable technology casing that will be in contact with a person's skin, has been developed. It was shown that the temperature sensor was able to obtain a stable reading when in contact with the enclosure, to prevent interference from the environment. Yet, with the pulse rate sensor, it was found that there was interference with the electronics inside the casing, and therefore an insulation from interference must be considered for future wearable devices.

There is scope for future work. It would be of interest to examine sensor readings and the calibration criteria required if the sensors were placed in a watertight casing.

REFERENCES

Dehghani, M., & Kim, K. (2019). The effects of design, size, and uniqueness of smartwatches: perspectives from current versus potential users. Behaviour & Information Technology, 38(11), 1143-1153. doi: 10.1080/0144929x.2019.1571111

Koshy, A., Sajeev, J., Zureik, M., Street, M., Wong, M., Roberts, L., & Teh, A. (2017). Accuracy of Smart Watches in Arrythmias: Smarts Study. Journal Of The American College Of Cardiology, 69(11), 337. doi: 10.1016/s0735-1097(17)33726-9

Lu, T., Fu, C., Ma, M., Fang, C., & Turner, A. (2016). Healthcare Applications of Smart Watches. Applied Clinical Informatics, 07(03), 850-869. doi: 10.4338/aci-2016-03-r-0042

Phaneuf, A. (2021). Latest trends in medical monitoring devices and wearable health technology. Retrieved 11 January 2021, from https://www.businessinsider.com/wearable-technology-healthcare-medical-devices?IR=T

Ramakrishna, S., Tian, L., Wang, C., Liao, S., & Teo, W. (2015). Medical devices. Woodhead Publishers.

Reeder, B., & David, A. (2016). Health at hand: A systematic review of smart watch uses for health and wellness.   Journal Of Biomedical Informatics, 63, 269-276. doi: 10.1016/j.jbi.2016.09.001

CHAPTER 4

DESIGN AND DEVELOPMENT OF A TRACKING SYSTEM FOR AUTOINJECTORS USING BLUETOOTH LOW ENERGY WITH AUTONOMOUS EMERGENCY ALERT

Qhamani Maqungu, Sudesh Sivarasu
ORCID ID: 0000-0002-8327-3797,
0000-0002-0812-568x
Division of Biomedical Engineering,
Department of Human Biology,
University of Cape Town,
Western Cape,
South Africa

ABSTRACT

Anaphylaxis has propelled the use of adrenaline autoinjectors (AAI) globally. This is to ensure patients administer themselves whenever they experience an allergic reaction, anywhere, to reduce the severe consequences that would result if medical services far located far. Common issues identified with AAI: They are forgotten, not simple to use, and often misplaced. This paper proposes a connected mobile system with an e-cap for AAI using wireless communication protocol, Bluetooth. The hardware in this paper comprises of an Arduino nano BLE module, LED, and magnetic buzzer. Several algorithms for tracking were used and quadratic line of best-fit, produced better distance approximation. The accuracy of the system was affected by electromagnetic interferences. Further development is required to improve the robustness of the system using other wireless technologies and algorithms.

Keywords: fast-locating, Bluetooth tracking, smart autoinjector, Bluetooth Low Energy (BLE)

INTRODUCTION

Anaphylaxis is a severe allergic reaction that is triggered by some food products (like peanuts), insect stings or rubber latex (Posner & CA, 2017). In a world with food of diverse cultures, shared recreational areas, the exposure to allergens is almost unavoidable. The disease affects critical physiological systems that are essential for human survival. These systems include cardiovascular, digestive, and the respiratory system. When the reaction occurs, common symptoms including hives, skin rashes, hypotension, nausea, and difficulty breathing, are present before it becomes deadly to the patient.

Anaphylactic patients intramuscular inject epinephrine via autoinjectors (AI) to mitigate the reaction as shown in Figure 1. AAI are injection devices designed to be portable for out-of-hospital use by patients. The adrenaline (epinephrine) is administered in the thigh for fast absorption. Patients are still required to visit an emergency room (ER) even after successful administration of the drug, to avoid biphasic reaction (Levin, et al., 2015).
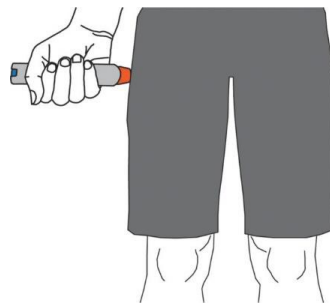

Figure 1: Autoinjector, Epi-Pen, placed on a thigh for epinephrine injection (Posner & CA, 2017)

Given that most available AAI, are mechanical spring-loaded, patients encounter issues when using these devices, including injecting themselves in the thumb instead of thighs (Potera, 2015). Furthermore, patients may not always carry the device with them (Sheikh, Simons, Barbour & Worth, 2012). In the panic before or after using the device, patients may fail to request medical follow-up, putting them at risk (Sheikh, Simons, Barbour & Worth, 2012).

It was found that a delayed administration of epinephrine is less effective as patients will suffer from asphyxia (Pumphrey, 2004). The delay is commonly due to patients not having the AAI within reach. Consequently, eight patients died despite having epinephrine administered within 30 minutes (Pumphrey, 2004).

Short-range tracking technology is used in most household portable items. Smart tags have utilised Bluetooth Low Energy (BLE) and Ultra-wideband (UWB) technology for tracking purposes. *An APPhylaxis* app enables a patient to locate their AAI smart case using a smartphone. The current AI market players have no device available that calculates distance between a patient and AAI itself, and ultimately inform emergency personnel when the AAI is triggered. The literature, however, discuss accessory devices including smart cases, and sleeves for AAI that provide either one or both features.

BLE is classified as Bluetooth 4.0 and above. The application of these devices is IoT- (Internet of things) related since they consume little energy. In this application, the hardware (BLE) is enclosed in a cap, that forms part of the AAI tip. The Global Positioning System (GPS) is used for locating an object on earth using satellites. GPS

modules can come as stand-alone or are found in smartphone devices. Geolocators are power-consuming and need rechargeable, high-density power sources. In this paper, the smartphone is used as host for the GPS system to exploit the rechargeability feature.

The mobile application provides a communication interface between a patient, the hardware, and healthcare providers. The application provides the patient's location in Google Maps. It shows nearby pharmacies with available AAI for patients experiencing an allergic shock.

MATERIALS AND METHODS

In the design and development, the system consisted of two sub-systems: the hardware, and the mobile application. A readily available development board was used, and the enclosure was 3D-printed. The overall system functional flow diagram is shown in Figure 2.
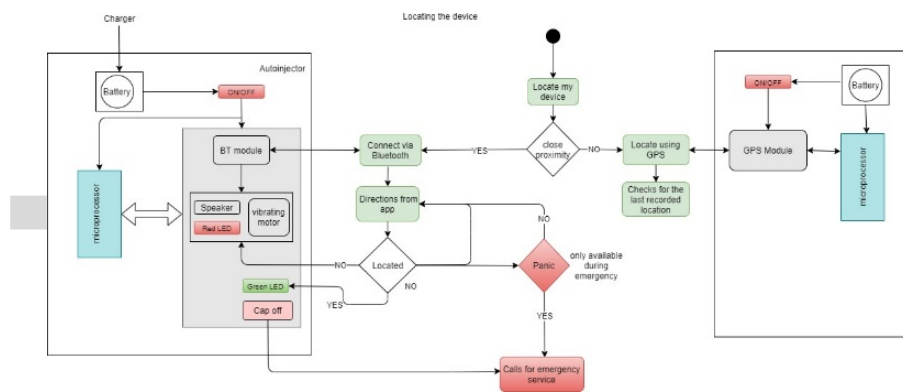
Figure 2: Functional flow diagram.

i. Hardware

An Arduino nano BLE 33 was chosen as the microcontroller as shown in Figure 3. This device does not only provide access to nRF52840 microcontroller but has an on- board BLE module, NINA B306 which is based on the nRF52840 Cortex processor. A magnetic buzzer, connected via an NPN transistor, and an RG LED, and a power switch were added peripherals to the development board. A human-safe buzzer that can be heard up to a distance of 10 meters, with an 80dB noise level was used as suggested by (Birgitta, et al., 1999), which is in compliant with ISO 1900.
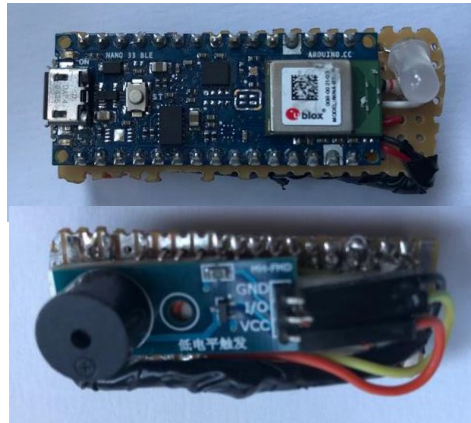
Figure 3: Hardware board with its peripherals.

A power bank was used as the power source, with the specifications: Li-polymer, 5000mAh, with output parameters, 5V/200mA. The RG LED was used for successful (green), and termination (red) of Bluetooth connection.

ii. Mobile application

The mobile application was developed in Kotlin, for Android devices. For database storage, Google Firebase was utilised for security and reliability. A flow diagram of the app for Bluetooth tracking is shown in Figure 4.
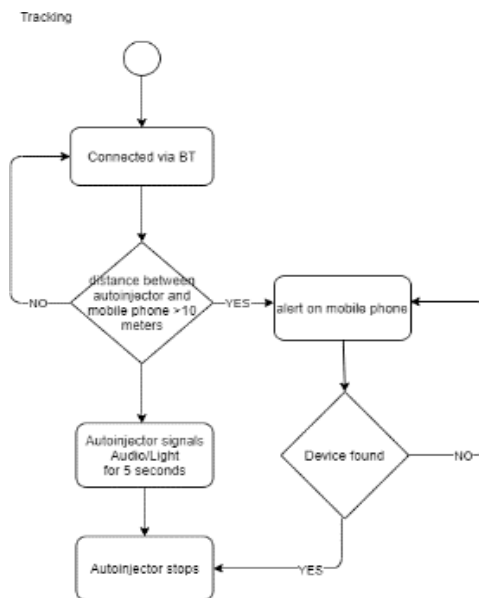
Figure 4: Flow Diagram for Bluetooth Tracking

iii. Distance approximation

To get distance, the received signal strength indicator (RSSI) was converted using methods to be discussed. The RSSI value is given in dBmW, which is how much milli watt power in a radio signal is transferred over a meter distance. The RSSI value

26

at one meter was recorded multiple times and averaged to a value of -51 dBm. This value was used to normalise the RSSI values at different points to minimise deviation results.

The best line of fit was generated on the data using a natural logarithm and a quadrating equation, as shown with Equation 1 and Equation 2 respectively.

$$distance = \; e^{(RSSI\,ratio - K)} \quad (1)$$

$$distance = ax^2 + bx + k \quad (2)$$

Local notifications are triggered when the patient is located far from the AAI. The patient is provided options to fast locate the device on the app using a panic button feature or follow the distance approximated by the app, in case of an emergency. The options include ringing a buzzer and controlling an LED or reading numbers off the mobile app showing how far the device is from the patient, respectively.

RESULTS AND DISCUSSION

Logarithm estimation proved to be less accurate compared to the quadratic polynomial estimation. Therefore, the quadratic method was implemented (*Equation 2*). It created less fluctuations when a patient was constantly moving. Shown in Figure 5 below.
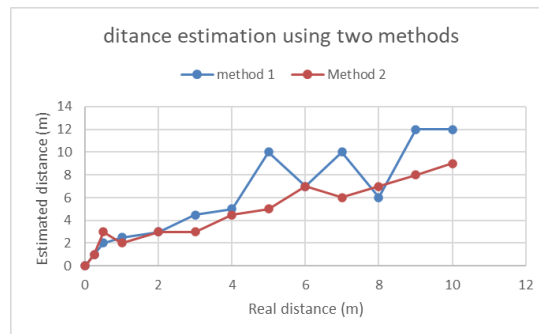
Figure 5: Comparison between distance-approximating techniques

An accurate estimation should produce a straight-line positive correlation. From the graphs, method two (quadratic equation) was chosen to be the final iteration for this method. These results were influenced by electromagnetic interference, i.e., Wi-Fi, Bluetooth, or microwaves. Bluetooth had more influence on the signal. Other factors included:
- Mobile phone's battery percentages
- Wall interference
- Metal plates located near the device (false antenna).

The method, however, was implemented on the mobile application for testing.

The geo- location was implemented successfully using google maps and it produced accurate geo-pinning, Figure 6 shows the results.
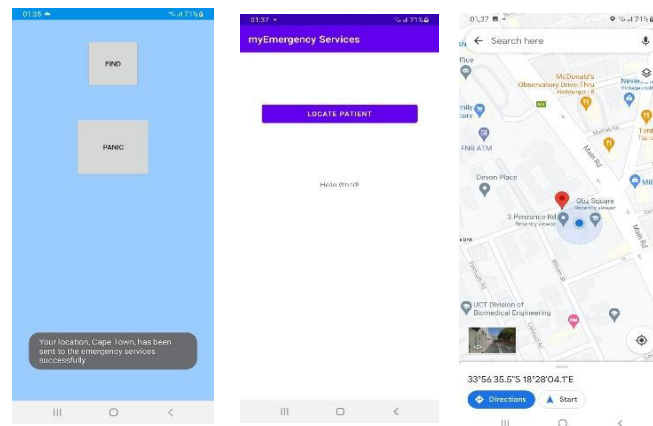
Figure 6: Geo-locating a patient demonstration

The location of the patient is sent to emergency services via a cloud message. Emergency services retrieve the location and direct to Google Map to show the patient's location

CONCLUSION
The device tracks within the range zero to 15 meters. The integration of a buzzer improved fast-locating ability. However, the distance approximation is less robust. False triggers (of being far) were observed and needed improvement. The geo-location was accurate, however, real-time cloud notifications to emergency services were not fully working.

ACKNOWLEDGEMENTS

REFERENCES
Birgitta, B., Thomas, L., & Dietrich, H. S. (1999). Community Noise. Stockholm University and Karolinska Institute. Retrieved from World Health Organisation: https://www.who.int/docstore/peh/noise/Com noise-4.pdf

Levin, M. E., Risenga, S. M., Kriel, M., Karabus, S., Manjra, A. I., Gray, C. L.,Spuy, D. A. (2015). Severe food allergy and anaphylaxis: Treatment, risk assessment and risk reduction. South African Medical Journal, 72-73. doi: 10.7196/SAMJ.9099

Posner, L., & CA, C. (2017). Update on the usage and safety of epinephrine auto-injectors, 2017.Dovepress, 9-18. doi:10.2147/DHPS.S121733

Potera, C. (2015). Misuse of Autoinjectors and Inhalers. AJN, American Journal Of Nursing, 115(3), 17. doi: 10.1097/01.naj.0000461799.44904.d3

Pumphrey, R. (2004). Anaphylaxis: can we tell who   is at risk of a fatal reaction?. Current Opinion In Allergy & Clinical Immunology, 4(4), 285-290. doi: 10.1097/01.all.0000136762.89313.0bSheikh, A., Sheikh, A., Simons, F., Barbour, V., & Worth, A. (2012). Adrenaline auto-injectors for the   treatment of anaphylaxis with and without cardiovascular collapse in the community. Cochrane Database Of Systematic Reviews. doi: 10.1002/14651858.cd008935.pub2

CHAPTER 5

LOW-COST LOAD SHEDDING-RESILIENT MEDICINE STORAGE WITH PHASE-CHANGE MATERIAL: THEORETICAL HEAT TRANSFER EVALUATION OF A DESIGN CONCEPT

Lan Xu, Neil Stacey, David Rubin, Diane Hildebrandt
ORCID ID: 0000-0003-1342-4710, 0000-0003-4902-5201,
0000-0003-0316-9197, 0000-0001-7873-8855
School of Chemical Engineering
University of Witwatersrand
Gauteng
South Africa

ABSTRACT

Diabetes mellitus is one of the most common non-communicable diseases; approximately 0.72 million people in South Africa require insulin treatment. Insulin—a hormone peptide drug— is temperature sensitive and undergoes thermal fibrillation when exposed to temperature above manufacturers' recommendations. Most insulin formations must be stored at 2°C - 8°C in a refrigerator when unopened to maintain its potency and to keep insulin within manufacturers' suggested expiry date. However, one of the unforeseen consequences of frequent power outages in South Africa—and many other developing nations—is thermal denaturation of insulin within household refrigerators caused by frequent power outages. In addition, users cannot tell if insulin has reduced pharmacological action. This publication presents a preliminary design for an in-refrigerator medicine storage container utilising phase-change material to stabilise the temperature of insulin or other medications during power outages, and to provide a visual indicator if a melting event has occurred, even if refrigeration has subsequently been restored, to alert the user that their insulin may have expired. It is found that the principal variables of interest to determine the time to melting are the thickness of the layer of phase-change material in the unit's walls, and the degree of insulation of the outer shell surrounding the phase-change material. It is also determined that asymmetric insulation parameters for the inner and outer surfaces of the container's walls are a crucial design feature for usability, permitting an initial freezing time that is more rapid than the melting time. The current design has been found to be unable to meet all usability criteria, primarily due to an unacceptably long freezing time, regardless of the values of the available parameters. It is therefore concluded that design revisions are required to meet all usability criteria.

Keywords: Diabetes, medicine storage, phase-change material, public health

NOMENCLATURE

Q	Rate of heat transfer
A	Area for heat transfer
ΔH	Change in enthalpy
M	Mass
t	Time
T	Temperature
U	Overall heat transfer coefficient
d	Thickness
k	Thermal conductivity
h	Film heat transfer coefficient
d	Thickness of material of construction
δ	Thickness of PCM layer

INTRODUCTION

The prevalence of diabetes in low- and middle-income countries has increased drastically over the past few decades—increasing urbanisation leads to physical inactivity and poor diet choices (Cullen, 2020). Within South Africa, 4 581 200 (12.8%) (International Diabetes Foundation, 2020) of the adult population has diabetes and about 15.5% of people with type 2 diabetes need insulin (Basu, et al., 2018). This issue is likely to worsen in the near future, as infection with COVID-19 has been found to be a risk factor for subsequent diabetes diagnosis (Barrett CE, 2022). Consequently, the number of new diabetes diagnoses is likely to increase above normal baseline for the duration of the pandemic. The public health needs of developing nations are not the focus of research and development (World Health Organisation, 2021), where there is a greater burden from increasing rate of diabetes cases and a lack of thermostable insulins. Moreover, limited access to reliable medication is exacerbated by insulin's cold chain requirements and frequent power outages.

Along the supply chain for insulin distribution, stakeholders such as manufacturers, distributors, and pharmacies have quality systems to maintain ideal storage conditions. Yet, when diabetics purchase insulin, the same standard is not maintained for several reasons (Braune, et al., 2018; Heinemann, et al., 2020). Currently, it is assumed that domestic refrigeration is reliable enough to store insulin, because developed nations have reliable power supplies. However, studies have shown that even during normal daily domestic refrigerator usage (without power outages) 11.3% of the time insulin degradation is an underestimated risk (Braune, et al., 2018). Insulin potency and quality is compromised by storing the insulin at non-ideal temperatures. Most household refrigerators should operate between 0°C - 8°C for food safety, but may vary depending on position, air circulation, time, and age of the fridge. Therefore, temperatures within a household fridge are almost never ideal for medication storage, even when the mean temperature (6.1°C) is within insulin

manufacturers' recommendation; the typical range (1.5°C - 16.1°C (James, et al., 2016)) is unsuitable.

Coincidentally, many of the developing regions that experience frequent power outages have hot climates, compounding the issues caused by socioeconomic equality and access to reliable diabetes care. Regions with this burden in descending order are: Sub-Saharan Africa, South Asia, the Middle East, and some South American countries. In South Africa, frequent power outages, referred to as "load shedding," are becoming more commonplace (Table 1) —a trend unlikely to change quickly. Therefore, with long and frequent power outages, it is likely diabetics will either waste money on more insulin to replace spoiled insulin, or accidentally use insulin with decreased potency—which is potentially life-threatening.

Table 1: Power outage trends in South Africa

Year	Duration of power outages (hours)	Energy shed (GWh)
2007	-	176
2008	-	476
-	-	-
2014	121	203
2015	852	1325
-	-	-
2018	127	192
2019	530	1352
2020	859	1798
2021	1136	2455

This compromised storage situation creates two urgent needs for insulin users in this context. The first of these is better thermal stability of storage and the second is a visual indicator when a given batch of medication has been exposed to out-of-range temperatures, alerting a user to potential thermal degradation. This solution is also subject to several constraints imposed by the South African context. South Africa has a median per-capita household income in the region of R1 200 per month, severely constraining the acceptable cost of any accessories to treatment. There are also limitations on access to healthcare services, meaning that a solution must be low-maintenance and not frequently require replacement parts. This means that common solutions to cold-chain management are unsuitable. Thermochromic stickers that detect out-of-temperature warming events are unsuitable because they would require replacement after each such event and would also require a cold chain for their distribution and delivery. Accurate digital temperature tracking, while potentially feasible, is comparatively costly and requires externalities including either battery replacement or charging, as well as either their own interface, or connectivity with outside electronic devices. Neither of these approaches to indicating out-of-temperature events address the core issue of thermal stability.

Our proposed solution is the use of a phase-change material (PCM) as a thermal stabiliser which, because of gravimetric and buoyancy properties, can also serve as a low-cost visual indicator by way of flotation of coloured beads of slightly differing density to the PCM. Such beads can be locked into one position base on the container's orientation during the freezing process and then, with the container's orientation altered for storage, only float to an alternate position if the phase change material melts. Hence, if there is a warming event there will be an irreversible positional change giving a visual indication. Afterward, re-freezing the material in the appropriate orientation will reset the beads' position for reuse.

The main usability criteria for this device are that it must have a sufficiently long time-to-melting, once solidified, to maintain thermal stability over the course of a sustained power outage. It must also have a sufficiently short time-to-freezing to allow users to freeze the phase-change material within a convenient amount of time. Ideally, the device should also hold enough excess thermal capacity to restore its internal temperature through multiple occasions of it being opened to retrieve insulin.

MATERIALS AND METHODS // INITIAL DEVELOPMENT CONSIDERATIONS

At this stage of the project, the objective is identifying the key design parameters and experimental targets for prototyping. This will be done on a theoretical basis by using a heat transfer model to identify which parameters affect the main usability criteria, and to determine whether the current design concept will be able to meet the criteria for usability, namely; a sufficiently long melting time to last through typical power outages, a sufficiently rapid freezing time for user convenience, and sufficient excess thermal capacity to repeatedly re-normalise temperature after the container has been opened to retrieve medication as needed.

i.   Physical properties and modelling assumptions

The proposed phase-change material, C-14 paraffin, has a melting point of 6°C, latent heat of melting of 230kJ/kg, density of 763kg/m^3, and thermal conductivity (in the liquid phase) of 0.14W/m*K. The proposed construction material for the device is polypropylene, which has thermal conductivity of 0.11 W/m*K. Air is assumed to have a heat capacity of 1.00kJ/kgK and a density of 1.2kg/m^3. The convective heat transfer coefficient for air is taken to be 10W/m^{2}*K.

The device is conceived to be a rectangular prism, with outer walls comprised of polypropylene, which will enclose a volume of C-14 paraffin as a phase-change material. For simplicity, the device can be envisioned as a cube, but the actual dimensions may vary. All six walls of the device are assumed to have the same dimensions and enclose an equal thickness of PCM. Final design may deviate from this approach, as it may turn out that different properties of convection from vertical and horizontal surfaces may require that the respective wall thicknesses of those surfaces differ.

For purposes of modelling, the following simplifying assumptions are made:
o The phase-change material has uniform temperature of 6°C during melting.
o The air temperature within the refrigerator is uniform.
o A plausible worst-case scenario is considered for simplicity, where the fridge interior has rapidly reached 20°C to determine the time-to-melting during strenuous conditions. Hence, a uniform air temperature of 20°C is assumed for the refrigerator. In practice, the temperature will initially be lower, and follow a gradually increasing profile. However, energy incursion into refrigerators is highly inconsistent, being driven more by opening/closing than by continuous heat loss and so, a refrigerator reaching a high internal temperature early in the course of a power outage is a scenario that will occur at times and so, any device intended to thermally stabilise medicine must be able to handle such a scenario. Hence, the performance benchmark that is considered is the time-to-melting under those conditions.
o For the freezing process, the internal temperature of the refrigerator is assumed to be uniform at 4°C.
o The difference between inner and outer skin surface areas is neglected as being minor.

ii. Governing equations

The device will be closed for storage, which means that heat transfer will occur through the outer skin only. Based on Fourier's Law, and the definition for an overall heat transfer coefficient (these are defined in equations 4 and 5), the rate of heat transfer during melting is given by:

$$Q = \Delta T . U_{\text{outer skin}} \tag{1}$$

During freezing, the device will be open, so the inner surfaces will also interact with the interior air of the refrigerator, so the rate of heat transfer is then given by:

$$Q = \Delta T . U_{\text{outer skin}} + \Delta T . U_{\text{inner skin}} \tag{2}$$

Based on the principle of conservation of energy, the following energy balances can be formulated, governing freezing and melting:

$$\Delta H_{\text{total}} = \Delta H_{\text{Phase Change}} * M_{\text{solid}} \tag{3}$$

$$\Delta H = \int_{t0}^{tfinal} Q dt \tag{4}$$

Equation 3 relates the quantity of material and/or frozen to the enthalpy change that has occurred, while Equation 4 relates the enthalpy change to the heat transfer over time. Equation 2 relates the heat transfer rate to the temperature differences and

hence, these equations together are sufficient to determine the rate of melting and/or freezing once the parameters are populated. The temperature parameters are a product of the outside conditions, while the other parameters are either material properties or are functions of the design geometry of the box.

$$U_{\text{outer skin}} = A_{outer\ skin} \Bigg/ \left(\frac{d_{outer\ skin}}{k_{outer\ skin}} + \frac{1}{h_{air}} \right) \qquad (5)$$

$$U_{\text{inner skin}} = A_{inner\ skin} \Bigg/ \left(\frac{d_{inner\ skin}}{k_{inner\ skin}} + \frac{1}{h_{air}} \right) \qquad (6)$$

Conveniently, because the PCM is at a fixed temperature during freezing or melting, when a constant internal air temperature is assumed for the refrigerator, both processes take place at a constant rate, and the freezing and melting times can be estimated as follows:

$$t_{melt} = \frac{M_{PCM}.\Delta H_{phase\ change}}{U_{outer\ skin}.(20°C - 6°C)} \qquad (7)$$

$$t_{freeze} = \frac{M_{PCM}.\Delta H_{phase\ change}}{U_{outer\ skin}.(6°C - 4°C) + U_{inner\ skin}.(6°C - 4°C)} \qquad (8)$$

Now, the total mass of the PCM is given by the total surface area of the container walls multiplied by the thickness, δ, of the PCM volume, multiplied by its density. Consequently, the above equations can be summarised as follows:

$$t_{melt} = \frac{\rho_{PCM}.\delta.\Delta H_{phase\ change}}{(20°C - 6°C) \Bigg/ \left(\frac{d_{outer\ skin}}{k_{outer\ skin}} + \frac{1}{h_{air}} \right)} \qquad (9)$$

$$t_{freeze} = \frac{\rho_{PCM}.\delta.\Delta H_{phase\ change}}{(6°C - 4°C) \Bigg/ \left(\frac{d_{outer\ skin}}{k_{outer\ skin}} + \frac{1}{h_{air}} \right) + (6°C - 4°C) \Bigg/ \left(\frac{L_{inner\ skin}}{k_{inner\ skin}} + \frac{1}{h_{air}} \right)} \qquad (10)$$

Equations 9 and 10 only have the thicknesses of the inner and outer skins, and the thickness of the PCM volume as independent variables, which makes it possible to assess two major usability criteria just in terms of those independent variables. This simplification is possible only if the inner and outer skin areas are close to equal, and only for simple geometries where outer surface area multiplied by thickness gives the total volume. For more complex geometries with heat transfer features to modify the respective surface areas, this simplification is not applicable.

The other critical usability criterion is tolerance to opening and closing of the unit for retrieval of medicine. There will be considerable user-variability in how much additional heat exchange takes place with each such event. However, it can be reasonably assumed that most users will open the container only briefly during a

power outage, to conserve the cold environment inside. Therefore, the worst-case scenario among the likely use cases is that when the container is opened, all of its air contents are replaced with interior air from inside the refrigerator and then the container will be closed with air at the refrigerator temperature now inside. It can be fairly assumed that heat transfer between the storage container and now-enclosed air will be rapid enough to prevent medicines warming above the desirable range and that the temperature inside the container will re-stabilise at 6°C in a reasonable timeframe. Hence, the area of concern is that the excess energy of the enclosed air will be added to the PCM each time the container is opened and closed.

This performance characteristic can be expressed as a fraction of the PCM volume that will be melted to re-stabilise temperature after a single opening event, and can be estimated using the following equation:

$$fractional\ melt = \frac{V_{container}.\rho_{air}.Cp_{air}.\Delta T}{V_{PCM}.\rho_{PCM}.\Delta H_{Phase\ change}} \tag{11}$$

The only variables remaining in this equation are the volumes of the container interior and that of the PCM; the other parameters are physical constants. Hence, by substituting the known physical constants, the fraction of phase-change material required to melt to normalise temperature after an opening event can be expressed as the following linear relationship to the ratio of interior container volume to PCM volume:

$$fractional\ melt = 0.0001.V_{ratio} \tag{12}$$

RESULTS AND DISCUSSION
i.   Fractional melting during opening and closing of storage container

The fractional melting per usage, as defined by Equation 12, is $0.0001.V_{ratio}$. For a container of square base measuring 18cm on each axis, a height of 12cm, PCM thickness of 1cm, the interior volume will be 3888 cubic cm, and the PCM volume will be 805 cubic cm, and thus the fractional melting per opening and closing event will be only 0.00048, or roughly 0.05%. This means that the overall excess thermal capacity available to compensate for opening/closing of the box will be far in excess of what is required.

This implies that the main consideration for opening/closing is in fact just ensuring that the interior skin's heat transfer is rapid enough that warmer interior air is cooled quickly enough to prevent much temperature rise in the medicines themselves. The low heat capacity of the air volume inside the container suggests that this will not be especially concerning and, therefore, if a user is careful to not keep the container open for extended periods during a power outage, the opening and closing of the container will not significantly affect its performance.

Because of this, heat incursion of this type is not a severe design constraint, leaving the volume of PCM relative to the interior volume of the container as a free variable, subject to other constraints.

ii.   Melting and freezing times
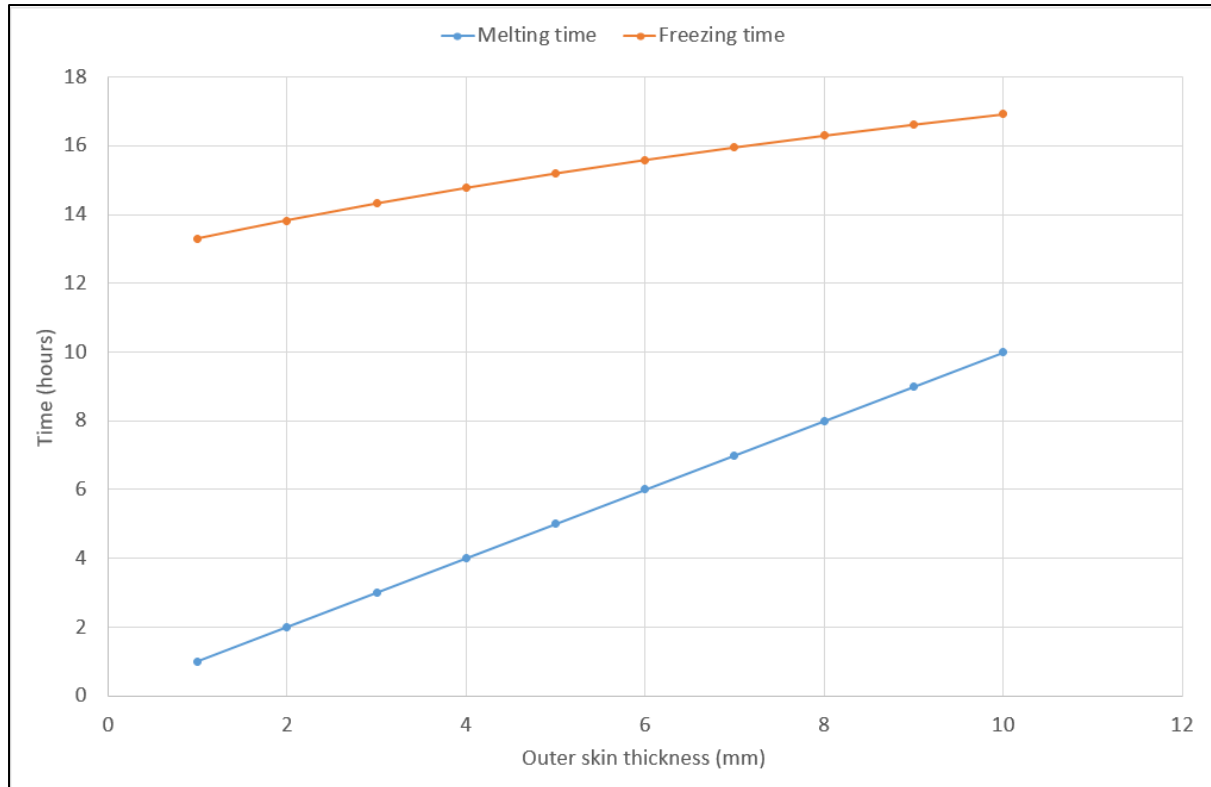
Figure 1: Melting and freezing times for a phase-change material container with 1cm thickness of phase-change material, 1mm thickness of inner skin surface, assuming refrigerator temperature of 4°C during freezing, and 20°C during melting.

Figure 1 demonstrates quite clearly that the design, as currently conceptualised, is not able to meet all usability criteria. While a suitable melting time is achievable, albeit with a comparatively thick outer skin, the freezing time is unacceptably high. Freezing time is directly proportional to thickness of PCM volume but lowering freezing time by reducing δ will also commensurately reduce melting time, adversely affecting another key usability criterion.

Reducing inner skin thickness would also reduce freezing time, but not by a significant enough amount to yield a viable design, because the limitations of convective heat transfer will still apply and so, the heat transfer through the inner skin cannot be increased by that large a factor through that modification. Moreover, decreasing the inner skin thickness to less than the 1mm thickness currently envisioned risks compromising its structural strength. Increasing the outer skin thickness much beyond the 1cm thickness that is the maximum value in Figure 1 is

also not viable because it will drive up the cost of the unit and make it excessively bulky.

The fundamental reason for the difficulty in achieving both of these usability criteria resides in the respective driving forces for heat transfer during melting and freezing. During freezing, the temperature difference between the refrigerator interior and phase-change material at its freezing point is very small, as low as 2°C, resulting in a very small driving force for removing heat from the PCM. During melting, the temperature difference, and therefore the resulting driving force, is considerably larger.

Consequently, fundamental design revisions are required to meet all usability criteria. Modifications that would potentially improve the relationship between the melting time and freezing time are as follows:

- o Insulation on the outer skin to reduce the rate of energy loss and allow for a reduction in PCM volume to reduce freezing time without compromising on melting time. The limitation on this approach is the requirement for excess thermal capacity to withstand the heat incursions when opening and closing the container, but it has been found that it would be possible to decrease thermal capacity very significantly before that constraint becomes onerous. Consequently, this is a highly promising modification.
- o Higher surface area for the inner skin than for the outer. This would require the inclusion of heat transfer features such as fins to increase surface area. There are limitations to how many such heat exchange features can be included without occluding an unreasonable amount of the storage volume, so this modification must be considered in conjunction with others.
- o More conductive material for the inner skin. This modification unfortunately has only small scope for increasing overall conduction, because of the additional role of the convective barrier to heat transfer. Moreover, conductive materials tend to be more expensive than the proposed material of construction, so this must be considered a modification with little promise.

CONCLUSION

It has been shown that a storage container utilising C-14 paraffin as phase-change material is potentially feasible as a means of thermally stabilising medication stored in a household refrigerator during power disruptions, as a sufficiently long melting time is achievable with reasonable design parameters. However, it has been found that an unreasonably long freezing time affects the usability of the proposed design and, consequently, design revisions are needed in order to meet the required usability criteria. It has also been shown that the main parameters of interest for usability are the thickness of the PCM layer and the heat transfer coefficients for the inner and outer skins respectively. It has been found that the inner skin heat transfer coefficient must be considerably higher than that of the outer skin in order to meet the usability criterion of freezing time being shorter than melting time. Once a revised

design that meets the usability criteria is developed, prototyping and laboratory testing should be focused on determining those heat transfer coefficients and achieving values for those parameters that meet the specified usability criteria.

ACKNOWLEDGEMENTS

REFERENCES

Barrett CE, K. A. A. P. e. a., 2022. Risk for Newly Diagnosed Diabetes >30 Days After SARS-CoV-2 Infection Among Persons Aged <18 Years — United States, March 1, 2020–June 28, 2021. *MMWR Morb Mortal Wkly Rep,* Volume 71, p. 59–65.
Basu, S. et al., 2018. Estimation of global insulin use for type 2 diabetes, 2018–30: a microsimulation analysis. *Lancet Diabetes Endocrino,* 7(1), pp. 25-33.

Braune, K. et al., 2018. Storage Conditions of Insulin in Domestic Refrigerators and Carried by Patients—Insulin Is Often Stored Outside Recommended Temperature Range. *American Diabetes Association,* pp. 1-7.

Cullen, M., 2020. *Type 2 Diabetes in Developing Countries.* [Online] Available at: https://borgenproject.org/diabetes-developing-countries/
Heinemann, L. et al., 2020. Insulin Storage: A Critical Reappraisal. *ournal of Diabetes Science and Technology,* pp. 1-13.

International Diabetes Federation, 2021. *IDF Diabetes Atlas: 10th Edition (South Africa Diabetes report 2000 — 2045).* [Online] Available at: https://diabetesatlas.org/data/en/country/185/za.html
International Diabetes Foundation, 2020. *IDF Africa Members.* [Online] Available at: https://www.idf.org/our-network/regions-members/africa/members/25-south-africa [Accessed 2021 August 15].

James, C., Onarinde, B. A. & James, S. J., 2016. The use and performance of household refrigerators: a review. *Comprehensive Reviewsin Food Science and Food Safety,* pp. 160-179.

World Health Organisation, 2021. *Keeping the 100-year-old promise making insulin access universal,* Geneva: World Health Organisation.

CHAPTER 6
DEVELOPMENT AND VALIDATION OF A MEDICAL DEVICE SOFTWARE TO SIZE AUTOINJECTOR COMPONENTS

Ntokozo Magubane, Sudesh Sivarasu
ORCID ID: 0000-0001-6336-0669,
0000-0002-0812-568x
Division of Biomedical Engineering
Department of Human Biology
University of Cape Town
Western Cape
South Africa

Malebogo Ngoepe
ORCID ID: 0000-0002-3639-9063
Centre for Research in Computational and Applied Mechanics
Department of Mechanical Engineering
University of Cape Town
Western Cape
South Africa

ABSTRACT

Auto-injectors are medical devices used to inject medication into the intramuscular or subcutaneous layer of the body. They can be used for different disease applications such as anaphylaxis, rheumatoid arthritis, episodic migraines, multiple sclerosis, diabetes, and many others. This study focuses on developing a software application to size autoinjector components for different disease applications. The kinematic properties of an autoinjector are analysed and explained using a mathematical model that focuses on the plunger motion during the injection process. The mathematical model is validated by a physical experiment that uses a high-speed camera to capture the motion of the plunger during the injection process. The plunger displacement increases linearly during the injection process while the plunger velocity increases linearly and then reaches a constant velocity for the remainder of the injection process. The software application is developed using the validated mathematical model and optimising the relevant equations to determine the component dimensions of an auto injector.

Keywords: autoinjectors, IM injections, mathematical model

INTRODUCTION

The autoinjector (AI) market is growing rapidly due the increasing demand for self-administration of medication and the growing prevalence of diseases that require intramuscular and subcutaneous injections (Global Industry Report, 2019-2026). Although AIs for some disease applications already exist, there is not an easy method to adapt these existing designs for other disease applications to meet market demand. Medications are injected into the intramuscular or subcutaneous layer for faster absorption as patients usually have limited time and minimal chances of survival during a shock. One of the biggest challenges in the auto-injector market is the increase in injectable natural drugs (Badkar et al, 2021). These drugs have complex formulations and concentrations, high viscosities and are prescribed in high dosages. For high viscosity drugs, a large spring force is needed to ensure an acceptably short injection time on the order of second (Zhong et,al 2020)

There are many models created to study the performance characteristics of an autoinjector, however none of the models are used to size autoinjector components. Predictions of injection time and injection force are important to ensure high preforming AIs. Injection time presents information on the variability of parameters in an auto-injector and is often calculated by considering the equilibrium of the static forces including stopper friction and pressure drop as described by the Hagen- Poiseuille equation (Thueer et al, 2018). This study aims to develop a medical device software to size autoinjector components and determine performance characteristics of autoinjectors for different disease applications.

MATERIALS AND METHODS

i.   Mathematical Model

The performance characteristics of an autoinjector were divided into three groups, namely kinematic properties, fluid properties and component dimensions. Table 1 shows the performance characteristics in their respective groups.

Table 1: The performance characteristics of an autoinjectors

Kinematic properties	Fluid properties	Component dimensions
- Plunger displacement - Plunger velocity - Frictional force between plunger and syringe barrel - Injection force - Injection time - Injection depth	- Fluid force - Drug pressure - Medication volume - Shear stress	- Syringe volume (syringe diameter and length) - Needle diameter - Needle length

This study focuses on the kinematic properties and the component dimensions. A mathematical model was developed to explain the kinematic properties. The kinematic properties were analysed by considering the plunger inside an autoinjector

and its motion. The forces that act on the plunger are 1) the spring force (because of the spring being compressed to force the plunger into motion), 2) the frictional force between the moving plunger and syringe and 3) the fluid resistance force as a result of the medication being injected into the patient.

The spring force (1) is defined as per Hooke's law and depends on the displacement of the spring and the initial preload. The preload used was defined as 81 mm and the spring force reads:

$$F_{spring} = k(0.081 - x) \tag{1}$$

The fluid force (2) is defined as the product of the drug pressure and syringe area. The drug pressure is a sum of the viscous pressure via the Hagen Poiseuille equation, the dynamic pressure losses via the Darcy Welsbach equation, the static pressure loss, and the pressure difference inside an auto-injector. The drug pressure is defined as:

$$\frac{8\mu L}{4R^4}\frac{dx}{dt} + f_d \frac{L}{d}\frac{Pv^2}{2} + pgh + P_{atm} - P_{tissue} \tag{2}$$

The frictional force (3) is equal to the product of static coefficient and the normal force when the plunger is stationary and the sum of the viscous and kinetic when the plunger is moving. The dynamic frictional force is:

$$\mu_k F_n sgn(x) + \mu_v \frac{dx}{dt} sgn(x) \tag{3}$$

The force acting on the plunger is coupled using force balance into a system of differential equations that are solved using MATLAB.

i.   Validation experiment
An experiment was conducted to validate the mathematical model. As part of this experiment, the spring properties were verified by compressing the spring and measuring the spring force and deflection using a Testometric force machine.

Two models were set up for the experiment:
o   An actuation model used to compress and release the spring coupling a spring holder, spring, and spring compressor.
o   An injection model with a vial, plunger, needle, fluid, and holder with displacement markings. Both models were clamped into the Testometric machine, and a light source was used to improve visibility. A high-speed camera was used to capture the motion of the plunger as it was forced into movement by the spring.

ii.   Graphical User Interface

A graphical user interface was used to determine autoinjector dimensions and performance characteristics. The software widgets are coded in Python Tkinter and functionality is based on the validated mathematical analysis conducted for this project. The user interface is validated using FDA software validation guidelines. These guidelines include (1) defining the software lifecycle as per the software life cycle for medical devices standard (IEC 62304); (2) defining the system requirements; (3) completing a risk register as per the risk management for medical devices standard (ISO 14971); (4) completing a design review at the end of the initial development phase to confirm that the system requirements are met; (5) conducting a traceability analysis to check how the source code compares to the design specification and ensuring that appropriate coding standards are adhered to.

RESULTS AND DISCUSSION

There is a linear relationship between plunger displacement and time during the injection process. The results recorded are for water of viscosity 1 cP at $25^{\circ}C$. The displacement shown in Figure 1 below remains zero before actuation of the autoinjector and remains constant when the spring is fully compressed.
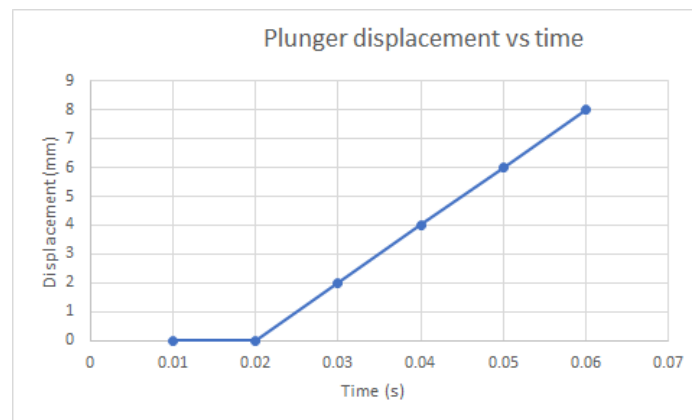
Figure 1: Plunger displacement vs time graph for water of viscosity 1cP at $25°C$

The plunger velocity shown in Figure 2 increases linearly with time and reaches peak when the spring is fully compressed. The system rebounds between 0.03 to 0.04 seconds before reaching a constant velocity of 0.2 m/s. When the plunger is in contact with the fluid, the fluid pressure increases rapidly and reaches a constant pressure of 29.8 Pa. The numerical and experimental results agree with a percentage error of 4.25%. The discrepancy in the results is associated with the limited results recorded in the validation experiment and should be accounted for by analysing the fluid properties of an auto-injector. The syringe acceleration was not recorded in this study.
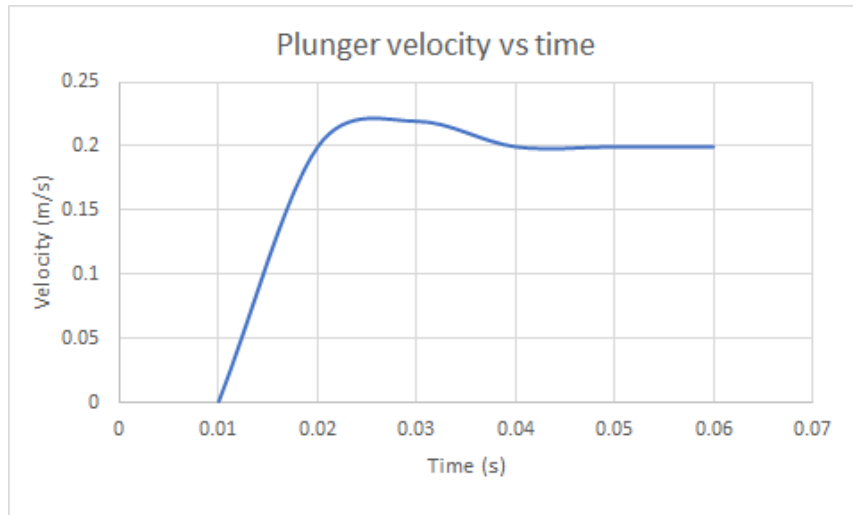
Figure 2: Plunger velocity vs time for water of viscosity 1cP at 25°C

The developed software allows a user to log in and define their user inputs. Thereafter, they can thereafter select the kind of analysis they would like to run, from (1) dimension; (2) injection force; (3) plunger displacement; (4) plunger velocity; (5) spring force (6) frictional force; (7) drug pressure and (7) fluid force.

The software authentication page is shown in Figure 3. The software:
  ○ Allows the user to log in using their correct authentication.
  ○ Allows the user to select their parameters of interest and input the name, viscosity, and dosage of the medication they intend to inject.
  ○ Uses numerical analysis to determine the industrial parameters, namely injection force and injection time, based on the user's input.
  ○ Allows the user to further determine the syringe diameter and length.
  ○ Allows the user to explore other performance parameters of an auto-injector such as spring force, plunger displacement and plunger velocity.
  ○ Stores users' results in a secure database so they can access the results later. Allows the user to delete the analysis results if they do not wish to save them

Figure 3: Authentication page of the developed software.

CONCLUSION

44

This project focused on developing a graphical user interface using an experimentally validated mathematical model. The user interface is coded using Python Tkinter and validated 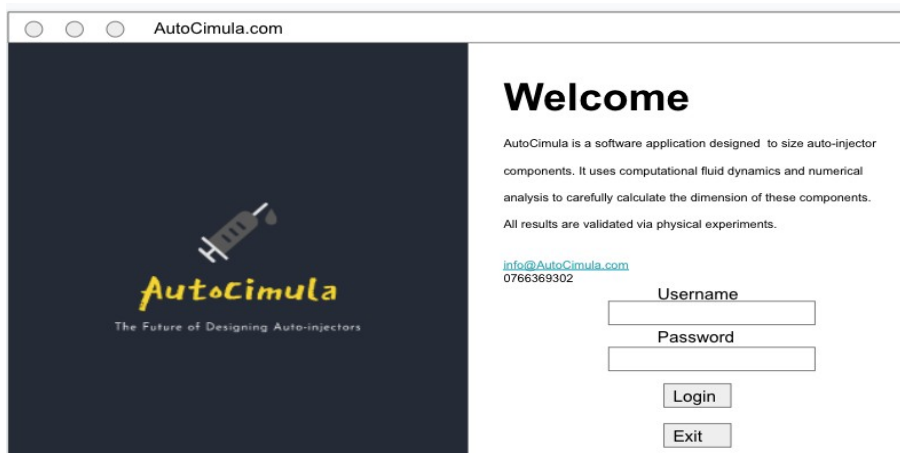using FDA software validation guidelines. The mathematical model developed in this study is based on the following assumptions: (1) the fluid is incompressible and Newtonian; (2) the flow is laminar through a syringe of constant circular cross-section; (3) the fluid is injected into a tissue of pressure 40 mmHg (5332 Pa). Further research is recommended to model the fluid properties using CFD.

ACKNOWLEDGEMENTS

REFERENCES

Auto-Injectors Market Size, Share | Global Industry Report, 2019-2026. (2022). Retrieved 29 March 2022, from https://www.grandviewresearch.com/industry-analysis/auto-injectors-market

Wilkins, J., & Iain, S. (2012). Mathematical modeling for faster autoinjector design [Ebook] (12th ed., pp. 41-45).

Zhong, X., Guo, T., Vlachos, P., Veilleux, J., Shi, G., Collins, D., & Ardekani, A. (2021). An experimentally validated dynamic model for spring-driven autoinjectors. International Journal Of Pharmaceutics, 594, 120008. doi: 10.1016/j.ijpharm.2020.120008

Badkar, A. V., Gandhi, R. B., Davis, S. P., & Labarre, M. J. (2021). Subcutaneous delivery of high-dose/volume biologics: Current status and prospect for future advancements. Drug Design, Development and Therapy, 15, 159–170. https://doi.org/10.2147/DDDT.S287323

Thueer, T., Birkhaeuer, L., & Reilly, D. (2018). Development of an advanced injection time model for an autoinjector. Medical Devices: Evidence and Research, 11, 215–224. https://doi.org/10.2147/MDER.S151727

CHAPTER 7

DEVELOPMENT OF AN INTEGRATED COVID-19 TRACKING AND MONITORING SYSTEM

Kashangabuye Jordan Masirika
ORCID ID:0000-0003-1967-4024
Cape Peninsula University of Technology
Department of Mechanical Engineering
Bellville
Cape Town
South Africa

ABSTRACT

During the COVID-19 pandemic, several policies were instituted to help mitigate the spread of the virus and contact traceability as the virus is spread through person-to-person and person-to-surface contact. One of these was a mandatory completion of a COVID-19 compliance form that captured the details of users of a premises before being granted access. This project proposes an integrated COVID-19 monitoring and tracking system that ensures that the filing process of the compliance forms is fully automated, thus eliminating person-to-person and person-to-surface contact. The automated system will use machine learning algorithms for facial recognition and Natural Language Processing developed in Python to interact with the client through voice prompts.

Keywords: tracking system, machine learning, algorithm, monitoring system, COVID-19, pandemic, facial recognition, natural language processing, deep learning

INTRODUCTION

On the 7th of January 2020, SARS-CoV-2 was confirmed as the causative agent of the Coronavirus Disease 2019, or COVID-19 in short. Since then, the virus has spread to more than 90% of countries in the world, including South Africa (South African Department of Health, 2021). This situation forced various countries around the world to devise ways to correctly track and prevent infection. SARS is a life-threatening respiratory disease caused by its associated SARS coronavirus. It is an animal virus that can affect humans after crossing the species barrier. The first human occurrences of the sickness are thought to have occurred in the Guangdong Province of the Chinese Republic in November 2002 (European Centre for Disease Prevention and Control, 2021). However, the symptoms were only discovered three months later. Following its discovery, the virus spread from individual to individual, largely by inhalation of droplets.

The virus' incubation phase lasted anywhere from three to 10 days. A high fever would develop, followed by non-specific symptoms, and in many cases, diarrhoea (Cherry & Krogstad, 2004). Due to the Chinese outbreak, the virus moved rapidly from China to other Asian countries. A minor number of cases was also reported in various countries, including four in the United Kingdom, and a large outbreak in Canada. Fortunately, it was brought under control in July 2003, thanks to a program that consisted of isolating individuals suspected of having the disease and screening all passengers flying from the afflicted nations for symptoms of illness. Another minor SARS outbreak was connected to a Chinese medical laboratory in 2004. It was assumed to have been caused by a person coming into close contact with a sample of the SARS virus, rather than transmission from animal to person or person to person (National Health Service, 2021).

LITERATURE REVIEW

This section highlights current COVID-19 tracking and monitoring systems used by various countries around the world. These will be compared and the strengths and weaknesses of each will be drawn out. The majority of countries use mobile tracking apps to record data that can be used for contact tracing in the event of a transmission.

i.   Aorogya Setu (India)

Among the countries most affected by this pandemic, India is placed second with approximately 29 million cases reported (Worldometer, 2021). This provides an idea of the severity of the situation for the Indian government. As such, they developed a tracking tool called Aarogya Setu. It is a mobile application developed by their Health Ministry to track and sensitise Indian citizens to flatten the curve. The app uses Bluetooth and GPS technologies to alert users when they are near a person infected with COVID-19 (Gupta, Bedi, Goyal, Wadhera & Verma, 2020). A self-assessment test feature was added that provided health and symptom related questions, and from the answers provided would determine the risk level for said user in different colour codes. This technology has room for Artificial Intelligence and Computer Vision to detect COVID-19 patients.

ii.   Private Kit: Safe Paths (United States of America)

This application was developed by the Massachusetts Institute of Technology. It contains the same features as the Aarogya Setu application. Its main goal is to simplify contact-tracing procedures to effectively reduce the spread of the disease. It uses GPS-based arrangement; but because this technology is difficult to anonymise, developers are looking into specialised solutions using encryption. The application gathers a user's location information by keeping a time-stamped log using little storage space, far less than what is needed for a single photo. The user's information is encrypted and never leaves their phone, with the purpose of preventing other users from recognising them. If a user tests positive for the virus, they can make use of a QR code to convey location information to public health researchers (Oliver et al., 2022).

The trend that can be seen with the two examples is that they are focused on tracking the user themselves. This is an efficient way to track and immediately alert people who might be at risk, but it relies heavily on the belief that people will actually register and use the application, even if it only runs in the background. An example of this can be seen with the South African COVID-19 tracking application, COVID Alert South Africa. South Africa currently has a total population of 58 million people, with 69% being active internet users i.e., 38 million using the internet on their smartphones (The World Bank, 2021; Johnson, 2021). Despite these numbers, the application only has a reported one million downloads, which is less than 3% of active internet users (Google Play Store, 2021). Additionally, the use of mobile applications does not allow for temperature testing. This means that even if a user has their data on any of the various tracking applications, they are still required to queue to have their temperature taken. The following sections will provide an overview on the hardware and software components involved in providing the tracking and monitoring capabilities. These sections will contain specific aspects of the device such as system, mechanical, electrical and algorithmic overviews.
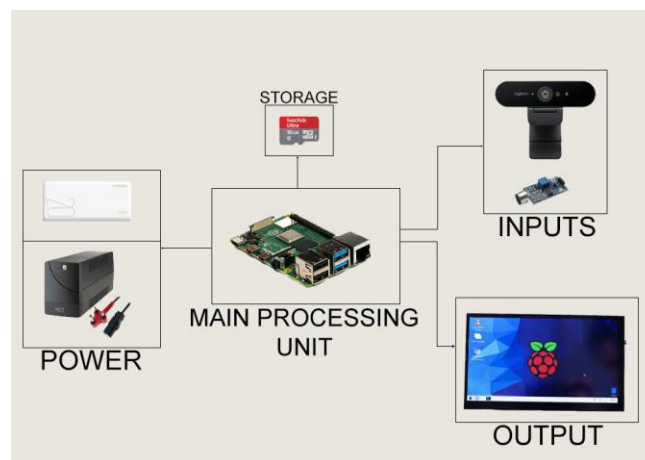
DESIGN

    i.   System Design

Figure 1. Overall system layout

Figure 1 shows the connection between the various parts of the system. Each of these will be studied to understand their use in the system. We have the camera and the microphone as the inputs, a seven-inch display as the, the storage housing the operating system (OS), and the power source.
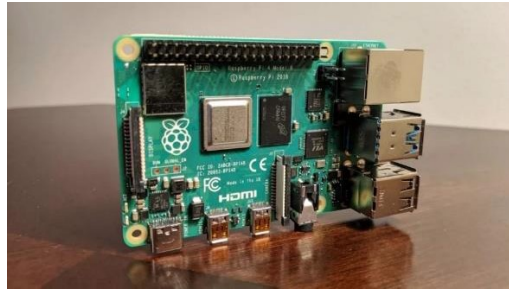
- Raspberry Pi 4

Figure 2. The Raspberry Pi 4 Model B

The Raspberry Pi 4 (Figure 2) is the latest version of the low-cost Raspberry Pi computer. It can be defined as a credit-card sized circuit board similar to those found in a computer, but much smaller. It can do a surprising variety of tasks. For starters, the Pi boards are used as media centres, file servers, vintage games consoles, routers, and network-level ad-blockers by amateur computer enthusiasts. That is, however, only a small sample of what is conceivable. People have used the Raspberry Pi to construct tablets, laptops, phones, robots, smart mirrors, capture images on the edge of space, and execute experiments on the International Space Station, among other things. With the Pi 4's increased speed, its ability to decode up to 4K resolution videos, quicker storage via USB 3.0, and faster network connectivity via real Gigabit Ethernet, many new applications are now possible. Its latest model, the 4B, uses a quad-core Cortex-A72 processor, with tripled performance compared to its predecessor, and is also the first Pi to offer dual 4K at 30 FPS, which is a bonus for creatives who need additional desktop space.

Despite being a miniature computer, the Raspberry Pi 4 still boasts a number of input and output ports that can be used for a wide of variety of applications. Figure 5 shows the ports used for data transfer: the old generation USB 2.0, with speeds capping out at around 60 Mbps, the first generation of USB 3.0 technology with data transfer speed going up to 600 Mbps, and a Gigabit Ethernet port to allow for faster internet connectivity compared to normal wireless connectivity.

It is also equipped with a pair of HDMI 2.0 ports, a USB Type-C power jack for power delivery, and a 3.5-millimeter jack that serves as an analogue audio/video-out port. However, in addition to the familiar aforementioned ports used in the majority of computers, the Raspberry Pi 4 also delivers enormous flexibility by including less common ports such as Camera Serial Interface (CSI), in order to connect basic camera proprietary or non-proprietary modules, a Display Serial Interface (DSI), in order to connect their proprietary seven-inch display and a microSD card slot that enables the ability to add storage to the system, as it comes with no onboard storage of its own.

49
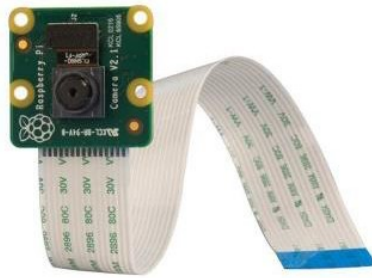
- Camera module

Figure 3. The camera module

The camera module (Figure 3) is a single channel, eight megapixels module supporting the CSI-2 bus interface. It can record at a maximum frame rate of 30 FPS. This camera board connects to any Raspberry Pi or compute module, allowing high-definition videos and still photographs. It uses Sony's IMX219PQ image sensor, which provides high-speed video imaging and sensitivity. Image contamination, such as fixed pattern noise and smearing, is also decreased. A 15 cm ribbon cable is linked to the camera module and connects straight into the Raspberry Pi's CSI connector. It boasts a number of features namely a still picture resolution of 3280 x 2464, an automatic 50/60Hz luminance detection as well as 720p and 1080p resolution at 60 frames per second. It is prudent to note that the camera mentioned above is used only for testing purposes. Despite its great benefits, it is not made to be deployed for heavy usage. *Figure 4* shows the camera that will be more appropriate for such a task.

Figure 4. Logitech Brio 4K HDR

It is the Logitech Brio 4K HDR (Figure 4), a professional grade web camera, with a maximum resolution of 4K Ultra HD at 30 FPS, Logitech's own RightLight™ 3 with HDR technology for accurate colour, alongside a 5x zoom for fine details. It has a diagonal adjustable field of view ranging from 65º to 90º. It is equipped with noise-reducing, dual, omni- directional microphones that provide premium audio performance. It connects through USB 3.0 or USB Type-C.

- Display screen

The Raspberry Pi LCD Touch Display is a Raspberry proprietary display that enables interaction between the user and the Raspberry OS. The 800 x 480 display connects to the board via an adapter board which handles power and signal conversion. Only two connections to the Pi are required: the power from the Pi's

General-Purpose Input/Output (GPIO) port and a ribbon cable that connects to the DSI port. It also has support for up to 10-finger touch and an on-screen keyboard for full functionality without a physical keyboard or mouse.

- Romoss™ 30000 MAh Power Bank

The Romoss™ 30000mah is a high-capacity power storage device that normally allows for the charging of multiple devices. Its lithium polymer batteries are safe and long- lasting. Fit Charge technology allows it to work with a variety of gadgets, including smartphones, tablets, and other electronic devices, while also preventing over-charging. Its ergonomic hand-held design conforms to its simplistic appearance and superior feel. Over-charge, over-current, reset, over-discharge, temperature, power-surge, anti-reverse, short-circuit, and RFI protection are among the 10 intelligent safety features present on the device. It features dual USB Output Ports, lighting, micro-USB, and Type-C input and is widely compatible with a range of devices. It is powered by a 30000 MAh (111Wh) battery and takes an input voltage of 5 V at 2.1 A, while outputting 5 V at 2.1 A or 5 V at 1 A. The connection of all previously mentioned modules is shown in Figure 5.

Figure 5. Connection between the previously mentioned modules

ii.   Mechanical Design

The mechanical design is made to accommodate all the previous components listed. In Figure 6, the camera and screen slot can be seen. The screen will be inserted from the top, and the camera will be screwed in. The total height of the stand is based on the average height in South Africa, which was reported to be 166.7 cm by Business Tech in 2016.
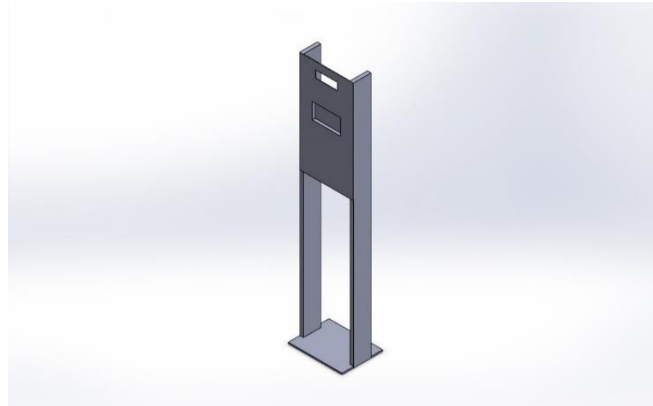
Figure 6. 3D view of the stand

Figure 7 shows both the various slots made for the power bank, the screen, and the Raspberry, as well the two materials constituting the stand: plexiglass and steel. The plexiglass is going to be bolted to the steel that will make up the frame of the stand.

The metal bar constitutes the support for the entire stand. It consists of two main parts: two 1700 x 120 x 25 mm steel bars to provide a frame for the stand and a plate that slides into the bars to provide balance. Mild steel was chosen for this project due its excellent properties. It has an unparalleled weldability and machinability. It is a type of low carbon steel (contains a maximum of 2.1% steel) that enhances the properties of the pure iron. Its outstanding characteristics have led to an increase in its use across a wide range of sectors. Among the various grades of mild steel present, the one considered for the purpose of this project is EN 1.0301, having equivalent grades such as AISI 1008, C10 or DC01. It has a very good weldability and is commonly used for extruded, forged, cold-headed, and cold-pressed parts.
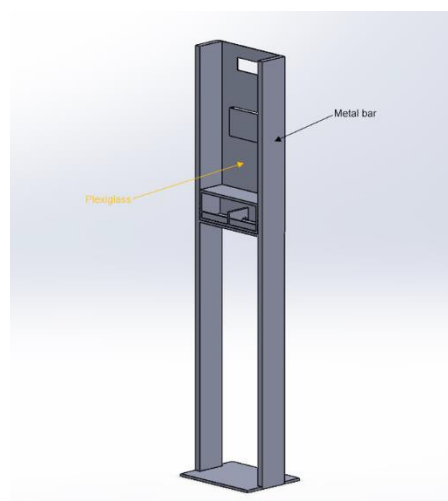
Figure 7. Additional view of the stand

Plexiglass on the other hand is a transparent thermoplastic often used in sheets due to its light weight and shatter resistance, compared to glass. Chemically, it is the synthetic polymer of methyl methacrylate. It is a robust, resilient, and lightweight material that can withstand more impact than glass. Due to its stronger environmental stability than most other plastics, such as polystyrene and polyethylene, it is also excellent for outdoor applications. Plexiglass is a highly beneficial invention because of these advantages, as well as additional features including a long service life, excellent light transmission, and ease of processing. The sheets used for this project are 3 mm thick and cut at specific lengths. Total measurement can be found in the appendix. The total weight that will need to be supported by the steel bars are the plexiglass sheets weights including the weight of the various components is shown in Table 1 below.

Table 1: Total weight to be supported

Element	Weight (g)
Screen	331.1224
Power bank	810
Raspberry Pi 4	46
Camera (Logitech Brio 4K)*	63
Total weight	1250.12

* The camera module used for testing has a negligible weight, so it was ignored.

iii.   Electrical Design

The Raspberry Pi 4 requires an input voltage of 5V to operate without problems. A lower voltage renders some features unusable. Due to its wide variety of ports, it enables us to reduce the number of devices requiring external power to only one, with every other device being plugged directly into it. The camera, with its embedded noise cancelling microphone, can be plugged into one of the USB 3.0 ports and the seven-inch touch screen display can be powered by the all-purpose pins present on the Raspberry.

There are multiple ways to provide the required voltage of 5 V to the system. Among those, three were chosen depending on their price range and their ability to be used during loadshedding periods in South Africa.

• Power bank

The Romoss™ mentioned previously is a high-capacity power storage device that possesses a number of intelligent and safety features, such as over-charge, over-current, power- surge, and short-circuit protection. These features are favourable to the Raspberry Pi 4 as the device is sensitive to unexpected electrical changes. Additionally, its 30000MAh battery capacity allows it to keep the device powered beyond the two-hour window that is normally the duration of power outages during

loadshedding. Finally, it is capable of being used while plugged into a power source (a wall socket, or any power source providing 230V).

- Uninterruptible Power Supply (UPS)

When the input power source or main power source of electrical equipment fails, a UPS (Figure 8) supplies emergency power. It differs from an auxiliary or emergency power system or backup generator in that it protects against input power interruptions almost instantly by delivering energy stored in batteries, supercapacitors, or flywheels. Depending on the budget, these can range from having a relatively short on-battery run-time, of a few minutes, to a decent amount of power delivery time, of two to four hours. It is a continuous power system. A UPS is often used to protect hardware such as computers, data centres, telecommunications equipment, or other electrical equipment against power outages that could result in injuries, fatalities, major business disruption, or data loss.

Figure 8. Mecer 2000VA Line Interactive UPS (Takealot, 2021)

The Mecer 2000VA UPS was chosen for this method due its AC voltage regulation, adequate frequency range, and a performant alarm system that immediately alerts the user in case of low battery, overload, and electrical faults in the unit. If a UPS system is chosen as the main power source for the Raspberry, it will need to be used in conjunction with Raspberry's proprietary power brick that will convert the 230V analogue voltage coming from the UPS to a stable 5V output voltage required.

- Power supply system with backup generator (Figure 9)

This method required the design of an in-house power supply system that can provide the required voltage to the Raspberry.
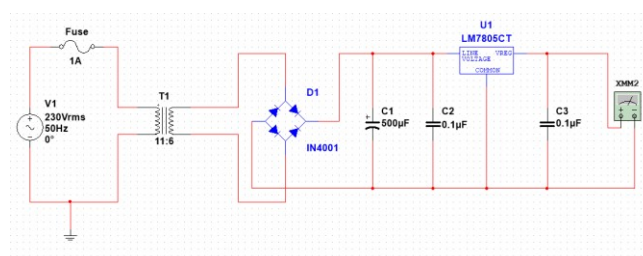

Figure 9. Power supply design

54

The power supply was designed using the NI Multisim tool and was able to provide a smooth 5V DC output voltage (Figure 10) thanks to the LM7805.
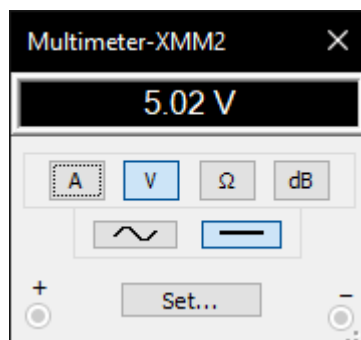
Figure 10. DC output voltage

A transformer, the Indel TS25/11, was used to provide the minimum required voltage of 7V, while also compensating for the 1.4V drop across the bridge rectifier made of IN4001 diodes. As for the capacitor, their values were determined from a combination of the required capacitance at the input and output of the LM7805, and the fact that the capacitor voltage needed to be at least 20% more than the secondary voltage. This required to determine the V$_{RMS}$ to select the proper capacitor.

$$V_{RMS} = \sqrt{2}\,V_{RMS} = \sqrt{2} * 9 = 12.72V$$

The proper capacitance can now be found as:

$$C = \frac{1}{2\pi f V_O} = \frac{1}{2\pi * 50 * 5} = 6.366 \times 10^4 F$$

The practical standard value close to this capacitance value is 500uF, thus it was selected. So far, the cost is kept relatively low due to the components used for the design. However, if this is to be implemented in South Africa, a backup generator will also be bought to account for emergency power generation in the event of power outages. Specifications for generators vary greatly, but their prices are higher than the other two alternatives discussed, thus making this the most expensive alternative.

iv.   Algorithm Design
The algorithm behind the entire system, from the graphical user interface (GUI) to the face detection algorithm itself, were designed and coded in Python programming language.
•Face detection
Face detection makes use of multiple technologies to work. To build the face recognition system, face detection will first be performed, then face embeddings will be extracted from each face using deep learning. A face recognition model will be trained based on those embeddings, and finally the recorded faces can be recognised

in both images and video streams using the Open-Source Computer Vision Library (OpenCV) as shown in Figure 11. This is a library of programming functions aimed at real-time computer vision. The library is available to use on multiple operating platforms, while also being free for use under the open-source Apache 2 License. Its application areas include, but are not limited to, facial recognition, gesture recognition, human-to-computer interaction, and object detection. For supporting some of the areas mentioned, it also included a statistical machine learning library that contains various functions such as boosting and a support vector machine. It was originally written in C++, but contains binding in Python, Java, and MATLAB.
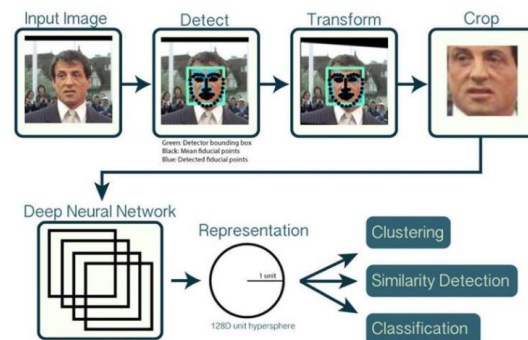
Figure 11. Overview of OpenCV's face recognition pipeline. (Amos, Lidwiczuk & Satyanarayanan, 2016)

To build the face recognition algorithm, deep learning was applied, which is a sub-field of machine learning concerned with algorithms inspired neural networks, with two steps: to apply face detection, which will detect the face location but not identify it, and in order to extract 128-d feature vectors called embedding that quantify each of the faces. This is shown in Figure 12. To increase detection accuracy, facial landmarks, key facial structures such as eyebrows, eyes, and noses, can be computed, making it possible to pre-process and align the face.with I = 1A and f = 50Hz (standard wall frequency in SA).
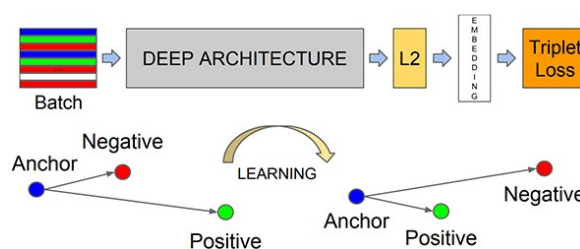
Figure 12. How face embedding is computed using a deep learning face recognition model (Schroff, Kalenichenko & Philbin, 2015).

The model responsible for quantifying each face is from the open-source OpenFace project, a Python and Torch implementation of face recognition with deep learning. This model computes a 128-d embedding that quantifies the face itself using the data inputted into the network, and the triplet loss function. The triplet loss function

is a loss function for machine learning where an anchor input is compared to a positive and negative input. Thus, to train the model with deep learning, each data input needs to include three inputs: an anchor image, a positive image, and a negative image. The anchor is the current face, the positive image is an image that contains multiple faces as well as that of the anchor face, and the negative image does not contain the anchor face. The neural network computes the 128-d embeddings for each face, then tweaks the weights of the network via the triplet loss function such that the embeddings of the anchor and the positive image are closer together, while the anchor and the negative image are farther away from each other. That way, the network can learn to quantify faces and return confident face recognition.

The face recognition and machine learning integration were done using Python programming language. Python was chosen for this project due it being an object-oriented, high-level programming language with dynamic semantics. Additionally, OpenCV integration resources are well documented online, thus making the code debugging process easier.

- Graphical User Interface

Due to the nature of this project, a GUI had to be developed to facilitate the entire process the device is attempting to replace. For that purpose, an open-source Python framework, named Kivy, was used. It is a set of libraries that enable the development of multi-touch application software with a natural user interface. It is distributed under the terms of the MIT License and can be run on the majority of operating systems. Kivy enables the creation of individual "screens" or pages which can be customised independently of each other and can be freely accessed only from the application. The screens are divided in layouts which are independent sections where a set of given data can be put. These data can range from text to images and videos. A total of seven screens were made.

The five main screens are the main screen, the register screen, the manage screen, and the pre- and post-detection screens.

- Main Screen (Figure 13)
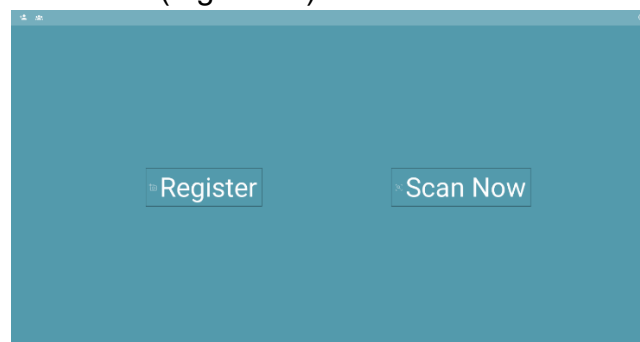
Figure 13. Main Screen

This screen is the second one to be shown. It contains links to the main parts of the software, namely 'registration', 'scanning', 'management', and 'application information' or 'about' section.

- o Register Screen (Figure 14)
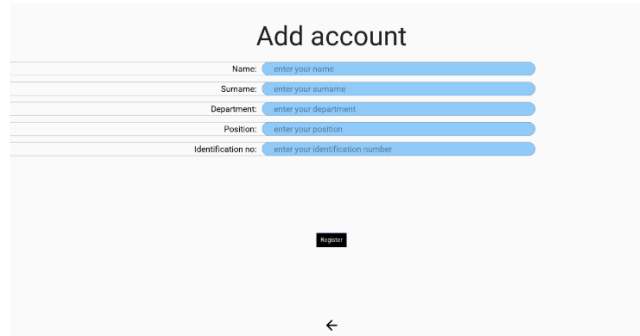
Figure 14. Register Screen

This screen enables the addition of data into the database. The database used during testing is Microsoft Excel. Upon filling out the required information as shown in Figure 14, a set of 10 snapshots of the user's face will be taken using OpenCV and saved onto the local database in a folder with the registered person's name and surname as shown in Figure 15. At the same time, their details will be saved in an Excel sheet.
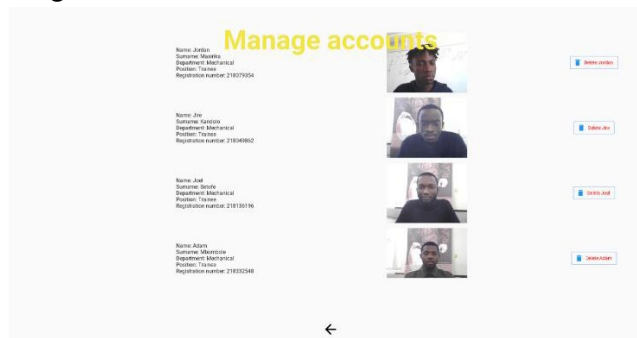
- o Manage Screen

Figure 15. Manage Screen

This screen enables management of the data saved on the database. It has a scrollable view that enables the viewing of all registered people. It also enables the deletion of any person using the button on the right.

- o Pre- and Post-detection Screens

Figure 16. Pre-detection Screen

When the software is put into action by selecting the 'Scan Now' option (Figure 13), it turns on the camera and starts reading the camera video feed in real time to detect faces. To detect all the facial features, the entirety of the face will need to be in the frame. Wearing a mask partially blocks the face. On this screen (Figure 16), a face is detected but there is no match with any of the pictures in the database due to features lacking.
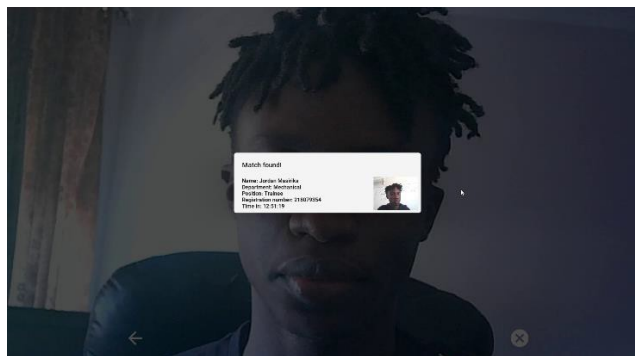
Figure 17. Post-detection Screen

Upon detecting the face (Figure 17), the details of the user are presented on the screen to make sure it is correct, and the COVID-19 compliance questions will be asked. There will be a window for answering the questions, a sound queue will play when the question is fully read. When the user replies to all the questions, they can access the building and their time is registered in another Excel sheet.

CONCLUSION

The goal of this project was to design a system that would eliminate the need for physical COVID-19 compliance forms as well as attendance filing. To do so, a system was designed focused on a Raspberry Pi 4 due to its high performance and features. This system involves the use of a number of additional components such as a camera and a screen to facilitate the two aforementioned problems. The Raspberry Pi was powered by a power storage system during in-house testing. An enclosure was also designed to hold the components involved. This enclosure was made of a combination of plexiglass and steel bars. To perform the attendance filing portion of this project, Python programming language was used in conjunction with machine

learning technology, more specifically a subset called deep learning, which will extract certain facial features and train a model to recognise them more efficiently. When reading the live feed from the camera, the algorithm will automatically detect the user's face if they are saved in the database, and to which a voice-prompt based interaction with the system will be initiated to assist the user in filling out COVID-19 compliance questions. The answers will be registered on an Excel sheet, which is saved locally, along with the time the user entered. Additionally, these details can be accessed at any given time should an urgent need, such as an infection outbreak and contact tracing requirements, arise.

RECOMMENDATIONS

The recommendations for this project can be divided into three sections: hardware, software and general.

i.   Hardware

Due to logistical reasons, a certain number of critical components could unfortunately not be ordered in time. Among them:

- The high-performance Logitech Brio 4K camera: the camera that was used during testing performs was somewhat acceptable but has a number of inherent flaws due its build and price range. It does not handle certain lighting conditions well which impede the face detection algorithm and result in either no detection or incorrect face detection. The use of the Logitech Brio would solve most of these issues.
- Dedicated noise cancelling microphone: because the system will be placed at entrances, which are fundamentally noisy due to constant entry or exit of people. An attempt at solving this problem was made through the algorithm itself, with the use of a library that adjusts the microphone to ambient noise, but this was not enough. The system is unable to pick up user replies in loud environments. For that, a performant noise cancelling microphone would solve most of these issues.
- Thermal reading: a fine addition to this system would be a temperature sensor that would also record the temperature of the person entering the premises. This will eliminate the need for an external temperature reading device.
- Automatic sanitiser spray system: the addition of a sanitiser dispenser system that would provide hand sanitiser once the person has answered the COVID-19 compliance questions and is ready to enter.

ii.   Software

Due to the complexity that they bring, certain functions could not be implemented in time. Among these are:

- A search bar function: embedded in the 'Manage Screen'. This will help find a specific individual faster should there be a large number of registered people in the database.

- Administrator privileges: requiring administrator credentials before accessing vital parts of the software such as the 'Manage Screen' since it contains details of all the people currently registered.
- Online storage capabilities: Industry 4.0 is one where the majority of devices and services are linked to some kind of cloud system. Elements present online can be accessed faster than those on physical devices.

iii.　　General recommendations

This section contains all steps that could not be achieved due to lack of time, logistical reasons, or unavailability of the needed resources.

The building of the first enclosure prototype would have allowed the testing of the system in the field, which would permit the discovery of any bugs. The testing that was performed was mostly in a controlled environment, thus the results cannot be compared to what could possibly happen should the device be placed in a real environment with a large number of uncertainties.

REFERENCES

Amos, B., Lidwiczuk, B., & Satyanarayanan, M. (2016).　　Openface:　A general-purpose face recognition library with mobile applications. Retrieved 31 March 2022, from https://cmusatyalab.github.io/openface/

Cherry, J., & Krogstad, P. (2004). SARS: The First　　Pandemic of the 21st Century. Pediatric Research,　　56(1),　　1-5.　　doi: 10.1203/01.pdr.0000129184.87042.fc

European Centre for Disease Prevention and Control. (2021).　　Retrieved 10 June 2021, from https://www.ecdc.europa.eu/en/covid-19/latest-evidence/coronavirsuses

Google　Play　Store.　(2021).　Retrieved　10　June　2021,　from https://play.google.com/store/apps/details?id=za.gov.health.covidconn

Gupta, R., Bedi, M., Goyal, P., Wadhera, S., & Verma, V.　　(2020).　Analysis of COVID-19 Tracking Tool in　　India. Digital Government: Research And Practice, 1(4), 1-8. doi: 10.1145/3416088

Johnson, J. (2021). Digital population in South Africa as of　　January　　2021. Retrieved 7 September 2021, from https://www.statista.com/statistics/685134/south-africa-digital- population/

National Health Service. (2021). Main Symptoms of　　Coronavirus　　(COVID-19). Retrieved 15 June 2021,　　from　　https://www.nhs.uk/conditions/coronavirus-covid- 19/symptoms/main-symptoms/

Oliver, N., Letouzé, E., Sterly, H., Delataille, S., De Nadai,   M., & Lepri, B. et al. (2022). Mobile phone data and   COVID-19:   Missing   an   opportunity?. Retrieved 31 March 2022, from http://arxiv.org/abs/2003.12347

Schroff, F., Kalenichenko, D., & Philbin, J. (2015). FaceNet: A   unified embedding for face recognition and   clustering.   2015   IEEE   Conference   On Computer   Vision   And   Pattern   Recognition   (CVPR).   doi: 10.1109/cvpr.2015.7298682

South African Department of Health. (2021). About COVID-   19 (Coronavirus). Retrieved 10 June 2021, from https://sacoronavirus.co.za/information-about-the-virus-2/

Takealot. (2021). Mecer 2000VA Line Interactive UPS.   Retrieved   22 October 2021, from https://www.takealot.com/mecer-2000va-line-interactive-ups/PLID34152441

The World Bank. (2021). Population, total - South Africa.   Retrieved   10 June 2021, from https://data.worldbank.org/indicator/SP.POP.TOTL?locations=ZA

Worldometer. (2021). Countries Where Coronavirus Has Spread. Retrieved 10 June 2021, from   https://www.worldometers.info/coronavirus/countries-where-coronavirus-has-spread/

CHAPTER 8

DESIGN AND DEVELOPMENT OF AN OPEN-SOURCE ADL-COMPLIANT PROSTHETIC ARM FOR TRANS-RADIAL AMPUTEES

Lara Timm, Maureen Etuket, Sudesh Sivarasu
ORCID ID: 0000-0003-02073-09649, 0000-0002-9581-3762, 0000-0002-0812-568X
University of Cape Town
Cape Town
South Africa

ABSTRACT

Presently, open-source prosthesis is not optimised to assist the dominant hand in performing bimanual ADL. This research study was thus geared towards the design and experimental validation of an open-source below-elbow prosthetic arm, called the ADL arm, that is functionally optimised for the performance of ADL in the unilateral trans-radial (TR) amputee population. The ADL arm is 3D printed; the design validation involved functional assessment - using the AHAP and simulated use assessment with healthy volunteer participants after obtaining Ethics approval. In accordance with AHAP, the ADL arm presented with an overall GAS of 68% and a partial GAS of >75 % for 4/5 ADL grasps. Usability Assessment involved the performance of ADL tasks coupled with the completion of the SUS. The perceived usability of the device was found to increase with increased device familiarity, yielding an overall score of 84.29. Through the tests conducted, the ADL arm was found to be functionally competent, relatively acceptable with proven ability to assist in the performance of ADLs in a simulated-use environment. A number of design modifications and clinical tests are however recommended to overcome the limitations of the current design and corroborate the results obtained in this study.
Keywords: Open source; Prosthesis; Trans-radial

NOMENCLATURE

ADL   Activities Of Daily Living
AHAP Anthropomorphic Hand Assessment Protocol
CC   Creative-Common
FDM   Fused Deposition Modelling
GAS   Grasping Ability Score
IADL   Instrumental Activities of Daily Living
OT   Orthopaedic Technician
ROM   Range of Motion
TR   Trans-radial
TD   Terminal Device

INTRODUCTION

TR amputation is traumatic, leading to the amputee having a limited ability to perform activities of daily living (ADLs) like eating, dressing, toileting, grooming and ambulation (Pasquina, Cooper & Lenhart, 2009). Below-elbow prostheses are hence prescribed. TR- (below- elbow) amputation refers to the partial removal of the upper limb between the elbow and wrist joints. Such amputations are performed for various reasons, including irreparable physical trauma, certain diseases, and birth defects (Ovadia & Askari, 2015; Jette, Spicer & Flaubert, 2017). The incidence of upper-limb amputations in South Africa (SA) is not well documented. As of 2020, there are approximately 11 000 major upper extremity amputees living in SA, where major amputations exclude amputations more distal than wrist level (Ziegler-Graham, MacKenzie, Ephraim, Travison & Brookmeyer, 2008).

In most scenarios, prosthetic intervention forms part of the post-surgical rehabilitative pathway for below-elbow amputees (Saradjian, Thompson & Datta, 2008). The high cost associated with prostheses, however, results in many amputees in low-to-middle income countries relying on government subsidized devices, which are cosmetic rather than functional, or none at all. Functional prostheses are preferred to their cosmetic counterparts as they allow for a wide range of varied motion hence supporting both the primary and secondary goals that make up the ADLs (Jette, Spicer & Flaubert, 2017; Østlie et al., 2012).

Open-source prostheses, made possible by the internet, are aimed at improving device accessibility, reducing device costs, encouraging collaborative design and a sustainable value chain (Alami et al., 2020). However, the open-source prosthetic arms that are currently available have two main goals: to be an inexpensive solution for child amputees who outgrow prostheses very quickly, or to replicate electric arm prostheses in an inexpensive and accessible manner (Alami et al., 2020; Enabling The Future, 2021).

Currently, a body-powered prosthetic arm intended to assist the dominant hand of a unilateral amputee in performing ADLs does not exist. By increasing personal autonomy, such a device would greatly benefit adult amputees in LMICs who do not have access to functional prostheses. Hence, this study focused on the development of a functional below- elbow prosthetic arm (the ADL arm) that is optimised to assist in the performance of bimanual ADLs. The ADL arm is designed to reliably perform the grasps required by the non-dominant hand in two handed ADL activities. Further, the study aims at validating the functionality and efficacy of the ADL arm by conducting functional and simulated-use testing.

MATERIALS AND METHODS

i.   Open-source Prosthesis Design

The ADL arm Prototype 1 was developed by selecting and combining favourable components of existing open-source designs available in the CC space

and designing novel components to achieve a solution functionally optimised for the performance of bimanual ADLs as summarised in Table 1.

Table 1: A summary of the open-source designs that were combined to form the ADL arm.

Mechanism	Derived from	Original license
Rotating thumb	Galileo Hand V2.0	CC-BY-NC
Hinged Elbow	Unlimbited Arm V2.1	CC-BY-NC-SA

ii.   The ADL Arm Version 1 (V1)

This ADL arm uses torque generated by flexion of the elbow joint to actuate the hand TD. The prosthesis is suspended using Velcro straps that secure the device to the biceps and forearm of the amputee as shown in Figure 1. These straps allow for easy adjustment to fit different users. Customisability is also achieved through 3D printing which allows for improved individual fit, comfort, and level of anthropomorphism (Alami et al., 2020; Gibson & Srinath, 2015).

The hand TD is voluntary closing. Each digit is restored to its resting position by an elastic element. Notable features of the design are the under-actuation mechanism, which facilitates adaptive grasp; the rotating thumb mechanism, which allows adduction and abduction of the thumb; and the rotating wrist mechanism, which allows pronation and supination of the TD.

Figure 1: ADL arm v1

Testing of the ADL arm V1 yielded results shown in Table 2 that led to its further development into a parametric prosthetic arm design that is more suitable for modification and fabrication with limited resources. This process is described in subsequent sections.

Table 2: Test results of ADL arm v1

Weight of hand TD	Hand grasp diameter	Tension developed in actuation code from elbow mechanism
127g	105mm	34.15N

iii.   Defining System Parameters

The design process began with a consideration of the parameters which affect the overall device efficacy as shown in Figure 2. The initial system parameters were identified by reviewing the available literature, through several discussions with a consulting OT, Michael Awood, and following the results obtained after testing the first prototype (ADL V1).

The system parameters included:

- The hand's ability to perform the grasps required for bimanual ADLs.
- The stability of the grip in these configurations.
- The stability of the attachment of the prosthesis to the residual limb.
- The physical effort required to use the device.
- The overall mass of the device.
- The system does not require existing prosthetic hardware to function.
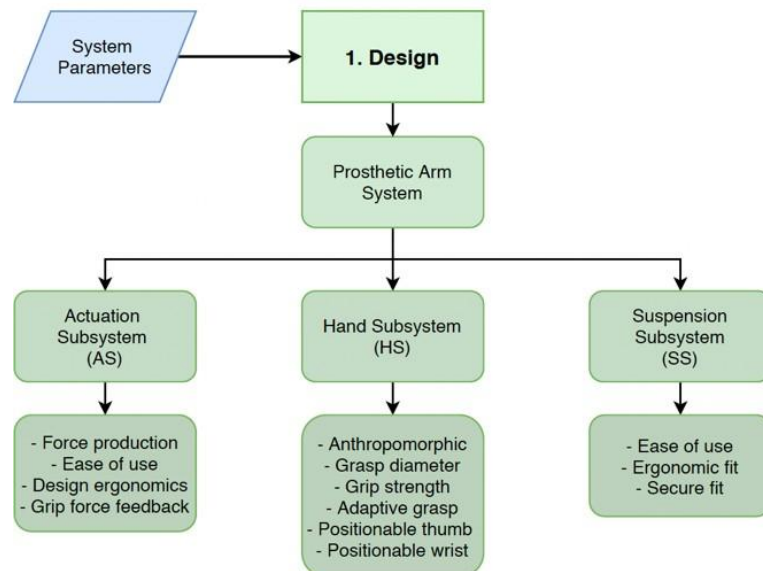
Figure 2: Prosthetic arm subsystems and essential considerations.

iv.   Design and Integration of Three Subsystems

The design of the prosthesis –ADL Arm V2 proceeded with the design and testing of the individual three subsystems: AS, HS and SS shown in Figure 2 and final assembly to form the ADL AMR V2 prototype.

v.   The ADL Arm Version 2 (V2)

The physical prototype of the ADL arm is an assembly of 3D printed parts and accessible hardware components. All 3D printed parts were fabricated using a Creality Ender 3 FDM printer. FDM printed parts suffer an inherent weakness in planes parallel to the print bed, between layers. Some parts, such as the proximal wrist, were designed as an assembly of smaller components. This was to ensure adequate strength of each part in the appropriate direction and to minimise the amount of required support material during printing.

This device is body-powered, featuring a hand terminal device (TD) with thumb abduction and adduction, and wrist pronation and supination functionality. Elbow flexion of the residual limb is used to actuate the hand TD. The hand TD is composed of five digits: four fingers and a thumb. Each digit features a channel that extends the length of its palmar side to house the actuation cord for that digit. The cord is fixed at the fingertip. Applying tension to the cord flexes the digit; releasing cord tension extends the digit. The digit is extended by the restorative spring elements.

Unlike prototype one, the final prototype implements a cable-lock mechanism as shown in Figure 3. This is advantageous as the device is voluntary closing, implying that elbow flexion must be maintained to keep a grip on the object. A cable lock maintains the grip on an object without requiring sustained physical effort from the user. With a cable lock, objects can be grasped away from the body, increasing an amputee's functional work envelope when wearing the device.

Figure 3: ADL arm v2

vi.   Design Validation – Functional Assessment

AHAP aims to reliably measure the grasping ability of anthropomorphic hands. In this case, grasping ability is defined as the hand's ability to effectively grasp and maintain a stable grip on an object while the arm moves around (Llop-Harillo, Pérez-González, Starke & Asfour, 2019).

The AHAP protocol consists of 26 tasks and uses 10 grasp types associated with performing ADLs. The results of the protocol reveal: A total Grasping Ability Score (GAS): which quantifies the hand's ability to perform the full set of grasps; A partial GAS: which quantifies the hand's ability to perform each specific grasping task; A qualitative indication of the advantages and disadvantages of the hand, its control mechanism, and its actuation mechanism; A starting point to identify the reasons for failed tasks/grasps. The protocol is designed to identify difficulties experienced with grasping and a classification thereof.

For each of the 26 tasks, a trained operator (the innovator) instructed the participant to carry out each step thrice using the ADL ARM V2. Priority was placed on 11 tasks that are representative of those used by bimanual ADLs. The grasp types

that were used as a measure for prosthetic success included medium wrap, adducted thumb, lateral grasp, index finger extension, and non-prehensile.

Of the 11 tasks performed using these grasps, a score of at least one had to be achieved for each of the five grasp types specified. That is to say that at least one object per grasp type, and not necessarily all object variations, must be grasped successfully. If the results met these criteria, the device would be considered a success at this stage. Scores were given in this order: a score of one was given for a successful grasp of the correct grasp type, 0.5 if the grasping posture differed from the specification, and zero if the prosthesis could not grasp the object. The definition of grasp success differs per grasp type, however, a score of 100 % is the best-case scenario and corresponds to functionality and anthropomorphism similar to that of a healthy human hand.

vii.   Design Validation – Simulated Use Assessment

Simulated Use Assessment was completed by seven healthy, right-hand dominant individuals. The designed bypass socket was used for this portion of testing as shown in Figure 4. In the first stage, a self-report questionnaire was used which allowed the innovator to quantify the usefulness of the prosthetic device for performing a range of ADL and IADL tasks.

Figure 4: The bypass socket of the ADL arm

The questionnaire was designed to measure:
- If the task can be performed without assistance.
- If the prosthesis was used in performing the task.
- The grasping role (direct/indirect/passive) of the prosthesis.
- The perceived difficulty experienced when performing the task.

In the second stage, the *overall device usability* was assessed following the acquisition of ethics approval from the UCT Human Research and Ethics Committee under reference number HREC REF 796:2020. Device usability was assessed using seven healthy participants in the laboratory setting divided into three categories: those with no familiarity with the device; those with theoretical experience with the device; and those who were involved in the testing of prototype one. System usability was scored according to the System Usability Scale (SUS) (Brooke, 1996). The SUS

questionnaire provides a quantitative measurement of device usability and user experience.

According to a study conducted by Bangor, Kortum and Miller (2008), the average SUS score is 68, while anything above 68 is considered above average. A 'good' score is one larger than 72:75, an 'excellent' score is larger than 85:58 and the 'best imaginable' score is 100. The obtained SUS will be evaluated against this scale.

RESULTS AND DISCUSSION

The physical and mechanical properties of the ADL ARM V2 were evaluated on a subsystem basis and following through with particular parameters of interest reported in Table 3 below:

Table 3: Test results of ADL arm v2

Weight of hand TD	Hand grasp diameter	Tension developed in actuation code from elbow mechanism
104g	114mm	43N

The ROM of the designed TD informs the grasp diameter, and, for the ADL ARM V2, it was comparable to the healthy hand. This achievable ROM allowed the hand to mimic the kinematics of the healthy hand, allowing it to securely grasp objects of a range of sizes, weights, and surface qualities.

The elbow mechanism was able to produce approximately 43 N of tensile force to transmit to the hand. However, this producible tensile force and the grip force measured in the hand were not the same. This may have been due to the shape of the hand TD and the hand grip dynamometer not being suitable for accurate measurement. Another reason for the discrepancy could have been a loss of energy as a result of friction within the digits, or simply that the transmission of cable tension to grip force is not a 1:1 ratio. It also became apparent during testing that the design of the elbow hinge was a limiting factor to how much force the elbow mechanism could produce, calling for further modifications to the elbow hinge and the cable alignment.

The overall GAS and partial GAS of the ADL arm was found to be 68 %. The ADL arm achieved a partial GAS of greater than 75 % for four of five bimanual ADL grasps. A major design flaw resulted in a partial GAS of 33:3 % for the lateral pinch grasp type. The performance in this grasp, as well as others, would be greatly improved by the inclusion of a mechanism to lock the distal joint of the digits in extension during grasp. In this way, the hand would be better able to apply force to an object with the pads of the digits.

The ADL assessment involved the completion of 86 ADL and IADL tasks; scored using the designed self-report questionnaire. The participants could perform all but seven tasks independently, and the perceived difficulty for tasks requiring the prosthesis was low overall.

Participants performed a number of tasks and then completed the SUS. The perceived usability of the device was found to increase with increased device familiarity, yielding an overall score of 84.29. This result indicated that participants found the experience with the device to be 'good' overall.

CONCLUSION

The ADL arm is functionally competent and has proven its ability to assist in the performance of ADLs in a simulated- use environment, using able-bodied participants. A number of design modifications are recommended to overcome the limitations of the current design, which should be tested in a large TR amputee population to corroborate the results obtained in this study.

ACKNOWLEDGEMENTS

REFERENCES

Alami, H., Rivard, L., Lehoux, P., Hoffman, S., Cadeddu, S., & Savoldelli, M. et al. (2020). Artificial intelligence in health care: laying the Foundation for Responsible, sustainable, and inclusive innovation in low- and middle-income countries. Globalization And Health, 16(1). doi: 10.1186/s12992-020-00584-1

Bangor, A., Kortum, P., & Miller, J. (2008). An Empirical Evaluation of the System Usability Scale. International Journal Of Human-Computer Interaction, 24(6), 574-594. doi: 10.1080/10447310802205776

Brooke, J. (1996). Usability Evaluation in Industry (pp. 189-194). Taylor & Francis.

Enabling The Future. (2021). Which Design?. Retrieved 21 October 2021, from https://enablingthefuture.org/which-design/

Gibson, I., & Srinath, A. (2015). Simplifying Medical Additive Manufacturing: Making the Surgeon the Designer. Procedia Technology, 20, 237-242. doi: 10.1016/j.protcy.2015.07.038

Jette, A., Spicer, C., & Flaubert, J. (2017). The promise of assistive technology to enhance activity and work participation. Washington: National Academies Press (US).

Llop-Harillo, I., Pérez-González, A., Starke, J., & Asfour, T. (2019). The Anthropomorphic Hand Assessment Protocol (AHAP). Robotics And Autonomous Systems, 121, 103259. doi: 10.1016/j.robot.2019.103259

Østlie, K., Lesjø, I., Franklin, R., Garfelt, B., Skjeldal, O., & Magnus, P. (2012). Prosthesis use in adult acquired major upper-limb amputees: patterns of wear, prosthetic skills and the actual use of prostheses in activities of daily life. Disability And Rehabilitation: Assistive Technology, 7(6), 479-493. doi: 10.3109/17483107.2011.653296

Ovadia, S., & Askari, M. (2015). Upper Extremity Amputations and Prosthetics. Seminars In Plastic Surgery, 29(01), 055-061. doi: 10.1055/s-0035-1544171

Pasquina, P., Cooper, R., & Lenhart, M. (2009). Care of the Combat Amputee. Washington: TMM Publications.

Saradjian, A., Thompson, A., & Datta, D. (2008). The experience of men using an upper limb prosthesis following amputation: Positive coping and minimizing feeling different. Disability And Rehabilitation, 30(11), 871-883. doi: 10.1080/09638280701427386

Ziegler-Graham, K., MacKenzie, E., Ephraim, P., Travison, T., & Brookmeyer, R. (2008). Estimating the Prevalence of Limb Loss in the United States: 2005 to 2050. Archives Of Physical Medicine And Rehabilitation, 89(3), 422- 429. doi: 10.1016/j.apmr.2007.11.005

CHAPTER 9:

DEVELOPMENT OF A CONTROL ALGORITHM FOR A BAG VALVE MASK VENTILATOR

Kandolo Jire Christian, Georgina Mampuru
ORCID ID: 0000-0001-8185-7564, 0000-0002-5793-693X
Cape Peninsula University of Technology
Cape Town
Western Cape

ABSTRACT

People infected with COVID-19 can experience trouble breathing since the virus primarily attacks the lungs. It is a highly contagious virus that can be transmitted easily. Leading to high numbers of hospitalised patients, and hospitals can become overwhelmed. Ventilation is the primary source of treatment in severe cases, shortages of equipment can occur leading to a high death rate. The present paper aims to design and develop a low cost, user-friendly and automated bag valve mask ventilator capable of supplying oxygen to a patient. During the pandemic, we were using traditional intensive care ventilators since manual ventilation prompt to some serious health risks. The device is using a simple hardware device such as Arduino.

Keywords: Ambu bag, bag valve mask, Arduino, ventilation, automated, COVID-19.

INTRODUCTION

COVID-19 is an infectious disease caused by a novel coronavirus. It is a highly contagious disease that began in Wuhan in China at the end of December 2019 (Iyengar, Bahl, Raju Vaishya & Vaish, 2020). Coronavirus disease 2019 (COVID-19) led to increased mortality rates by overwhelming medical infrastructure at the regional level. Mechanical ventilators, which are essential for treating both influenza and COVID-19 patients in severe acute respiratory failure, are in critically short supply in some locations. During pandemics, intensive care units (ICUs) do not have sufficient ventilators to treat all the patients requiring them which forces triage and rationing This is despite national stockpiles of proprietary, mass-manufactured ventilators, which are simply not numerous enough due to prohibitive costs to service society during an extreme pandemic (Petsiuk et al., 2020).

MATERIALS AND METHOD

i.   Hardware Design

For the hardware parts as illustrated in the Figure 1, the mechanical concept replaces the action of a human pressing the bag. Manual ventilation with excessive volume and pressure can cause severe complications for patients, particularly vulnerable patients suffering from Acute Respiratory Distress Syndrome (ARDS), including those infected with COVID-19. Since acute care facilities are currently treating large numbers of COVID-19 patients, understanding the implications of poor BVM techniques among this insurgent population (Culbreth & Gardenhire, 2021). The design of the compressing mechanism is a crucial stage in development.
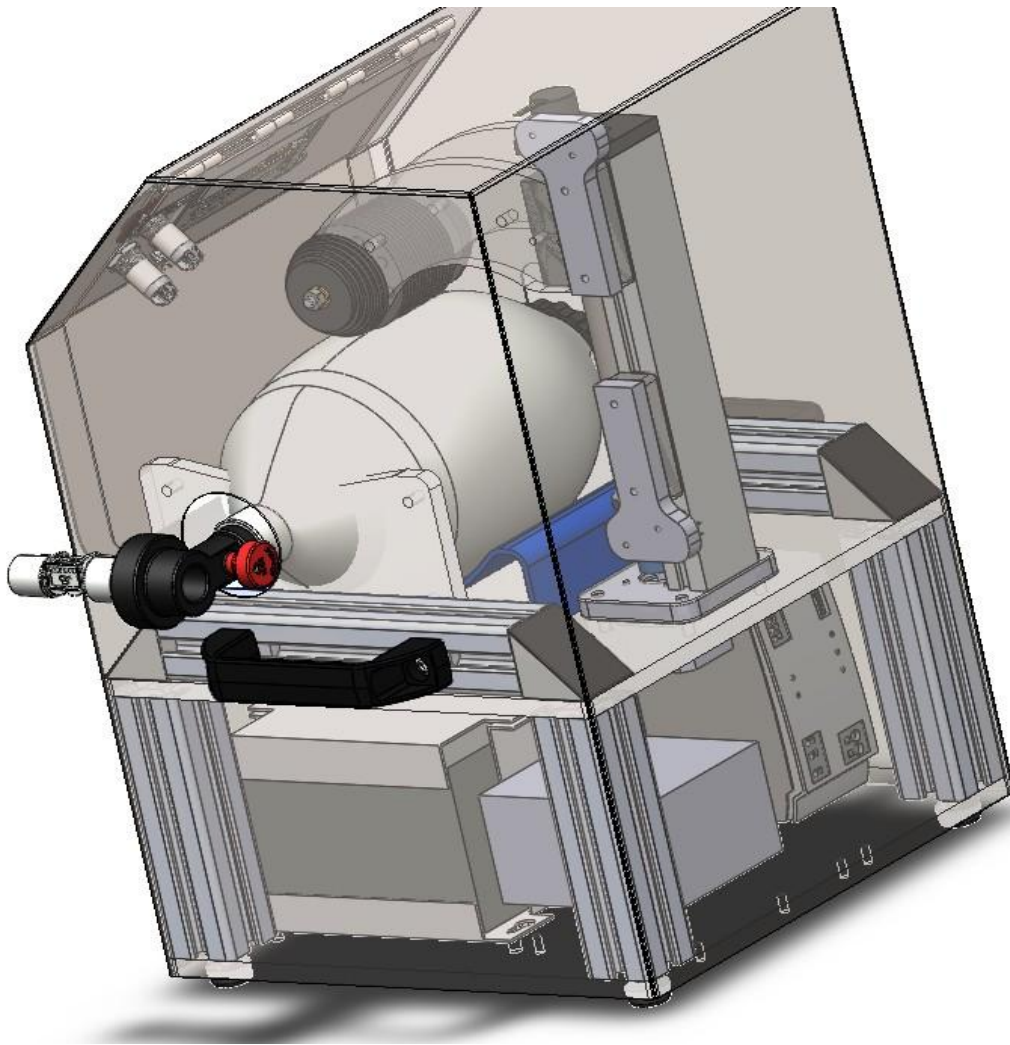
Figure 1: 3D drawing of the Bag valve mask ventilator

ii.   Electrical Design

To simplify the cost of equipment we opted for cheap but reliable devices. The main electrical component is the Arduino board. In this application we used a Controllino (Figure 4) which is an industry-grade PLC with open-source software, fully compatible with Arduino. We are using a brushless DC motor (Figure 3), and to control the speed, we have a speed controller (Figure 2). Raspberry Pi is used here to improve our software architecture. The integration of these components is shown in Figure 5.

Such Examples of low-cost designs can be found in (Chang et al., 2021). Such example is the Masi ventilator that could be rapidly and manually manufactured. The ventilator has the capabilities to manage COVID-19 patients with severe acute respiratory distress syndrome (ARDS). Most COVID-19 patients who develop acute respiratory distress syndrome (ARDS) often require prolonged mechanical ventilation.

Figure 2: Motor Controller

Figure 3: DC motor
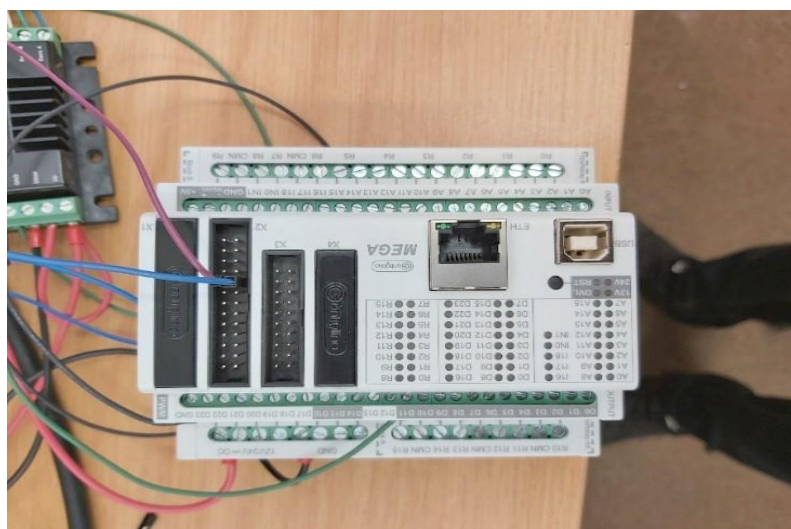
Figure 4: Controllino boar

Figure 5: Flow Diagram

Upper limit switch

Magnetic Encoder
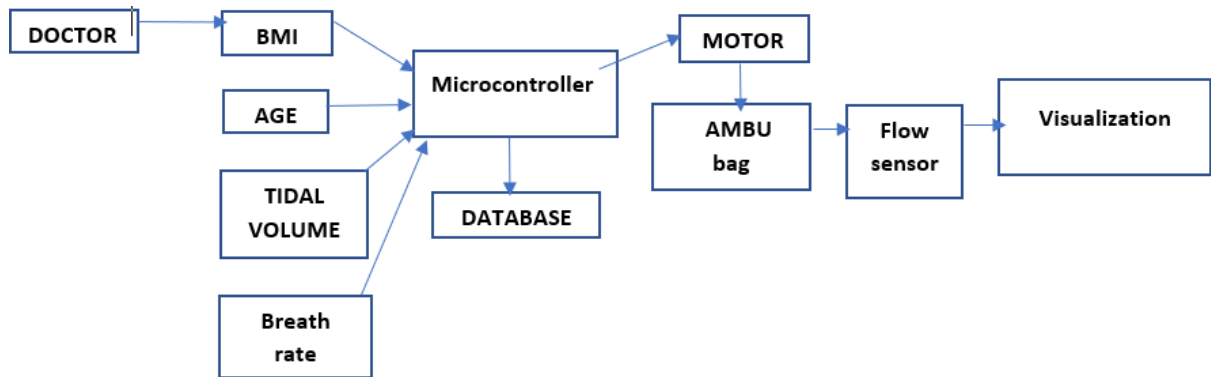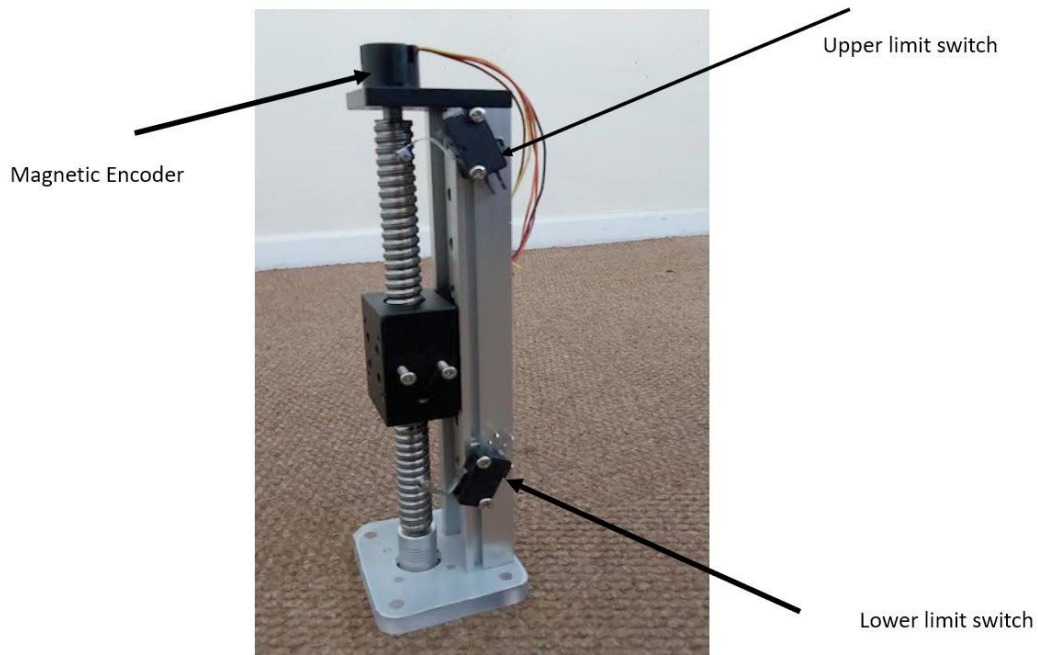
Lower limit switch

Figure 6: Scaler with different component

Figure 6 shows the scalar and its main part which are limit switches that helps stop the motor from both positions. We have a scaler that will be moving following the movement of the motor and speed. Our goal is to deliver oxygen to a patient. But patients have different needs. The figure below expresses the clinical breath per minute required for each kind of patient.

Newborn	40 - 60 breaths per minute
< 1 year	30 - 40 breaths per minute
1 - 2 years	25 - 35 breaths per minute
2 - 5 years	25 - 30 breaths per minute
6 - 12 years	20 - 25 breaths per minute
> 12 years	15 - 20 breaths per minute
Adult	10 - 12 breaths per minute

Figure 7: Different breath per minute (BPM)

RESULTS AND DISCUSSION

The different Breath Per Minute for each age group is shown in Figure 7. As we observe there are different breath per minute (BPM) rates. The algorithm is supposed to correct or implement the correct BPM required. We are achieving this by varying the speed and the position of the motor on the scaler. This is achieved by the magnetic encoder shown in Figure 8 below. An Incremental Magnetic Encoder provides an integrated solution for angular detection within a complete 360° rotation. The use of magnetic technology for motion control and sensing activities eliminates mechanical contact and enables this device to be free from mechanical wear and tear. The three-channel output provides an additional index channel for every full rotation or revolution of 360°. An additional advantage is that the encoders near the upper limit switch rotational speed limits are typically only limited by the application's bearing speed.

Figure 8: Interaction between different components.

Figure 8 represents how the different components interact. The Controllino board is the controlling component. Our goal is to make the Ambu bag deliver oxygen automatically using a motor. This is achieved by setting different speeds controlled by the speed controller at different positions controlled by the magnetic encoder. To get a better 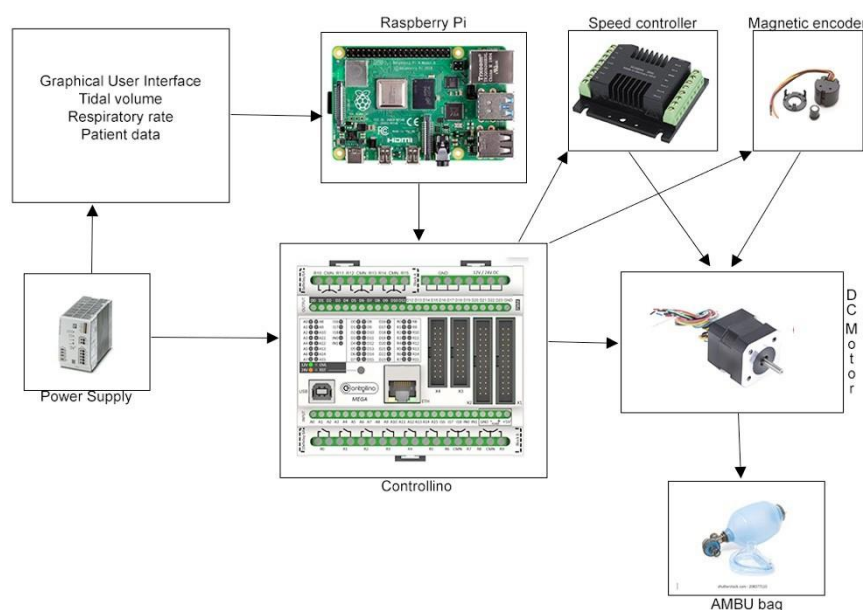picture, a magnetic encoder works through a set of pulses that represent the rotation of the motor. This means each rotation corresponds to a pulse. For a certain number of pulses, the motor will rotate, and this will be interpreted as a point that the scaler has reached. The breath cycle is made up of two main phases, inspiration, and expiration. The scaler has an upward movement and a downward movement which is decompressing or (Expiration). The algorithm will use those two, major concepts to successfully represent those movements. The objective here is to study the required number of pulses to reach a certain position corresponding to a certain volume of air supplied. The speed is a factor of breath per minute, which means the number of breaths that can be supplied to a patient under certain conditions.

Since this a medical device it is necessary to have a testing phase to see if it follows the standard to be used by health professionals. As shown in Table 1, MIT describes that the apparatus required for testing ventilators are:

Table 1: Apparatus required for testing ventilators

Apparatus	Function
Multimeter	Monitors current during cycle and monitors the thermocouple
Thermocouple, Thermal camera, Thermal gun	Monitor component temperature, including motor, gearbox & motor drive
Stopwatch & Counter	Used to manually verify system timing. Consulting the pressure or volume trace from the pressure transducer and spirometer or breathing simulator will provide greater fidelity.
Pressure Transducer & Data Logger	Monitors pressure profile in breathing circuit throughout the cycle
Spirometer	Records airflow and tidal volume Example: Vernier Spirometer.
Video / Digital camera	Used to record test sequences, including sounds and specific observations
White sheet	Used to collect particles debris under the mechanical device.
Breathing Simulator	These are hospital-grade systems used to validate ventilator operation

The South African Health Product Regulatory Authority (SAHPRA) is the body in charge of regulating and certifying medical devices in the country. The device must be approved by SAPHRA. Therefore, the device would also need to comply with the ISO standards below:

- Conformity assessment and certification of the quality management system (as per
  ISO1348515:2016) and testing of products to meet the specified standard is also important.
- ISO 13485 for good manufacturing Practice (GMP).
- ISO 10651-5:2006 specifies the requirements for resuscitator sets.
- IS0 10651-3: I997. specifies requirements for portable lung ventilators designed for use in emergencies and transport.
- ISO 80601-2-80:2018, medical electrical equipment — Part 2-80: Requirements for basic safety and essential performance of ventilatory support equipment for ventilatory insufficiency.
- Protection of Personal information Act (POPIA) requirements

CONCLUSION

COVID-19 caught the world by surprise and did not allow for much preparation. While the pandemic is ongoing, we remember the peak of the pandemic where hospitals were overcrowded due to high infection rates. The main problem was how to treat everyone without enough ventilators. The easiest solution is to use a manual oxygen supplier (i.e., Ambu bag) but this solution is not recommended over the long term since human misuse could occur. We proposed to supply hospitals and health workers with a fully automated device. The main aspect was to make it affordable, easy to use and to develop a working algorithm that will make it perform as traditional ventilators. Software like python and open-source devices and hardware, like Arduino were selected.

ACKNOWLEDGEMENTS

REFERENCES

Chang, J., Acosta, A., Benavides-Aspiazu, J., Reategui, J., Rojas, C., & Cook, J. et al. (2021). Masi: A mechanical ventilator based on a manual resuscitator with telemedicine capabilities for patients with ARDS during the COVID-19 crisis. Hardwarex, 9, e00187. doi: 10.1016/j.ohx.2021.e00187

Culbreth, R., & Gardenhire, D. (2021). Manual bag valve mask ventilation performance among respiratory therapists. Heart & Lung, 50(3), 471-475. doi: 10.1016/j.hrtlng.2020.10.012

Iyengar, K., Bahl, S., Raju Vaishya, & Vaish, A. (2020). Challenges and solutions in meeting up the urgent requirement of ventilators for COVID-19 patients. Diabetes & Metabolic Syndrome: Clinical Research & Reviews, 14(4), 499-501. doi: 10.1016/j.dsx.2020.04.048

Petsiuk, A., Tanikella, N., Dertinger, S., Pringle, A., Oberloier, S., & Pearce, J. (2020). Partially RepRapable automated open source bag valve mask-based ventilator. Hardwarex, 8, e00131. doi: 10.1016/j.ohx.2020.e00131

CHAPTER 10:

DEVELOPMENT OF AN ULTRAVIOLET C IRRADIATION DEVICE: INITIAL FINDINGS FOR THE TREATMENT OF SPIKED WHOLE BLOOD

Jonathan Oehley, Sudesh Sivarasu
ORCID ID: 0000-0002-7988-7673, 0000-0002-0812-568X
Division of Biomedical Engineering
Department of Human Biology
University of Cape Town
Western Cape
South Africa

Vernon Louw
ORCID ID: 0000-0002-2885-3342
Division of Clinical Haematology
Department of Medicine
Groote Schuur Hospital
University of Cape Town
Western Cape
South Africa

Lynthia Paul
ORCID ID: 0000-0002-5844-0637
Division of Medical Microbiology
Department of Pathology
University of Cape Town
Western Cape
South Africa

ABSTRACT

Sepsis is a life-threatening condition that occurs when the body's response to a source of infection is damaging to its own tissues. Sepsis is responsible for substantial health loss worldwide, particularly in sub- Saharan Africa. Increasing rates of antibiotic-resistant bacteria severely reduce the ability of physicians to treat the underlying infection that causes sepsis, especially when the infection is multidrug-resistant. Ultraviolet irradiation of the blood was historically used to treat infections.

This project explores this therapy as a novel treatment modality for multidrug-resistant sepsis through the development of a device to perform ultraviolet irradiation of the blood. This study reports on the initial findings of the in-vitro irradiation of bacterial-spiked, expired, whole blood with ultraviolet light. Spiked whole blood was exposed to ultraviolet light under different experimental conditions using a custom-made testing rig. The initial findings have suggested that the inactivation of bacteria in whole blood may be dependent on a variety of conditions. Further work is being done within this project to identify and quantify these conditions. These findings will then be utilised to guide further testing and development of the device design proposed in this project.

INTRODUCTION

Sepsis is a life-threatening condition that occurs when a host's dysregulated response to an infectious organism causes organ dysfunction (Singer et al., 2016). No sepsis-specific treatments currently exist beyond the use of antibiotics (Cohen et al., 2015). Antibiotic therapy is currently the key to reducing morbidity and mortality of sepsis (Thompson, Venkatesh, & Finfer, 2019). However, there is concern that the rate of antibiotic development may not be adequate to address the increasing levels of multidrug-resistant bacteria found in sepsis cases (Goldstein et al., 2019).

Antibiotic resistance has been associated with negative outcomes for patients with sepsis. Sepsis caused by multidrug-resistant bacteria is associated with higher mortality in patients (Capsoni et al., 2019). Additionally, patients with infections that are complicated by multidrug-resistance are more likely to have longer and more costly hospitalisations (Adams, Susi, & Nylund, 2019), highlighting a need for a novel treatment modality for multidrug-resistant sepsis.

Ultraviolet blood irradiation, where blood is exposed to ultraviolet C (UVC) light outside the body, was a therapy used to treat infections over 80 years ago (Hamblin, 2017) . During treatment, blood was withdrawn from the body, exposed extracorporeally to ultraviolet light, and then reinfused back into the patient. Multiple studies in this era reported the resolution or marked improvement of patients with sepsis under ultraviolet blood irradiation treatment (Miley & Christensen, 1947; Rebbeck, 1942, 1951).

The treatment of patients with multidrug-resistant sepsis is a complex problem. However, the effective treatment of spiked blood products could potentially indicate the suitability of a method as a treatment for multidrug-resistant sepsis. Thus, a device for the treatment of infected blood products is under development in this project to evaluate the suitability of UVC irradiation as a therapeutic modality for multidrug-resistant sepsis.
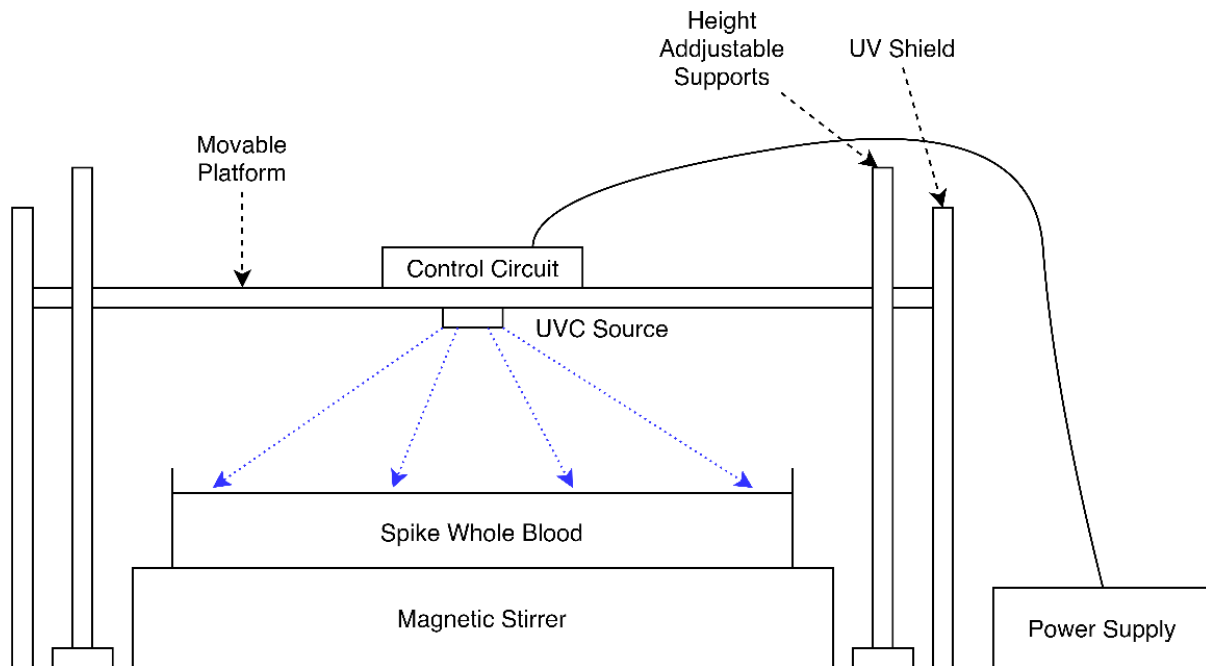
Figure 1: Experimental setup used during the irradiation experiments.

MATERIALS AND METHODS

Approvals from both the Human Research Ethics Committee (411/2021) and the Health Sciences Faculty Biosafety Committee (SS/001a/2021-2024) of the University of Cape Town were obtained before initiating the testing in this project.

i.   Material Sourcing and Preparation

Expired whole blood was obtained from the Western Cape Blood Services and stored between 2°C and 6°C at the Division of Medical Microbiology Laboratory, at the University of Cape Town. Trypticase soy agar (TSA, Biolab) was prepared according to the manufacturer's instructions. *Staphylococcus aureus* ATCC25923 was used to spike the whole blood. The *S. aureus* isolate was maintained on Brucella agar containing horse blood. For the experiments, the isolate was streaked on blood agar plates and incubated overnight (for 18 to 20 hours). Bacterial cells from the overnight colonies were resuspended in phosphate-buffered saline (PBS) to obtain a concentration of approximately 10^6 colony forming units per ml (CFU/ml).

ii.   Experimental Setup and Method

A testing rig (Figure 1) was developed to provide a UVC source for the irradiation experiments. The testing rig's platform was adjusted so that the UVC source was 20mm above the surface of the blood. During the experiments, the spiked blood was placed in a Petri dish and stirred on a magnetic stirrer. The experimental conditions for each of the conducted experiments are summarised in Table 1. For each test, samples were taken from the blood before irradiation, after irradiation (plated immediately) and at an additional sampling time after irradiation (Figure 2).

82

Experimental Condition	Experiment 1	Experiment 2	Experiment 3
Quantity of Blood Used	25ml	25ml	5ml
Magnetic Stirring	200rpm	200rpm	Off
Blood Age	55 days	61 days	67 days
Irradiation Duration	100 s	300 s	300 s
Approximate UVC Dose	20 mJ/cm^2	60 mJ/cm^2	60 mJ/cm^2
Additional Sampling Times	90, 180 seconds	30 mins	30 mins
Control Medium	-	PBS	Trypticase Soy Broth
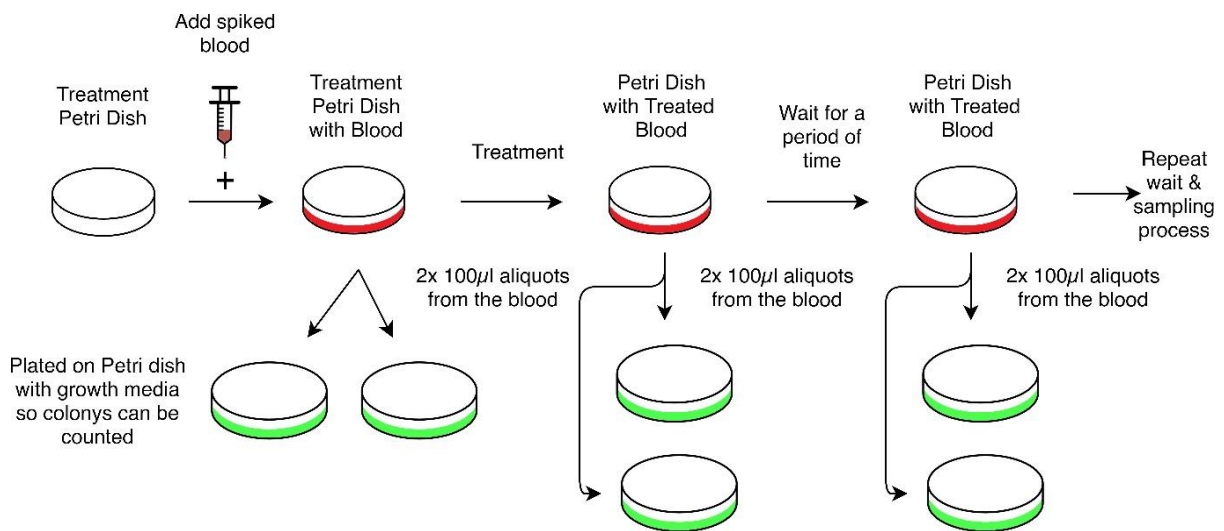
Figure 2: Flowchart of the experimental procedure.

When sampling the blood for measurement, aliquots were serially diluted in PBS and plated in duplicate technical repeats on TSA plates. The TSA plates were incubated at 37°C under aerobic conditions for 24 hours. Colony forming units were then manually counted and recorded. The final colony counts were determined by the average of plates with between 30 and 300 colonies for each sample.

RESULTS AND DISCUSSION

Firstly, these results are from a series of preliminary tests and are intended for internal testing of the methodology and equipment. Thus, any insights and conclusions should be considered preliminary pending further investigation. The blood samples in Experiment 3 were contaminated with other microbes and, thus, there were no quantitative results from Experiment 3. The results from the other two recorded experiments are presented in Figure 3.

Overall, the results in Figure 3 that there was no substantial reduction in the quantity of viable bacteria in the sample either after irradiation or after waiting for an additional delay post- irradiation as specified in Table 1.

Additionally, while the samples in Experiment 3 were contaminated and not counted, it was noted that there was not any discernible qualitative reduction in the quantity of colony growths on the plates. The trypticase soy broth control in Experiment 3 was not contaminated, but also showed no inactivation of bacteria. However, there was complete inactivation of bacteria in phosphate-buffered saline (PBS) control in Experiment 2.
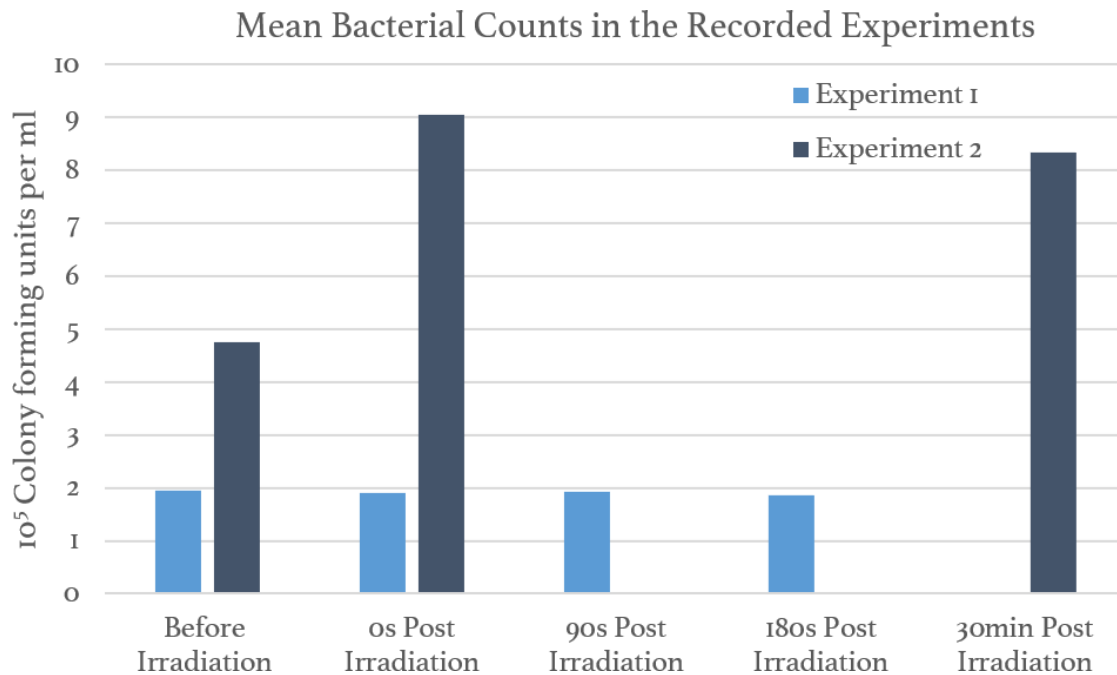
Figure 3: Mean bacterial counts in the whole blood samples at different time points during the experiments conducted in this study. Experiments 1 and 2 had different post-irradiation sampling times. The mean CFU/ml was determined by averaging the plates with between 30 and 300 colonies for each blood sample.

The inactivation of *S. aureus* has been demonstrated by other studies in various mediums under different conditions (Kim & Kang, 2018; Terpstra et al., 2008). The PBS control in Experiment 2 demonstrated the capability of the experimental setup to inactivate *S. aureus* under the conditions described in Table 1. Despite this, the bacteria were not inactivated in the whole blood samples or the trypticase soy broth control. This suggests that compounds in these mediums could be absorbing the UVC light and impacting the bactericidal effect of the UVC light.

One of the developers of the historic ultraviolet blood irradiation therapy reported the ability of UVC light to inactivate *S. aureus* in whole blood (Knott, 1948), and the therapy developed from his work was subsequently used to treat *S. aureus* infections (Rebbeck, 1942).

Therefore, the lack of inactivation seen so far in this project could be due to the combination of conditions used in these experiments. The experimental conditions which could be affecting the inactivation results are listed in Table 2.

Table 2: List of experimental conditions which could affect the inactivation of bacteria in whole blood

Key Conditions of Interest		Additional Conditions
UVC dose	UVC wavelength	Quantity of blood used
Age of blood	Quantity of bacteria	Duration for additional sampling
Container and blood flow characteristics during irradiation		Temperature of blood

The key conditions of interest all have a large potential to affect the experimental outcome. As it is hypothesised that ultraviolet blood irradiation produces some form of an immune-modulating effect (Boretti, Banik, & Castelletto, 2020), the age of the blood could make a significant difference to the results. This is because various cells of the blood break down over time which could change the immune response of the blood to the UVC radiation. While spiking the blood with high quantities of bacteria (10^6 CFU/ml) allows for a measurement of the log inactivation achieved by the device, clinically relevant levels of bacteria are much lower at 1-100 CFU/ml (Lamy, Dargère, Arendrup, Parienti, & Tattevin, 2016; Reimer, Wilson, & Weinstein, 1997). Thus, changing the quantity of bacteria used to spike the blood could also affect the results. Finally, the wavelength of UVC light, dose of UVC light, the container holding the blood, and the way the blood flows in the container could all affect how the light is absorbed by the blood and, thereby, the inactivation results. The ongoing work in this project will vary these conditions of interest to attempt to determine the conditions required to inactivate bacteria in whole blood.

CONCLUSION

The initial findings of this project have shown the ability of the experimental setup to inactivate *S. aureus* in phosphate-buffered saline in an initial test. However, the lack of bacterial inactivation in the blood samples suggests that the inactivation of bacteria in whole blood may be dependent on a variety of conditions. Further work is being done to identify the relevant conditions and then quantify the effect of these conditions. These findings will then be utilised to guide the further testing and development of the device design proposed in this project.

ACKNOWLEDGEMENTS

thank Prof. Jonny Peter, Dr Elizabeth Prentice, Dr Sean Wasserman, and the larger working group for the project from UCT and beyond who have assisted and advised during this project.

REFERENCES

Adams, D. J., Susi, A., & Nylund, C. M. (2019). Clinical characteristics, risk factors, and outcomes of patients hospitalized in the US military health system with carbapenem-resistant Enterobacteriaceae infection. *Am J Infect Control, 48(6), 644-649*. doi:10.1016/j.ajic.2019.10.006

Boretti, A., Banik, B., & Castelletto, S. (2020). Use of Ultraviolet Blood Irradiation Against Viral Infections. *Clinical Reviews in Allergy & Immunology*. doi:10.1007/s12016-020-08811-8

Capsoni, N., Bellone, P., Aliberti, S., Sotgiu, G., Pavanello, D., Visintin, B., . . . Brambilla, A. M. (2019). Prevalence, risk factors and outcomes of patients coming from the community with sepsis due to multidrug resistant bacteria. *Multidiscip Respir Med, 14(1)*. doi:10.1186/s40248-019-0185- 4

Cohen, J., Vincent, J.-L., Adhikari, N. K. J., Machado, F. R., Angus, D. C., Calandra, T., . . . Pelfrene, E. (2015). Sepsis: a roadmap for future research. *The Lancet Infectious Diseases, 15*(5), 581-614. doi:10.1016/S1473-3099(15)70112-X

Goldstein, E., MacFadden, D. R., Karaca, Z., Steiner, C. A., Viboud, C., & Lipsitch, M. (2019). Antimicrobial resistance prevalence, rates of hospitalization with septicemia and rates of mortality with sepsis in adults in different US states. *International journal of antimicrobial agents, 54*(1), 23-34. doi:10.1016/j.ijantimicag.2019.03.004

Hamblin, M. R. (2017). Ultraviolet Irradiation of Blood: "The Cure That Time Forgot"? *Advances in experimental medicine and biology, 996*, 295-309. doi:10.1007/978-3-319-56017-5_25

Kim, D.-K., & Kang, D.-H. (2018). UVC LED Irradiation Effectively Inactivates Aerosolized Viruses, Bacteria, and Fungi in a Chamber-Type Air Disinfection System. *Applied and Environmental Microbiology, 84*(17), e00944-00918. doi:10.1128/aem.00944-18

Knott, E. (1948). Development of ultraviolet blood irradiation. *The American Journal of Surgery, 76*(2), 165-171.

Lamy, B., Dargère, S., Arendrup, M. C., Parienti, J.-J., & Tattevin, P. (2016). How to Optimize the Use of Blood Cultures for the Diagnosis of Bloodstream

Infections? A State-of-the Art. *Frontiers in microbiology, 7.* doi:10.3389/fmicb.2016.00697

Miley, G., & Christensen, J. A. (1947). Ultraviolet blood irradiation therapy: Further studies in acute infections. *The American Journal of Surgery, 73*(4), 486-493. Rebbeck, E. (1942). Ultraviolet irradiation of autotransfused blood in the treatment of postabortional sepsis. *The American Journal of Surgery, 55*(3), 476-486.

Rebbeck, E. (1951). Further studies with ultraviolet blood irradiation therapy (Knott technic) in septic abortions. *The American Journal of Surgery, 82*(6), 736-740. Reimer, L. G., Wilson, M. L., & Weinstein, M. P. (1997). Update on detection of bacteremia and fungemia. *Clinical Microbiology Reviews, 10*(3), 444-465. doi:10.1128/cmr.10.3.444-465.1997

Singer, M., Deutschman, C. S., Seymour, C. W., Shankar-Hari, M., Annane, D., Bauer, M., . . . Angus, D. C. (2016). The Third International Consensus Definitions for Sepsis and Septic Shock (Sepsis-3). *Jama, 315*(8), 801-810. doi:10.1001/jama.2016.0287

Terpstra, F. G., van 't Wout, A. B., Schuitemaker, H., van Engelenburg, F. A., Dekkers, D. W., Verhaar, R., . . . Verhoeven, A. J. (2008). Potential and limitation of UVC irradiation for the inactivation of pathogens in platelet concentrates. *Transfusion, 48*(2), 304-313. doi:10.1111/j.1537- 2995.2007.01524.x

Thompson, K., Venkatesh, B., & Finfer, S. (2019). Sepsis and septic shock: current approaches to management. *Internal medicine journal, 49*(2), 160-170. doi:10.1111/imj.14199

CHAPTER 11:

THE USE OF HOLLOW FIBRE MEMBRANE DIALYSERS IN A LIQUID-LIQUID CONFIGURATION FOR RESPIRATORY SUPPORT

Izak Minnie, Stewart Gibson, Neil Stacey
ORCID ID: 0000-0003-0135-4479, 0000-0001-7254-1277, 0000-0003-4902-5201
School of Chemical and Metallurgical Engineering
University of the Witwatersrand
Johannesburg
South Africa

ABSTRACT

Conventional extracorporeal membrane oxygenation utilises a gas-to-liquid transfer regime to oxygenate blood from a stream of oxygen gas. This work serves as an exploratory study of the liquid-to-liquid transfer of dissolved gases, which may prove advantageous for general applications of ECMO as it allows for higher partial pressures of oxygen as well as the use of isotonic solutions as a means of improving patient haemostability. This concept is of particular interest to an ongoing project which has investigated the use of repurposed hollow fibre membrane dialysers as a means of providing emergency respiratory support using existing equipment. The liquid-liquid regime mass transfer properties of the hollow fibre membrane dialysers were investigated by determining the mass transfer coefficients of carbon dioxide and salt through the membrane as well as the sieving coefficient and leakage rate. Three cartridge types (high flux Braun, low flux Braun and Leoceed 21N) were investigated using a liquid-liquid configuration with carbonated or saline water used as a blood substitute in contact with distilled water. The high flux cartridge demonstrated a high leakage rate making it unsuitable for the proposed use. The two low flux cartridges demonstrated adequate carbon dioxide removal of 75.8% and 64.4% of the recommended 200ml/min for the Braun and Leoceed cartridges, respectively. All three cartridges displayed sieving coefficients close to one, indicating a high rate of salt transfer and subsequent need for solute balance in the final application. The results of this work showed a higher mass transfer coefficient for the liquid-liquid transfer regime compared to prior studies using a gas-liquid transfer regime. This result suggests that a liquid-liquid configuration is not just useful for emergency respiratory support but could outperform existing ECMO techniques. Further study into the use of liquid-liquid HFMD for respiratory support, using blood and conditions more representative of the final intended use, is warranted.

Keywords: Hollow Fibre Membrane Dialysers; Carbon Dioxide Mass Transfer Coefficient; Liquid-Liquid Mass Transfer; Gas-Liquid Mass Transfer; Salt Mass Transfer Coefficient; Leakage.

INTRODUCTION

The ongoing COVID-19 pandemic has resulted in considerable challenges regarding planning and resource management in the healthcare sector (Mirco et al., 2020). Specifically, the provision and application of respiratory support on a global scale has proven difficult (Lyons & Callaghan, 2020).

Respiration is the addition of oxygen to the circulatory system and concurrent removal of carbon dioxide. This gas exchange is important for most bodily functions and if it is not fully functional can lead to a variety of problems regarding hypoxemia or hypoxemia (insufficient or excessive oxygen levels) and hypocapnia or hypercapnia (insufficient or excessive carbon dioxide levels) (Fasano & Sequeira, 2017). Hypoxemia is of particular concern as it can result in cellular hypoxia, organ dysfunction, and death (Martin & Grocott, 2013) through the excessive production of inflammatory cytokines that further worsen lung injuries (Hojyo et al., 2020; Ragab et al., 2020). Hypercapnia can also worsen existing lung injuries through immunosuppression (Takahashi et al., 2018).

One respiratory problem of concern is acute respiratory distress syndrome (ARDS). ARDS is caused by fluid build-up in the alveoli, decreasing the amount of oxygen uptake and leading to hypoxemia (Mayo Clinic, 2020). Pre-COVID-19, ARDS was responsible for roughly 10% of ICU admissions in the United States of America and had a high mortality rate (Claar & Hyzy, 2017). With the onset of the pandemic, between 15% and 30% of COVID-19 patients developed ARDS leading to a substantial increase in hospital admissions and subsequent equipment shortages (Maclaren et al., 2020) as severe COVID-19 cases required ventilatory support (Dondorp et al., 2020).

Respiratory support can be provided using several methods such as high flow nasal oxygen (HFNO), endotracheal intubation, continuous positive airway pressure (CPAP), bilevel positive airway pressure (BiPAP), non-invasive ventilation (NIV), and equipment such as face masks, nasal cannula, hyper oxygenated oxygen chambers and mechanical ventilators (Gorman et al., 2021; Matthay et al., 2020; Pfeifer et al., 2020; H. Xu et al., 2011).

While the above-mentioned methods can provide respiratory support in many cases, there are certain situations or potential problems that could preclude their use. These include the uncertainty regarding increased risk of infection to healthcare workers when administering some treatments such as HFNO (Lyons & Callaghan, 2020; Pfeifer et al., 2020), lung injury caused by ventilators (Maclaren et al., 2020) such as barotrauma, atelectrauma, and oxytrauma (Dondorp et al., 2020), the toxicity of oxygen when breathed at high concentrations for an extended period of time (Martin & Grocott, 2013), high morbidity and mortality of invasive ventilation (Munshi & Hall, 2021), high failure rates of non-invasive ventilation for viral influenzas and

coronaviruses (Gorman et al., 2021), inefficiency in treating some respiratory diseases such as pneumoconiosis and pulmonary fibrosis (H. Xu et al., 2011) and mechanical ventilation causing hypercapnia (Takahashi et al., 2018).

EXTRACORPOREAL MEMBRANE OXYGENATION (ECMO)

In the case where a patient is not responding to conventional treatments, extracorporeal membrane oxygenation (ECMO) can be used to provide respiratory support (Pfeifer et al., 2020; Ramanathan et al., 2020). During the COVID-19 pandemic, ECMO has been recommended for severe cases as it has been shown to reduce mortality and improve quality of life (Maclaren et al., 2020; Matthay et al., 2020; Mishra et al., 2010; Ramanathan et al., 2020).

    i.   Workings of ECMO

ECMO acts as a cardiopulmonary bypass, where deoxygenated blood is removed, pumped through an artificial membrane lung where gas exchange occurs, and then returned (Maclaren et al., 2020). The most common ECMO membrane is a hollow fibre format polymethyl pentane (PMP) membrane that separates the blood from the gas stream, providing oxygen and removing carbon dioxide (Evseev et al., 2019; Yeager & Roy, 2017). While the primary function of the ECMO method is the oxygenation of blood, requiring a blood flow of 3-6L/min for acceptable oxygenation, in a low flow set-up, carbon dioxide removal can still be achieved (Gattinoni et al., 2019; Makdisi & Wang, 2015; Sidebotham et al., 2012). ECMO can be set up in two ways: veno-venous (VV) or veno-arterial (VA) differing in where the oxygenated blood is returned to the patient (Fasano & Sequeira, 2017). VV ECMO only provides support to lung function and is the more common application, while VA ECMO provides both lung and heart capabilities (Sidebotham et al., 2012). The gas transfer in ECMO is significantly affected by the blood flow through the equipment, additionally, oxygen transfer is determined by pre-membrane oxygen saturation and pre-membrane carbon dioxide levels while the carbon dioxide transfer is determined by the gas flow, haemoglobin levels, and pre-membrane carbon dioxide levels (Park et al., 2013).

    ii.   Limitations of ECMO

While ECMO is proven to be an effective form of respiratory support, it is resource-intensive, highly specialised, and expensive (Maclaren et al., 2020; Mishra et al., 2010). This, coupled with the planning and personnel training required, means that ECMO facilities are restricted to advanced care centres (Matthay et al., 2020; Ramanathan et al., 2020). The Extracorporeal Life Support Organization (ELSO), a global organisation focused on education, training, research, and management of extracorporeal life support, lists only South Africa and Egypt as registered ECMO centres on the African continent (ELSO, 2021). Due to its high resource use and limited availability, ECMO is only recommended for use in essential cases and when all traditional methods have been attempted (Shekar, 2022; Maclaren et al., 2020).

HOLLOW FIBER MEMBRANE DIALYSERS (HFMD)

In resource-poor environments where ECMO capabilities are not available, it has been proposed to use hollow fibre membrane dialysers for respiratory support as dialysis is a widely used technique, with existing clinical approval and a lower resource cost (Rubin, Stacey, Matambo, Vale, et al., 2020). Dialysers are used for haemodialysis therapy and continuous renal replacement therapy (CRRT) where they replace kidney function by filtering small and medium toxins and managing electrolyte and acid balances in the body (Tange & Yoshitake, 2019; ter Beek et al., 2020).

i.   Workings of HFMD

The workings of a dialyser and ECMO machine are similar as both use a hollow fibre design (Yeager & Roy, 2017) with a membrane to separate blood from the secondary exchange flow. The differences are in the membrane type, flow rate, and counter-current flow. HFMD commonly uses a polysulfone membrane that is more permeable than membranes used in ECMO as it is required to exchange not just gas but larger toxins and fluids as well (Tange & Yoshitake, 2019; ter Beek et al., 2020). Dialyser cartridges are also smaller than ECMO resulting in a lower blood flow which means a single cartridge set-up is not capable of providing full oxygenation of blood (Rubin, Stacey, Matambo, Vale, et al., 2020; Sidebotham et al., 2012). This smaller size and subsequently lower blood prime volume could be an advantage of HFMD cartridges as it avoids issues such as requiring blood transfusions that accompany the large priming volume of ECMO (Gimbel et al., 2016). Lastly, HFMD works with a liquid dialysate and not a gas stream as used in ECMO (Rubin, Stacey, Matambo, Vale, et al., 2020).

ii.   Blood oxygenation using HFMD

During the application of conventional dialysis, it has been found that the partial pressure of oxygen in the blood passing through the dialyser had increased (Tange & Yoshitake, 2019). Simulated dialysis using bovine blood has also shown that oxygenating the dialysate results in increased levels of blood oxygenation (Tange et al., 2012; Tange & Yoshitake, 2019). However, there is contradictory evidence on the effect of dialysate oxygenation on blood carbon dioxide levels (Tange et al., 2012; Tange & Yoshitake, 2019). A combination of membrane lung, hemodiafiltration, and acid addition has been shown to remove carbon dioxide from blood (Takahashi et al., 2018).

In terms of respiratory support, CRRT has been shown to improve oxygenation in paediatric patients with ARDS (Yang et al., 2016), and using a gas stream as in ECMO, oxygenation of blood has been achieved using HFMD (Rubin, Stacey, Matambo, Vale, et al., 2020). The latter has been proposed as a means of providing partial respiratory support to COVID-19 patients suffering from a respiratory deficit. It was found that a single HFMD cartridge, with 500ml/min flowing through it, would be capable of supplying as much as 15% of a patient's oxygenation requirements, thereby

potentially compensating for even a severe respiratory deficit with a setup that more closely resembles dialysis, an outpatient procedure, than a highly intensive medical intervention such as ECMO.

Oxygenation by a gas stream in HFMD cartridges appears to hold promise as an emergency measure and as a means of retaining reserve healthcare capacity for respiratory support, but also poses certain issues, including possible leakage due to the permeable nature of its membrane (L. Xu, 2020). This, coupled with the low blood flow rates and oxygen partial pressure limitations in pressurised gas and saturated water/dialysate, means HFMD is generally insufficient for full respiratory support. Furthermore, the gas configuration can lead to emboli. Although not particularly dangerous in the VV configuration, as emboli can be filtered when passed through the lung, emboli can cause serious harm in a VA configuration. It must be noted that emboli comprised of pure oxygen are likely to be far more easily absorbed into the bloodstream than air emboli comprised mainly of nitrogen, and therefore the risk of emboli in the VV configuration is reduced by the intrinsic properties of the method and, with proper handling and monitoring, is unlikely to be a severe threat. Nevertheless, it cannot be discounted entirely, nor can the possibility of membrane fouling be occurring as a result of foaming at the interface.

POTENTIAL ADVANTAGES OF A LIQUID-LIQUID CONFIGURATION FOR ECMO

The proposed novel approach to ECMO involves a highly oxygenated liquid stream to be brought into contact with the bloodstream to supply oxygen and remove carbon dioxide. Operationally, this approach could prevent the serum leakage associated with ECMO through one of two means. Firstly, if a hydrophobic oxygen-carrying liquid is used, then water and water-soluble blood components will not readily be transferred into the oxygen carrier stream. Secondly, if a hydrophilic or water-based oxygen carrier is used, then it can be formulated to be isotonic in nature, thereby eliminating the osmotic driving force for leakage and ion loss.

Another potential advantage of using a liquid oxygen carrier is that it could be oxygenated at pressures significantly exceeding atmospheric pressure, resulting in a supersaturated solution with an oxygen partial pressure greater than can be achieved in gas-liquid configurations, which are fundamentally limited by the need to keep trans-membrane pressure low to avoid mechanical stress on the membrane material.

The most promising candidates for liquid oxygen carriers are Perfluorocarbons and an aqueous solution of Hemopure®. Perfluorocarbons (PFCs) are a category of hydrophobic molecules comprised of Carbon and Fluorine atoms, with an ability to store and release copious amounts of oxygen (Carroll, 2021; Jägers et al., 2020; Tawfic & Kausalya, 2011). PFCs have an oxygen capacity 40 times larger than water and twice that of blood (201 ml_{O2}/L_{Blood} (Pittman, 2011)) and an even larger carbon dioxide capacity (Jägers et al., 2020).

Hemopure® is an aqueous solution containing bovine-derived hemoglobin, able to absorb oxygen in the same manner as blood does. Each of these candidates have advantages and disadvantages. For Hemopure®, it is not possible to usefully elevate the partial pressure of oxygen above atmospheric pressure. This is because Hemopure® follows a similar oxygen-dissociation curve to that which characterises blood, and for which the capacity to absorb oxygen plateaus at higher partial pressures as the active sites on the haemoglobin become saturated. Perfluorocarbons, by contrast, exhibit a Raoult's Law behaviour where there is a strong linear relationship between oxygen partial pressure and dissolved oxygen content, thereby allowing for super-saturation beyond partial pressures of one atm. Hemopure®, on the other hand, is advantageous because it is an aqueous solution and thus lends itself to the addition of other solutes for the benefit of patient stability.

However, the current study is a preliminary investigation of membrane gas transfer in the liquid-liquid configuration and therefore selecting an optimal oxygen carrier is outside the scope of work undertaken at this stage. Further, the operational and ethical requirements of experimentation with blood are more onerous than appropriate for an initial pilot study. The principal area of concern in this study is whether gas transfer takes place in the liquid-liquid configuration, or whether the gas transfer is obstructed by liquid filling of pores. Hence, the primary goal is to estimate a mass transfer coefficient for a convenient respiratory gas, to determine whether it is comparable to the mass transfer coefficient for the same gas in the gas-liquid configuration. For reasons of convenience, carbon dioxide is chosen as the studied gas, and water is used as the solvent. This results in an inexpensive experimental setup with minimal operational obstacles, which is therefore easily reproducible for corroboration or new testing with alternative membrane materials.

METHODS AND MATERIALS

i. Experimental set-up

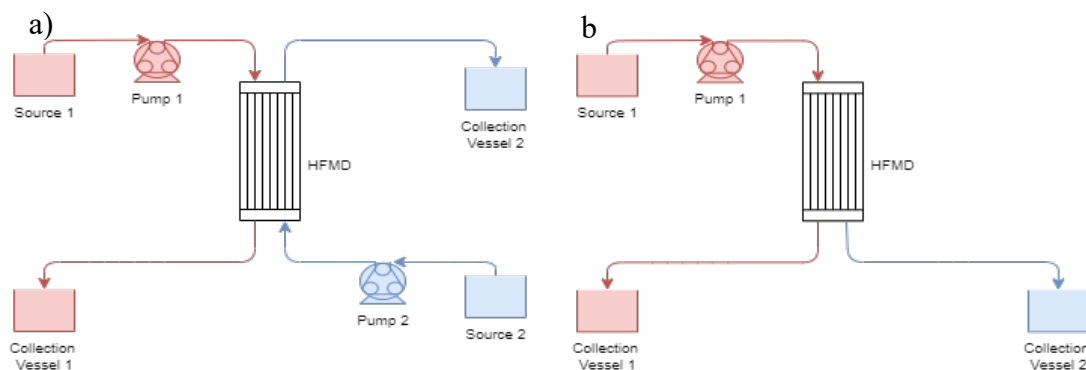The basic experimental set-up can be seen below in Figure 1.

Figure 1: Experimental set-up of hollow fibre membrane dialyser (HFMD) with a) two liquid loops, loop 1 (red) and loop 2 (blue) running through shell and tube respectively or b) one loop (red) running through the shell or tube while the other is open to the atmosphere.

As seen in Figure 1a, the set-up uses two pumps: the tube-side pump in the red circuit runs at around 500ml/min and the shell-side pump in the blue circuit runs at around 1000ml/min. Unfortunately, due to equipment constraints, flow control of the pumps was limited, especially with the fish pump used on the shell side. Three HFMD cartridges were considered, the details of which can be seen in Table 1.

Table 1: HFMD cartridge details

Brand	Braun Diacap	Braun Diacap	Leoceed 21 N
Cartridge type	High Flux (B Braun, 2009)	Low Flux (B Braun, 2009)	Low Flux (Asahi Kasei Medical, 2012)
Priming Volume (ml)	90	58	108
Polysulfone Membrane Effective Surface Area (m^2)	1.5	1	2.1
Internal Fiber Diameter (μm)	200	200	185
Wall Thickness (μm)	40	40	35
Manufacturer's Specified Blood Flowrate Range (ml/min)	200 – 500	200 – 500	200 - 400
Maximum Transmembrane Pressure (kPa)	80	80	80

The liquid and conditions used in each loop were varied based on the experimental parameters required.

ii.   Liquid-Liquid carbon dioxide mass transfer coefficients

Carbon dioxide is an important gas that needs monitoring during oxygen therapy. The normal partial pressure of carbon dioxide in arterial blood is between 35- and 45- millimetres of mercury (Messina & Patrick, 2021). As mentioned, high (greater than 45mmHg) and low (less than 35mmHg) levels of carbon dioxide can have severe effects on the body (hypercapnia and hypocapnia). Therefore, the mass transfer of carbon dioxide in a HFMD is important as it will determine whether the use of HFMD for oxygen therapy is viable or not.

To evaluate the mass transfer coefficients of carbon dioxide across the HFMD membrane, carbonated distilled water (pH 3.9 – 4.2) was run through the red loop while distilled water was run through the blue loop (Figure 1a). After a priming period, the carbon dioxide content at each inlet and outlet of the HFMD cartridge was determined using a pH meter along with the Acid-Base equations below.

o   Acid-Base equilibria

Seventy per cent of carbon dioxide is transported through an acid-base, catalysed interconversion between carbonic acid (H2CO3), bicarbonate (HCO3-), and

94

hydrogen (H+) ions [14]. The acid-base equation can be given below with the equilibrium constant, K, given by (Boyd, 2015):

$$CO_2 + H_2O \leftrightharpoons H^+ + HCO_3^-$$ K = 10^-6.35

Reaction 1

The equilibrium expression of the reaction above can thus be written as follows:

$$K = \frac{[H^+][HCO_3^-]}{[CO_2(aq)]} = \frac{[H^+]^2}{[CO_2(aq)]} = 10^{-6.35} \tag{1}$$

and as pH is defined as:

$$pH = -\log[H^+] \tag{2}$$

The pH of water can be used to determine the dissolved carbon dioxide concentration.

o   Fick's Law

The mass transfer coefficient of both gases through the membrane can be modelled using the following equation:

$$k_o A = \frac{q_{gas}}{LM\Delta p_{gas}} \tag{3}$$

where:

k_o = mass transfer coefficient (mg/ (min kPa m^2))

A = membrane area (m^2)

q_{gas} = rate of gas transfer (mg/min)

$LM\Delta p_{gas}$ = logarithmic mean of partial pressure differences at the top and bottom of the cartridge (kPa) calculated as follows:

$$LM\Delta p_{gas} = \frac{\Delta p_{gas}^{top} - \Delta p_{gas}^{bottom}}{\ln(\frac{\Delta p_{gas}^{top}}{\Delta p_{gas}^{bottom}})} \tag{4}$$

The partial pressures for both gases in water can be calculated using Henry's law:

$$p_{gas} = \frac{[gas]}{K_H} \tag{5}$$

with K_H values of 1.3×10^{-5} and 3.4×10^{-4} mol/(m^{3}Pa) for oxygen and carbon dioxide, respectively.

iii.   Liquid-liquid salt mass transfer coefficient

Since the primary use of HFMDs is to remove toxins from the blood (Khandpur, 2020), special attention needs to be paid to the transfer of electrolytes when using the membrane for respiratory support. A significant drop in a patient's electrolyte level,

known as hyponatremia, may cause headaches, dizziness and, in severe cases, lack of consciousness. It is imperative to consider this as it will justify the need for an electrolyte support solution if there is excessive ion loss from the blood to the dialysate. To evaluate the mass transfer coefficients of NaCl across the HFMD membrane, salt was dissolved in distilled water (6 – 12g/L) and run through the red loop while distilled water was run through the blue loop (Figure 1a). At each inlet and outlet of the HFMD cartridge, the salt content was determined using an EC/TDS meter.

The salt mass transfer coefficient can be determined through a minor adjustment to Equation 3 by determining the log mean concentration instead of the log mean pressure.

iv.   Sieving coefficient

The sieving coefficient is the measure of the equilibration of a substance through a semipermeable membrane (Kashani et al., 2012). Simply put, the sieving coefficient is the measure of how easily a substance passes from the blood plasma to the filtrate in a HFMD. The sieve coefficient equation is given by the following equation (Neri et al., 2016):

$$SC = \frac{C_{filtrate}}{C_{plasma}} \qquad (6)$$

where:

SC = sieving coefficient
$C_{filtrate}$ = concentration of solute in the filtrate that passed through the membrane
C_{plasma} = average concentration of the solute in the plasma

A sieving coefficient of one indicates that the substance equilibrates on both sides of the membrane and a sieving coefficient of zero indicates that the substance does not cross the membrane at all.

To determine the sieving coefficient, a salt solution as prepared by dissolving table salt (NaCl) in distilled water (10g/L). This water was run through the hollow fibers of the cartridge in a closed-loop configuration with no opposing gas or liquid flow (Figure 1b). After allowing time for priming of the system, the leakage was collected from the shell-side of the cartridge. Using an EC/TDS meter, the total dissolved solids and electrical conductivity of the reservoir and collected leakage were determined.

v. Leakage tests

Hollow fibre membrane dialysers are specifically designed for the transfer of toxins from the blood to the dialysate through the mixing of fluids (Khandpur, 2020). However, during this mixing, some of the blood remains in the dialysate and vice versa, this is known as leakage. Leakage is synonymous with bleeding as blood is lost from the body. If too much blood is lost, the body goes into hypovolemic shock, which impedes the heart's ability to pump sufficient blood (Machalinski, n.d.). As a result, tissues do not receive enough oxygen, leading to tissue damage.

To evaluate the leakage of fluid from one side of the membrane to the other, the two loops were run in three configurations for each cartridge:

- o Distilled water was run through the inside of the hollow fibres with no opposing gas or liquid flow in the cartridge shell. Any water that leaked through the fibres was collected and a tube-side leakage rate was determined (Figure 1b).
- o Distilled water was run through the cartridge shell with no opposing liquid or gas flow inside the hollow fibres. Any water that leaked through the fibres was collected and a shell-side leakage rate was determined (Figure 1b).
- o Both loops were filled with distilled water and ran in a closed-loop configuration. The drop in the tube-side reservoir was used to determine the net liquid exchange rate between the two streams.

RESULTS AND DISCUSSION

The results are presented with outliers removed based on the IQR method. Most of the outliers removed had flowrates significantly different to the average of the run and this is likely the cause of their outlying values. Results are reported to be ± 1 standard deviation.

i. Liquid-Liquid mass transfer coefficients
o Carbon dioxide mass transfer coefficient

The rate of carbon dioxide removal in HFMD depends on membrane area, pore size, and pore material. It was found that membrane fibres with small pores and hydrophobic construction are better suited for carbon dioxide absorption (Sumin et al., 2010). All three cartridges, Braun Low Flux, Braun High Flux, and Leoceed21N, comprise of a polysulfone membrane, which has a hydrophobic nature (Espinoza-Gómez & Lin, 2003). Therefore, it is expected that the two low flux cartridges have higher carbon dioxide mass transfer coefficients than the high flux cartridge. Additionally, one would expect the mass transfer for a species across the membrane to be constant as the membrane area, pore size and pore material should be constant. The carbon dioxide mass transfer coefficients as a function of initial carbonated source pH are shown in Figure 2.
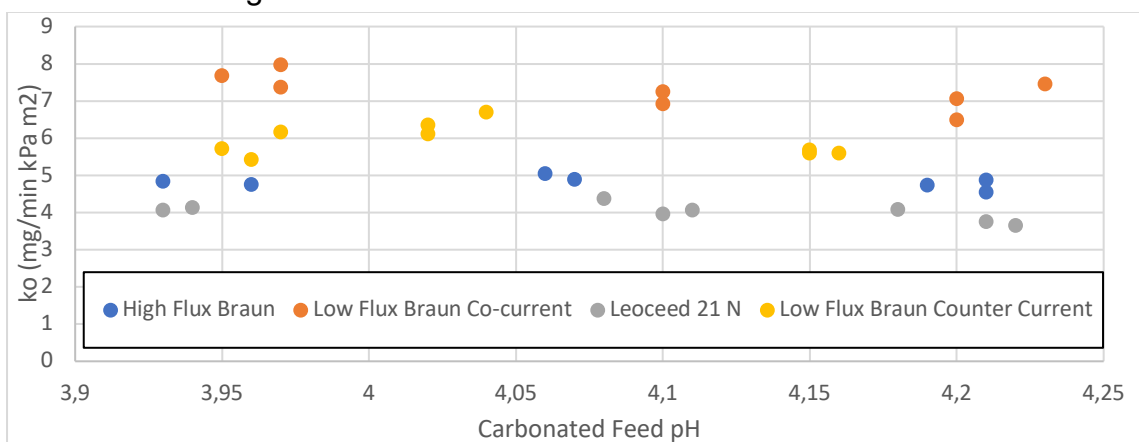

Figure 2: Carbon dioxide mass transfer coefficient variations with changing initial pH.

97

The low flux Braun cartridge in the co-current configuration resulted in the highest mass transfer coefficient, while the Leoceed 21N resulted in the lowest. A summary of the average mass transfer coefficients for each cartridge can be seen in Table 2.

Table 2: Mass transfer coefficient data

		Braun High Flux	Braun Low Flux Co-current	Braun Low Flux Counter-current	Leoceed 21N
Mass transfer coefficient (mg/min kPa m^2)	Tube-side	5.19 ± 0.38	8.61 ± 0.71	5.78 ± 0.46	4.50 ± 0.22
	Shell-side	4.43 ± 0.38	5.93 ± 0.69	5.93 ± 0.70	3.52 ± 0.35
	Average	4.81 ± 0.15	7.27 ± 0.43	5.92 ± 0.40	4.01 ± 0.21
Pearson correlation coefficient between pH and mass transfer coefficient		-0.33	-0.64	-0.24	-0.56

The difference in the mass transfer coefficient seen between the shell- and tube-side data is due to a mass balance inequality where the mass of carbon dioxide lost from the tube-side is higher than the mass gained by the shell-side. This discrepancy is most likely due to two systematic errors. Firstly, the measurements made were discrete and not continuous which made it difficult to see whether equilibrium had been reached when the measurement was taken. This implies that equilibrium had not yet been reached and that some of the missing carbon dioxide had been adsorbed onto the membrane. Secondly, the time between collection and pH measurements of the liquid discharge on both sides, coupled with insufficient equipment to fully cover the collection vessels, resulted in the off gassing of carbon dioxide on both sides. This off-gassing would increase the pH measurement indicating that the tube-side lost more carbon dioxide than in reality and, simultaneously, that the shell-side gained less carbon dioxide. Due to these reasons, the average mass transfer coefficient is considered the most reliable.

The Pearson correlation coefficient shows a slight negative correlation between pH and mass transfer coefficient across all cartridges, with the effect being most pronounced in low flux co-current set-ups. This is a surprising result as we expect the coefficient to remain constant regardless of initial concentration. However, this result must be investigated further as it is derived from a limited set of data points (n = 7 – 9) for each cartridge and could be a result of flowrate variations that can influence the mass transfer coefficient as found by Lan Xu (L. Xu, 2020).
- o Carbon dioxide removal

While the carbon dioxide mass transfer coefficient data is a valuable piece of information regarding the use of HFMD in gas transfer applications for use in a clinical setting, the much more relevant information is the rate of carbon dioxide removal as that will dictate whether the device can prevent hypercapnia in patients requiring respiratory support.

Using ECMO as a basis for comparison, membrane oxygenators aim to remove 200ml CO_2/min for an average adult (Baker & Low, 2015). The carbon dioxide removal rate found in this project can be seen in Figure 3. The graph illustrates that all four configurations display exponential relationships between carbon dioxide removal and pH. The equations and R^2 values of each cartridge can be seen in Table 3.

Table 3: Trendline data for carbon dioxide removal

Configuration	Exponential Relationship	R^2
Low Flux Braun Counter-current	$y = 7E+09e^{-4.37x}$	0.9221
Low Flux Braun Co-current	$y = 3E+10e^{-4.804x}$	0.9833
Leoceed 21N	$y = 7E+09e^{-4.412x}$	0.9957
High Flux Braun	$y = 3E+09e^{-4.241x}$	0.9825

Figure 3: Carbon dioxide removal rate as a function of inlet pH
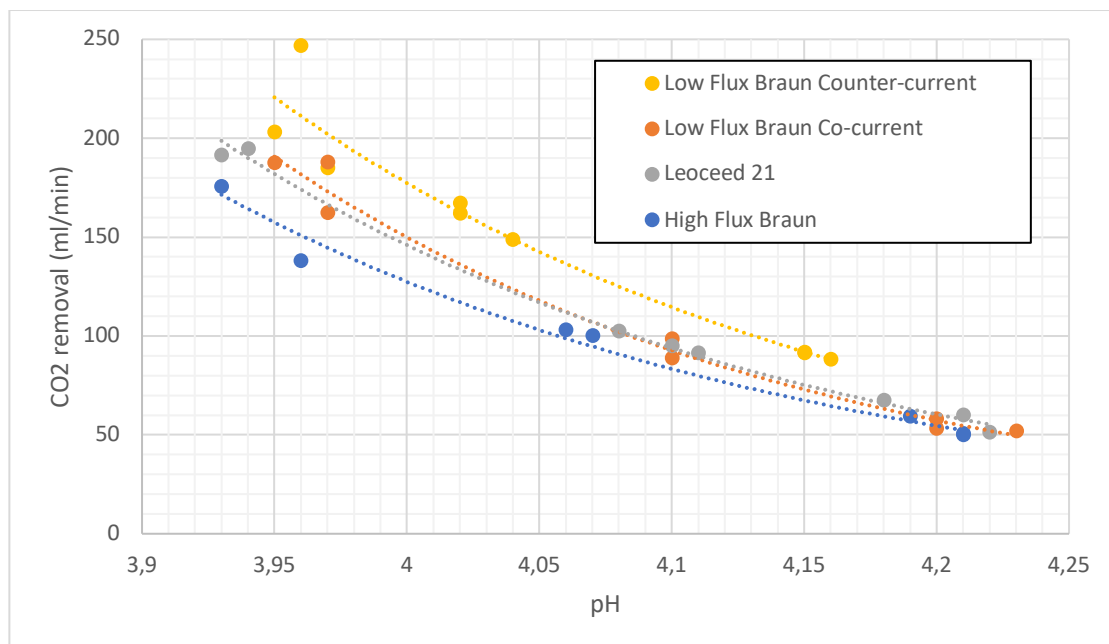
At low pH values (3.95) the HFMD cartridges come close to fulfilling the carbon dioxide removal requirements with >75% removal in all cases. However, it decreases to only around 33% at higher pH values (4.2).

The carbon dioxide partial pressure in venous blood is 6.1kPa (Arthurs & Sudhakar, 2005), using equations 1, (2, and (5 this corresponds to a pH of 4.52. This

is a much higher pH than the range considered during experimentation, and due to the differences between blood and water, a direct comparison is not entirely valid, but it can serve as a broad indication of the expected performance of the HFMD cartridge in a clinical setting. Using the relationships presented in Table 4, the percentage of required carbon dioxide removal achieved by each cartridge can be seen below.

Table 4: Percentage of ideal carbon dioxide removal achieved at a pH of 4.52

Configuration	CO_2 removed (ml/min)	Percentage
Low Flux Braun Counter-current	18.48	9.2%
Low Flux Braun Co-current	11.14	5.6%
Leoceed 21N	15.29	7.6%
High Flux Braun	14.19	7.1%

Based on the carbon dioxide removal results presented, multiple HFMD cartridges would be required to achieve even partial respiratory support.

o   Comparison to Liquid-Gas configuration

The work presented is a variation of work done by Lan Xu in 2020, where the carbon dioxide mass transfer coefficient and carbon dioxide removal of HFMD cartridges was investigated using a liquid-gas configuration (L. Xu, 2020). The work done by Xu focussed on the Low Flux Braun and Leoceed 21N cartridges run at a pH of 4 with varying flow rates. A comparison between the results of that study and the present work is presented in Table 5, calculated from trendline data based on a pH of 4 and flowrate of 500ml/min.

Table 5: Comparison between liquid-liquid and liquid-gas HFMD carbon dioxide transport

		Lan Xu (L. Xu, 2020)	This work
Low Flux Braun	Mass transfer coefficient (mg/min kPa m^2)	3.632	5.92
	CO_2 Removal (ml/min)	51.83	179.32
Leoceed 21N	Mass transfer coefficient (mg/min kPa m^2)	2.086	4.01
	CO_2 Removal (ml/min)	68.12	151.59

The difference in the Leoceed21N results may be due to the configuration. This paper investigated co-current flow, whereas Xu (L. Xu, 2020) investigated counter-current flows, indicating that co-current flow has a higher leakage rate than counter-current flow. However, the difference is also due to the difference in exchange medium. This can be further confirmed by comparing the low flux Braun counter-current mass transfer coefficients, indicating that liquid-liquid exchange has a higher mass transfer than gas-liquid exchange.

This increase in carbon dioxide transfer as well as the presence of a suitable medium to prevent or balance solute losses as explained in subsequent sections means the liquid-liquid configuration is preferred for the application of emergency HFMD respiratory support. The improvements in performance shown by a liquid-liquid configuration also have significant implications for the ECMO field as current ECMO techniques implement a gas-liquid configuration. Thus, patients using ECMO can experience better respiratory support, by simply replacing the gas stream with an oxygen-carrying support fluid. Fluids with high oxygen-carrying abilities, such as perfluorocarbons and Hemopure® solutions, can be used.

o   Salt mass transfer coefficient

The results for the salt mass transfer coefficient were handled in an equivalent way to the carbon dioxide results, with the exception that the results presented were based solely on the tube-side mass transfer and not the average. This was done as membrane adsorption and lack of time to equilibrate caused large deviations in the shell-side results.
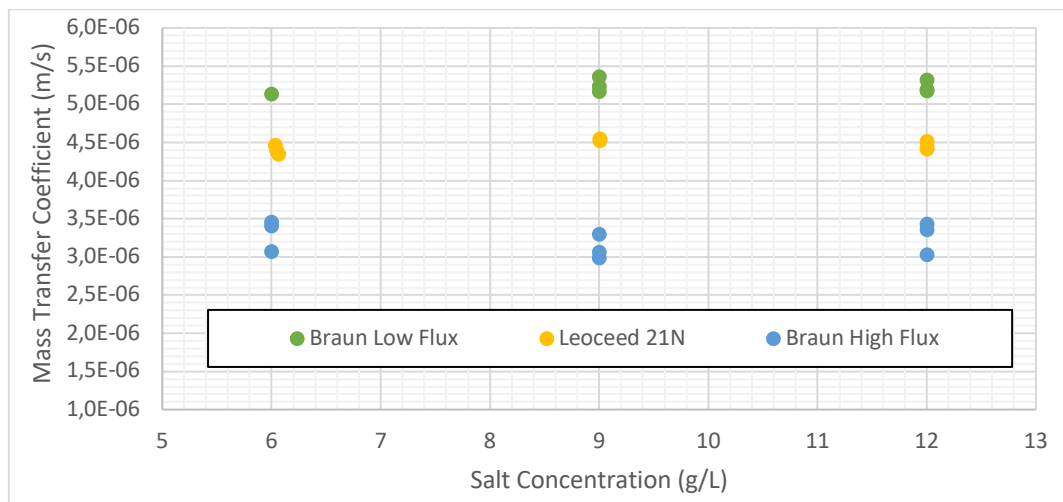

Figure 4: Variation of salt mass transfer coefficient with initial salt concentration

Figure 4 displays the salt mass transfer coefficient against the initial tube-side salt concentration. Table 6 gives the average coefficient as well as the Pearson

correlation for each cartridge. The high flux cartridge mass transfer is virtually independent of initial salt concentration while the low flux cartridges show a slightly positive correlation.

Table 6: Mass transfer data for NaCl

	Braun High Flux	Braun Low Flux	Leoceed 21N
Mass transfer coefficient (m/s)	3.2E-06 ± 1.8E-0.7	5.2E-06 ± 7.6E-08	4.5E-06 ± 6.5E-08
Pearson correlation coefficient	-0.05	0.26	0.36

During the use of the HFMD cartridge for respiratory support, consideration must be given to the blood composition as well as the gas transfer. The salt mass transfer coefficients determined above can give an indication of the requirements for clinicians to balance the solutes of interest as is done in regular dialysis.

ii. Leakage tests

The first leakage test was to determine the amount of leakage from the inside of the fibres out to the cartridge shell. The results can be seen in Table 7.

Table 7: Tube Side Leakage Data

Run	Braun High Flux			Braun Low Flux			Leoceed 21N		
	Volume (ml)	Time (s)	Flowrate (mL/min)	Volume (ml)	Time (min)	Flowrate (mL/min)	Volume (ml)	Time (min)	Flowrate (mL/min)
1	100	58.83	101.99	50	10.03	4.98	50	5.14	9.73
2	100	58.95	101.78	50	10.05	4.98	50	5.17	9.68
3	100	58.32	102.88	50	10.02	4.99	50	5.13	9.75
4	100	58.84	101.97	-	-	-	-	-	-
5	100	57.85	103.72	-	-	-	-	-	-
Average (mL/ min)	102.47 ± 0.73			4.98 ± 0.01			9.72 ± 0.03		

The second leakage test determined the leakage rate from the cartridge shell into the fibres. From this test, only the Leoceed 21N showed any leakage with a leakage rate of 6.10 ± 0.63mL/min across three runs.

The third leakage test determined the net leakage experienced by the tube-side during operation. The results can be seen in Table 8.

Table 8: Net Leakage Rate Data

| Run | Braun High Flux | | | Braun Low Flux | | | Leoceed 21N | | |
	Volume (ml)	Time (min)	Flowrate (mL/min)	Volume (ml)	Time (min)	Flowrate (mL/min)	Volume (ml)	Time (min)	Flowrate (mL/min)
1	400	2.35	170.21	16.67	10.13	1.65	50	4.67	10.71
2	400	2.38	168.15	16.67	6.77	2.46	50	4.64	10.78
3	400	2.43	164.37	16.67	7.73	2.16	50	4.66	10.72
4	400	2.42	165.53	-	-	-	-	-	-
Average (mL/min)	167.06 ± 2.27			2.09 ± 0.34			10.74 ± 0.03		

Apart from the Braun low flux cartridge, the net leakage across the membrane increased with the introduction of the shell-side liquid stream. This increase is likely due to a higher transmembrane pressure caused by the flow of the second stream, forcing more fluid through the membrane.

On average, human blood volume is 75ml/kg (Nadler et al., 1962), resulting in an average blood volume of 5 250ml for a 70kg human male. While side effects start appearing at around 15% blood loss, significant effects appear above 30%, and, above 40%, there is a substantial risk for organ failure, coma, and death (Johnson & Burns, 2021). With a net leakage rate of 167.06ml/min, this 40% threshold would be reached in around 12,5min. This makes the high flux cartridge unsuitable for use as a respiratory support device. The lower leakage rates of the other cartridges could be compensated for by blood or other fluid transfusions.

The high leakage rate of the high flux cartridge is likely due to its higher permeability to allow for larger molecules such as β2-microglobulin to pass through the membrane (Donadio et al., 2017). The leakage through all three cartridges could also be attributed to the differences between the water used in this work and the blood used in the usual dialysis procedure. The use of inadequate pumps with limited control could also have contributed as the flow rates and pressures could not be easily controlled. To fully assess the leakage risk, more sophisticated pumps, along with more representative fluids, will have to be employed. However, this study shows that high flux cartridges are not acceptable for use in a clinical setting.

iii. Sieving Coefficient

The results of the sieving coefficient can be seen in Table 9.

Table 9: Sieving Coefficient Data

	Braun High Flux	Braun Low Flux	Leoceed 21N
Initial Salt concentration (g/L)	10.00	10.00	10.00
Leakage Flowrate (ml/min)	76.22 ± 1.75	4.72 ± 0.06	8.41 ± 0.57
Sieve Coefficient	0.992 ± 0.002	0.967 ± 0.003	0.977 ± 0.002

With a sieving coefficient close to one, all three cartridges display a nearly unrestricted transport of Na^+ and Cl^- across the membrane. This is as expected as these ions are small molecules (MW<500 Da) that can pass through both low and high flux membranes (Donadio et al., 2017). The high flux cartridge has the highest sieving coefficient due to its increased porosity and reliance on convective transport to allow for the removal of larger molecules (MW>500 Da) in addition to small molecules (Donadio et al., 2017).

If the HFMD is to be used for respiratory support in a liquid-liquid configuration, these molecules, and others like it, will have to be balanced by a physician. As mentioned, this is another advantage of the liquid-liquid configuration when compared to the liquid-gas configuration where a balancing medium is absent (L. Xu, 2020).

CONCLUSION AND RECOMMENDATIONS

The global COVID-19 pandemic has shown the need for and importance of proper planning and resource management of healthcare resources. In this study, we have shown qualitatively that HFMD cartridges can remove carbon dioxide when using carbonated water in a liquid-liquid configuration. The use of high flux cartridges is not recommended as it has severe leakage effects that will require significant intervention to prevent harm to the patient. The remaining two cartridges were both able to achieve a substantial portion of the recommended carbon dioxide removal rate of 200ml/min. The Braun low flux performed the best with 75.8% removal, while the Leoceed 21N removed 64.4% of the required amount. These results are more than twice that found in previous research using a liquid-gas configuration under the same conditions of flowrate and pH. This not only proves that liquid-liquid HFMD should be considered for respiratory support but that the liquid-liquid configuration should be investigated as a possible improvement in the established ECMO field. Additionally, all cartridges were found to easily transport salt ions, confirming that a clinician will have to monitor and balance the blood solutes to prevent harm to the patient, as is done in conventional dialysis.

The main outcome of the study is confirmation that gas transfer does take place in the liquid-liquid configuration, with the unexpected finding that the transfer of CO_2 is more rapid in the liquid-liquid configuration. This result is of great potential interest to the general operation of ECMO, but it is not certain to extend to the transfer of oxygen. It is also uncertain if the results are applicable when blood and an oxygen carrier are used as the two liquid streams.

Therefore, the findings here serve mainly as an indication that further research is merited to investigate the feasibility of liquid-liquid ECMO:

- o The liquid-liquid oxygen transfer characteristics should be evaluated in parallel with the carbon dioxide transfer data to gain a more comprehensive understanding of the potential for respiratory support. This was not possible in the presented research due to a lack of oxygen measurement equipment as well as the liquid medium used not being suitable for measurement due to the low solubility of oxygen in water.
- o The flowrate control on both sides of the cartridge must be improved to eliminate its variance and thus improve the conclusions that can be drawn from other relationships.
- o The experiments must be repeated using more representative liquids such as blood, Hemopure® solutions, and/or PFCs to get quantitative results for clinical use.

ACKNOWLEDGMENTS

CONFLICTS OF INTEREST

The authors have no conflicts of interest to declare.

FUNDING

ETHICAL APPROVAL

Consent statement/Ethical approval: Not required.

REFERENCES

Arthurs, G., & Sudhakar, M. (2005). Carbon dioxide transport. *Continuing Education in Anaesthesia Critical Care & Pain*, 5(6), 207–210. doi: 10.1093/BJACEACCP/MKI050

Asahi Kasei Medical. (2012). Leoceed series | Asahi Kasei Medical Co., Ltd. Retrieved 1 December 2020, from http://www.gml-dialyza.cz/downloads/products/Leoceed.pdf

Braun, B. (2021). Product Range of Dialysis disposables. Retrieved 29 September 2020, from https://avitum.com.pl/_files/ulotki_oferta_handlowa/materialy-do-dializy.pdf

Baker, R. W., & Low, B. T. (2015). Membrane Separation. *Reference Module in Chemistry, Molecular Sciences and Chemical Engineering*. doi: 10.1016/B978-0-12-409547-2.11674-9

Boyd, C. E. (2015). pH, Carbon Dioxide, and Alkalinity. In *Water Quality* (pp. 153–178). Springer, Cham. doi: 10.1007/978-3-319-17446-4_8

Carroll, D. (2021). A breath of fresh perfluorocarbon. Retrieved 16 November 2021, from https://engineering.cmu.edu/news-events/news/2017/11/20-nelson-perfluorocarbon.html

Claar, D. D., & Hyzy, R. C. (2017). Refractory Hypoxemia and Acute Respiratory Distress Syndrome Adjunctive Therapies: An Open Question? *Annals of the American Thoracic Society*, *14*(12), 1768–1769. doi: 10.1513/ANNALSATS.201707-547ED

Donadio, C., Kanaki, A., Sami, N., & Tognotti, D. (2017). High-Flux Dialysis: Clinical, Biochemical, and Proteomic Comparison with Low-Flux Dialysis and On-Line Hemodiafiltration. *Blood Purification*, *44*(2), 129–139. doi: 10.1159/000476053

Dondorp, A. M., Hayat, M., Aryal, D., Beane, A., & Schultz, M. J. (2020). Respiratory Support in COVID-19 Patients, with a Focus on Resource-Limited Settings. *The American Journal of Tropical Medicine and Hygiene*, *102*(6), 1191. doi: 10.4269/AJTMH.20-0283

Shekar, K. (2022). Extracorporeal Life Support Organisation COVID-19 Interim Guidelines [Ebook]. Elso. Retrieved from https://www.elso.org/Portals/0/Files/pdf/ELSO%20covid%20guidelines%20final.pdf

ELSO. (2021). ELSO Center Directory | Extracorporeal Membrane Oxygenation | ECLS. Retrieved 7 November 2021, from https://www.elso.org/Membership/CenterDirectory.aspx. Retrieved: 1 April 2022

Espinoza-Gómez, H., & Lin, S. W. (2003). Development of Hydrophilic Ultrafiltration Membrane from Polysulfone-Polyvinylpyrrolidone. *Revista de La*

Sociedad Química de México, 47(1), 53–57. http://www.scielo.org.mx/scielo.php?script=sci_arttext&pid=S0583-76932003000100008&lng=es&nrm=iso&tlng=en

Evseev, A. K., Zhuravel, S. V., Alentiev, A. Y., Goroncharovskaya, I. V., & Petrikov, S. S. (2019). Membranes in Extracorporeal Blood Oxygenation Technology. *Membranes and Membrane Technologies, 1*(4), 201–211. doi: 10.1134/s2517751619040024

Fasano, A., & Sequeira, A. (2017). Extracorporeal Blood Oxygenation. *Modeling, Simulation and Applications, 18*, 205–226. doi: 10.1007/978-3-319-60513-5_5

Gattinoni, L., Vassalli, F., Romitti, F., Vasques, F., Pasticci, I., Duscio, E., & Quintel, M. (2019). Extracorporeal gas exchange: When to start and how to end? *Critical Care, 23*(Suppl 1), 1–7. doi: 10.1186/s13054-019-2437-2

Gimbel, A. A., Flores, E., Koo, A., García-Cardeña, G., & Borenstein, J. T. (2016). Development of a biomimetic microfluidic oxygen transfer device. *Lab on a Chip, 16*(17), 3227–3234. doi: 10.1039/C6LC00641H

Gorman, E., Connolly, B., Couper, K., Perkins, G. D., & McAuley, D. F. (2021). Non-invasive respiratory support strategies in COVID-19. *The Lancet Respiratory Medicine, 9*(6), 553–556. doi: 10.1016/S2213-2600(21)00168-5

Hlastala, M. P., & Souders, J. E. (2012). Perfluorocarbon Enhanced Gas Exchange. *American Journal of Respiratory and Critical Care Medicine, 164*(1), 1–2. doi: 10.1164/AJRCCM.164.1.2104021A

Hojyo, S., Uchida, M., Tanaka, K., Hasebe, R., Tanaka, Y., Murakami, M., & Hirano, T. (2020). How COVID-19 induces cytokine storm with high mortality. *Inflammation and Regeneration, 40*(1). doi: 10.1186/S41232-020-00146-3

Jägers, J., Wrobeln, A., & Ferenz, K. B. (2020). Perfluorocarbon-based oxygen carriers: from physics to physiology. *Pflügers Archiv - European Journal of Physiology 2020 473:2, 473*(2), 139–150. doi: 10.1007/S00424-020-02482-2

Johnson, A. B., & Burns, B. (2021). Hemorrhage. *Complications in Small Animal Surgery*, 72–78. https://www.ncbi.nlm.nih.gov/books/NBK542273/

Kandler, M. A., Von der Hardt, K., Schoof, E., Dötsch, J., & Rascher, W. (2001). Persistent improvement of gas exchange and lung mechanics by aerosolized

perfluorocarbon. *American Journal of Respiratory and Critical Care Medicine*, *164*(1), 31–35. doi: 10.1164/ajrccm.164.1.2010049

Kashani, J., Shih, R. D., Cogbill, T. H., Jang, D. H., Nelson, L. S., Levy, M. M., Parker, M. M., Castanares-Zapatero, D., Laterre, P.-F., Castanares-Zapatero, D., Laterre, P.-F., Barney, J. B., Abraham, E., Murugan, R., Kellum, J. A., Sonneville, R., Ely, E. W., Sharshar, T., Maharaj, D., … Sun, B. (2012). Sieving Coefficient. *Encyclopedia of Intensive Care Medicine*, 2077–2077. doi: 10.1007/978-3-642-00418-6_3300

Khandpur, R. S. (2020). Hollow Fibre Dialyser. *Compendium of Biomedical Instrumentation*, 965–967. doi: 10.1002/9781119288190.CH178

Lyons, C., & Callaghan, M. (2020). The use of high-flow nasal oxygen in COVID-19. *Anaesthesia*, *75*(7), 843–847. doi: 10.1111/anae.15073

Machalinski, A. (n.d.). *Hypovolemic Shock: Symptoms, Stages, Causes, Diagnosis, and Treatment*. Retrieved October 25, 2021, from https://www.webmd.com/a-to-z-guides/hypovolemic-shock

Maclaren, G., Fisher, D., & Brodie, D. (2020). Preparing for the Most Critically Ill Patients with COVID-19: The Potential Role of Extracorporeal Membrane Oxygenation. *JAMA - Journal of the American Medical Association*, *323*(13), 1245–1246. doi: 10.1001/jama.2020.2342

Makdisi, G., & Wang, I. (2015). Extra Corporeal Membrane Oxygenation (ECMO) review of a lifesaving technology. *Journal of Thoracic Disease*, *7*(7), E166–E176. doi: 10.3978/J.ISSN.2072-1439.2015.07.17

Martin, D. S., & Grocott, M. P. W. (2013). Oxygen therapy in critical illness: Precise control of arterial oxygenation and permissive hypoxemia. *Critical Care Medicine*, *41*(2), 423–432. doi: 10.1097/CCM.0B013E31826A44F6

Matthay, M. A., Aldrich, J. M., & Gotts, J. E. (2020). Treatment for severe acute respiratory distress syndrome from COVID-19. *The Lancet Respiratory Medicine*, *8*(5), 433–434. doi: 10.1016/S2213-2600(20)30127-2

Mayo Clinic. (2020). ARDS - Symptoms and causes. Retrieved 6 October 2021, from https://www.mayoclinic.org/diseases-conditions/ards/symptoms-causes/syc-20355576

Messina, Z., & Patrick, H. (2021). Partial Pressure of Carbon Dioxide. StatPearls Publishing.

Mirco, N., Andrea, C., Angelo, G., Brambillasca, P., Federico, L., Michele, P., Giuseppe, G., Daniele, B., Francesco, F., Richard, N., Luca, L., Maurizio, C., & Carlo, M. (2020). At the Epicenter of the Covid-19 Pandemic and Humanitarian Crises in Italy: Changing Perspectives on Preparation and Mitigation. *Catalyst: Innovations in Care Delivery*, *Figure 1*, 1–5. doi: 10.1056/CAT.20.0080

Mishra, V., Svennevig, J., Bugge, J., Andresen, S., Mathisen, A., Karlsen, H., Khushi, I., & Hagen, T. (2010). Cost of extracorporeal membrane oxygenation: evidence from the Rikshospitalet University Hospital, Oslo, Norway. *European Journal of Cardio-Thoracic Surgery : Official Journal of the European Association for Cardio-Thoracic Surgery*, *37*(2), 339–342. doi: 10.1016/J.EJCTS.2009.06.059

Munshi, L., & Hall, J. B. (2021). Respiratory Support During the COVID-19 Pandemic: Is It Time to Consider Using a Helmet? *JAMA*, *325*(17), 1723–1725. doi: 10.1001/JAMA.2021.4975

Nadler, S. B., Hidalgo, J. U., & Bloch, T. (1962). Prediction of blood volume in normal human adults. *Surgery*, *51*(2), 224–232. doi: 10.5555/URI:PII:0039606062901666

Neri, M., Villa, G., Garzotto, F., Bagshaw, S., Bellomo, R., Cerda, J., Ferrari, F., Guggia, S., Joannidis, M., Kellum, J., Kim, J. C., Mehta, R. L., Ricci, Z., Trevisani, A., Marafon, S., Clark, W. R., Vincent, J.-L., Ronco, C., & alliance, on behalf of the N. S. I. (NSI). (2016). Nomenclature for renal replacement therapy in acute kidney injury: basic principles. *Critical Care*, *20*(1). doi: 10.1186/S13054-016-1489-9

Park, M., Costa, E. L. V., Maciel, A. T., Silva, D. P. e, Friedrich, N., Barbosa, E. V. S., Hirota, A. S., Schettino, G., & Azevedo, L. C. P. (2013). Determinants of Oxygen and Carbon Dioxide Transfer during Extracorporeal Membrane Oxygenation in an Experimental Model of Multiple Organ Dysfunction Syndrome. *PLoS ONE*, *8*(1), 54954. doi: 10.1371/JOURNAL.PONE.0054954

Pfeifer, M., Ewig, S., Voshaar, T., Randerath, W. J., Bauer, T., Geiseler, J., Dellweg, D., Westhoff, M., Windisch, W., Schönhofer, B., Kluge, S., & Lepper, P. M. (2020). Position Paper for the State-of-the-Art Application of Respiratory Support in Patients with COVID-19. *Respiration*, *99*(6), 521–542. doi: 10.1159/000509104

Pittman, R. N. (2011). Chapter 4: Oxygen Transport. In *Regulation of Tissue Oxygenation*. Morgan & Claypool Life Sciences.

Ragab, D., Salah Eldin, H., Taeimah, M., Khattab, R., & Salem, R. (2020). The COVID-19 Cytokine Storm; What We Know So Far. *Frontiers in Immunology*, *0*, 1446. doi: 10.3389/FIMMU.2020.01446

Ramanathan, K., Antognini, D., Combes, A., Paden, M., Zakhary, B., Ogino, M., MacLaren, G., Brodie, D., & Shekar, K. (2020). Planning and provision of ECMO services for severe ARDS during the COVID-19 pandemic and other outbreaks of emerging infectious diseases. *The Lancet. Respiratory Medicine*, *8*(5), 518. doi: 10.1016/S2213-2600(20)30121-1

Riess, J. G. (2009). Understanding the Fundamentals of Perfluorocarbons and Perfluorocarbon Emulsions Relevant to In Vivo Oxygen Delivery. *Artificial Cells, Blood Substitutes, and Biotechnology*, *33*(1), 47–63. doi: 10.1081/BIO-200046659

Rubin, D. M., Stacey, N. T., Matambo, T., & Hildebrandt, D. (2020). Oxygen transfer characteristics of a hollow fiber dialyser: toward possible repurposing of dialysers as blood oxygenators in the context of constrained availability of respiratory support. *MedRxiv*, *Xx*, 2020.04.06.20055236. https://www.medrxiv.org/content/10.1101/2020.04.06.20055236v2%0Ahttps://www.medrxiv.org/content/10.1101/2020.04.06.20055236v2.abstract

Rubin, D. M., Stacey, N. T., Matambo, T., Vale, C. Do, Sussman, M. J., Snyman, T., Mer, M., & Hildebrandt, D. (2020). Toward Respiratory Support of Critically Ill COVID-19 Patients Using Repurposed Kidney Hollow Fiber Membrane Dialysers to Oxygenate the Blood. *Journal of Healthcare Engineering*, *2020*. doi: 10.1155/2020/8862645

Sidebotham, D., Allen, S. J., McGeorge, A., Ibbott, N., & Willcox, T. (2012). Venovenous Extracorporeal Membrane Oxygenation in Adults: Practical Aspects of Circuits, Cannulae, and Procedures. *Journal of Cardiothoracic and Vascular Anesthesia*, *26*(5), 893–909. doi: 10.1053/J.JVCA.2012.02.001

Sumin, L., Youguang, M., Shuhua, S., & Chunying, Z. (2010). The effect of hydrophobic modification of zeolites on CO_2 absorption in different solvents. *Brazilian Journal of Chemical Engineering*, *27*(2), 327–338. doi: 10.1590/S0104-66322010000200011

Takahashi, N., Nakada, T., & Oda, S. (2018). Efficient CO_2 removal using extracorporeal lung and renal assist device. *Journal of Artificial Organs 2018 21:4*, *21*(4), 427–434. doi: 10.1007/S10047-018-1058-X

Tange, Y., Migita, H., Yoshitake, S., Isakozawa, Y., Takesawa, S., Imamiya, T., & Yoshida, T. (2012). Dialysate with High Partial Pressure of Oxygen Enhances Oxygenation in Blood during Simulated Circulation of Hemodialysis. *Advanced Biomedical Engineering*, *1*(0), 43–46. doi: 10.14326/ABE.1.43

Tange, Y., & Yoshitake, S. (2019). Oxygen delivery to the blood stream by the dialysis fluid during continuous renal replacement therapy ex vivo. *Journal of Artificial Organs 2019 22:2*, *22*(2), 104–109. doi: 10.1007/S10047-018-1085-7

Tawfic, Q. A., & Kausalya, R. (2011). Liquid Ventilation. *Oman Medical Journal*, *26*(1), 4. doi: 10.5001/OMJ.2011.02

ter Beek, O. E. M., Pavlenko, D., & Stamatialis, D. (2020). Hollow fiber membranes for long-term hemodialysis based on polyethersulfone-SlipSkin™ polymer blends. *Journal of Membrane Science*, *604*, 118068. doi: 10.1016/J.MEMSCI.2020.118068

Xu, H., Li, Y., Gao, W., Zhang, H., & Xu, L.-X. (2011). Hyperoxygenated Solutions in Clinical Practice: Preventing or Reducing Hypoxic Injury: *Journal of International Medical Research*, *39*(5), 1589–1606. doi: 10.1177/147323001103900502

Xu, L. (2020). *Hollow Fiber Membrane Dialysers: Gas transfer properties of Hollow Fibre Membrane Dialysers repurposed for respiratory support in critically ill COVID-19 patients. doi: 10.13140/RG.2.2.33285.83680*

Yang, W., Hong, J., Zeng, Q., Tao, J., Chen, F., Dang, R., Liang, Y., Wu, Z., & Yang, Y. (2016). Improvement of Oxygenation in Severe Acute Respiratory Distress Syndrome With High-Volume Continuous Veno-venous Hemofiltration: *Global Pediatric Health*, *3*, 2333794X1664569. doi: 10.1177/2333794X16645699

Yeager, T., & Roy, S. (2017). Evolution of Gas Permeable Membranes for Extracorporeal Membrane Oxygenation. *Artificial Organs*, *41*(8), 700–709. doi: 10.1111/aor.12835

CHAPTER 12:
DESIGN AND DEVELOPMENT OF A BIPAP NON-INVASIVE VENTILATOR: PROTOTYPE DEVELOPMENT

Joel Philpott, Sudesh Sivarasu
ORCID ID: 0000-0003-4037-9193, 0000-0002-0812-568X
Division of Biomedical Engineering
Department of Human Biology
University of Cape Town
Western Cape
South Africa

Richard Raine
ORCID ID: 0000-0003-2075-7396
Division of Pulmonology
Department of Medicine
University of Cape Town
Western Cape
South Africa

ABSTRACT

Many diseases affect the efficacy of the respiratory system, and thus ventilatory support is required to improve the patient's prognosis. One of the methods of providing this support is by using non-invasive, positive pressure, BiPAP ventilation. The purpose of this project is to develop a prototype of a medical device that can provide this support. This is achieved by understanding the requirements of the device, generating concepts that can satisfy these requirements, selecting a concept and constructing it. The selected concept makes use of two blower fans, the first to provide the inspiratory pressure support, and the second to provide the expiratory pressure support. The pressure delivered to the patient is controlled using an axial solenoid valve and a one-way valve. A PID control loop is then used to control the speed of the fans. The system developed is not able to meet all the requirements but would be able to do so with slight improvements. These improvements include redesigning the axial solenoid valve to reduce the pressure drop across the valve, redesigning the flow path of the circuit to reduce the pressure drop in sharp corners, and changing the inspiratory fan control loop implementation strategy. The flow rate sensor also needs to be improved to allow the device to perform accurate volume-controlled ventilation.

Keywords: BiPAP, non-invasive, ventilation, pressure controlled, flow control valve, flow rate sensor

NOMENCLATURE

NPV	Negative Pressure Ventilation
PPV	Positive Pressure Ventilation
BiPAP	Bilevel Positive Airway Pressure
CPAP	Continuous Positive Airway Pressure
IPAP	Inspiratory Positive Airway Pressure
PEEP	Positive End Expiratory Pressure
WHO	World Health Organisation
PID	Proportional Integrative Derivative
I: E	Inspiratory: Expiratory

INTRODUCTION

Many diseases have harmful impacts on patients' lungs, resulting in reduced blood oxygen levels and ultimately respiratory failure (Patel, 2020). To improve their prognosis, it is essential to provide support to the patient's respiratory system before it fails (Shelly & Nightingale, 1999). This support can either be invasive or non-invasive. Invasive therapy refers to mechanical ventilation administered via an endotracheal tube (a tube through the mouth into the throat near the larynx) or a tracheostomy tube (a tube through an incision in the trachea) (Shelly & Nightingale, 1999). Non-invasive therapy refers to respiratory therapy applied via a face mask.

Non-invasive therapy can be further split into two categories: Negative Pressure Ventilation (NPV) and Positive Pressure Ventilation (PPV). Negative pressure ventilation is the application of negative pressure to the outside of the thoracic region, assisting in opening the patient's airways (Marcotte, 2020). This ventilation method is, however, not effective when the patient's lung compliance is reduced, and the devices are typically cumbersome to use (Grasso, et al., 2008). PPV is the application of positive pressure inside the patient's lungs. This is achieved by blowing air into the patient's lungs through a mask, thereby preventing their lungs from collapsing.

Non-invasive PPV can be achieved through two different strategies: Continuous Positive Airway Pressure (CPAP) and Bilevel (also known as Bi-phasic) Positive Airway Pressure (BiPAP). CPAP provides constant pressure to the patient, regardless of whether they are inhaling or exhaling (Sharma, et al., 2011). BiPAP, on the other hand, provides two different pressure levels: a lower pressure when the patient is exhaling, and higher pressure when they are inhaling. The higher pressure is the Inspiratory Positive Airway Pressure (IPAP), and the lower pressure is the Positive End Expiratory Pressure (PEEP). BiPAP ventilation is more comfortable than CPAP ventilation, especially at higher pressures, and is therefore used more frequently to treat severe cases of respiratory distress (Patil, 2020).

The COVID-19 pandemic has placed significant strain on the healthcare systems in many countries, leaving patients untreated, or inadequately treated (Menon & Padhy, 2020). This project, therefore, aims to develop a non-invasive BiPAP ventilator that can be used in the treatment of patients infected with the SARS-COV2 virus. The device differs from conventional ventilators by changing the pneumatic circuit. Conventional ventilators use a single fan module and control the speed of the fan to control the pressure output. This device uses two fans, with one fan controlling the expiratory pressure, and the second controlling the inspiratory pressure. The fans do not need to change speed rapidly, allowing for more accurate control of the pressure levels. The following research question is therefore addressed in this article: Can the use of a dual fan pneumatic circuit combined with the use of an axial solenoid valve reduce the reliance on the change of speed of the fan to produce BiPAP ventilation?

MATERIALS AND METHODS

Firstly, the required performance characteristics of the device are identified. These will ensure the device developed meets the market standards in terms of performance as well as the requirements of the World Health Organisation (WHO). To limit the scope of the project, and because the device developed is only a prototype, some of the requirements are excluded. The requirements are shown in Table 1.

Table 1: BiPAP Non-Invasive Ventilator Requirements

Requirement	Value	Source
Inspiratory flow	1 – 120 l/min	(WHO, 2020)
Inspiratory pressure	4 to 35 cmH$_2$O	(WHO, 2020) (MHRA, 2020), (SASA, 2020)
Respiratory rate	10 to 30 breaths/min	(MHRA, 2020), (SASA, 2020)
PEEP	0 to 25 cmH$_2$O	(WHO, 2020) (SASA, 2020)
I:E ratio	1:1 to 1:6	Clinician
Ventilation Modes	Volume and pressure controlled	(WHO, 2020) (SASA, 2020)

While considering the intellectual property landscape, different concept generation strategies are used to develop solutions that would satisfy the requirements above. These concepts are then screened by their functional performance, as well as regulatory and reimbursement considerations. The resulting pneumatic circuit of the device is shown in Figure 1 below.
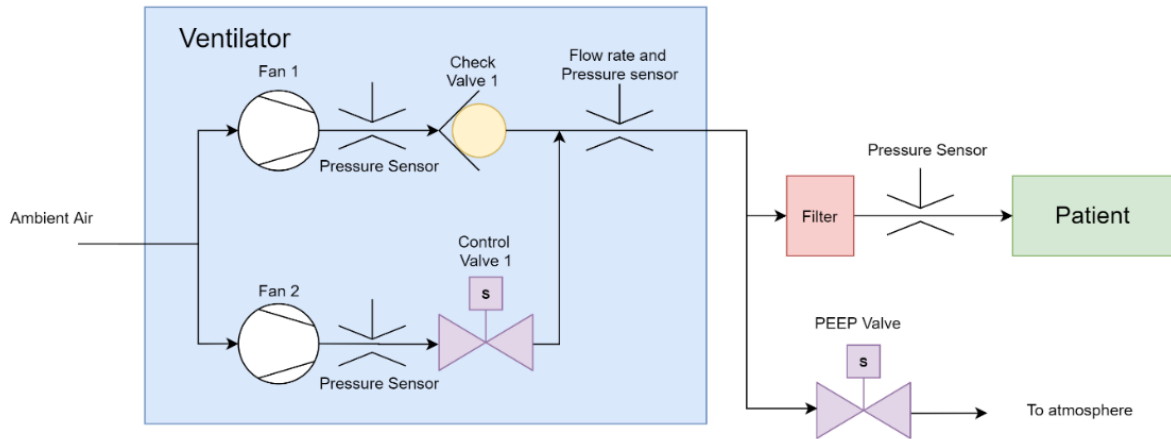
Figure 1: Selected Concept

All components are purchased as off-the-shelf parts except the flow rate sensor and the control valve 1. The design of these components is discussed below.

    i.   Flowrate Sensor

Flowrate sensors are typically expensive components, so to reduce the cost of the device, a flowrate sensor that makes use of the Venturi effect is designed. This relies on the principle that a fluid flowing creates a negative pressure next to it, and the faster the fluid is flowing, the greater the negative pressure. If the diameter of a pipe is reduced, the velocity of the fluid flowing through the pipe changes, thus causing a pressure differential. The flow rate can be calculated using Bernoulli's equation shown below (Muson, Young, & T.H., 1994).

$$Q = A_2 \sqrt{\frac{2}{\rho} \cdot \frac{\Delta P}{1-\left(\frac{A_2}{A_1}\right)^2}} \qquad (1)$$

In the equation, A_2 represents the smaller area of the pipe, A_1 the larger area of the pipe, the density of the air, and Q the flowrate. By iterating through different differential pressure sensors and optimising the design for the most accurate flow rate reading, it is calculated that the ideal diameters for A_1 and A_2 are 20mm and 7.5mm respectively. The design is 3D printed, and the inner area is drilled and reamed to ensure dimensional accuracy. The assembled flow sensor is shown in Figure 2.
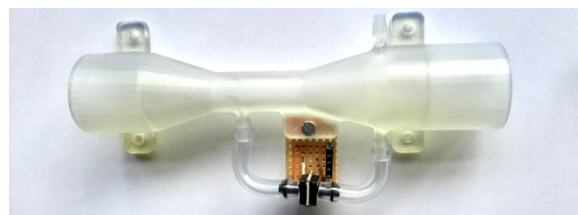

Figure 2: Assembled Flowrate Sensor

ii.   Control Valve

The control valve is required to open when the patient inhales, and close when they exhale. It must therefore close quickly, and seal well to ensure the correct pressure is applied to their lungs. Various design iterations are built and tested, and the final iteration is shown in Figure 3.
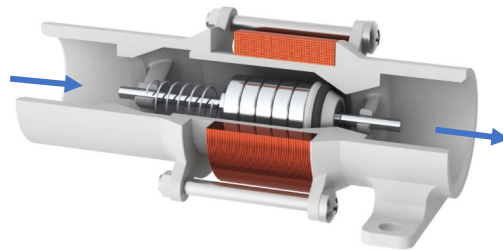

Figure 3: Flow Control Valve

This design makes use of a movable plunger in the flow path to open and close the valve. When the solenoid coil around the outside is not activated, the air pressure, as well as the spring, pushes the plunger to the right, sealing it against the casing. When the solenoid coil is activated by applying a voltage to it, the magnetic field of the solenoid and the permanent magnets on the plunger interact, pushing the plunger to the left, up the flow path. This allows air to flow through the valve and to the patient. The air passes between the magnets and the coil, so it does not need to go through any sharp corners, thus reducing the pressure drop across the valve.

iii.   Device Assembly

The purchased and manufactured components are assembled, using 3D printed parts to connect all the components. All the connections are designed to press-fit together, and tape is used where necessary to seal the connections. The resulting device is shown in Figure 4.
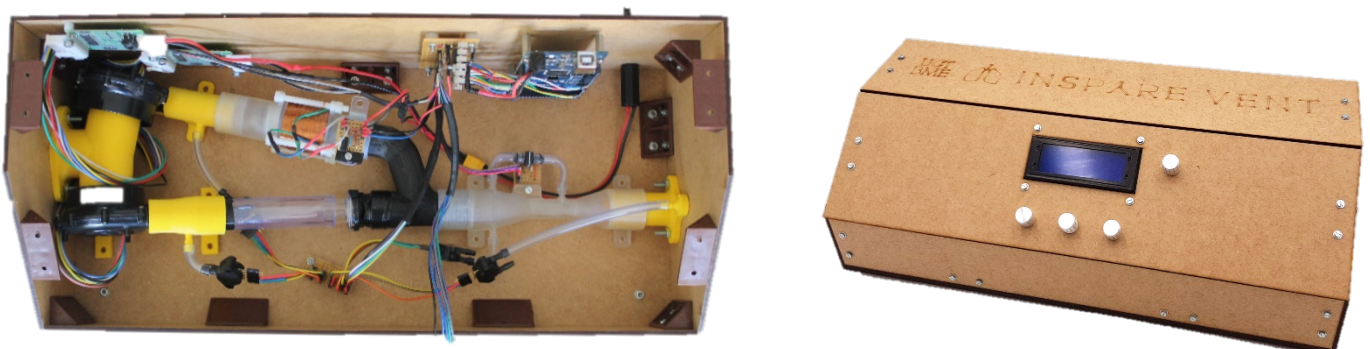

Figure 4: Assembled Prototype

116

The four potentiometers on the front face of the device are used to control the breathing rate, PEEP pressure, IPAP pressure, and I:E ratio. Veroboard is also used to make all the required electronic connections and ensure that the connections do not loosen during operation.

iv. Algorithm

One of the key components of the device is the algorithm used to control the pressure delivered to the patient. To identify what algorithm would be suitable, a test is done on the system without any feedback. The IPAP and PEEP fans are set at a constant speed and the control valve is controlled with a square wave. The results of this test are shown in Figure 5.
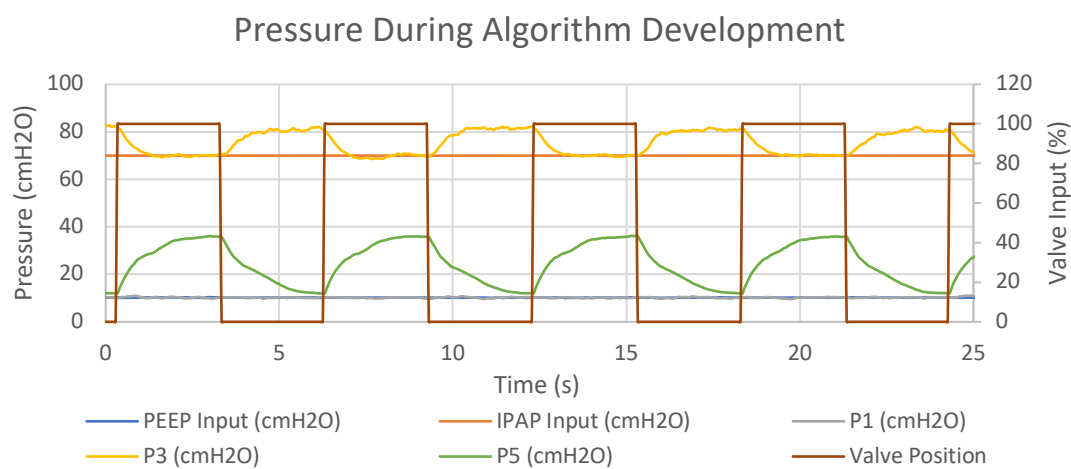

Figure 5: Pressure Readings During Algorithm Development

The P1 reading is taken just after the PEEP fan, the P3 reading is taken just after the IPAP fan, and the P5 reading is taken at the patient end. It is noted that the P1 readings do not change when the control valve opens and closes. A continuous Proportional Integrative Derivative (PID) control loop can therefore be run on the value from P1. It is also noted that the P3 reading drops significantly when the valve opens and rises again when the valve closes. Because of this, a PID loop is implemented for the second half of the inspiration phase. The pressure readings are therefore allowed to settle to a relatively constant value before the speed of the fan is changed.

RESULTS AND DISCUSSION

The design is tested using a passive test lung with a volume of 1.0 l, and compliance of 20ml/cmH$_2$O, in the place of a patient. The first characteristic of the ventilator tested is the flow rate delivered to the patient. The results of this test are shown in Figure 6.
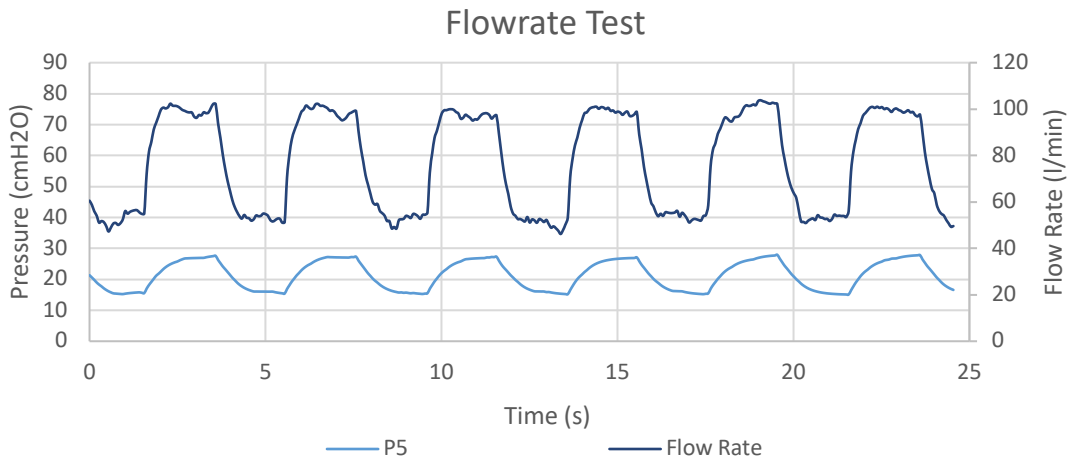
Figure 6: Flowrate Test Result

The device achieves a maximum flow rate of 103.81 l/min, which is less than the 120 l/min requirement. During component testing, it is found that the fans can produce the required flow rate, so the flow path of the air needs to be optimised to increase the flow rate. This can be achieved by improving the design of the flow control valve and reducing the pressure drop across the valve. This change would also increase the maximum pressure delivered to the patient. Figure 7 shows the maximum pressure delivered to the patient during the inspiratory phase. The maximum inspiratory pressure is measured to be 33.45 cmH_2O, less than the 35 cmH_2O requirement.
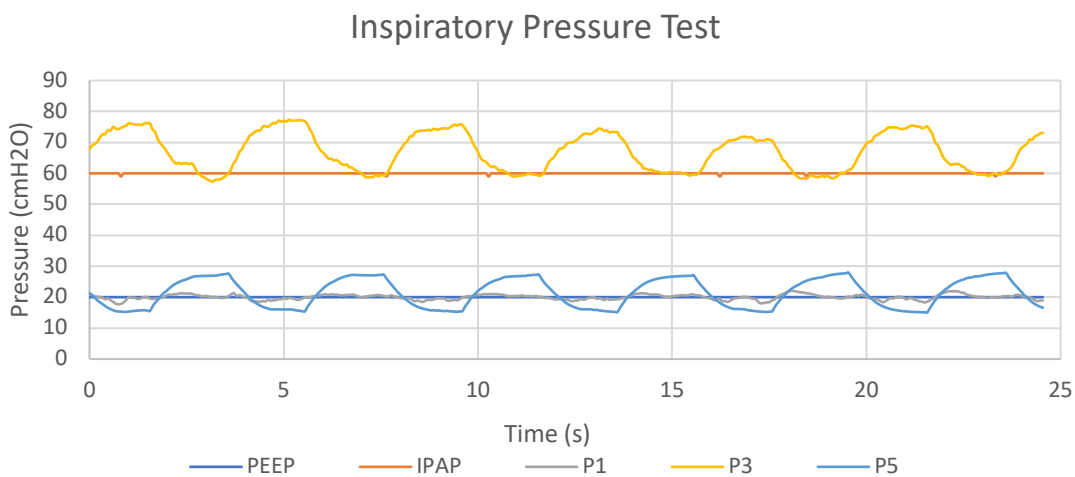

Figure 7: Inspiratory Pressure Test

One of the issues with the control algorithm that became clear during testing is that as the time of the inspiratory phase decreases, so does the time that the PID loop is run for the IPAP fan. This results in an unstable loop, where the speed of the IPAP fan and thus the IPAP pressure delivered to the patient oscillates between breaths. This is seen in the test with an Inspiratory: Expiratory (I:E) ratio of 1:6 (inhalation is one-seventh of the total cycle). The results of this test are shown in Figure 8.
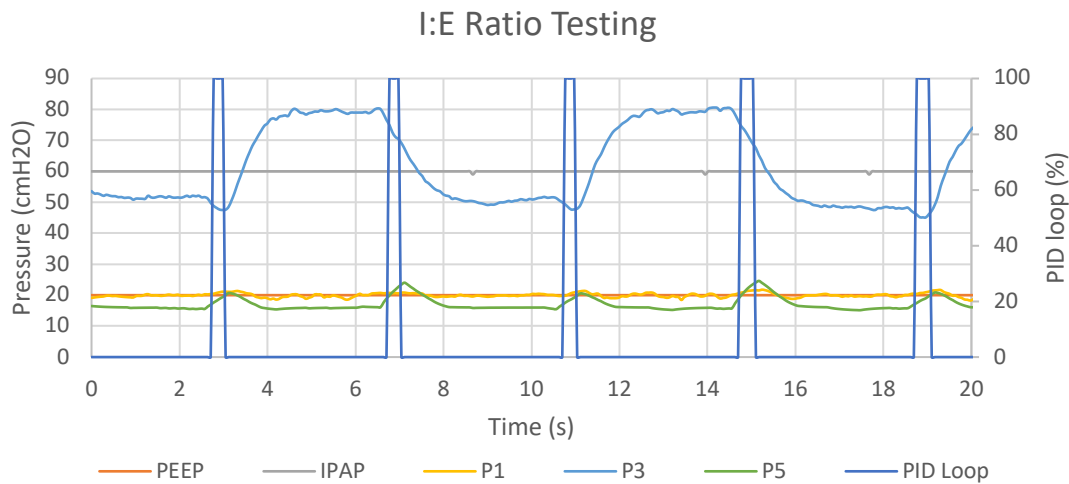

Figure 8: Inspiratory Pressure Test

The time that the PID loop is used is indicated by the dark blue line labelled "PID Loop". For an I:E ratio of 1:6, the IPAP PID loop is only used for 7.1% of the cycle. The resulting oscillation of the fan speed is seen in the P3 readings, the pressure just after the IPAP fan. Similar oscillation in the IPAP fan speed is seen with an increased breathing rate (30 breaths per minute), as shown in Figure 9.
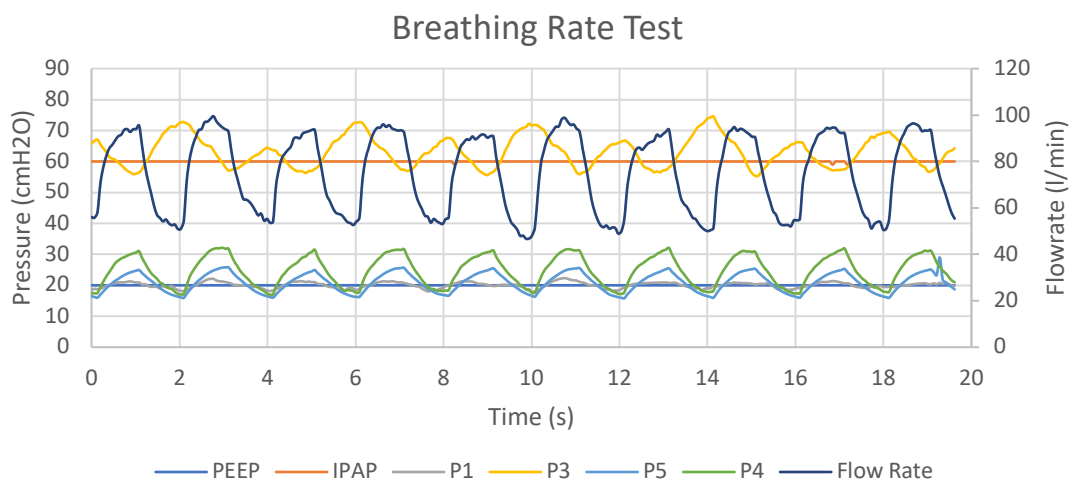

Figure 9: Breathing Rate Test

119

Lastly, the PEEP pressure is tested. The required maximum PEEP pressure is 25 cmH$_2$O and the device can supply this pressure. The PEEP fan stabilises at a fixed speed for all the tests indicating the control algorithm for the PEEP fan works correctly.

CONCLUSION

The constructed device was able to meet some of the requirements, but not all of them. The flow control valve used in the device should be redesigned to reduce the pressure drop across the valve and increase the maximum flow rate. The control algorithm for the IPAP fan should also be improved to increase its stability. Improvements should be made to the flow rate sensor to allow accurate, volume-controlled ventilation. Although it can provide basic pressure controlled non-invasive ventilation, further development is required for the device to have the same performance characteristics as conventional single fan ventilators.

REFERENCES

Grasso, F., Engelberts, D., Helm, E., Frndova, H., Jarvis, S., Talakoub, O., . . . Kavanagh, B. (2008). Negative-Pressure Ventilation. *American Journal of Respiratory and Critical Care Medicine*, 412-418. doi: 10.1164/rccm.200707-1004OC

James, F. K. (2019, May 17). *healthline*. Retrieved from What is Hypoxemia?: https://www.healthline.com/health/hypoxemia

Marcotte, B. (2020, April 17). *Ventilators: Three centuries in the making*. Retrieved from Medical Press: https://medicalxpress.com/news/2020-04-ventilators-centuries.html

Menon, V., & Padhy, S. (2020). Ethical dilemmas faced by health care workers during COVID-19 pandemic: Issues, implications and suggestions. *Asian Journal of Psychiatry*, 102-116. doi: 10.1016/j.ajp.2020.102116

MHRA. (2020, April 10). Rapidly Manufactured Ventilator System. Medicines & Healthcare Products Regulatory Agency.

Muson, B., Young, D., & T.H., O. (1994). *Fundamentals of Fluid Mechanics, 2nd Ed.* John Wilet and Sons, Inc.

Patel, B. K. (2020, April 24). *Repiratory Failure*. Retrieved from MSD Manual: https://www.msdmanuals.com/home/lung-and-airway-disorders/respiratory-failure-and-acute-respiratory-distress-syndrome/respiratory-failure

Patil, S. (2020). BiPAP vs CPAP in Treatment of OSAS. *Chest*, A2408-A2409. doi: 10.1016/j.chest.2020.09.008

SASA. (2020). Standards for Supply/Manufacture of Ventilators to South Africa During the COVID-19 Pandemic. South African Society of Anaesthesiologists.

Shaikh, J. (2020, October 15). *What Are Blood Oxygen Levels? Chart*. Retrieved from MedicineNet: https://www.medicinenet.com/what_are_blood_oxygen_levels/article.htm

Sharma, S., Agrawal, S., Damodaran, D., Sreenivas, V., Kadhiravan, T., Lakshmy, R., . . . Kumar, A. (2011). CPAP for the Metabolic Syndrome in Patients with Obstructive Sleep Apnea. *New England Journal of Medicine*, 2277-2286. doi: 10.1056/NEJMoa1103944

Shelly, M. P., & Nightingale, P. (1999). ABC of intensive care: Respiratory support. *BMJ*, 1674-1677. doi: 10.1136/bmj.318.7199.1674

WHO. (2020, April 15). *World Health Organisation Institutional Repository for Information Sharing.* Retrieved from Technical specifications for invasive and non-invasive ventilators for COVID-19: Interim guidance: https://apps.who.int/iris/handle/10665/331792

CHAPTER 13

FEASIBILITY OF REPURPOSING HOLLOW FIBRE MEMBRANE DIALYSERS FOR OXYGENATING BLOOD IN RESOURCE CONSTRAINED ENVIRONMENTS

Alexander Francis, Doron Joffe, Lan Xu, Neil Stacey, David Rubin
ORCID ID: 0000-0003-0729-3750, 0000-0003-1953-9420, 0000-0003-1342-4710, 0000-0003-4902-5201, 0000-0003-0316-9197
School of Chemical Engineering
University of Witwatersrand
Gauteng
South Africa

ABSTRACT

Previous research has demonstrated the viability of kidney dialysers repurposed as extra-corporeal membrane oxygenation devices to provide sufficient supplemental oxygen support for those suffering from COVID-19. This study focused on determining the mass transfer coefficient for carbon dioxide in kidney dialyser cartridges at varying pH levels. CO_2 mass transfer coefficients of 5.5 and 6.95 $mg/kpa \cdot min$ were achieved, depending on the type of hollow fibre membrane dialyser — this corresponds to a CO_2 removal rate of between of 80% and 90% of the total CO_2 produced by the body. The mass transfer coefficients achieved with water as the medium suggest that sufficient CO_2 removal for respiratory requirements can be achieved with hollow fibre membrane dialysers. This should motivate further experimentation with blood to determine the feasibility of using the cost-effective hollow fibre membrane dialysers to supplement conventional extra-corporeal membrane oxygenation technologies in resource-constrained hospital wards. It is also found that hollow fibre membrane dialysers have high sieving coefficients for dissolved ions, which indicates that dissolved solids and plasma ions will leak from the cartridge and supplements will need to be given to patients to account for these losses. The sieving coefficient for the kidney dialyser cartridge was calculated to be an average of 0.983. The results in this study are promising, adding additional parameters to the body of knowledge for devising operational protocols. However, more specific experimentation using blood is warranted.

Keywords: COVID-19; Respiratory Support, Emergency healthcare capacity

NOMENCLATURE

ECMO	Extra-Corporeal Membrane Oxygenation
HFMD	Hollow Fibre Membrane Dialyse

INTRODUCTION

The COVID-19 pandemic has resulted in millions of deaths and many more infections. It may also cause long-term lung injury in those who survive — with pneumonia and respiratory-failure being the main causes of mortality. As COVID-19 affects countries in waves, oxygen treatment is at its highest demand near the peak of each wave. In extreme cases, the demand is unable to be met due to a lack of supplemental oxygen treatment devices.

Both ECMO and HFMDs operate through diffusion of solutes to and from the patient's blood stream. It has been suggested to repurpose renal hollow fibre membrane dialysers as ECMO machines to reduce the shortfall of supplemental oxygen treatment devices (Rubin et al, 2020). There are many risks involved with the use of an ECMO device. Primarily, a safe ECMO device must concomitantly oxygenate and decarbonate blood to appropriate levels in a patient with respiratory distress. The mass transfer characteristics for carbon dioxide in hollow fibre membrane dialyser cartridges need to be investigated to assess the suitability of the cartridges as a possible treatment option for patients suffering from respiratory distress during resource scarce situations. The hollow fibre membrane dialyser needs to transfer sufficient oxygen into the blood to prevent or limit hypoxia and hypoxemia. Additionally, excessive carbon dioxide removal from the blood can result in hypocapnia, while insufficient carbon dioxide removal can result in hypercapnia.

The goal of ECMO is to maintain the patient's blood oxygen saturation at a minimum of 90% and between 92% - 95% for pregnant women while simultaneously maintaining healthy CO_2 levels in the blood (Whittle, Pavlov, Sacchetti, Atwood & Rosenberg, 2020). Healthy blood oxygen levels are at 95% saturation and above (Davis, 2021). This is in contrast to patients suffering from COVID-19 where blood oxygen saturation as low as 50% has been observed (Loyola Medicine, 2020).

Once the disease processes associated with COVID-19 infection have reduced a patient's oxygen levels, the patient will begin to take deeper and quicker breaths. This exacerbates the inflammatory response and unintentionally causes lung damage. At this stage, the patient is still expelling CO_2 and will not feel discomfort because the blood is still at normal pH levels. Chemical feedback from CO_2 levels in the blood, rather than O_2 levels, governs the respiratory drive, which is why patients do not experience discomfort (Leusen, 1953; Epstein et al., 1995; Vaporidi et al., 2020). Tissue damage worsens over time as the patient unwittingly suffers from dangerously low oxygen levels ($PaO_2 < 60mmHg$) until hospitalisation is required (Dhont, Derom, Van Braeckel, Depuydt & Lambrecht, 2020; Tobin, Laghi & Jubran, 2020). The patient will eventually develop hypercapnia which results in dyspnoea (Zubieta-Calleja & Zubieta-DeUrioste, 2020). Once a patient is hospitalised, it is crucial to implement oxygen therapy before the patient becomes critically ill.

A vital parameter of any ECMO application is the gas transfer rate that can be achieved to and from the patient's blood stream. A membrane with high resistance to mass transfer will be inadequate to meet oxygenation requirements and adequate quantities of CO_2 will not be removed. Conversely, excessive gas transfer may lead to the onset of hypocapnia where the blood CO_2 levels drop below the normal reference range of 35 mmHg (Sharma and Hashmi, 2021). Experimental precedent exists for successfully using a low-flux hollow fibre dialyser with a polysulfone membrane to achieve oxygen transfer rates of approximately 37.5 ml/min at a blood flow rate of 500ml/min (Rubin et al., 2020). It has been suggested that using two dialysis devices in parallel could provide up to 75ml/min (Rubin et al., 2020). Although this would not satisfy a critically ill patient's oxygen requirement, it would be useful for patients with some breathing capability as a means of compensating for a respiratory deficit.

Only a fraction of a patient's regular O_2 supply needs to be recovered to counter the adverse effects of hypoxia. Therefore, (Rubin et al., 2020) proposed using hollow fibre membrane dialysers to meet the demand for supplemental oxygen. This is because haemodialysis cartridges are in abundance and can supply limited respiratory support. If the mass transfer properties of oxygen and carbon dioxide of the dialyser are known, there is potential for hollow fibre membrane dialysers to be used in the place of ECMO machines because they are cheaper and are medical grade. The high rate of hospitalisation of COVID-19 patients has led to shortages of respiratory support equipment in certain regions of the world (Kliff et al., 2020). Substituting ECMO machines for hollow fibre membrane dialysers could have a significant impact in Africa, where resources and medical equipment are scarce.

Seventy per cent of carbon dioxide in blood is transported through a series of catalysed acid base reactions involving carbonic acid, bicarbonate, and hydrogen ions. The remainder of carbon dioxide transport is facilitated by carbaminohaemoglobin (23%) and dissolution in plasma (7%) (Biga et al., 2020). The acid-base relationships are defined in Reaction 1 and Reaction 2. Reaction 1 is catalysed by the enzyme carbonic anhydrase (Biga et al., 2020).

A process known as oxygenator wetting can occur where blood plasma infiltrates the membrane micropores and inhibits gas transfer (Yeager and Roy, 2017). Oxygen transfers far less rapidly through water than air and thus, the ECMO functionality is compromised (Yeager and Roy, 2017). Blood products would need to be replenished in the patient's blood stream via blood transfusion or a drip. The extent of leakage of dissolved solids and ions from the cartridge can be numerically quantified through the sieving coefficient. The coefficient describes the relationship between the concentration of the fluid at the membrane inlet and the concentration of the filtrate (Hulko et al., 2018). It can be used to predict solute loss in blood. A coefficient of one indicates that the solute passes freely through the membrane (Hulko et al., 2018). This

is a vital parameter because it indicates the extent to which blood products need to be replaced via a drip or blood transfusion to supplement for solute losses.

The aim of this study was to determine the mass transfer coefficient for carbon dioxide in water at varying pH levels for the two haemodialysis cartridges shown in Table 1. This will indicate whether the cartridges can remove sufficient carbon dioxide and their viability as makeshift ECMO devices can be assessed. Additionally, this study aimed to determine the sieving coefficient of the cartridges. Both parameters are necessary for developing a clinical plan for implementation of emergency repurposing of HFMDs as makeshift ECMO devices. The sieving coefficients for dissolved solids and ions will indicate the rate at which blood products will have to be replaced in a patient undergoing treatment. For the proposed treatment to be viable, the removal rate of CO_2 must be adequate to support respiration. However, in the situation where the CO_2 removal rate is excessively high, some amount of CO_2 will need to be added to the oxygen stream to maintain normal CO_2 levels in the blood.

MATERIALS AND METHODS

i.   Apparatus and experimental procedure (Figure 1)
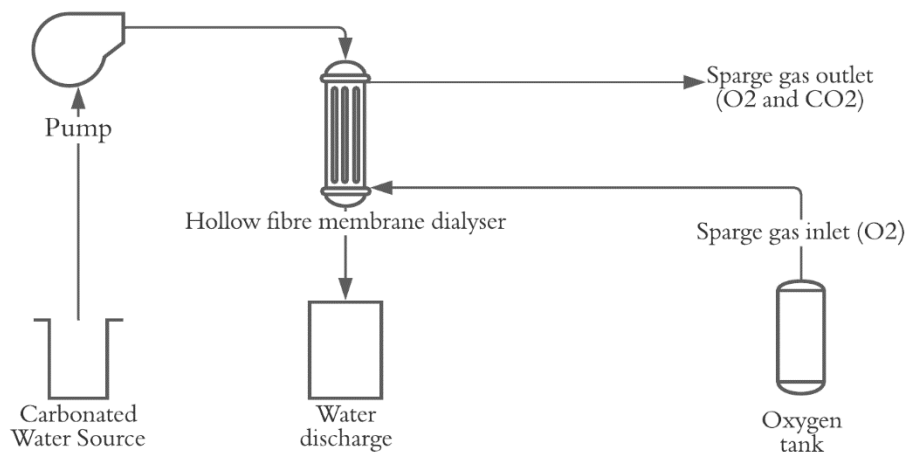

Figure 1: Experimental setup for determining mass transfer coefficient of carbon dioxide (Xu, 2020)

The experiments were performed at a laboratory in Johannesburg, at an altitude of 1 750m with an atmospheric pressure of about 84kPa and a temperature of about 28°C during the course of experimentation.

To determine the mass transfer coefficient, carbonated water needed to be pumped counter current to a pure oxygen stream through the cartridge. Carbonation of distilled water was done using a canister of high-pressure CO_2, followed by dilution to reach the target pH. The water was pumped at a rate of 500ml/L and the oxygen sweep gas flowed at a rate of 1.5L/min. The pH of the water source was measured as

well as the pH of the water after discharge. Subsequent to discharge, the water was diluted by a factor of five and reused as the carbonated water source for the next run. The cycle was repeated until the pH of the water remained unchanged after running through the cartridge. This indicated that an equilibrium had been reached and no further gas transfer was possible. To ensure experimental accuracy, prior to each run, the circuit was primed with twice the recommended priming volume of the cartridge.

The experimental procedure to determine the sieving coefficient was similar. Table salt was added to distilled water to produce the water source. The dissolved solids concentration was measured instead of the pH. The properties of the two types of haemodialysis cartridges used are shown in Table 1. These cartridge types were selected because it has previously been found that high-flux cartridges exhibit high rates of leakage when operated with a gas stream making them unsuitable for this purpose (Xu, 2020).

Table 1: Haemodialysis cartridges used

Cartridge	Low-flux Leoceed-21N	Low-flux Braun Diacap
Membrane surface area (m^2)	2.1	1.08
Internal Fibre Diameter (µm)	185	200
Priming volume (ml)	108	58
Manufacturer's specified blood flow rate (ml/min)	200 – 500	200 – 500

ii.   Computational methods

The mass transfer coefficient can be found using Equation 1, which is derived from Fick's law. The driving force for carbon dioxide transfer is the partial pressure difference of carbon dioxide across the membrane

$$k_0 = \dot{q}_{CO2} \Big/ A \cdot LM\Delta p_{CO2} = \dot{q}_{CO2} \Bigg/ \left(A \cdot \left[\frac{\Delta p_{CO2}{}^{top} - \Delta p_{CO2}{}^{bottom}}{ln\left(\frac{\Delta p_{CO2}{}^{top}}{\Delta p_{CO2}{}^{bottom}}\right)} \right] \right) \tag{1}$$
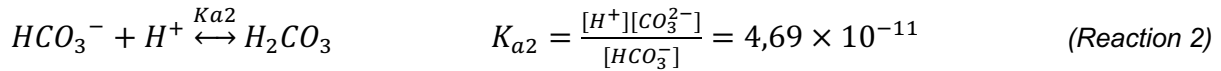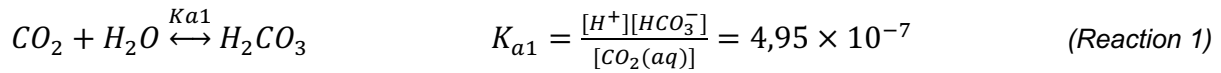
where

- k_0 (mg/min·kPa·m^2) is the mass transfer coefficient.
- A (m^2) is the membrane area, given by the manufacturer and indicated in Table 1.
- ΔPCO_2 (KPa) is the partial pressure difference of carbon dioxide.
- q_{CO2} (mg/min) is the rate of carbon dioxide transferred.

iii.   Acid-base equilibria and mass balance

The relationship between carbonic acid and water can be used to calculate the

carbon dioxide concentration difference between the water source and discharge. It can further be used to determine the partial pressure of carbon dioxide. The concentration of hydrogen ions in the water can be calculated using Equation 2

$$[H^+] = 10^{-pH} \tag{2}$$

$$CO_2 + H_2O \overset{Ka1}{\longleftrightarrow} H_2CO_3 \qquad K_{a1} = \frac{[H^+][HCO_3^-]}{[CO_2(aq)]} = 4{,}95 \times 10^{-7} \qquad \textit{(Reaction 1)}$$

$$HCO_3^- + H^+ \overset{Ka2}{\longleftrightarrow} H_2CO_3 \qquad K_{a2} = \frac{[H^+][CO_3^{2-}]}{[HCO_3^-]} = 4{,}69 \times 10^{-11} \qquad \textit{(Reaction 2)}$$

where
- Ka is a dissociation constant and is a dimensionless number.

K_{a1} largely determines the pH of the solution for two reasons. Firstly, Reaction 2 dominates because $K_{a1} \gg K_{a2}$. Moreover, the enzyme carbonic anhydrase rapidly hydrates carbon dioxide to carbonic acid. Additionally, since HCO_3^- does not dissociate in the medium (lower K_{a2}), the concentration of HCO_3^- and H_3O^+ are almost equal. Thus:

$$K_{a1} = \frac{[H_3O^+]^2}{[CO_2(aq)]} = 4{,}95 \times 10^{-7} \tag{3}$$

Using Henry's law, the carbon dioxide partial pressure can be used using Equation 4. The Henry's constant (KH) for carbon dioxide in water is 3.4 × 10-2 mol/L·atm.

$$p_{CO2} = \left. CO_{2\,(aq)} \middle/ K_H \right. \tag{4}$$

When pure oxygen is used as the sweep gas and enters from the bottom, the partial pressure of carbon dioxide in the sweep gas is zero and thus $\Delta p_{CO2, \text{bottom}}$ = Pa$_{CO2 \text{ out, liquid}}$. At the top, carbon dioxide in the liquid transfers through the membrane into the gas. The carbon dioxide present in the gas outlet is calculated by doing a mass balance on the carbon dioxide over the liquid inlet and outlet. The partial pressure of carbon dioxide in the gas outlet can then be calculated. The partial pressure difference at the top is taken as the difference between the partial pressure of carbon dioxide in the liquid inlet and gas outlet streams.

iv.   Carbon dioxide transfer rate

The rate of carbon dioxide passing the membrane (q_{CO2}) is found using the pH measurements. The number of H+ ions can be determined by Equation 2. The aqueous CO_2 concentration (mol/l) can be found using the acid-base equilibrium constant described by Equation 3, appropriate unit conversion to mg/m^3 must be made.

v.   Sieving coefficient

The extent of leakage of dissolved solids and ions from the cartridge can be numerically quantified through the sieving coefficient, defined in Equation 5 below. The electrical conductivity (EC) of the solution gives an indication of the concentration of dissolved plasma ions. The ratio between the EC of the solution before and after passing through the cartridge membrane indicates the extent of the leakage of dissolved ions

$$S = \frac{C_r}{C_d} \qquad (5)$$

where
- S is the sieving coefficient.
- Cr is the solute concentration in the receiving stream (after passing through the membrane). Cd is the solute concentration in the donating stream (prior to passing through the membrane).

RESULTS AND DISCUSSION

i.   Mass transfer coefficient for CO_2

The mass transfer coefficients for both cartridges were calculated. Maximum mass transfer coefficients of 6.95 $mg/kpa*min$ and 5.5 $mg/kpa*min$ were obtained in the Braun and Leoceed cartridges, at CO_2 inlet concentrations of 8.5 mmol/L and 5.6 mmol/L, respectively.

As shown in Figures 2 and 3, the relationship between the mass transfer coefficient and the inlet CO_2 coefficient fits a logarithmic profile with R^2 values of 0.85 and 0.92 for the Braun and Leoceed cartridges respectively. The relatively high R^2 values indicate that the logarithmic trendlines fit the data points relatively accurately and can be used to forecast values at inlet concentrations that were not tested.
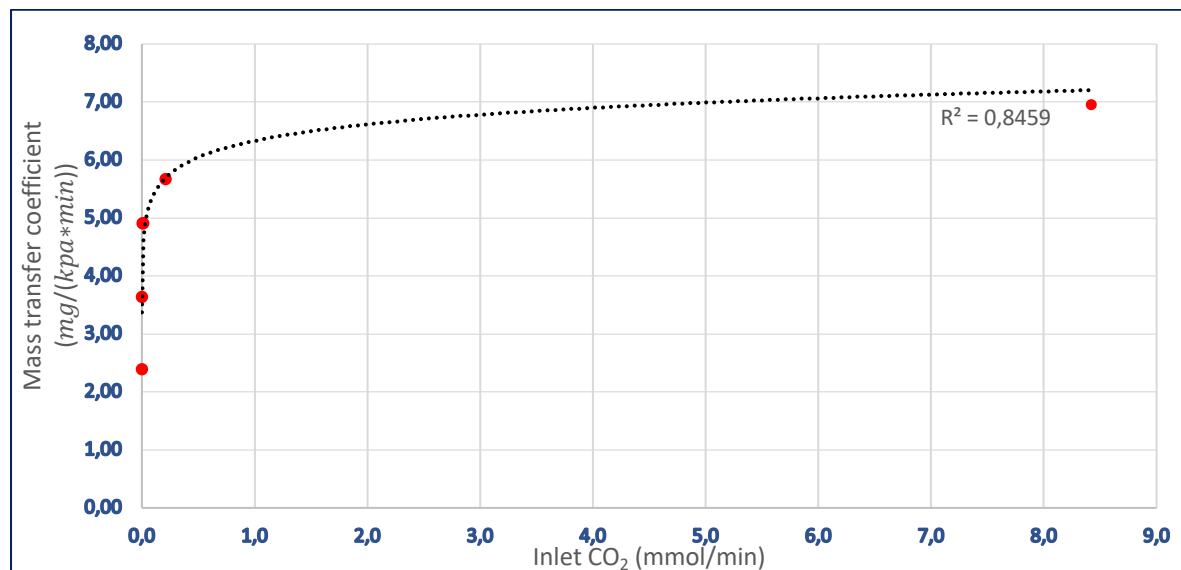

Figure 2: Relationship between CO2 mass transfer coefficient and inlet CO2 concentration in the Braun cartridge.
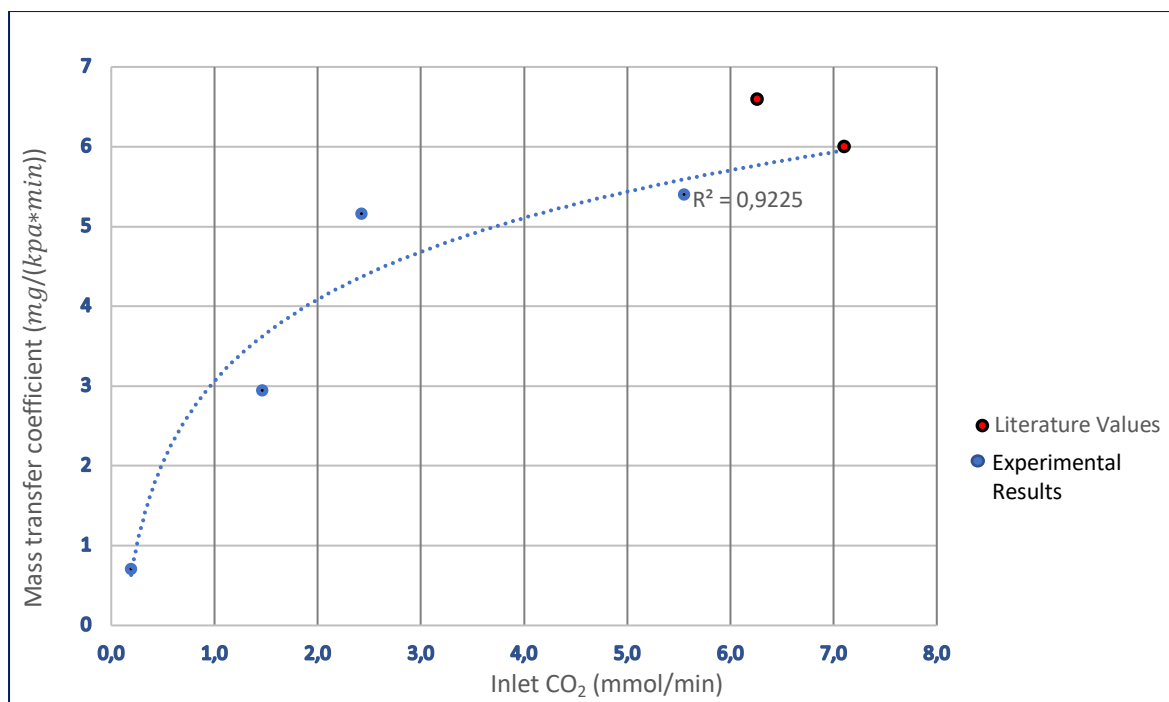
Figure 3: Relationship between CO_2 mass transfer coefficient and inlet CO_2 concentration in the Leoceed cartridge.

It is evident that the mass transfer coefficient for both cartridges is strongly dependent on the inlet CO_2 concentration, but mass transfer coefficients are typically dependent on the membrane material and the type of transporting medium, not inlet concentrations. The apparent dependence on concentration may indicate that there is a two-step process taking place during the dialysis procedure. There could be a reactive equilibrium in the liquid followed by mass transfer through the membrane. Higher CO_2 inlet concentrations will increase the rate of the forward reaction in the reactive equilibrium and subsequently increase the apparent overall mass transfer coefficient. This phenomenon merits further study in experiments purpose-designed to examine it, as its presence suggests that CO_2 dissolution/diffusion systems may be more accurately considered to be a multi-reaction equilibrium system.

The trendlines show an x-axis asymptote occurs when the carbonated water has reached an equilibrium — no further CO_2 removal from the liquid is possible. The y-axis asymptote represents the maximum possible mass transfer coefficient of the cartridge. The x-axis asymptote for the Braun cartridge occurs at a CO_2 concentration of approximately 7.33×10^{-4} mmol/L (corresponding pH $\approx$ 6.22). The y-axis asymptote for the Braun cartridge is at the maximum transfer coefficient value previously reported. Experiments conducted with the Leoceed cartridge did not use inlet concentrations near the asymptote points; therefore, the exact asymptote values cannot be accurately reported. However, the logarithmic trendline suggests that the values will be similar to those of the Braun cartridge.

The Braun and Leoceed cartridges were tested at dissimilar ranges of inlet CO_2 concentrations. However, by using the logarithmic trendlines to extrapolate values at inlet concentrations that were not tested, it can be determined that, on average, the Braun cartridge has a higher overall mass transfer coefficient for each respective CO_2 inlet concentration. This is counterintuitive because the Braun cartridge has a lower surface area than the Leoceed cartridge. Subsequently, the Braun cartridge should have a lower overall mass transfer coefficient. Thus, further experimentation is needed to obtain more data points and eliminate the need for extrapolating trend lines.

Similar results were found in literature for experiments that have been conducted on a Leoceed cartridge. However, the liquid that was used in those experiments was blood (Rubin et al., 2020). If the logarithmic profile for the Leoceed cartridge is extrapolated to match the inlet concentration that was used in the literature experiments, Figure 3 indicates the literature values are slightly higher than the experimental values. This is expected because in blood the CO_2 conversion to the bicarbonate ion is catalysed by the enzyme carbonic anhydrase. Therefore, the reaction rate producing hydronium and bicarbonate ions will always be higher in blood than in water, which would be expected to result in a higher apparent mass transfer coefficient in blood than in water.

ii.   Quantity of CO_2 removed

The volume of CO_2 that can be removed from the liquid each minute can be calculated based on the calculated mass transfer coefficients. In Figure 4 the relationship between CO_2 transferred cross the membrane and the water inlet CO_2 concentration is shown. For both cartridges the trend is linear and the equation of the line of best fit for the Braun cartridge is y = 0.725x - 0.0035 with an R^2 value of 1 while the equation for the Leoceed cartridge is y = 0.6449x - 0.0879 with an R^2 value of 0.9988. The high R^2 values for both graphs indicate that the data points are clustered close enough that both functions can be deemed valid to approximate the data.

To determine whether sufficient carbon dioxide is removed by the cartridge, the difference in the carbon dioxide content in the arteries and veins in the human body must be known. The arteries carry oxygenated blood that has a lower carbon dioxide content relative to the de-oxygenated blood found in veins. The concentration of carbon dioxide in arterial blood is 21.5mmol/L compared to 23.5 mmol/L in venous blood (Arthurs & Sudhakar, 2005). The difference in the carbon dioxide content between the venous and arterial blood is thus only 2mmol/L. The aim should be to remove this amount of CO_2 from the blood because excessive removal can lead to hypocapnia in the patient. Insufficient removal can result in accumulation of carbon dioxide in the blood, and the subsequent onset of hypercapnia in the patient.
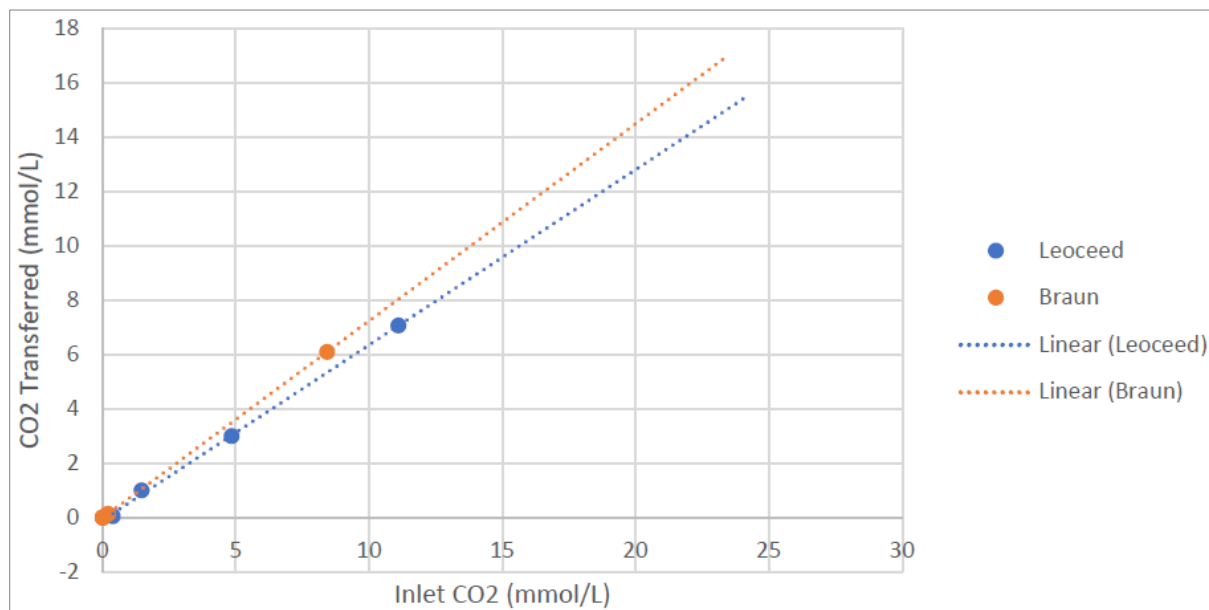
Figure 4: Relationship between CO_2 transferred (mmol/L) and water inlet CO_2 concentration (mmol/L)

Both cartridges remove too much carbon dioxide and are projected to remove as much as 16mmol/L of carbon dioxide from the water at a carbon dioxide concentration similar to that found in venous blood. Such excessive removal of carbon dioxide would be detrimental to a patient's health. However, this problem can be solved easily. The amount of carbon dioxide transferred across the membrane can be reduced by increasing the carbon dioxide content in the sweep gas. Consequently, the driving force for mass transfer of carbon dioxide across the membrane will be reduced and the aim of reducing the carbon dioxide concentration in the blood by only 2mmol/L can be achieved. COVID-19 patients frequently exhibit so-called 'silent hypoxia', a condition where SpO_2 is reduced without elevated CO_2 levels and discomfort typically associated with respiratory distress. Consequently, it can be argued that removing additional CO_2 is not necessarily desirable in many COVID-19 patients.

The "distilled water" provided for the experimentations had pH levels slightly below six. This suggests a presence of ions which may have detrimentally affected the results. The mass transfer coefficient for carbon dioxide in water in both cartridges is deemed sufficiently large to remove enough carbon dioxide from blood. However, adjustments will need to be made to the sweep gas to reach the target of removing 2mmol/L of carbon dioxide from venous blood. The mass transfer coefficient results highlight the potential of the technology and warrant further research on human blood (as opposed to water). The results from this study are not directly comparable to those that would be obtained through the use of blood, although they can be used to make a fair estimation.

131

iii.   Leakage and sieving coefficient results

Sieving coefficients were calculated at various dissolved solid inlet concentrations. The results plotted in Figure 5 below indicate that the sieving coefficient for the Braun dialysis cartridge fluctuates around 0.98. There is no trend in the sieving coefficient and the dissolved solids concentration has no effect on the sieving coefficient. This indicates that the sieving coefficient is independent of the original dissolved solids concentration.
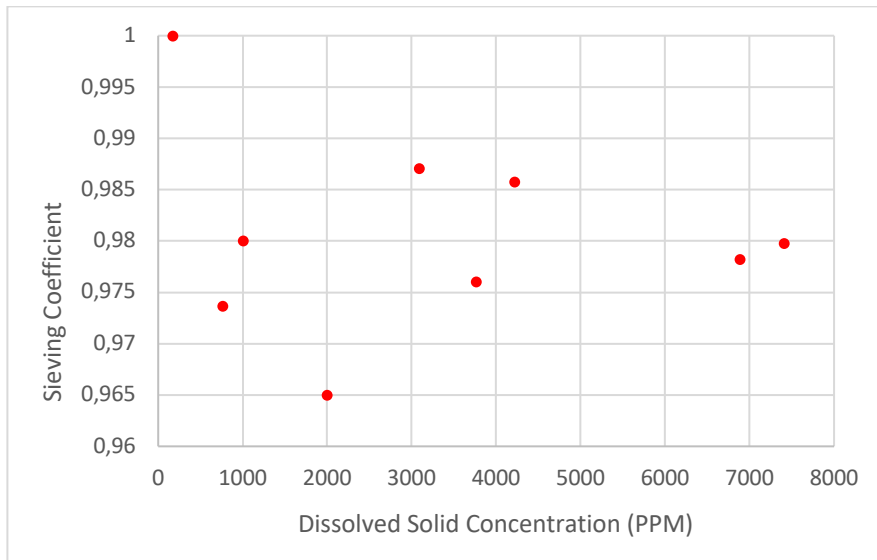

Figure 5: Relationship between the sieving coefficient and dissolved solid concentration

The electrical conductivity of the solution was measured alongside the dissolved solids concentration and the ratio of the electrical conductivity between the source and discharge was calculated. The average electrical conductivity ratio was 0.981 and was also unaffected by the varying levels of dissolved solids concentration. The electrical conductivity ratio was plotted against the sieving coefficient and a change in one of them led to a proportional change in the other. This is shown in Figure 6, and it validates the data collected during the experimentation, as one would expect the dissolved solids and electrical conductivity of the solution to decrease or increase proportionally. The loss of ions and dissolved solids can be attributed to accumulation inside the cartridge and the leakage that occurs.
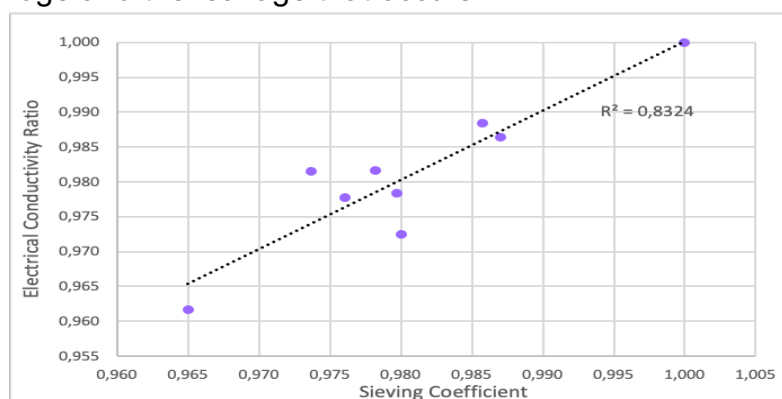

Figure 6: Correlation between the electrical conductivity ratio before and after the membrane and the sieving coefficient.

132

About 2% of the dissolved solids and ions in the water is lost when passing through the dialysis cartridge. In practice, when operating on a patient, there will be about a 2% loss in the blood products for each time the patients' entire blood volume passes through the cartridge. This a significant loss in blood products considering that some patients suffering from COVID-19 require oxygen therapy over a period of days and possibly weeks. If this method is to be used, the patient may require a drip or blood transfusion to supplement the loss of blood products.

CONCLUSION

The mass transfer coefficient for CO_2 permeating the hollow fibre membrane dialysers exceeds the minimum target for adequate CO_2 removal. This initially suggests the feasibility of the technology. However, some uncertainty about this result remains because the mass transfer coefficient was not constant over the range of pH levels at which it was tested. This is inconsistent with linear Fick's Law behaviour. This could indicate that a two-step process occurs such that a reactive equilibrium in the liquid occurs followed by the transfer of carbon dioxide through the membrane. This casts some doubt on the direct applicability of this result when operating with blood, because the liquid-phase reactions will have different reaction kinetics in blood. The haemodialysis cartridges have the potential to be used as a makeshift ECMO device in a resource constrained setting.

The sieving coefficient for the dissolved ions tested was calculated as 0.983, which suggests that those ions pass freely through the membrane material along with the solvent. This suggests there will be about a 1.7% loss in water-soluble blood products every time a patient's total blood volume is pumped through the cartridge, based on the observed leakage rates. These losses will have to be replaced, most likely intravenously. The results from this study are promising, but further experimentation using blood is required to determine mass transfer coefficients more accurately.

ACKNOWLEDGEMENTS

REFERENCES

Biga, L., Harwell, A., Hopkins, R., Kaufmann, J., LeMaster, M., Matern, P., & Morrison-Graham, K.   (2020). Transport of Gases. In L. Biga, S. Dawson, A. Harwell, R. Hopkins, J. Kaufmann & M. LeMaster et al., Anatomy and Physiology (1st   ed.).   Oregon   State   University.   Retrieved   from https://open.oregonstate.education/aandp/chapter/22-5-transport-of-gases/

Davis, C. (2021). Safe, Normal, Low Blood Oxygen Levels: Pulse Oximeter Chart. Retrieved 26 September 2021, from https://www.onhealth.com/content/1/normal_low_blood_oxygen_pulse_oximeter_levels

Dhont, S., Derom, E., Van Braeckel, E., Depuydt, P., & Lambrecht, B. (2020). The pathophysiology of 'happy' hypoxemia in COVID-19. Respiratory Research, 21(1). doi: 10.1186/s12931-020- 01462-5

Hulko, M., Haug, U., Gauss, J., Boschetti-de-Fierro, A., Beck, W., & Krause, B. (2018). Requirements and Pitfalls of Dialyzer Sieving Coefficients Comparisons. Artificial Organs, 42(12), 1164-1173. doi: 10.1111/aor.13278

Kliff, S., Satariano, A., Silver-Greenberg, J. and Kulish, N. (2020). There Aren't Enough Ventilators to Cope with the Coronavirus. Retrieved 17 November 2021, from https://www.nytimes.com/2020/03/18/business/coronavirus-ventilatorshortage.html

Leusen, I. (1953). Chemosensitivity of the Respiratory Center. American Journal Of Physiology-Legacy Content, 176(1), 39-44. doi: 10.1152/ajplegacy.1953.176.1.39

Rubin, D., Stacey, N., Matambo, T., Vale, C., Sussman, M., & Snyman, T. et al. (2020). Toward Respiratory Support of Critically Ill COVID-19 Patients Using Repurposed Kidney Hollow Fiber Membrane Dialysers to Oxygenate the Blood. Journal Of Healthcare Engineering, 2020, 1-6. doi: 10.1155/2020/8862645

Tobin, M., Laghi, F., & Jubran, A. (2020). Why COVID-19 Silent Hypoxemia Is Baffling to Physicians. American Journal Of Respiratory And Critical Care Medicine, 202(3), 356-360. doi: 10.1164/rccm.202006-2157cp

Vaporidi, K., Akoumianaki, E., Telias, I., Goligher, E., Brochard, L., & Georgopoulos, D. (2020). Respiratory Drive in Critically Ill Patients. Pathophysiology and Clinical Implications. American Journal Of Respiratory And Critical Care Medicine, 201(1), 20-32. doi: 10.1164/rccm.201903- 0596so

Whittle, J., Pavlov, I., Sacchetti, A., Atwood, C., & Rosenberg, M. (2020). Respiratory support for adult patients with COVID-19. Journal Of The American College Of Emergency Physicians Open, 1(2), 95-101. doi: 10.1002/emp2.12071

Loyola Medicine. (2020). Hypoxia Covid. Retrieved 17 November 2021, from https://www.loyolamedicine.org/about-us/news/new-study-explains-potentialcauses-for-happy-hypoxia-condition-in-patients-with-the-covid19-virus

Xu, L., 2020. Hollow Fiber Membrane Dialysers: Gas transfer properties of Hollow Fibre Membrane   Dialysers repurposed for respiratory support in critically ill COVID-19 patients. doi: 10.13140/RG.2.2.33285.83680

Zubieta-Calleja, G., & Zubieta-DeUrioste, N. (2020). Pneumolysis and "Silent Hypoxemia" in COVID-   19. Indian Journal Of Clinical Biochemistry, 36(1), 112-116. doi: 10.1007/s12291-020-00935-0

CHAPTER 14

DESIGN AND DEVELOPMENT OF A COST-EFFECTIVE CPAP DEVICE WITH OXYGENATION AND AN AUTOMATED MDI DELIVERY SYSTEM

Muhammad Arshad Eyasim, Sudesh Sivarasu
ORCID ID: 0000-0001-9571-6586, 0000-0002-0812-568X
Division of Biomedical Engineering
Department of Human Biology
University of Cape Town
Western Cape
South Africa

ABSTRACT

Patients suffering from Covid-19 and Chronic Obstructive Pulmonary Disease (COPD), or asthma comorbidities receive Continuous Positive Airway Pressure (CPAP) therapy as one of the treatment options. They additionally require regular administration of a bronchodilator medication using a Metered Dose Inhaler (MDI) to open the airways of the lungs to make breathing easier. However, some challenges have been identified with existing techniques of using MDI with CPAP; a nurse must remain at the bedside to manually time the actuations and actuate the MDI. One of the current methods does not provide Positive End-Expiratory Pressure (PEEP), thereby reducing the medication's effectiveness. The current global Covid-19 pandemic has resulted in the limited number of Intensive Care Unit (ICU) resources such as bedside nurses and ventilators. Therefore, a need for a device that can provide oxygenation and automated MDI medication delivery has been identified to reduce the number of ICU admissions, increase the effectiveness of MDI treatment, and reduce the number of patients requiring intubation. This design project entails the development of a prototype as well as verification and validation tests. The prototype was built by focusing on the functional blocks and iterating the core component of the design. The prototype was then verified and validated. It was found the Proof of Concept of the device meets the requirements and works as intended. In conclusion, the project highlights how the needs are met and the drawbacks of the design are identified. Recommendations are then made on the improvement of the device's functionality and usability features.

Keywords: CPAP, MDI, Bronchodilator, Automated, Covid-19, COPD, Asthma

NOMENCLATURE

COPD   Chronic Obstructive Pulmonary Disease
CPAP   Continuous Positive Airway Pressure
FiO_2 Fraction of Inspired Oxygen
ICU   Intensive Care Unit
MDI   Metered Dose Inhaler
PEEP   Positive End-Expiratory Pressure

INTRODUCTION

The number of cases in the current global Covid-19 pandemic is on the rise, and many of these patients have COPD or asthma comorbidities. Pneumonia and Hypoxemia in Covid-19 patients with pre-existing illnesses such as COPD or asthma are the disease state fundamentals of interest within the target group. Many people in the target group require oxygen therapy, such as CPAP therapy, as well as the delivery of a bronchodilator using an MDI. The MDI delivery is currently conducted using two methods. The first technique, shown in Figure 1, employs an inline MDI T-piece adaptor, which requires a nurse to manually time and actuate the MDI. The second approach, shown in Figure 2, necessitates the removal of the mask to administer the drug orally using an MDI spacer.

Figure 1: Inline MDI T-piece adapter (Armstrong Medical, 2021)

Figure 2: MDI spacer (Doyle & McCutcheon, 2021)

A study on the severity and mortality associated with COPD and smoking in patients with Covid-19 found that COPD patients had a higher severity risk of 63% compared to patients without COPD with a severity risk of 33.4%, and Covid-19 patients with COPD have a higher mortality rate of 60% (Alqahtani et al., 2020). Africa has the second highest prevalence of COPD in the world and Cape Town has the highest COPD prevalence in Africa (Blanco et al., 2019). The symptoms are worse for people who already have asthma when they are infected with the Covid-19 virus (Wiginton, 2021). Based on a recent study by Naidoo & Naidoo (2021) on scarce ICU resources, they found that approximately 16% of Covid-19 infected cases require ICU admission and that this percentage in a South African setting will put additional pressure on the country's ICU resources which are already in usage by other patients with medical conditions that require ICU support. Thus, the need statement formulated to address the problem identified is a way of addressing the delivery of MDI medication using a CPAP device by integrating an automated MDI delivery system, allowing for a

decreased number of ICU admission, increased effectiveness of MDI treatment and a decreased number of patients requiring intubation.

Currently, there is no commercial solution available to address the identified issue. The proposed solution is a CPAP device with oxygenation and an automated MDI delivery system. This device allows users to set CPAP and MDI settings such as inspiratory pressure, dosing frequency, and dosing interval. A prototype is to be built, verified and validated. The prototype must meet all user and design requirements, identified needs, and Proof of Concept.

MATERIALS AND METHODS

The design thinking 6-3-5 brainstorming method (Wilson, 2013) was used amongst six participants to ideate on various components of the device. The best ideas were collated, and nine concepts were generated. A final concept was obtained after selecting and screening the concepts.

i.   Functional Block of Prototype

After obtaining the final concept, functional blocks were identified based on the needs criteria for the preliminary step in the prototype development. The functional blocks are: a fan that can provide adjustable continuous pressure, a way to adjust and determine Fraction of Inspired Oxygen (FiO$_2$), an automated MDI delivery system, an easily accessible and reloadable medication canister, supplied air must be warmed and humidified, the device must provide PEEP and have safety features.

ii.   Technical Specifications

The technical specifications of the prototype are drawn using the specifications prescribed by the World Health Organization for non-invasive ventilators for Covid-19 (2020) as shown in Table 1.

Table 1: Technical specifications

CPAP device		MDI actuation device	
Pressure [cmH$_2$O]	3 to 20	Number of dosages	0 to 10
PEEP [cmH$_2$O]	5 to 20	Interval between dosages [hrs]	4 to 12
FiO$_2$ [%]	21 to 100		

iii. Design Iterations
o Fan outlet
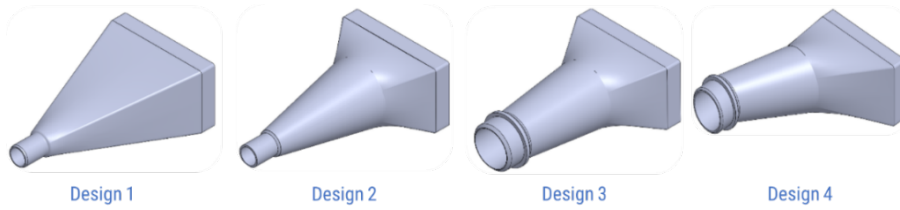The initial design iteration was conducted on the fan outlet, shown in Figure 3.

Figure 3: Fan outlet design iterations

The internal diameter was changed to 22mm after Design 2 to maintain a constant diameter across the system to minimise pressure drops. It was found that Design 4 is the best with the lowest backpressure and smoother readings.

- ○ MDI actuation device

The first iteration uses a lever arm that is placed directly on the canister end. When the lever rotates, it will press against the canister and actuate it. This design failed as the torque was too small causing the lever arm to be stuck on the canister end. The second iteration uses a slider-crank mechanism whereby the slider presses against the canister and actuates it. This design also failed as the force exerted onto the canister was too small. Servos with higher torque specifications were tried, but they also did not work. The last iteration uses a cam actuation mechanism to actuate the canister, as shown in Figure 4.
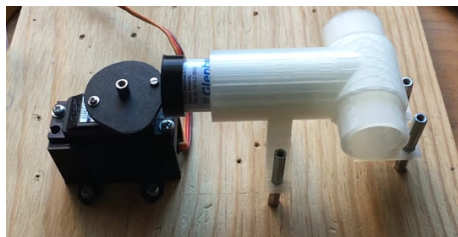

Figure 4: Cam actuation mechanism

This mechanism worked well. However, a cap had to be placed on the canister to enable actuation. Without the cap, the nose of the cam is jammed in the concave surface of the canister.

- ○ Prototype Construction

After all the iterations, coding, and components layout, the prototype was finally assembled using various off-the-shelf and 3D printed parts. Figure 5 shows the UI, the PEEP valve and the sliding door, Figure 6 shows the air inlet filter, Figure 7 shows the power and oxygen inlet and Figure 8 shows the dual circuitry ports.
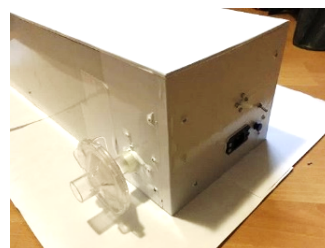

Figure 5: Front view of the prototype

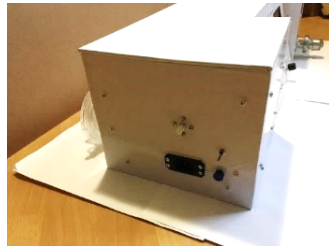*Figure 6: Rear view of the prototype*

Figure 7: Left view of the prototype

Figure 8: Right view of the prototype

- ○ Microcontroller and electrical connections

An Arduino Mega ATmega2560 microcontroller is used in the device as the controls system. Figure 9 shows the electrical layout of the Arduino connections with the other electronics.
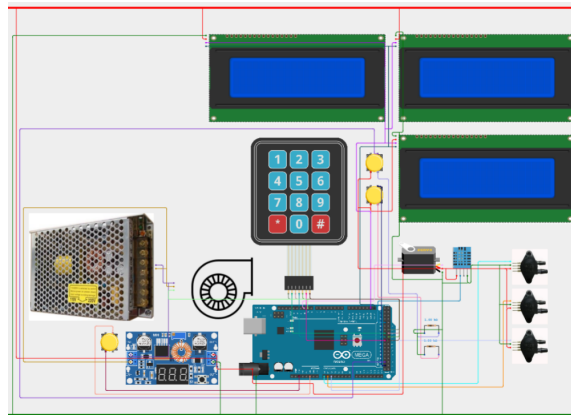

Figure 9: Device electronics connections

A DHT11 temperature and humidity sensor is used to monitor the temperature and humidity of the supplied air. The first pressure sensor is used in the feedback loop to regulate the CPAP settings. The second and third pressure sensors are used to measure the differential pressure across the Venturi flow meter along the air and oxygen stream respectively to in turn calculate the flow rate of gas in each stream.

- ○ Low Pass Noise Filter

A low pass noise filter was used for the pressure readings. Figure 10 shows the results from pressure readings before and after applying the low-pass noise filter.
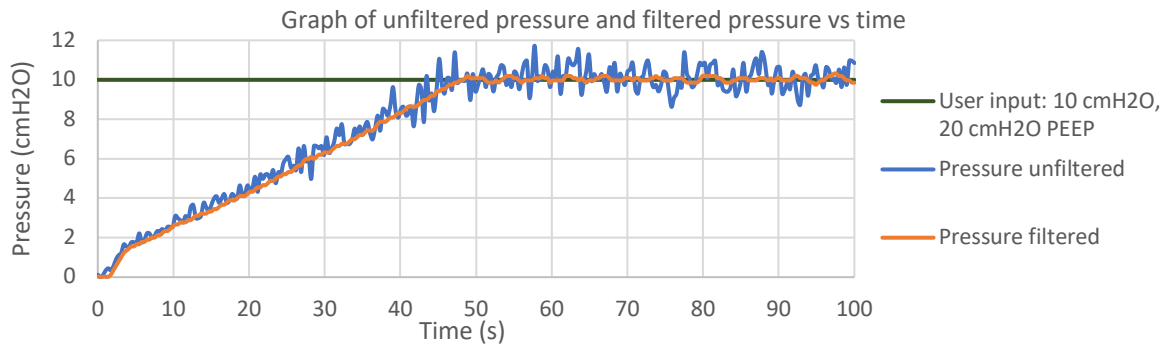

Figure 10: Unfiltered and filtered pressure vs time

Graph 1 shows that before applying the low-pass noise filter, the readings are very noisy. After applying the filter, the readings are smoother.

RESULTS AND DISCUSSIONS
   i.   Verification and Validation
   o   Provide Continuous Pressure Based on User Input
The verification test for the pressure specifications was conducted at the minimum pressure setting of 3 cmH_2O and the maximum pressure setting of 20 cmH_2O at a minimum PEEP of 5 cmH_2O and a maximum PEEP of 20 cmH_2O for each test. However, for a user input of 20 cmH_2O, the fan was not able to achieve this pressure at its maximum speed due to its specifications. Thus, the pressure range that can currently be achieved is 3 to 13 cmH_2O. This is mainly due to the fan specifications which can be changed for a higher specification fan.

The pressure is validated by comparing the pressure output of the device to the pressure supplied to the mask by measuring the pressure at the end of the circuitry which would be the same as the pressure delivered to the mask. Figure 11 shows the results.
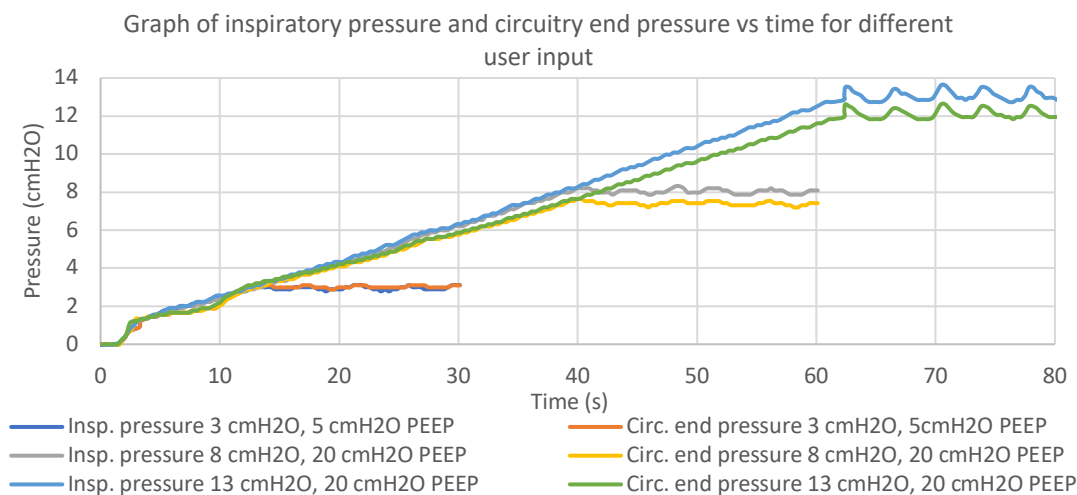

Graph of inspiratory pressure and circuitry end pressure vs time for different user input

Figure 11: Inspiratory and circuit end pressure vs time for different user input

Figure 11 shows that the inspiratory pressure is very close to the pressure at the circuitry end. However, the difference between the inspiratory and circuitry end pressure increases slightly with increasing inspiratory pressure. This difference can be accounted for by calibrating the fan. Hence, the inspiratory pressure produced, based on the user input, is validated as the pressure at the circuitry end is very close to the user input pressure.

   o   Actuation of MDI Based on User Input Settings
The MDI actuations were verified using the Arduino IDE serial plotter feature. Figure 10 shows the results for user input settings of two for the number of dosages and six seconds for the interval between dosages.
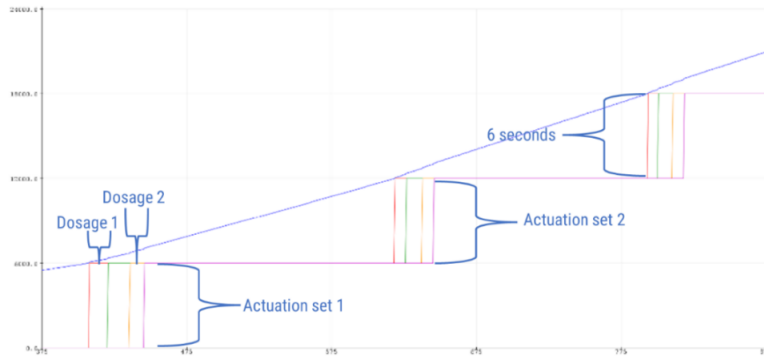
Figure12: MDI actuation signals

Figure 12 shows that the servo is actuated two times every six seconds. The MDI actuation test was conducted with a range of user input settings for the number of dosages and interval between dosages. It was found that the actuation of the MDI is working as intended based on the user input settings. The actuation of the MDI based on the user input settings is validated by testing the actuation at different user inputs and by visually confirming that the actuation occurred.

The validation was conducted by inputting a wide range of settings for the actuations and intervals between the actuations. The actuation was visually confirmed, and the serial monitor on the Arduino IDE software was then used to check the time. Thus, for each setting, when the servo was actuated, the "actuated" print and timestamp on the serial monitor of the Arduino IDE interface was also checked and found to be working as intended.

o Adjustable Fraction of Inspired Oxygen Level

Due to the scope of this project, the prototype was not tested with actual oxygen, but with air instead. Equation 1 was used to plot Figure 13 using the airflow rate at these specific pressures and using the standard oxygen wall supply flow rate of hospitals, which ranges from 0 to 15 Lpm (Ely & Clapham, 2003).

$$FiO_2 = \frac{O_2 \ flow \ rate + 0.2(Air \ flow \ rate)}{Air \ flow \ rate + 0.2} \tag{1}$$
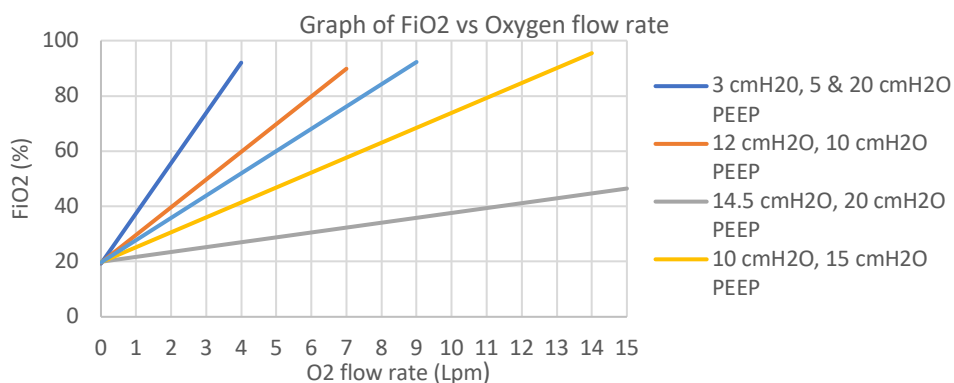

Figure 13: FiO2 vs time

Figure 13 shows a linear relationship between FiO_2 and oxygen flow rate. This graph is derived using air only. That is, right now 10 cmH_2O user input is achieved from air only, whereas in actual use with oxygen, the 10 cmH_2O would be a combination of the pressure exerted by the air-oxygen mixture which will together equal 10 cmH_2O. Therefore, in actual use, a user input of 10 cmH_2O means a lower pressure from the air supply, which would also be represented by a line of lower pressure in the current graph. Since all the pressure lines have the same relationship, the relationships between FiO_2 and oxygen flow rate in the current graph will still be valid in actual use, but at lower pressures.

As actual oxygen was not used for the tests, a secondary air source was used in place of oxygen to test for FiO_2. At the time of validation, few possible air sources were tested to be used instead of oxygen due to availability. However, their flow rates were higher or lower than the standard medical oxygen flow rates of 3 to 15 Lpm. Thus, to validate the FiO_2, an outlet air bypass was used at the circuitry which was then directed to the oxygen inlet of the air stream inside the device. The setup was then tested using different user inputs and the data on air and 'oxygen' flowrates were recorded and the FiO_2 was calculated using equation (1). Figure 14 shows the FiO_2 obtained for different user input pressures at 20 cmH_2O PEEP.
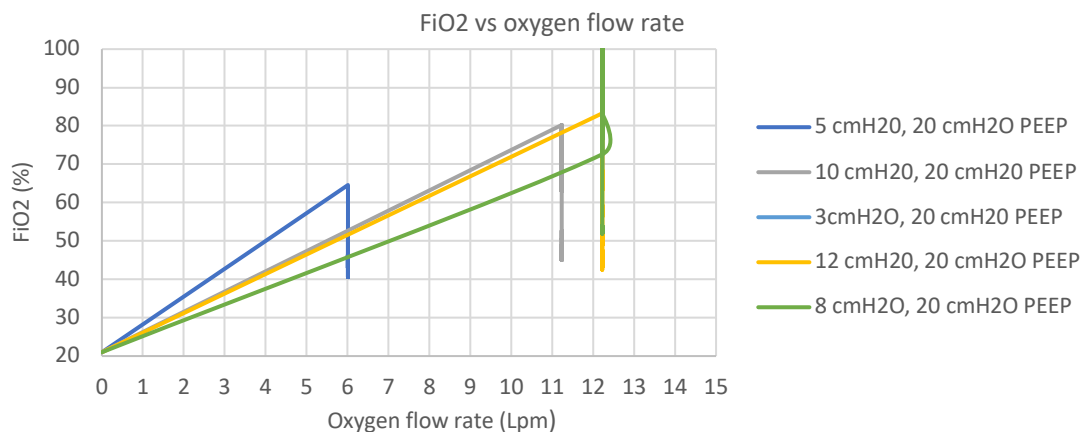
Figure 14: FiO2 vs O2 flowrate different user inputs

This graph shows the results for the FiO_2 at different pressure and O_2 flow rates. At each flow rate, the line was extended to 0 Lpm, 21%. The graph shows that at any user input, increasing the oxygen flow rate increases the FiO_2 and the fan simultaneously adjusts its speed to match the pressure and flow rate required to achieve the FiO_2 and pressure.

ii. Proof of Concept and Test results

The Proof of Concept of the prototype was met by verifying and validating whether the device can provide continuous pressure, actuate the MDI and adjustable FiO_2 based on user input. The maximum inspiratory pressure range that can currently be achieved with the device is 3 to 13 cmH_2O. It was also found that with increasing pressure the pressure at the mask is slightly lower than the output of the device. This

pressure drop is expected and can be calibrated by increasing the output pressure of the device slightly higher than the user input pressure so that the pressure at the mask is the same as the user input. The MDI actuation device was found to be working effectively and accurately in respect to time. Theoretically, it was verified that the adjustable FiO_2 will work. The test was then validated showing that the verification test and the validation test graphs are very similar. Thus, the working principle of this concept works. Hence, the Proof of Concept of the device was successfully met.

COSTING

The total cost of prototyping was R5 667. Considering the mass production of the device and various parts, the cost is expected to be reduced to R 4000. Thus, with a 25% markup, the retail price of the device to distributors will be R5 000. The developed device is cheaper than traditional CPAP devices without oxygenation, which cost upwards of R 8 900, but it is more expensive than CPAP devices that use air entrainment such as the Nippy 3+ or CPAP masks that cost upwards of R 4 800 and R 1 200 respectively (Afrimedics, 2021; Dotmed, 2021; Medex Supply, 2021). The device developed, which integrates an automated MDI delivery system, is thus considered to be cost-effective compared to both the cheaper and more expensive CPAP devices as they do not include the MDI delivery system. The cheaper CPAP devices have many limitations such as restricted flow rate in the Nippy 3+, and no display to monitor various parameters and fixed FiO_2 with CPAP masks.

DRAWBACKS

The drawbacks of the prototype are that the accuracy and sensitivity of the pressure sensors are unreliable, the fan specifications are too low for this application, the prototype is very large, it needs to be reset at power up for the Arduino to work and the reloadability of the MDI canister is not user-friendly.

RECOMMENDATIONS

Based on the prototype, the following recommendations on the improvement of the device are made: a way to substitute the cap needed for the MDI canister by using a different cam design that will not get jammed in the canister's concave end, a standard off-the-shelf flowmeter can be used for better accuracy and reliability, the flow dynamics of the device must be analysed and improved to increase the efficiency of the pressure delivery, the sliding door can be motorised for ease of use and to ensure it is closed fully, the reloading of the canister can also be improved by using an actuator that pushes the canister out for reloading and lastly, the device can be improved to detect inspiration and then actuate the MDI after the interval set.

CONCLUSION

A Proof of Concept for a CPAP device with oxygenation and an automated MDI delivery system has been successfully designed and developed. The device has been tested and validated to show that it works as intended. Based on its additional features, the device is cost-effective compared to existing solutions. This project presented a

methodology that can be used for further iterations to create improved commercial solutions. Further improvements were recommended to adapt the design to the global market in terms of functionality and ease of use.

ACKNOWLEDGEMENTS

REFERENCES

Afrimedics. (2021). Portable auto Cpap Machine DS-6 AUTO CPAP. Retrieved 25 September 2021, from https://www.afrimedics.co.za/product/portable-auto-cpap-machine-ds-6-autocpap/?sfdr_ptcid=13621_617_673695122&sfdr_hash=d18ffb68f5f2948fd794621db2bb5562

Alqahtani, J., Oyelade, T., Aldhahir, A., Alghamdi, S., Almehmadi, M., & Alqahtani, A. et al. (2020). Prevalence, Severity and Mortality associated with COPD and Smoking in patients with COVID-19: A Rapid Systematic Review and Meta-Analysis. *PLOS ONE*, *15*(5), e0233147. doi: 10.1371/journal.pone.0233147

Armstrong Medical. (2021). Spirale® Drug Delivery System. Retrieved 20 September 2021, from https://www.armstrongmedical.net/product/spirale/

Blanco, I., Diego, I., Bueno, P., Casas-Maldonado, F., & Miravitlles, M. (2019). Geographic distribution of COPD prevalence in the world displayed by Geographic Information System maps. *European Respiratory Journal*, *54*(1), 1900610. doi: 10.1183/13993003.00610-2019

Dotmed. (2021). For Sale NIPPY 3+ Ventilator. Retrieved 26 September 2021, from https://www.dotmed.com/listing/ventilator/nippy/3+/2281165

Doyle, G., & McCutcheon, J. (2021). Clinical Procedures for Safer Patient Care. Retrieved 20 October 2021, from https://opentextbc.ca/clinicalskills/chapter/inhaled-and-topical-medications/

Ely, J., & Clapham, M. (2003). Delivering oxygen to patients. *BJA CEPD Reviews*, *3*(2), 43-45. doi: 10.1093/bjacepd/mkg011

Medex Supply. (2021). Flow Safe II CPAP with large adult mask 5/Box. Retrieved 16 October 2021, from https://medexsupply.com/flow-safe-ii-cpap-with-large-adult-mask-5-box/?pid=104260

Naidoo, R., & Naidoo, K. (2021). Prioritising 'already-scarce' intensive care unit resources in the midst of COVID-19: a call for regional triage committees in South Africa. BMC Medical Ethics, 22(1). doi: 10.1186/s12910-021-00596-5

Technical specifications for invasive and non-invasive ventilators for COVID-19. Apps.who.int. (2020). Retrieved from https://apps.who.int/iris/rest/bitstreams/1275111/retrieve.

Wiginton, K. (2021). *Coronavirus and Asthma*. WebMD. Retrieved from https://www.webmd.com/asthma/covid-19-asthma.

Wilson, C. (2013). Using Brainwriting For Rapid Idea Generation. Smashing Magazine. Retrieved from https://www.smashingmagazine.com/2013/12/using-brainwriting-for-rapid-idea-generation/

CHAPTER 15
HOSPITAL OXYGEN TANK VALVE DEFROSTING SYSTEM

Jasveer Pillay, Aliya Singh, Kerina Virasamy,
Pragesh Govender, Riaan Stopforth
ORCID ID: 0000-0002-0640-7480, 0000-0003-1754-447X, 0000-0001-9837-7794,
0000-0001-5173-4379, 0000-0002-8878-2232
Stopforth Mechatronics
Robotics and Research Lab
University of KwaZulu-Natal
Durban
South Africa

ABSTRACT

This research aimed to develop a liquid oxygen tank valve defrosting system that could be used in hospitals to enable a steady supply of oxygen even during cold weather or periods of high oxygen demand. The system was intended to be used as a viable alternative to the hosing systems currently used in many South African hospitals by being partially autonomous and environmentally friendly in its design and operation. Based off conducted research and interviews from hospital personnel, focus was placed on developing a defrosting system that used flowing water to melt ice. The development of the defrosting system was successful, and the system was able to conduct the independent tests reliably. Although the conducted testing did not involve using the defrosting system on a real liquid oxygen gas tank's frozen valve, various analyses were conducted with respect to flow rate performance, effects of water loss and the degradation of performance due to cold temperatures. Based off practical testing on ice, it was concluded that the system should be able to perform similarly if used on the liquid oxygen tank valves of hospitals and that the defrosting system should theoretically prove effective even under high oxygen demand or cold weather. The developed defrosting system should be an effective solution to the stated predicament of frozen oxygen tank valves in hospitals and is theoretically a viable alternative to the hosing system currently used by many South African hospitals.

Keywords: liquid oxygen tank, gas tank, frozen valve, defrost valve, melt ice, spray water, shower, water pump, defrosting device, defrosting system

INTRODUCTION

The following sections outline the background, aims and objectives, review of existing systems, and research contributions.

i.   Background

The valves found in liquid oxygen tanks used in hospitals tend to develop a build-up of ice. In situations where there is a high demand for oxygen in a hospital or during cold weather, the ice accumulation hinders oxygen delivery to patients. The issue of frozen oxygen tank valves is more prevalent in recent times as there exists a higher-than-average demand for oxygen in South African hospitals during the COVID-19 pandemic (Anand, 2021; Poonipershad, 2021).

ii.   Aims and Objectives

In response to the above-mentioned scenario, this research aimed to develop a liquid oxygen tank valve defrosting system that could be used in hospitals to deliver a steady oxygen supply even during cold weather or periods of high oxygen demand. The system was intended to be partially autonomous and environmentally friendly in its design and operation to be a viable alternative to the hosing system generally used in South African hospitals. The following points list the objectives of the defrosting system design:

- The system was made to effectively defrost the oxygen tank valve, even during periods of high oxygen demand or cold weather.
- Predominantly COTS components were used to ensure the system could be easily implemented, maintained and be sustainable in its construction.
- A water recycling system was utilised by using a reservoir system, thereby contributing to a sustainable design, and reduced operational costs.
- The system was designed to be partially autonomous in its major functions.
- The system was designed to be easily incorporated into existing oxygen tank set-ups in most South African hospitals.

iii.   Review of Existing Systems

The defrosting system currently used by hospitals involves manually operating a hosepipe to spray water on the valves, which is done daily for approximately one hour (Anand, 2021). Based off interviews conducted, the hosepipe system could be improved by automating most of the process and using a more sustainable design that reduces water wastage (Anand, 2021; Poonipershad, 2021). KJM Industries have implemented a system of showers to defrost ice from oxygen tank vaporisers during the COVID-19 pandemic (Matheson & KJM, 2021). Their reasoning for implementing their system was that it allowed defrosting without the need for heaters, which are considered hazardous near oxygen tanks (Matheson & KJM, 2021). KJM Industries' system was designed to defrost the vaporisers of oxygen tanks, and it is unproven to be a viable solution for defrosting oxygen tank valves.

Based on the research conducted, it was understood that valves found in liquid oxygen tank systems are known to freeze in addition to the vaporiser unit and its piping (Matheson & KJM, 2021). The oxygen tank components known to freeze were confirmed through investigative research and consultations with hospital

personnel (Anand, 2021). It was determined that the vaporiser was most prone to freezing and the vaporiser-tank valve was least prone to freezing. However, a frozen vaporiser-tank valve would hinder oxygen delivery more so than when the other components freeze (Anand, 2021). Hence, the focus was placed on designing the defrosting system to defrost oxygen tank valves and not the vaporiser or other components.

Freeze protection valves are used in systems to prevent or reduce ice build-up (Thermomegatech, 2011). Freeze protection valves are typically used in water-based systems, such as water inlet or supply piping (Hughes, 2021). Freeze protection valves can be considered a commercially-off-the-shelf (COTS) component, hence provided that the freeze protection valve is of appropriate compatibility with the oxygen tank, it can be installed with relative ease (Thermomegatech, 2011). Freeze protection valves were not included in the design as it was unproven to be a suitable solution to the freezing of liquid oxygen tank valves as freeze protection valves are commonly used in water-based applications (Hughes, 2021).

In many industrial applications, valves are enclosed in blanket heaters or heated enclosures known as "hotboxes" (Pape & Watlow, 2008). These heating enclosures are typically made from silicone rubber and contain heating elements that generate heat within the enclosure around the valve (Pape and Watlow, 2008). Alternate systems used to heat valves with external heat sources include using heating element designs such as tubular, cable or cartridge heaters (Pape & Watlow, 2008). These heating element designs are generally placed in direct contact with the valve or in the open air near the valve (Pape & Watlow, 2008). Though the heating solutions mentioned above have proven efficient in many applications, external heat sources are not favourable solutions when designing for systems in close proximity to liquid oxygen (Dugdale, 2020). Liquid oxygen is highly combustible, and fire hazards are not allowed near systems using liquid oxygen (University of Florida, 2016). Though the external heat sources do not produce an open flame, it can be considered a safety hazard (University of Florida, 2016). For these reasons, external heat sources were not used in the defrosting system's design.

iv.   Research contributions
The contributions of this research are the following:
- The development of a new defrosting system to address the issue of hospital oxygen tank valves freezing.
- Implementation of water-saving subsystems in the defrosting system to reduce operational costs and environmental damage compared to current solutions.
- Implementation of autonomous functionality in the defrosting system to

ensure practical and reliable operation compared to current solutions.

- Predominant use of COTS components in the defrosting system to ensure that the system can be assembled and implemented with relative ease.

MATERIALS AND METHODS

The following sections outline the development of the defrosting system's design, and the testing methodology used for each of the practical tests that were conducted.

i.   Development of the defrosting system's design

After taking the research and interviews conducted with hospital personnel into consideration, a defrosting system was designed to spray water onto the valve to defrost it. The method of spraying water on frozen components was an effective method in defrosting oxygen tank vaporiser units and could be applied to the valve system, which would have a similar frost build-up to the oxygen tank vaporiser (Matheson & KJM, 2021). This defrosting method was confirmed to be used by hospitals in South Africa as interviews were conducted with hospital workers (Anand, 2021; Poonipershad, 2021). Hence, this research's defrosting system should be effective in defrosting the valves of the oxygen tanks as it makes use of similar water spraying solutions.

The system was intended to be made from predominantly COTS components to ensure it could be easily implemented, maintained and be sustainable in its construction. The design was composed entirely of COTS components and only requires components such as rigid-polyvinyl-chloride (RPVC) piping and pump tubing to be cut to appropriate lengths. Table 1 depicts the major COTS components used in the defrosting system's construction.

Table 1: Defrosting System COTS Components

Component	Product Name	Product ID/Barcode	Supplier	Qt	Price
Water Reservoir	Stack & Store 22LT	0065	Just Plastics	1	R89.90
Nozzle	G/Master Nozzle Snap	6009694539869	Builders	1	R36.75
Pump Tubing	Waterfall MX12MM Clear Tubing	06009801316796	Makro	1	R78.99
Water Pump	Water pump 2 Core Flow 1500 3M	6920042803091	Builders	1	R698.00
Water Containment	Sheeting Alpex WHT 1.5MX1M 250MIC	00017278	Mambo's Storage	1	R22.99

Covers (Plastic Sheeting)			& Home		
Water Containment Covers (Rigid Acrylic)	Point of Sale Screen	N/A	Rusticworx (Online)	1	R385.25
Zipper	Haberdashery Misc 202	N/A	Craft Concept	2	R11.00

Adhesive for Framework	HASULITH	N/A	Craft Concept	1	R90.00
Cable Tie Connectors	Quick Ties Cable Ties (4.8X200MM)	9415886937028	Builders	1	R49.00
Power-Outlet Timer	MajorTech Timer Digital 8 On/Off MTD7	6008229002182	Builders	1	R340.00
Cord	Extension Lead HD SBS 1.5MMX10M WHT	6002844060022	Builders	1	R260.00
Electrical Outlet Box	ONESTO Outdoor Enclosure Large	OPS02	Electra Lighting & Electrical	1	R94.00
Frame Tubing	Pipe PVC 40MMX6M	PLT-1250	Plumbit (Online)	1	R107.67
Frame Connectors	BEND 87.5D PL SW 40MM	6001566019479	Builders	4	R11.00
Wire Grate	Fence Welded Mesh 50X50 (1.8M) (1.6M)	N/A	DIY Shop (Online)	1	R50.00

The system was designed for recycling most of the water used to spray the valve. The reservoir system implemented into the design was comprised of a reservoir base, water pump and water containment cover. Theoretically, most water would be recycled into the system effectively as the water containment covers would redirect most of the water into the reservoir. Additionally, components such as the wire grate, electrical outlet box and water containment covers were chosen and implemented with careful consideration to the risk management of the system in accordance with ISO 14971:2007, as each component ensured safety of the user and surrounding equipment during operation (ISO, 2007).

A key objective of the defrosting system was to design it to be incorporated into a variety of oxygen tank set-ups found in most South African hospitals. Through research and interviews with hospital workers, the dimensional constraints of the oxygen tank set-up were approximated, and a system could be designed to fit most scenarios. The dimensional constraints used were 1m x 0.3m x 0.2m and were obtained through interviews with hospital personnel and on-site measurements taken at King George Hospital (Anand, 2021). Additional design considerations were taken into account to accommodate oxygen tank set-ups that were not typical as the components that make up the defrosting system design can be cut to shorter lengths, or alternate components can easily be sourced and incorporated. Having components that could easily be dimensioned and swapped for more suitable alternatives was made possible because it was made entirely from COTS components. Hence, none of the parts would need to be specially manufactured to fit specific scenarios.

The design of the defrosting system can be seen in Figure 1. Figure 1 does not depict the electrical cabling and digital timer that would be present in the completed defrosting system design.
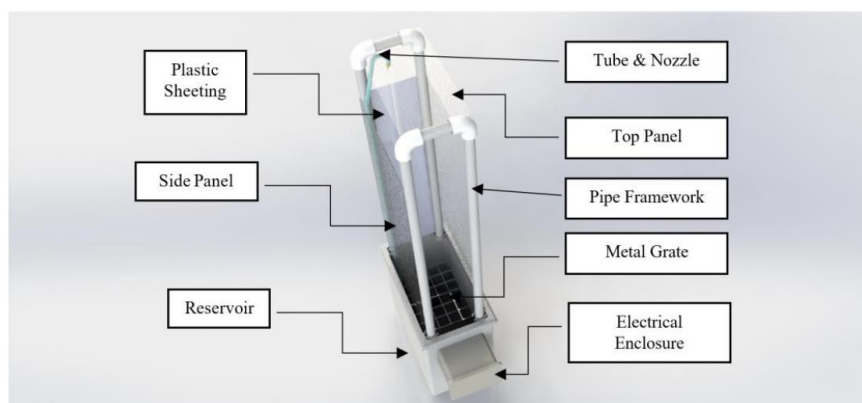

Figure 1: Design of defrosting system

To determine the preliminary performance of the defrosting system, a prototype version of the system was developed for experimentation. Three general tests were devised, and the objectives of the experiments were to determine the actual flowrate of the water pump in the given configuration, the approximate rate of water loss during operation, and to determine if cold water temperatures would significantly reduce the effectiveness of the defrosting system. Measuring tape was used to measure the different head heights, a stopwatch was used to record the time and a thermometer was used to record the water temperature. Three different tests were conducted using different experimental procedures to achieve the desired set of data and are briefly elaborated on in the following sections. The general set-up for the experiments can be seen in Figure 2. Each of the three tests were conducted with consideration to the risk management of the system in accordance with ISO 14971:2007, as the different electrical cables and relevant connections were encased or kept away from water sources during operation (ISO, 2007).
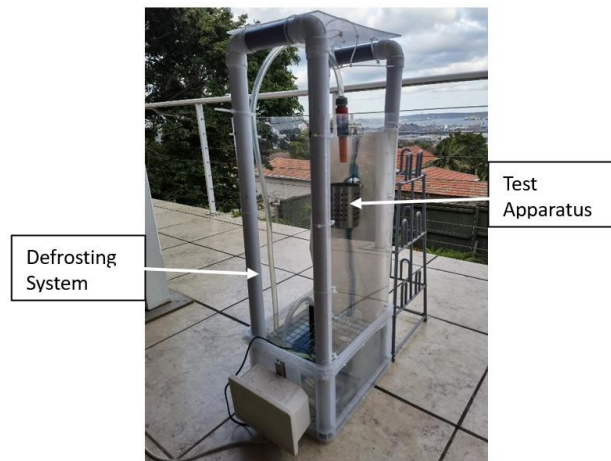

Figure 2: General set-up for experiments

ii.   Testing methodology for flow rate test

The defrosting system prototype was filled with water and the water pump was switched on. The outlet was held at varying head heights and the time taken to fill a 250ml cup was recorded. This procedure was repeated at an alternate pump setting to gauge the performance range of the pump under the specified conditions.

iii.   Testing methodology for water loss tests

The water loss tests involved conducting three separate tests. Two tests were to evaluate the water lost due to water splashes. Each test was conducted on the same prototype but with and without a front panel. This was done to evaluate if it was necessary to include a front panel in the design. The tests were conducted by measuring the difference in water level head height of the reservoir after allowing the system to operate for 24 hours. The final water loss test was done to evaluate on average how much water would be lost due to evaporation, hence the reservoir of the prototype was filled and left to stand for approximately four weeks. The new water level height was thereafter recorded with a tape measure.

iv.   Testing methodology for temperature test

This test involved measuring the time taken for the prototype system to melt crushed ice in a perforated container. The time taken to melt through approximately 0.12m of ice as well as the time to melt all the ice in perforated container were recorded separately. These steps were repeated numerous times to allow the melted crushed ice to gradually lower the temperature of the reservoir water and therefore yield different data in each iteration. The entire procedure was conducted once more to ensure consistency of results.

RESULTS AND DISCUSSION

The following sections outline the results obtained from each of the tests conducted on the prototype design followed by a brief analysis of the data.

i.   Results and discussion for flow rate test

The experimental procedure for the flow rate test was performed and the results can be seen in Figure 3 and Figure 4. The average time to taken to fill the 250ml container was recorded at different pump settings and head heights and is represented graphically in Figure 3.
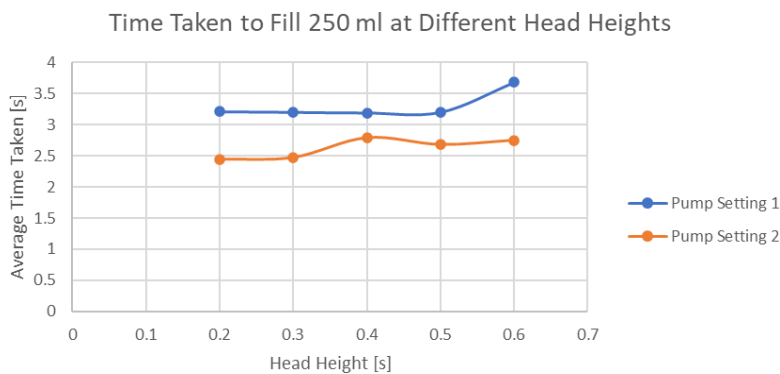

Figure 3: Graph for time taken to fill 250ml at different head heights

The corresponding flow rate for each reading was calculated based off the average time taken to fill the 250ml container and the results are represented graphically in Figure 4.
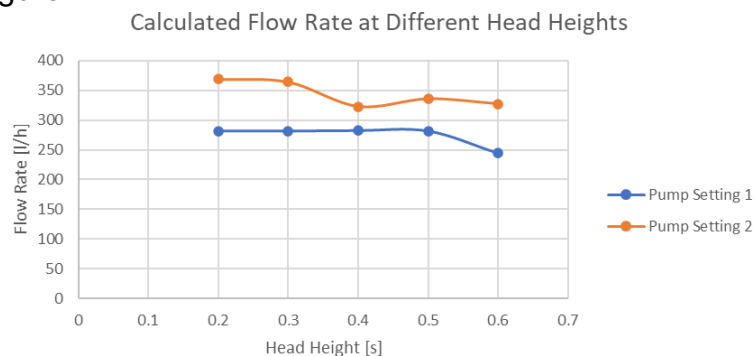

Figure 4: Graph for calculated flow rate at different head heights

Analysis of the flow rate test showed that the defrosting system did not deliver a constant flow rate of 1000 l/h, but rather delivered a maximum flow rate of 281.25 l/h at pump setting 1 and a maximum flow rate of 368.85 l/h at pump setting 2. Both settings delivered their maximum respective flow rates at the lowest head height tested which was 0.2 m. This was in accordance with theoretical expectations as lower head heights would provide better pump performance. Despite the defrosting system not reaching the target flow rate, it still performed as expected in melting ice as can be seen in following tests. A possible reason for why a flow rate of 368.85 l/h is sufficient despite the not meeting the target specification is likely due to the target being set higher than needed for the required task. The target specification was obtained from the flow rate used at hospitals. Possible reasons for the under-performance of the pump, despite having a marketed operating flow rate of 1500 l/h, could be due to the pump being defective, inaccurate testing or equipment, or the pump being incorrectly configured.

ii.   Results and discussion for water loss tests

The experimental procedure to find the amount of water lost due to splashing was performed and the results can be seen in Table 2. The initial and final water levels for each system set-up was recorded and the amount of water lost was calculated.

Table 2: Water lost due to splashing test results

System Set-up	Initial Water rLevel [m]	Final Water rLevel [m]	Water Lost in Head [m]	Water Lost in Vol. [litres]
Without Panel	0.155	0.130	0.025	2.4050
With Panel	0.160	0.159	0.001	0.0962

The experimental procedure to find the amount of water lost due to evaporation was performed and the results can be seen in Table 3. The initial and final water levels were recorded, and the amount of water lost was calculated. The test was conducted in Durban, South Africa, between 23 September 2021 and 21 October 2021. The average temperature, humidity and dew point during the testing period was approximated based off data from TimeAndDate (2021).

Table 3: Water lost due to evaporation test results

Initial Water Level [m]	Final Water Level [m]	Water Lost in Head [m]	Water Lost in Vol. [litres]	Average Temp. [°C]	Average Humidity [%]	Average Dew Point [°C]
0.150	0.078	0.072	6.9264	20.5	76	15.5

Analysis of the water loss tests yielded results that aided in predicting expected water loss under different conditions. It could be seen that prior to the addition of the front panel, the water lost due to splashes of water during operation would have been significant, as it lost 0.025m of height in terms of water level. Without additional water added, the reservoir would have lost approximately 0.065m head of water in 2.6 days, hence the pump would not be able to function with a water level of 0.085m. The addition of the front panel significantly reduced the amount of water lost due to splashing during operation. In contrast, it saved approximately 96 % of the water lost prior to the modification.

The water loss test regarding the water lost to evaporation showed one example of the amount of water that could be lost given the conditions specified in the test. This value is significant but is only applicable to specific scenarios as the result was highly dependent on environmental factors such as the temperature, humidity and dew point within a specific location and time range. Further testing in operation would need to be conducted to determine if the added water in the form of ice, as well as from naturally occurring rainwater would make up for the water loss.

iii.   Results and discussion for temperature test

The experimental procedure for the temperature test was performed twice and the results can be seen in Figure 5 and Figure 6. The time to taken to melt the crushed ice at different water temperatures and the developed moving average trendline in both tests is shown in Figure 5.
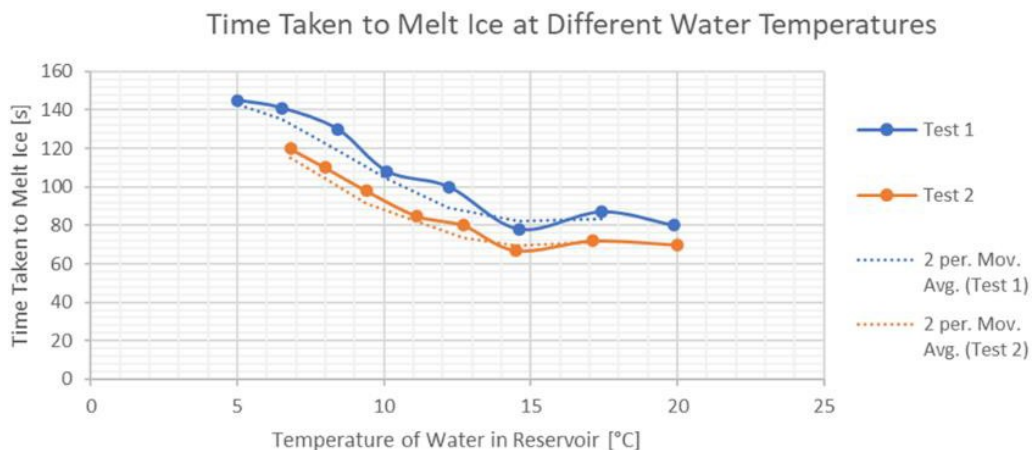

Figure 5: Graph of time taken to melt ice at varying temperatures

The time taken to melt the 12mm ice layer at different water temperatures and the developed exponential trendline in both tests is shown in Figure 6.
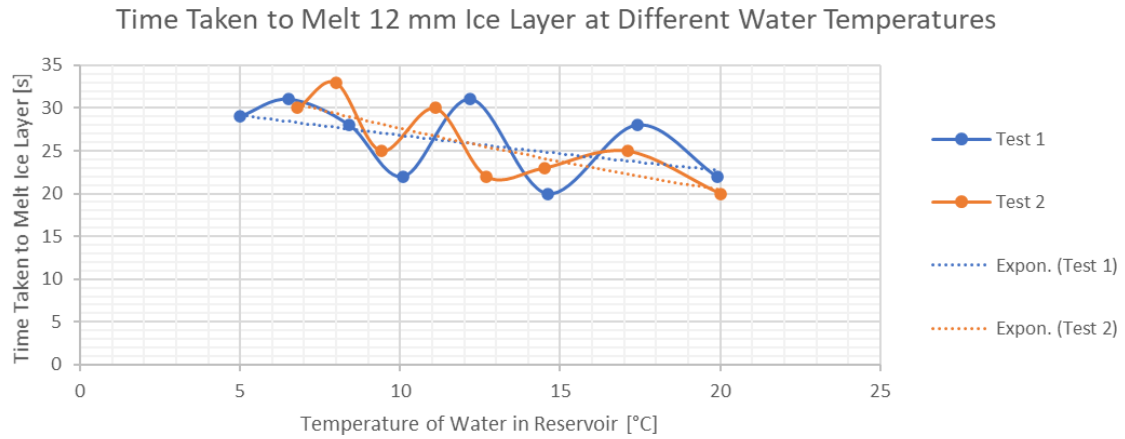
Figure 6: Graph of time taken to melt 12mm ice layer at varying temperatures

Statistical analysis was conducted on the temperature test data for Test 1 and Test 2 with respect to the recorded time readings. The results can be seen in Table 4 and Table 5.

Table 4: Test 1 statistical analysis of temperature test

	Time to Melt Ice [s]	Time to Melt 12mm Ice Layer[s]
Mean	108.625	26.375
Variance	640.98	16.73
Standard Deviation (σ)	25.32	4.09
Confidence Level (99%)	108.625 ± 23.058	26.375 ± 3.726
Outliers	80, 78, 141, 145	20, 31

Table 5: Test 2 statistical analysis of temperature test

	Time to Melt Ice [s]	Time to Melt 12mm Ice Layer[s]
Mean	82.25	26
Variance	194.69	18
Standard Deviation (σ)	13.95	4.24
Confidence Level (99%)	82.25 ± 12.708	26 ± 3.864
Outliers	67, 98, 110	20, 30, 33

Statistical analysis of the time taken to melt ice, corresponding to Figure 5, Table 4, and Table 5, yielded the following results: the mean, variance and standard deviation were 108.625, 640.98 and 25.32 respectively for Test 1 and 82.25, 194.69 and 13.95 respectively for Test 2. Hence, there were significant differences in the calculated statistical values for Test 1 and Test 2 and such discrepancies could have been attributed to environmental factors that weren't considered or human error. However, their respective trendlines as seen in the graphical representation of the tests display similar trendlines, and thus those were used for further analysis.

Statistical analysis of the time taken to melt the 12mm ice layer, corresponding to Figure 6, Table 4, and Table 5 yielded the following results: the mean, variance and standard deviation were 26.375, 16.73 and 4.09 respectively for Test 1 and 26, 18 and 4.24 respectively for Test 2. It was observed that both tests yielded relatively consistent statistical values, and thus the data was used for further analysis.

The tests conducted to analyse the effects of increasingly colder reservoir water temperatures on the overall effectiveness of the system's ability to melt ice was useful. In the test conducted to see the time taken to melt the entire container of ice, a similar graph shape was observed between both separately conducted tests. This observation was confirmed by noting the identical shape of both tests' moving average trendlines. It could be observed that although the effectiveness of the system's ability to melt the container of ice was reduced with colder reservoir temperatures, the differences were not of concern as it was never entirely or practically ineffective. The difference in time was approximately one minute to melt the ice in the container.

The temperature test also yielded results for the time it took to melt a 12mm layer of ice in the container, and it showed that, at the warmest reservoir temperature, it took an average of 20 seconds to melt, whereas at the coldest temperature, it took an average of 30 seconds. These results are acceptable as the rate of ice melting was decreased but did not make the defrosting system ineffective.

CONCLUSION

The defrosting system design successfully developed and fulfilled the aims and objectives of this research. The defrosting system was developed to use water sprays as the method of defrosting based off conducted investigations. The physical defrosting system was successfully constructed and used for independent testing. Practical tests were conducted using the defrosting system on ice which demonstrated that the system could reliably melt ice at varying water temperatures, despite using an under-powered pump. Analysis of the water loss tests showed that the defrosting system's water containment covers retained roughly 96% of water that would have been lost due to splashes, thereby ensuring much of the water could be recycled. The developed defrosting system should be an effective solution to the predicament of frozen oxygen tank valves in hospitals and should theoretically be a viable alternative to the hosing system employed by South African hospitals currently.

The contributions of this research were achieved in the following ways:
- A defrosting system for hospital oxygen tank valves was developed that was fundamentally different from the known solutions used generally by South African hospitals and should meet required design specifications.

- The defrosting system design ensured little water would be lost during operation by use of a water pump, reservoir, and splash covers, as confirmed through independent testing.
- The defrosting system design used a digital outlet timer to ensure that the pump would autonomously operate at specified time intervals, thereby ensuring the defrosting system would operate with minimal human input.
- The defrosting system design was comprised entirely from COTS components, thereby reducing manufacturing and assembly complexity.

ACKNOWLEDGEMENTS

REFERENCES

Anand, M. (2021, April 26). Artisan Foreman at King George Hospital. (J. Pillay, Interviewer)

Dugdale, D. (2020, December 1). Oxygen safety: MedlinePlus Medical Encyclopedia. Medline Plus. https://medlineplus.gov/ency/patientinstructions/000049.html

Hughes. (2021). Freeze Protection Valve. Retrieved April 2, 2021, from https://www.hughes- s afety.com/freeze-protection-valve.html

ISO, 2007. ISO 14971: 2007 Medical devices- Application of risk management to medical devices. [Online]. Available at: https://www.iso.org/standard/38193.html. [Accessed 20 October 2021]

Matheson & KJM. (2021, March 30). COVID Readiness - Bulk Hospital Vaporiser Guidance. Retrieved from https://hcai.ca.gov/wp-content/uploads/2020/12/02-Pressure-Drop-12-22-20.pdf

Pape, J., & Watlow. (2008, April 1). Using Heat to Protect Valves | 2008-04-01 | Process Heating. Using Heat to Protect Valves. https://www.process-heating.com/articles/86464-using-heat-to-protect-valves

Poonipershad, D. (2021, April 28). Specialist Anaesthetist at St Augustine's Hospital. (J. Pillay, Interviewer)

Thermomegatech. (2011, November 30). Freeze Protection Valves Keep Your Water Lines from Freezing. https://www.thermomegatech.com/freeze-protection-valves/

TimeAndDate. (2021, October 26). *Climate & Weather Averages in Durban, South Africa*. https://www.timeanddate.com/weather/south-africa/durban/climate

University of Florida. (2016, December 2). Liquid Oxygen » Environmental Health & Safety » University of Florida. Information Specific to Liquid Oxygen. https://www.ehs.ufl.edu/programs/lab/cryogens/oxygen/

CHAPTER 16
DEVELOPMENT OF A PEEP (CATPUL) VALVE FOR VENTILATORS: A COMPUTATIONAL APPROACH

Uchenna Ogemdi Okwuosa, Oscar Philander
ORCID ID: 0000-0003-1779-935X, 0000-0002-6702-6913
Adaptronics AMTL
Cape Peninsula University of Technology
Cape Town
South Africa

ABSTRACT

A major manifestation of the Covid-19 virus is acute respiratory syndrome. This brought about the massive need for respiratory support devices. The pandemic caused shortages of these critical devices, such as PEEP valves, which every ventilator must have to make supporting Covid-19 patients possible. PEEP valves are used to create a positive exhalation end pressure to prevent the patient's lungs from collapsing. This paper presents the developed a CATPUL PEEP valve designed to meet the South African and African continent markets. The CAD model of an AmbuPEEP valve and the CATPUL was designed with SolidWorks and CFD analysis was performed using Simscale software to characterise and compare the results of the two valves. The result of Ambu valve at 2mm valve opening was 1931 Pa pressure and29.74 m/s maximum flow velocity. The CATPUL recorded a maximum pressure of 1937 Pa and 29.77 m/s maximum velocity at the same valve opening. This shows that the designed valve outperformed the one on the market in terms of flow across the valve based on the computational analysis.

Keywords: PEEP, valve, CFD, Covid-19, Expiratory, Exhalation, Lungs, alveoli.

NOMENCLATURE

CAD	Computer Aided Design
CPAP	Continuous Positive Airway Pressure
PEEP	Positive End Expiratory Pressure
D	Diameter
d	Diameter
CFD	Computational Fluid Dynamics

INTRODUCTION

Resuscitating equipment is highly needed in an emergency facing health care systems all over the world. The outbreak of Covid-19 made these obvious and exposed deficiencies and unpreparedness in responding adequately to the demands of respiratory support. The unforeseen pandemic caused a shortage of ventilators and other respiratory support devices. These still mounting pressures on health care facilities all over the world is causing a global scramble for these limited supplies (Brierley, 2020). The South African Minister of Trade and Industry identified continuous positive airway pressure (CPAP) respiratory support device as important and critical to save lives in South Africa (Roelf, 2020). This assertion was made due to the nature of respiratory support needs arising from coronavirus infection. CPAP is needed to keep the lungs of a Covid-19 patient open to allow easy breathing by generating positive end expiratory pressure (PEEP) (Meara, 2020). Meara reported the importance of CPAP in combating Covid-19. Among them is its use at the early stages of infection to improve respiratory conditions. This will prevent critical situations requiring invasive devices. This report was corroborated by the research work done by Ashish et al. (2020). CPAP gained attention due to its ability to generate PEEP on a continuous basis to prevent the lungs from collapsing. This is particularly needed when about 15% of the Covid-19 patients need oxygen therapy and 5% will be critically ill as reported by Schutz, (2020).

Positive End Expiratory Pressure (PEEP) valves, as reported by McEvoy (2020), have been in existence since 1938. It has played a great role in the treatment and management of patients suffering from acute respiratory syndrome (Harman, 2020). The success and its usefulness are being amplified during the Covid-19 pandemic as an add-on to the mechanical ventilator to improve oxygenation of patients (Mason, 2014).

Prior to the Covid-19 pandemic, the African continent had no local capabilities to design and manufacture this device. This, as observed by the author, left the continent to the mercy of the West for the supply of this device. Due to the global shortage, companies like (EPCM: an engineering design and project management company), CapeWell, etc. (EPCM, 2020), institutionally based research centres (TIA Adaptronic AMTL: a research centre in CPUT, etc.), groups (Umoya, etc.), companies (EPCM and Medical Marine Offshore, etc. and individuals in South Africa (Roelf, 2020), and other African countries like Rwanda (Xinhua, 2020), swiftly sprang into action to produce ventilators and accessories in response to the challenge. This actionable response sees some of these companies' producing ventilators and accessories using locally sourced materials and skills.

To ensure adequate internal response, the South African government rolled out research and development funds towards developing local capabilities. All these efforts culminated into Umoya developing an adjustable PEEP valve and ventilator. Capewell, on the other, hand focuses on the spring of the PEEP valve using funds

from the South African government (PtSA, 2020). As part of South African agencies' response to the demand of PEEP valves, merSETA is currently funding a capacity building project meant to equip learners with the skills needed to respond effectively to produce medical related devices, including the PEEP valve.

Different parties, including researchers around the world, in an attempt better tackle the Covid- 19 virus, developed PEEP valves adaptable to different ventilators. The inline PEEP valve from Bunting et al. (2020) was used on a differential multi-ventilator to maintain adequate positive pressure at the exhalation end without venting the air to the atmosphere. During the development of a ventilator, Boire et al. (2021) also developed a solenoid-controlled PEEP valve with a record maximum performance error of 0.1 cmH2O during testing. However, considering the airways resistive pressure drop, the study by Hartung et al. (2016) to determine the errors on the existing PEEP valves, shows that the error in the PEEP ranges between 1.8 and 6.2 cmH2O and it is proportional to operating time and pressure. On the sensitivity of the valve to flow rate with respect to age, the work of Hawkes et al. (2011) shows that a Neopuff valve is sensitive to flowrate and warn that users/operators must pay attention to set the patient's PEEP needs accurately.

MATERIALS AND METHODS

A replica CAD model of an Ambu PEEP valve and the developed valve was designed in SolidWorks to a high degree of accuracy as shown in Figure 1 and Figure 2, respectively. These valves were characterised using Simscale CFD software. The basic differential features of these valves are seen at the upper part of the valves.
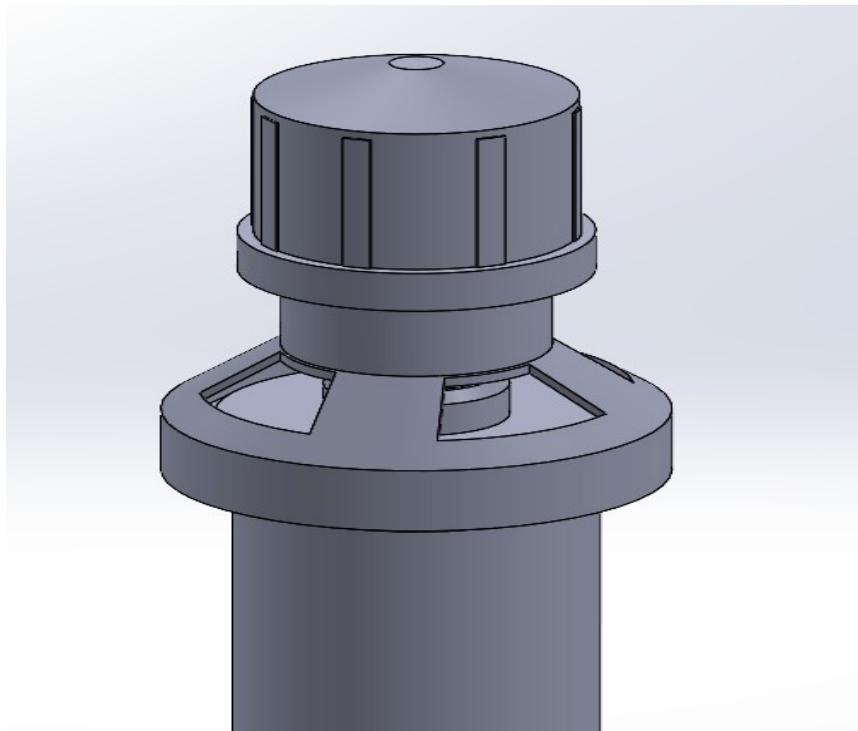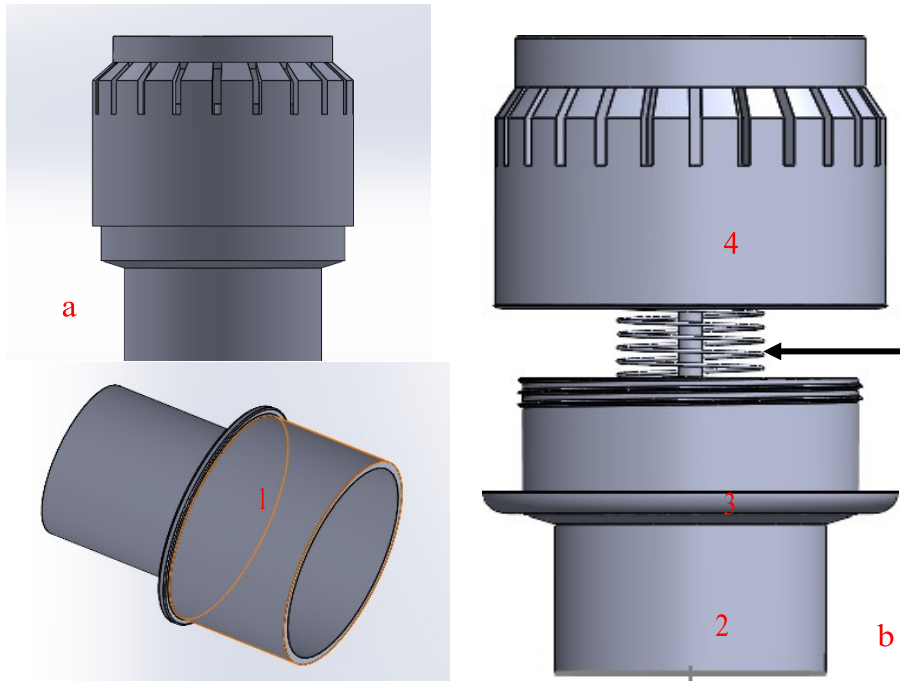

Figure 1: Ambu PEEP valve

Figure 2: CATPUL PEEP valve

i.   Functional description of the CAPTUL PEEP valve

The valve is used depending on the patient socket or the ventilator fitting with or without a design adaptor (component 1). During operation, the valve is set according to the patient's needs by adjusting the upper part (component 4) which screws through component 2. The calibration is placed on the body of the component and setting is done by adjusting the upper half until the bottom part of the valve lock (component 3) coincides with the calibration line desired.

ii.   CAPTUL PEEP valve development overview

Figure 3 shows the development processes considered during the development of this device. It shows the different stages of the development ranging from CAD design, the engineering analysis process, the prototyping stage, manufacturing (two stages: 3D printing and Injection moulding) and then the testing of the device. The processes between the CAD design and the engineering analysis involved some iterative steps until the desired flow result was achieved.
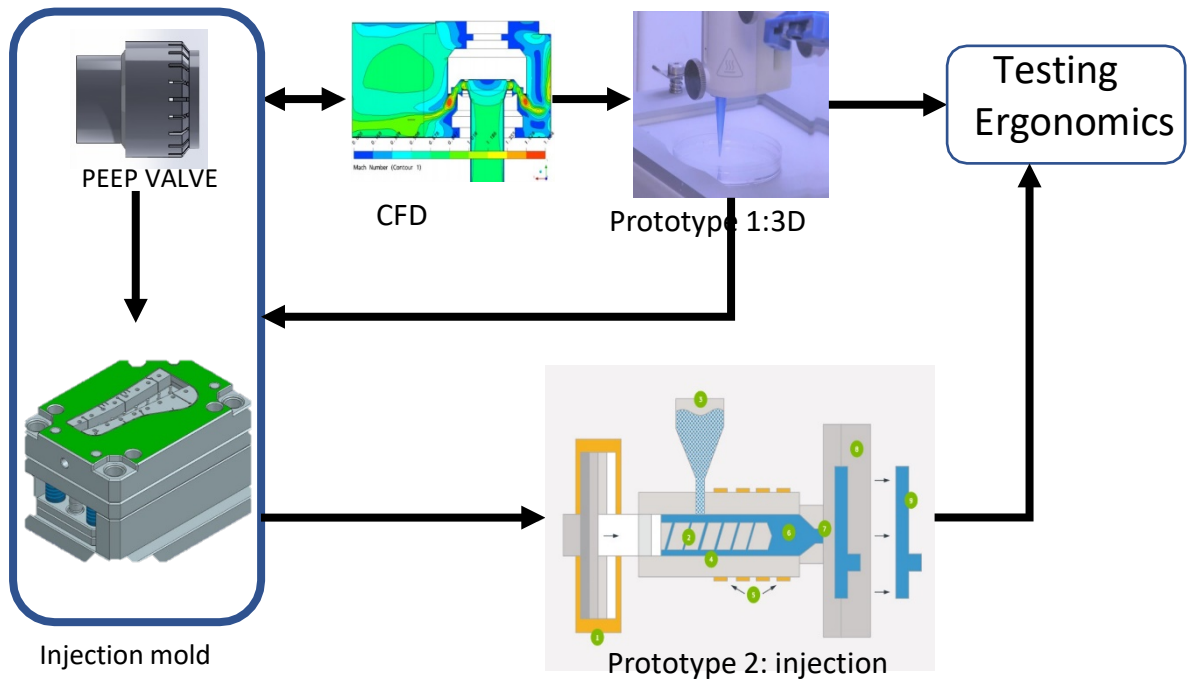
Figure 3: Development process overview (Indiamart, n.d.; Protolabs, n.d.; Song et al., 2014)

CFD CHARACTERISATION OF THE VALVE

Simscale computational code was employed to characterise the two valves designed using the finite volume method. The code solves the turbulence in the valve associated with the patient exhalation air flow conditions. K-omega ($k - w\ SST$) (Menter, 1994), a Reynolds average Navier- Stocks (RANS) turbulent closure was used to capture the turbulent flow characteristics of the exhalation air. $k - w\ SST$ captures effectively the airflow from the human respiratory system (Faizal et al., 2020; Srivastav et al., 2018).

The governing equation of unsteady compressible flow is:

$$\rho \frac{D_i}{D_t} = -pdiv\ u + div(kgradT) + \phi + S_i \qquad (1)$$

k turbulent kinetic energy - ω(dissipation rate) SST model to capture the turbulent viscosity is given in the equations below, obtained from (Versteeg & Malalasekera, 2007).

$$\frac{\partial}{\partial t}(\rho k) + div(\rho kU) = div\left[\left(\mu + \frac{\mu_t}{\sigma_k}\right)grad(k)\right] + P_k - \beta^* \rho k \omega \qquad (2)$$

and

$$\frac{\partial}{\partial t}(\rho\omega) + \frac{\partial}{\partial x_i}(\rho\omega u_i) = \frac{\partial}{\partial x_i}\left(\Gamma_\omega \frac{\partial \omega}{\partial x_j}\right) + G_\omega - Y_\omega + S_\omega \tag{3}$$

Where S_k and S_ω are the user defined source terms given as

$$S_k = \frac{1}{\rho}\tau{:}\nabla u - \beta^*\omega k$$

$$S_\omega = \frac{\gamma}{\mu_\tau}\tau{:}\nabla u - \beta\omega^2 + 2(1 - f_1)\frac{1}{\omega}\nabla k.\nabla\omega$$

Where: γ, β^*, β, σ_k, σ_ω are model constants given as 0.533, 0.09, 0.075, 2.0 and 2.0 respectively (Versteeg & Malalasekera, 2007).

i.   Computational domain and grid generation

Ability to effectively capture the turbulent flow characteristics depends on the size of the computational domain and its accurate discretisation into small cell volume (elements). The size of the domain downstream (5D x 10D downstream and 1d x 10D upstream) was carefully selected to allow smooth transition of the flow downstream without high turbulence leading to back flow as shown in Figure 4. Where 'D' is the diameter of the upper unit of the valve and 'd' the diameter of the plug. To reduce the computational power and cost, half of the domain was discretised (Figure 5) to an orthogonal mesh quality of 0.78088 and cell count of 5.8 million. To effectively capture the flow physics, the mesh was made finer around the diaphragm as shown in *Figure 5b.*
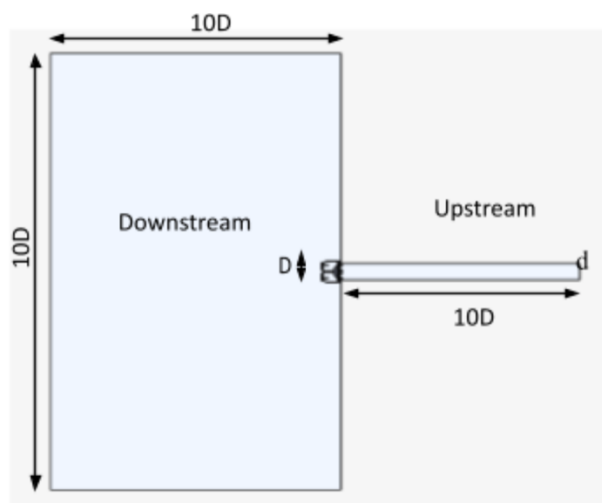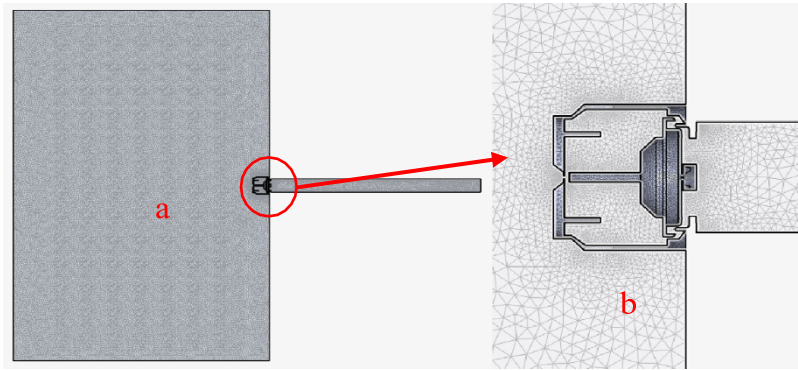

Figure 4: Computation domain

Figure 5: Generated computational grid

ii.   Boundary condition

Boundary condition is an essential part of CFD for an accurate prediction of the flow physics. Pressure inlet and pressure outlet were set for the inlet and outlet boundary conditions. The pressure inlet represents the pressure of the exhalation air from the patient while the pressure outlet was measured downstream of the valve. The inlet pressure was simulated from 0 to 20 cmH2O.

CFD ANALYSIS RESULTS PRESENTATION AND DISCUSSION

The study entails the analysis of flow within the PEEP valve of an off-the-shelf and CATPUL PEEP valve developed for the merSETA medical device development project. The result presents both the qualitative and quantitative results of the pressure, flow velocity and the velocity vector of the both the Ambu PEEP and CATPUL PEEP valve.

i.   Qualitative analysis results

This result section presents the pressure, velocity and velocity vectors contours which shows the flow pattern within the valves.

ii.   Pressure contour plot

Figure 6a-d presents the XY plane contour plot of the exhalation airflow static pressure for 2 cmH2O at 1 mm and 2 mm valve opening, respectively. The figures show the pressure of the exhaled air flowing from the patients before opening the valve diaphragm, and the pressure after escaping through the opening before leaving the valve through the vent provided. The contour plots show that the pressure of the exhaled air is high. Significant pressure drop can be seen within the region of the diaphragm as the flow forces the diaphragm to open. From the figure, we can see that the pressure at all regions of the CATPUL PEEP valve [(Figure 6b and d) with opening of 2mm and 1mm, respectively] are 11973 Pa and 2148 Pa, respectively. Ambu valve (Figure 6a and c) recorded a maximum pressure of 1931 Pa and 2187 Pa at 2 mm

valve opening. Although the pressure downstream is high compared to Ambu version, it does not cause any backpressure in the system as shown in Figure 8.
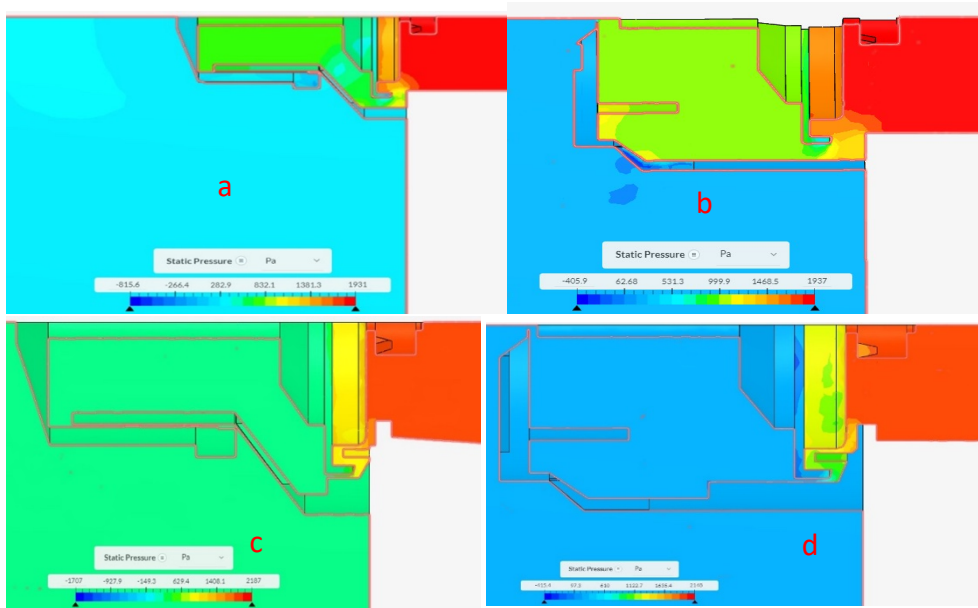
Figure 6: Ambu and CATPUL PEEP valve pressure contour

o Velocity contour plot

Figure 7 a-d presents the XY plane contour plot of the exhalation airflow velocity before opening the valve diaphragm and after escaping, leaving the diaphragm opening. Based on the parameters simulated, the figures showed the velocity downstream of the CATPUL valve is 29.77 m/s while that of the Ambu valve 29.73 m/s. The Ambu valve recorded a maximum flow velocity of 25.59 m/s at diaphragm region compared to 24.81 m/s recorded by the CATPUL valve. The lower velocity means a higher pressure for the CATPUL valve during operation, and this is advantageous.

Figure 7: Ambu and CATPUL PEEP valve velocity contours

o Velocity vector

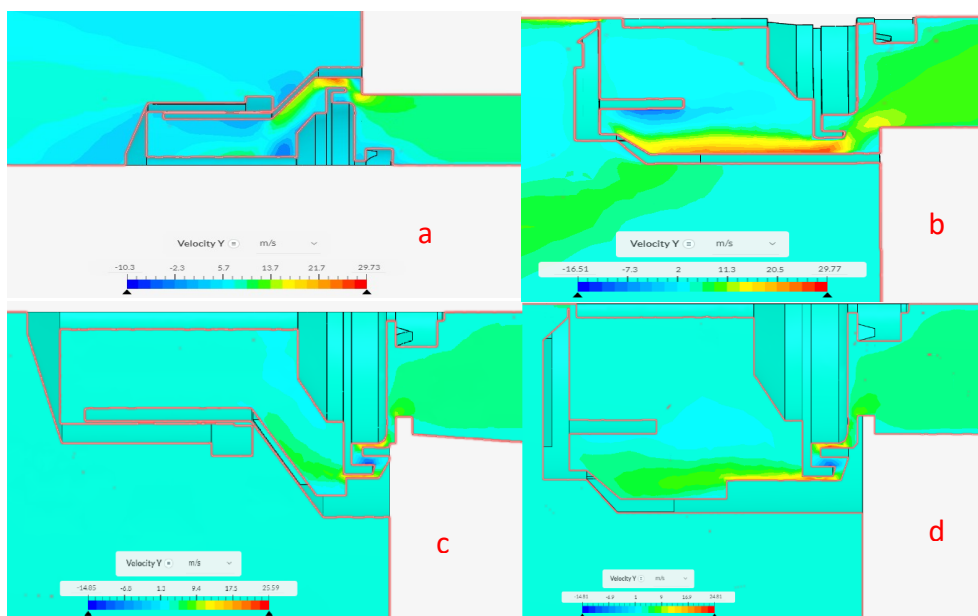The flow stream of the exhaled air is presented in Figure 8. The velocity vector shows the flow direction and behavioural pattern of the air both downstream and upstream. It also clearly showed that the air flows seamlessly through the openings of the diaphragm without backflow. Also, the vectors indicate that the pressure within the valves is higher than the surrounding air, preventing it from entering the valve to create undesirable backpressure.
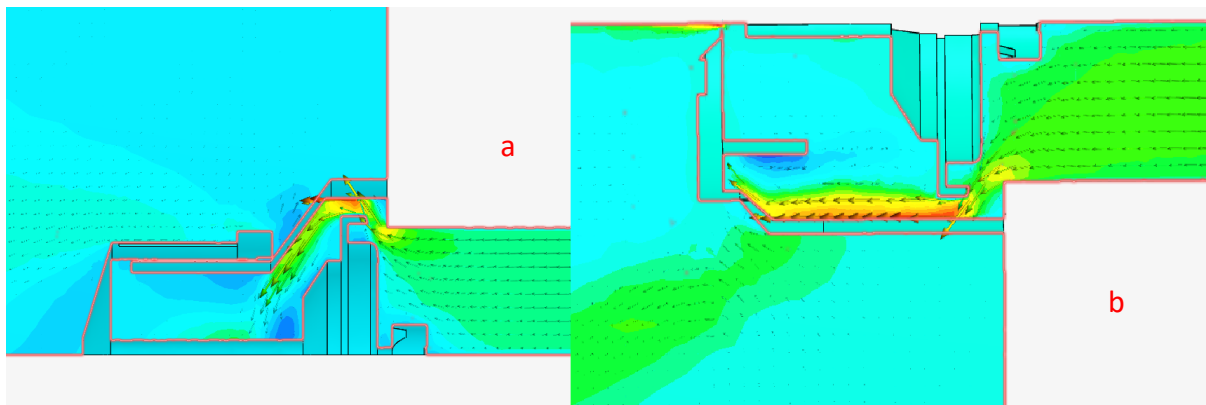

Figure 8: Ambu and CAPTUL PEEP valve velocity vector

o CFD analysis results summary

As presented in Figures 6, 7 and 8, the CATPUL PEEP valve design and analysis proves to be a good replacement for the Ambu counterpart. The CAPTUL valve gives a better performance as higher opening pressure is recorded. This means less work is required from the patient's respiratory system to open the valve during use. The velocity vector presented in Figure 8 shows that the CATPUL valve (Figure 8b) has a good flow and venting pattern. The flow circulation downstream of the valve is insignificant to cause backpressure capable of preventing the operation of the valve.

CONCLUSION

The computational study of the PEEP valve for patient's support is done comparing the performance of the Ambu and CAPTUL PEEP valve. $k - \omega$ turbulent model was adopted to simulate the turbulent viscosity within the valve. The flow pattern from the two valves analysed shows a similar flow trend with a close flow parameter at different valve openings signifying different patients' breathing needs. The analysis shows that the pressure and the flow velocity of the two valves are closely matched with the CAPTUL valve, recording a higher operational pressure of 1937 Pa against 1931 Pa recorded by the Ambu valve.

ACKNOWLEDGEMENTS

REFERENCES

Ashish, A., Unsworth, A., Martindale, J., Sundar, R., Kavuri, K., Sedda, L., & Farrier, M. (2020). CPAP management of COVID-19 respiratory failure: A first quantitative analysis from an inpatient service evaluation. *BMJ Open Respiratory Research*, *7*(1), e000692. doi: 10.1136/bmjresp- 2020-000692

Bunting, L., Roy, S., Pinson, H., & Greensweig, T. (2020). A novel inline PEEP valve design for differential multi-ventilation. *American Journal of Emergency Medicine*, *38*(10), 2045–2048. doi: 10.1016/j.ajem.2020.06.089

EPCM. (2020). *Ventilators - An Overview within the Covid-19 Context - EPCM Holdings*. https://epcmholdings.com/ventilators-an-overview-within-the-covid-19-context/

Faizal, W. M., Ghazali, N. N. N., & Khor, C. Y. (2020). Computational fluid dynamics modelling of human upper airway: A review. *Computer Methods and Programs in Biomedicine*, *196*, 105627. doi: 10.1016/j.cmpb.2020.105627

Hartung, J. C., Wilitzki, S., Thio-Lluch, M., Te Pas, A. B., Schmalisch, G., & Roehr, C. C. (2016). *Reliability of Single-Use PEEP-Valves Attached to Self-Inflating Bags during Manual Ventilation of Neonates-An In Vitro Study*. https://doi.org/10.1371/journal.pone.0150224

Hawkes, C. P., Dempsey, E. M., & Ryan, C. A. (2011). The Neopuff 's PEEP valve is flow sensitive. *Acta Paediatrica, International Journal of Paediatrics*, *100*(3), 360–363. doi: 10.1111/j.1651- 2227.2010.02086.x

Indiamart. (n.d.). *CAD / CAM Designing Firm Plastic Injection Mould Tool Design, | ID: 22903903212*. Retrieved December 26, 2021, from https://www.indiamart.com/proddetail/plastic-injection- mould-tool-design-22903903212.html

J.R. Boire, B. Roberts, T. Calow, M. J. & J. B. M. (2021). Flow meter, PEEP valve development and performance testing for use in a volume-controlled emergency use ventilator (EUV-SK1). *CMBEC44*. https://proceedings.cmbes.ca/index.php/proceedings/article/view/929/901

Mason, P. (2014). *Rationale for including PEEP valves in extended care of critically ill casualties Phillip Mason, MD*.

McEvoy, M. (2020). *Why PEEP? - EMS Airway*. https://www.emsairway.com/2020/06/02/why- peep/#gref

Meara, K. (2020). *Existing Treatment Saves the Lives of Covid-19 Patients*. https://www.contagionlive.com/view/existing-treatment-saves-the-lives-of-covid-19-patients

Menter, F. R. (1994). Two-equation eddy-viscosity turbulence models for engineering applications. *AIAA Journal*, *32*(8), 1598–1605. doi: 10.2514/3.12149

Protolabs. (n.d.). *Plastic Injection Moulding, Rapid Prototyping | Protolabs*. Retrieved August 23, 2021, from https://www.protolabs.co.uk/services/injection-moulding/plastic-injection-moulding/

PtSA. (2020). *PtSA News Newsletter of the Production Technologies Industry in South Africa Sponsored by Intratech (Pty) Ltd*.

Roelf, W. (2020). *South Africa produces its first ventilators to fight COVID-19 | Reuters*. https://www.reuters.com/article/us-health-coronavirus-safrica-ventilator-idUKKCN24W1VD

Schutz, E. (2020). *COVID-19: SA's looming ventilator shortage•Spotlight*. https://www.spotlightnsp.co.za/2020/04/06/covid-19-sas-looming-ventilator-shortage/

Song, X., Cui, L., Cao, M., Cao, W., Park, Y., & Dempster, W. M. (2014). *A CFD analysis of the dynamics of a direct-operated safety relief valve mounted on a pressure vessel*.

Srivastav, V. K., Paul, A. R., & Jain, A. (2018). *Capturing the wall turbulence in CFD simulation of human respiratory tract*. https://doi.org/10.1016/j.matcom.2018.11.019

Versteeg, H. K., & Malalasekera, W. (2007). An Introduction to Computational Fluid Dynamics. In

World Wide Web Internet And Web Information Systems (Vol. 1). doi: 10.2514/1.22547 Xinhua. (2020). *Rwandan engineers develop first locally made ventilator - Xinhua | English.news.cn*. http://www.xinhuanet.com/english/2020-04/21/c_138996664.htm

CHAPTER 17
AFFORDABLE ORTHOTIC MOON BOOT ALTERNATIVE

Aliya Singh, Riaan Stopforth
ORCID ID: 0000-0003-1754-447X, 0000-0002-8878-2232
School of Engineering
University of KwaZulu Natal
Durban
South Africa

ABSTRACT

This research paper details the engineering design process undertaken to develop an affordable alternative to commercially available orthotic moon boots. The project conceptualisation was conducted using an approach that aligns the design with the key focus of cost-effectiveness and fundamental functionality. Therefore, non-essential, cost-adding, and superfluous factors that are present in the existing production of orthotic moon boots were identified and omitted from this design. Stringent engineering design processes were used to redesign and optimise the materials and methods that are currently employed in the manufacturing of commercially available moon boots. The total cost of production of the redesigned moon boot amounted to R175.90, which was approximately 88% lower than commercial products. Therefore, this research proves to be extremely invaluable as it would widen accessibility to orthotics for various demographics.

Keywords: Affordable, Moon Boot, Orthotic

NOMENCLATURE

μ Mean

σ_2 Variance

σ Standard Deviation

INTRODUCTION

Moon boots, also known as orthopaedic walker boots, are orthotic devices which are commonly prescribed to assist in the treatment and recovery of patients with a range of leg and foot injuries or diseases. Moon boots target use for the treatment of several injuries such as severe ankle sprains, and fractures of the leg and foot in the fibular, tarsal, metatarsal, and tibial regions (Rizzone & Gregory, 2013).

These devices are also used to facilitate post-surgical management and rehabilitation of tendons and ligaments (Pollo, et al., 1999). They are also utilised by diabetic patients who are subjected to foot-related complications – these patients develop neuropathy or polyneuropathy as their condition progresses, resulting in the loss of sensation in the feet, leading up the lower leg, and ultimately leading to foot ulceration. Moon boots assist in fast healing of diabetes-induced foot ulcerations by decreasing pressure on the feet (Bledsoe & Bledsoe, 2008). In South Africa's developing economy, most of the population relies heavily on public healthcare. Therefore, acquiring these devices at the current cost of approximately R1 500 is generally unaffordable (Dis-Chem, 2021). As such, the development of an affordable moon boot is vital since it would permit wider accessibility and allow for a larger population of patients to reap the associated health-aligned benefits offered by moon boots. A considerable amount of work has been done in the medical orthosis field to further develop and refine the functionality of moon boots, but there has been little to no tangible results that aim to lower the purchase price of these devices (Arvela, et. al, 2010). Research has indicated that the well as high profit margins that are put in place by producers and retailers. Therefore, by reducing manufacturing costs of moon boots and eliminating the need for third parties, the cost price of moon boots can be significantly lowered for purchase by the customer. This is achieved by constructing the moon boot from less specialised, and commonly accessible components, equipment, and methods; whilst simultaneously ensuring that the functionality, ergonomics, and reliability of the device is comparable to commercially available products.

MATERIALS AND METHODS

The materials and methods used in the design of the moon boot alternative are detailed in the subsections below.

i.   Materials

The moon boot is constructed entirely from COTS. Therefore, no component requires specialised manufacturing. This aids in maintaining a low manufacturing cost, as the COTS themselves are widely accessible, affordable, and common. The moon boot can be classified into five sub-components, namely the firm L- shaped shell that is fitted along the calf and foot of the patient, reinforcements, lining, fasteners, and a sole. The firm shell structure was achieved through the utilisation of UPVC pipe elements, the padded inner lining was created through a mixture of foam types, i.e., closed cell foam and open cell foam, the non-slip sole was replicated using adhered rubber circles, and the adjustable fastener aspect was achieved by using Velcro straps. The utilisation of two diagonal bracings and a right-angled bracket, which are secured by eight pop rivets, ensures that the moon boot is structurally secure by adding resistance to the lateral load applied by the user, dispersing the load evenly. The bracing also prevents unwanted flexure in the moon boot, and reduces the strain experienced by the primary joint. Strategic placement of the open and closed cell foam layers allows for a comfortable orthotic, due to it being well-cushioned, and shock

resistant. Furthermore, the device is designed to be breathable and reduce the degree of discomfort experienced by the user, like commercial moon boots (Amaha, et al., 2017). The use of Velcro straps as the primary fasteners allows for the boot to be put on or removed easily, without requiring the assistance of a third party. This also aids the hygiene of the patient, as the orthotic can easily be removed for cleaning purposes. Additionally, Velcro permits a wide range of adjustability. Overall, the boot is made stronger using bracing, and the likelihood of failure through repetitive use is greatly reduced. The design does not include any component that is fast-diminishing and would require frequent replacement.

ii.　　Methods

The investigations, experimental testing, and data analysis of the moon boot consisted of two experiments, i.e., a usability test conducted on two user groups and a finite element analysis (FEA) conducted via *Solidworks* and *Autodesk Inventor* software. A usability test, as outlined in the International Electrotechnical Commission (IEC) standard IEC 62366-1: 2015 and IEC 62366-2: 2016 by the International Organization for Standardization (ISO), was used to establish a method for testing the effectiveness, efficiency, and user satisfaction of the medical device (ISO, 2015), (ISO, 2016). The test was also used to determine any use errors associated with the device, such that risk management in accordance with ISO 14971: 2007, which was associated with medical devices (ISO, 2007). Experimental testing of the moon boot using FEA software provided a method for observing the structural behaviour and performance of the moon boot over the course of the product's lifecycle without destructively testing the product (CaliberDesign, 2015).

RESULTS AND DISCUSSION

The results and discussions of Experiment 1 and Experimental 2 are detailed below.

i.　　Experiment 1: Usability Test

The aim of Experiment 1 was to determine the usability and use errors associated with the moon boot, as per ISO guidelines. For each usability test, there were three people involved, i.e., the test participant, test observer, and test moderator. The test moderator refers to the person who conducted the participant test training, post-test interviews and data analysis. The observer refers to a neutral unbiased person who recorded any comments and criticisms made by a participant during the usability test, and who conducted the usability test questionnaire to ensure that fair and accurate results were obtained. The test participants were split into two user groups, consisting of five participants each, to achieve data and commentary from, firstly, a group representing the general population of people who had no history of lower limb injuries or a professional medical background, and secondly, a group representing the intended users of the moon boot such as people with lower limb injuries or who had a professional medical background. The overall scores for each user group are illustrated in the graph shown in Figure 1.
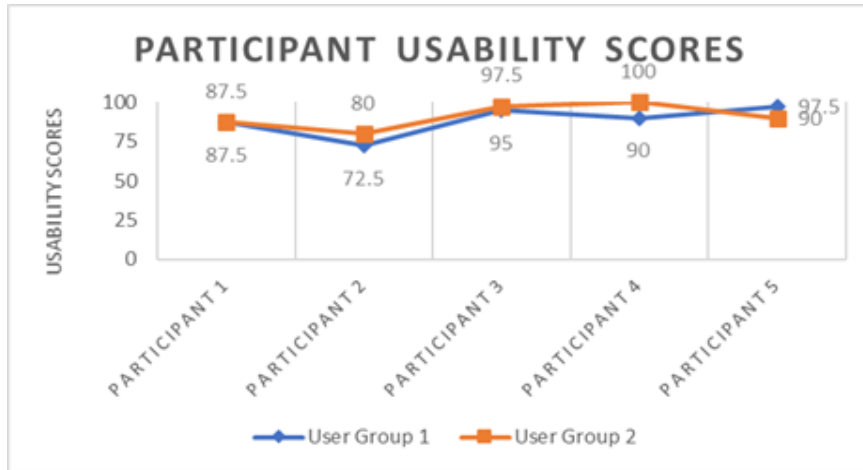
Figure 1: A graph illustrating participant usability scores for each user group

The overall scores were analysed using the scale shown in Figure 2 to determine the usability of the moon boot (Bangor, et al., 2008).
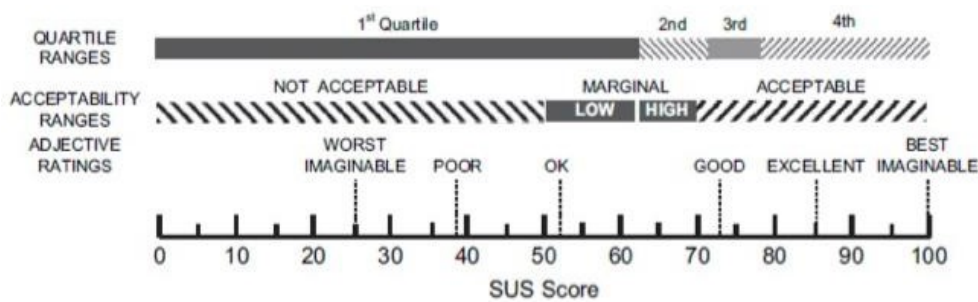
Figure 2: Usability score scale

Using the scale illustrated in Figure 2 and the graph shown in Figure 1, the usability of the device ranged from 72,5 to 100, with each rated out of 100, which translated to an adjective rating of 'good' to 'best imaginable'. Therefore, it can be concluded that the usability of the moon boot was ultimately successful. However, the validity of the data points was tested further using statistical analysis on both the combined user group scores as summarised in Table 1.

Table 1: Statistical analysis of experimental data points

Statistical Data	Combined User Group Scores
Average	89,75
Standard Deviation	8,54
Number of Outliers	2
Values of Outliers	80 and 100
Average without Outliers	89,69

Through the analysis of the statistical data obtained from Table 1, the following observations were made:

- From the 10 data points, only two data points did not fall within the range of one standard deviation of the mean.
- The outliers, 80 and 100, were the lowest and highest values of the data set, respectively.
- Eliminating the outliers and subsequently recalculating the mean resulted in a value of 89,69.
- Eliminating the outliers were unnecessary since the recalculated mean only had a percentage error of 0,07%.
- Both the original mean with the outliers and the recalculated mean without the outliers are approximately 90, which when ranked on the scale shown in Figure 10, demonstrates that the product has an acceptable usability score between the adjective ratings of 'excellent' to 'best imaginable'.
- Therefore, it can be concluded that the data points obtained are valid.

ii. Experiment 2

The aim of Experiment 2 was to obtain a low Von Mises stress value, low displacement value, and a high safety factor value using *Solidworks* Computer Aided Design (CAD) models which were input into *Autodesk Inventor* software to simulate the behaviour of the moon boot under simulated force values that were much greater than the parameters for which the moon boot was designed, i.e., the moon boot was designed for a patient with a weight of 500N. Therefore, a downward force load of 800N was chosen to simulate the weight of a patient, and a horizontal force load of 400N to simulate the force of a patient's leg when walking. A constraint was also input on the sole of the moon boot. The results of the Von Mises stress, safety factor and displacement simulations are shown in Table 2.

Table 2: FEA Simulation Results

Von Mises Stress Simulation	Safety Factor Simulation	Displacement Simulation
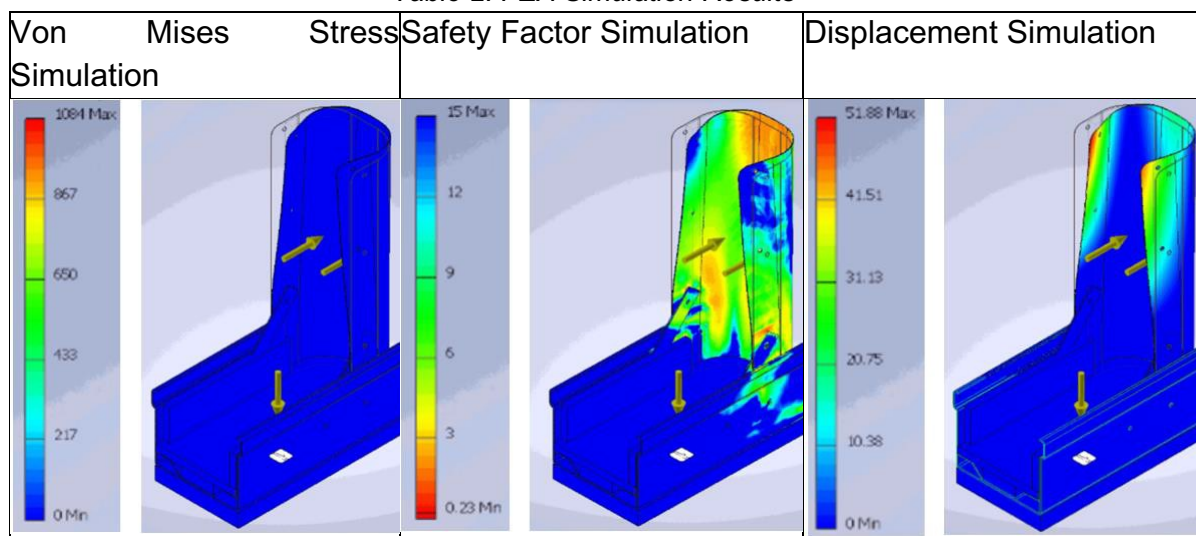
Through the analysis of each simulation, the following observations were made:

- o Any deformation of the moon boot would theoretically occur at the upper edges and would bend inward.
- o The Von Mises stress simulation indicated 0MPa throughout the moon boot for an exaggerated applied force. Therefore, it can be concluded that the moon boot design is highly unlikely to deform.
- o The safety factor simulation and displacement simulation indicated higher safety factor values and lower displacement values in the lower foot, ankle and back of the calf areas of the boot.
- o From the safety factor simulation, a desirable large safety factor was observed for most of the moon boot structure with certain areas resulting in a safety factor of approximately two, which was an acceptable value for the exaggerated force applied to the moon boot.
- o Therefore, from all three FEA simulations, it can be concluded that the moon boot is safe for patient use, structurally sound and theoretically up to standard compared to commercially available products.

CONCLUSION

The importance of the redesigned affordable orthotic moon boot alternative is reiterated due its role in pain reduction and swelling, and assistance in minimising the period of recovery of intended use patients. The outcomes of the final design illustrate that the redesigned moon boot was ultimately successful and comparable to commercially available orthotics, at a fraction of the cost.

ACKNOWLEDGEMENTS

Acknowledgement is given to Professor R. Stopforth, Mr P. Govender, all multidisciplinary professionals, participants and users involved in the design, testing, and evaluation of the moon boot design.

REFERENCES

Amaha, K. et al., 2017. Shorter recovery can be achieved from using walking boot after operative treatment of an ankle fracture. *Asia-Pacific Journal of Sports Medicine, Arthroscopy, Rehabilitation and Technology,* Volume 7, pp. 10-14. doi: 10.1016/j.asmart.2016.09.001

Arvela, E. et al., 2010. Arm Vein Conduit vs Prosthetic Graft in Infrainguinal Revascularization for   Critical Leg Ischemia. *Journal of Vascular Surgery,* 52(3), pp. 616-623. doi: 10.1016/j.jvs.2010.04.013

Bangor, A., Kortum, P. T. & J, T. M., 2008. An empirical evaluation of the system usability scale. Journal of Human-Computer Interaction, Volume 6, pp. 574-594. CaliberDesign, 2015. Why Use FEA?. [Online]. Available at: https://www.caliberdesign.co.nz/wp-content/uploads/2015/05/Caliber-   Design-HowToGuide-Intro-to-FEA.pdf. [Accessed 23 October 2021].

Bledsoe, G. R. & Bledsoe, B. O., 2008. *Walking boot for diabetic and other patients.* United States, Patent No. 7,418,755.

Dis-Chem, 2021. *Dis-Chem Pharmacies.* [Online] Available at: http://www.dischem.co.za/shop-by-department/health/health/assisted-living/immobilisation-and-support/post-op-support [Accessed 29 April 2021].

ISO, 2007. ISO 14971: 2007 Medical devices- Application of risk management to medical devices. [Online]. Available at: https://www.iso.org/standard/38193.html. [Accessed 20 October 2021].

ISO, 2015. ISO Standard No. 62366-1: 2015 Medical Devices-Part 1: Application of usability engineering to medical devices. [Online]. Available at https://www.iso.org/standard/63179.html. [Accessed 20 October 2021].

ISO, 2016. ISO Standard No. 62366-2: 2016 Medical Devices- Part 2: Guidance on the application of usability engineering to medical devices. [Online]. Available at:http://www.iso.org/standard/69126.html. [Accessed 20 October 2021].

Pollo, F. E., Gowling, T. L. & Jackson, R. W., 1999. Walking boot design: A gait analysis study. *Orthopedics,* Volume 22, pp. 503-507.

Rizzone, K. & Gregory, A., 2013. Using Casts, Splints, and Braces in the Emergency Department. *Clinical Pediatric Emergency Medicine,* 14(4), pp. 340-348. doi: 10.1016/j.cpem.2013.11.003

THE DESIGN AND DEVLOPMENT OF A LOW-COST HIGH FLOW NASAL OXYGEN DEVICE: A FUNCTIONAL ANALYSIS

Brandon Reabow, Sudesh Sivarasu
ORCID ID: 0000-0002-4534-2640, 0000-0002-0812-568X
Division of Biomedical Engineering
Department of Human Biology
University of Cape Town
Western Cape
South Africa

ABSTRACT

High Flow Nasal Oxygen (HFNO) medical devices are utilised to non-invasively oxygenate Coronavirus disease 2019 (COVID-19) and acute respiratory distress syndrome (ARDS) patients with mechanisms of clinical benefit. Most recently, HFNO has proven to be effective against hypoxemic symptoms by providing a range of oxygen concentration levels (FiO_2) and aims to improve patient compliance and comfort with heating and humidification of inspiratory gases. HFNO has been shown in studies to be feasible in resource-constrained settings, relying on an affordable solution to drive an increased number of supplied devices to healthcare facilities to effectively treat patients independently of intensive care units (ICU). Therefore, a Proof of Concept was developed under an iterative design approach. A full cost summary of materials was R8 100, compared to at least R45 000 for current South African market competitors. Additionally, the solution was functionally tested to determine levels of verification in technical specifications and validation in addressing clinician and patient needs. The solution achieved associated 10 - 60 l/min flow rates; stable FiO_2 from 50 - 100% (with a minimum of 40%); and inspiratory gas temperatures and humidity of up to 40 °C and 90% relative humidity (RH). Further design and development need to be conducted to output a high-performing and safe medical device as guided by ISO 80601-2-90.

Keywords: HFNO, COVID-19, ARDS, resource-constrained, low-cost, affordable, ICU, Proof of Concept, medical device

NOMENCLATURE

FiO_2	-	Device oxygen and air concentration level
SpO_2	-	Patient oxygen saturation level
VFR	m^3/s	Volumetric flow rate
C	-	Discharge coefficient for partial fluid viscosity
ΔP	Pa	Differential pressure

A_1	m^2	Upstream venturi cross-sectional area
A_2	m^2	Downstream venturi cross-sectional area
ρ	kg/m^3	Fluid density
VFR_{oxygen}	m^3/s	Volumetric flow rate of oxygen gas
VFR_{air}	m^3/s	Volumetric flow rate of ambient air

INTRODUCTION

Patients with COVID-19 and ARDS experience symptoms related to respiratory failure. These include hypoxemic or low oxygen saturation levels (SpO$_2$) and require intervention in oxygenation treatments. HFNO has been extensively used to treat COVID-19 patients, or patients with similar respiratory failure. The reason for this relates to the non-invasive characteristic of the treatment because patients do not need to be intubated, consequently improving chances for patients tolerating treatment without sedation.

- HFNO provides mechanisms of clinical benefit that relate to the following: (Slain et al., 2017; Vega & Pisani, 2021; WHO, 2021)
- Stable inspiratory oxygen flow at high flows.
- Nasal cannulas reduce breathing effort. Open-flow systems promote carbon dioxide washout.
- Continuous positive airway pressures result in positive end-expiration pressure (PEEP) effect reaching up to 7cmH$_2$O.
- Active heating and humidification attenuate discomfort, sinus pains, and drying of mucosa.

Studies have shown that the use of HFNO mitigates risks involved in treating patients with more invasive mechanical ventilators, as associated mortality rates for these devices can be high. The use of HFNO to treat initial acute hypoxemic symptoms allows for patients to be weaned off ventilation treatments before reaching invasive mechanical ventilation (Calligaro et al., 2020).

HFNO has proven to be used in varying application settings. The use of HFNO within resource-constrained settings is feasible (Calligaro et al., 2020). HFNO may be used within ICU's and general pulmonology wards, and to the extent of home use (Calligaro et al., 2020; ResMed, 2021). This results in not requiring ICU facilities which reduces length of stay in ICU for ventilated patients and reduces staffing requirements without compromising patient care (Bice et al., 2013). Additionally, ICU and ventilator expertise are less of a requirement (Liu et al., 2021). Transportation of unstable patients is appropriate with HFNO treatments (Kedzierewicz et al., 2021). Moreover, high flow therapy is limited by the source of oxygen, whereby typical oxygen concentrators for home-use can produce up to 10 l/min (Hardavella et al., 2019). Therefore, hospital wall oxygen provides the most suitable approach for supplying HFNO devices with oxygen for meeting high flow rate benefits. Studies need to be

conducted for HFNO treatment in pre-hospital settings but have been used as a first choice from home to emergency transport. These introduce exceeding battery energies associated with high energy consuming components for heating and humidification, as well as low oxygen delivery times with oxygen tanks like a 4.5-L ME36 cylinder (Kedzierewicz et al., 2021).

HFNO is classified as non-invasive within a high flow nasal oxygen category. The treatment is aimed at providing high flow oxygen delivery with heated humidification. The effectiveness of the treatment is associated with the high-velocity gas expelling from the cannula of a patient interface. Therefore, the system is based off flow rate requirements with maximum flow rates generally delivered between 50 and 70 l/min (WHO, 2021). This provides the necessary airway pressures and advantageous PEEP effect without requiring sealing of a patient interface. Additionally, as enlisted by the World Health Organization (WHO), technical specifications may be adopted to provide a basis for the development of the HFNO proposed solution. (WHO, 2021)

HFNO has many components constituting to the device. These may be broken up into stages described as inspiratory gas flows through the device and consecutively includes: oxygen regulation and mixing, humidification and heating, and the patient interface stages. The oxygen regulation and mixing stage make use of active flow generation in types of air-oxygen blenders or built-in flow generators, whereas passive entrainment systems provide for an additional method of mixing. Oxygen/air mixtures can have a range of FiO_2 from 0.2 to 1.0 and are usually dependent on input or generated flow rates (Nishimura, 2019; WHO, 2021). Dry gas, especially over long-term delivery, may cause mucociliary malfunction, epithelial damage, mucus plugging, ulceration of mucosa, and in this context, ventilator-induced lung injury (VILI) (Cerpa et al., 2015). Therefore, active heated humidifiers are used to primarily provide humidification at high flows. Additionally, a heated patient circuit is used to provide effective gas heating, as well as provide humidity regulation. Finally, a patient interface consisting of a nasal cannula provide an open system connection to the patient. Equipped with high flow rates, HFNO can provide more stable inspiratory flow rates and humidity, since low flow rate systems comparatively provide unmatched device settings due to inspiratory flow rates less than HFNO flow rates (Nishimura, 2019). Existing solutions for HFNO are internationally recognised, imported, and supplied in local supply chains. The cost range in the South African market is between R45 000 and R60 000 (*High-Flow Nasal Cannula Oxygen COVID-19 cases*, 2020). Therefore, the project aims to design and develop a high flow nasal oxygen device that is low-cost for improved accessibility and chance of local manufacturing to address the needs of resource-constrained and low-income settings for healthcare facilities.

DESIGN AND METHODS

Approaching a final concept with iterative design and development, the aim was to prototype an initial Proof of Concept with basic functionality that could be verified

and validated. Therefore, the following requirements and their methods were considered throughout the project:

- o *Low cost:* To promote affordable solutions within most resource-constrained and low- to middle-income country (LMIC) settings. Due to premature cost analysis, the bill of materials must not exceed a quarter of the minimum cost margin within South Africa, which requires for the materials to cost a maximum of R11 250.
- o *Local manufacturing:* To fulfil the national goal of promoting local economic growth, most of the manufacturing processes were conducted with no tooling and mostly 3D printed using Ender 3 Pro and FormLabs resin printers.
- o *Clinical needs:* With collaboration, design features need to provide convenience and effectiveness and solve current challenges wherever possible. Needs will be defined and assessed for the Proof of Concept based on clinical aspects to validate the design methods used.
- o *Functional design:* The solution within this initial project scope needs to output a functional solution that is verified and validated within current laboratory facilities. Thus, facilities within the University of Cape Town (UCT) Medical Devices laboratory (MDL) will be utilised to verify technical specifications as guided by WHO (WHO, 2021). Problem needs will be matched against the Proof of Concept in a qualitative manner.

The final concept subsystem units are divided into the following: oxygen regulation and mixing unit, heating and humidification unit, and the patient interface. The final prototype is shown in Figure 1.

Figure 1: Proof of Concept prototype solution developed.

i.   Oxygen regulation and mixing unit

The oxygen regulation and mixing unit incorporates a manual analog control solution whereby input oxygen and ambient air flow rates may be controlled in a low-cost manner. The unit utilises a Venturi entrainment device to entrain ambient air from the hospital wall oxygen outlet. Oxygen and air flow rates were determined by separate Venturi chambers that generate differential pressures across a decrease in diameters along the gas flow path. This differential pressure is measured, and Bernoulli's equation is used to calculate volumetric flow rates. The form of Bernoulli's equation

used is shown in Equation 1. With the user able to control flow rates of oxygen and air, the FiO_2 is manually controlled. There is a relationship between these two flow rates that calculate the output FiO_2, referred to in Equation 2 (Ely & Clapham, 2003). The nomenclature provides reference to the use and units of these equations.

$$VFR = C \sqrt{\frac{2\Delta P}{\rho}} \ \frac{A_1}{\sqrt{\left(\frac{A_1}{A_2}\right)^2 - 1}} \quad (1) \qquad | \qquad FiO_2 = \frac{VFR_{oxygen} + 0.2 VFR_{air}}{VFR_{oxygen} + VFR_{air}} \quad (2)$$

The testing of this unit involved the use of a portable tank compressor equipped with filters to provide compressed air at a maximum of 2.2 bars. The device would internally regulate the pressure between 0 and 4 bar, simulating the conditions from hospital oxygen wall supplies (SARAO, 2020). The MPX5100DP and the MPX5010DP differential pressure sensors were procured to provide analog measurement readings. These sensors are inexpensive, coupled with the Venturi chamber to produce affordable flow meters. Signal filtering techniques were used to mitigate noisy sensor measurements, particularly for differential pressure, volumetric flow rates, and calculated outputs which include total flow rate and FiO_2. These techniques involved digital low-pass filtering, passive laminar inducing components, and running averages. The flow rates were verified with the highly accurate Sensirion SFM3000 flow meter in the UCT MDL. A basic Liquid Crystal Display (LCD) was used to present all required measurements and calculations. This allowed for accurate usability and display of measurements. Ultimately, results were captured for the controlled oxygen and entrained ambient air flow rates, as well as the calculated summated total flow rate and FiO_2 percentages. A custom control valve for the entrained air was developed with six different settings: setting "0" referring to the least air entrained and setting "5" referring to the most air entrained. Therefore, a higher setting number will provide for a lower FiO_2 output for a given oxygen flow rate input.

ii.   Heating and humidification unit

The method to heat and provide humidity to the inspiratory gases requires active heater element components. The mechanical design was developed to transport gas from the oxygen regulation and mixing unit to the patient interface efficiently, with the procured water chamber by Inspira and heated breathing circuit by BMC. Two sensing units, at chamber-end and patient-end, were incorporated to measure relative humidity and temperature; and monitor effectiveness of active humidification of the water chamber and heating regulation of the breathing circuit. By applying air flow through the unit and allowing for the chamber water and heat exchanger to warm up, results show the characteristics of heating and humidification along the path to the patient. With the use of a basic control system, Pulse Width Modulated (PWM) triggers were utilised to control average voltages supplied to the water chamber and heated breathing circuit power elements. This will be controlled via a user menu implemented with a rotary encoder. Moreover, two DHT22 temperature and humidity sensors were used for chamber-end and patient-end measurements. Additionally, a temperature

sensor is placed in the chamber heater element to prevent overheating. All voltages and sensor measurements are presented on an LCD as the unit's user interface.

    iii.   Patient interface

A patient interface was developed to deliver inspiratory gases through a nasal cannula. The nasal cannula provides high-velocity gas deliverance into the nostrils of a patient. Throughout testing, the patient interface was only demonstrated and not connected to any person with the device on. Nevertheless, the interface provides adjustable fitment around the face with comfortable padding to insulate frontal sinuses. Additionally, a removable face shield may be placed onto the interface to minimise aerosolization effects associated with HFNO, standard oxygen masks and nasal cannula; and limit infectious spreading of respiratory-related diseases (Li et al., 2020).

RESULTS AND DISCUSSION

    i.   Oxygen regulation and mixing unit

The sensor measurements and calculations were captured from a single test whereby total flow rates were stepped in increasing 10l/min flow rates, for each entrained air control valve setting (0 - 5). Figure 2 and Figure 3 illustrate the dependency of total flow rates and FiO_2 for an input oxygen flow rate and each entrainer valve setting.
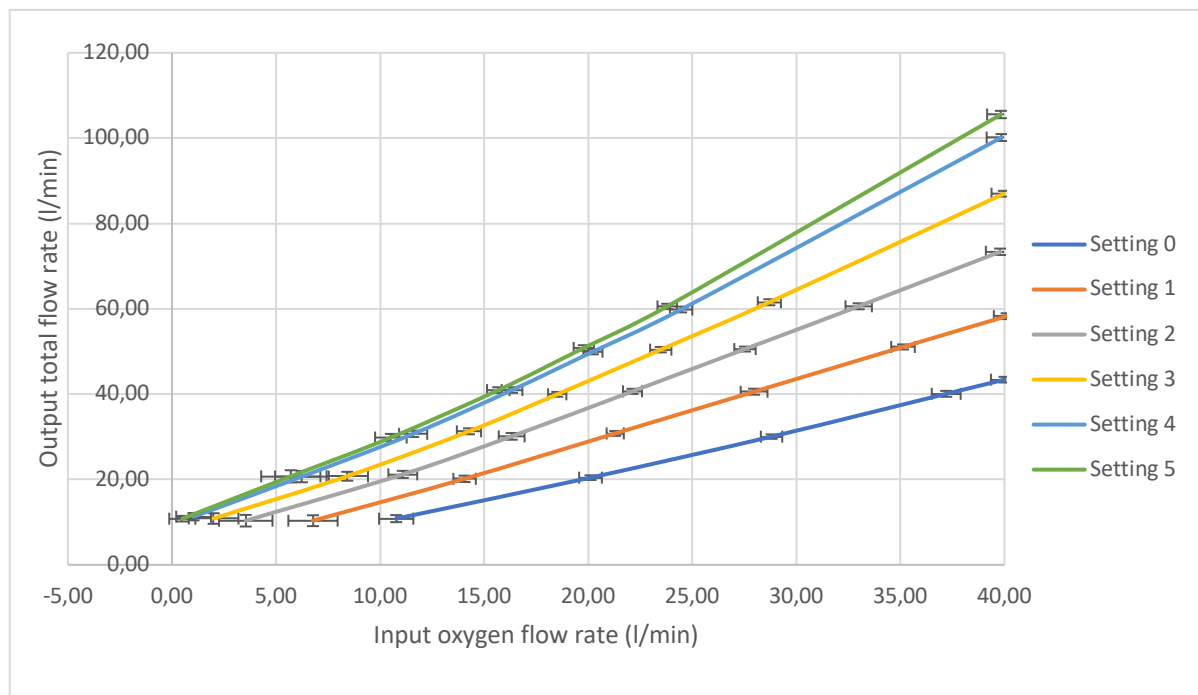

Figure 2: Mean flow rates for input oxygen and total flow for each setting on the entrainer valve, with standard deviation error bars showing measurement precision.
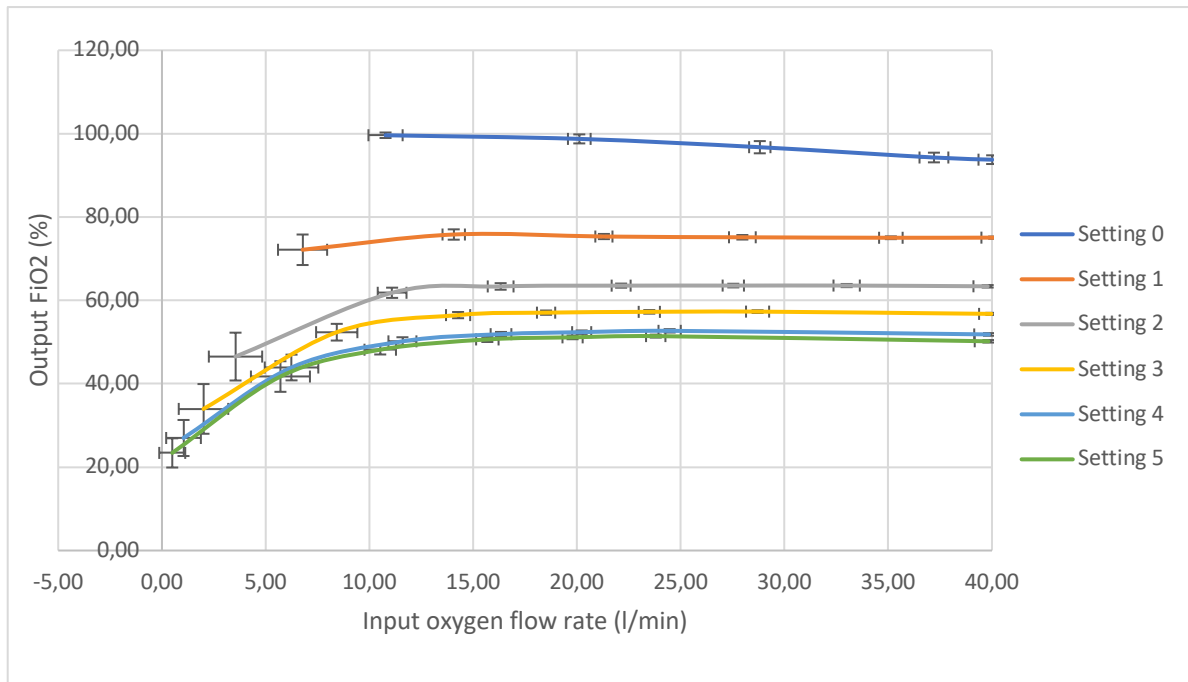
Figure 3: Mean input oxygen flow rates and output FiO₂ for each setting on the entrainer valve, with standard deviation error bars showing measurement precision.

The following aspects of the results for the unit are discussed:

o *Noisy low flow rate measurements:* Large standard deviations were recorded for FiO₂ percentages, whereby a ± 5.96 % was captured for Setting 3 at 10.86 l/min total flow. This was due to the noisy conditions of the differential pressure sensors where, at low flow rates, differential pressures seemed to have fluctuating characteristics. Although all efforts were made to limit this, the current setup with the chosen sensors or the Venturi chambers may need to be re-investigated. Therefore, the technical specification was limited to 10 l/min. Moreover, the entrained air flow rates were captured with lower standard deviations compared to the oxygen flow rates.

o *Entrainer valve trends*: Across the spectrum of settings 0 to 5, a non-linear FiO₂ trend may be shown, as referred to in Figure 3. The air inlet is shaped with a T-shaped cross-section, allowing to mitigate this effect and linearize the air flow per setting rotation. This has not seemed to work to the full effect.

o *Entrainment performance:* Referring to Figure 2, for an increasing setting number, the total flow rate increasingly deviates from the input oxygen flow rate. This illustrates good functionality with respect to the summation of entrained air and oxygen flow rates as the entrainer valve is opened. Furthermore, due to the high-velocity Venturi nozzle within the Venturi entrainer, the entrained air may exceed the oxygen inlet flow rates, allowing for excessively large flow rates of up to 105 l/min. This is at the inlet oxygen condition of 2.2 bar gauge pressure and may be regulated to limit flow rates for low FiO₂ settings. Moreover, leakages do occur, as shown in the Setting 0 at higher flows, whereby the total flow rate and oxygen flow rate deviate to a mean vale of 3.39 l/min. Although PTFE thread tape and O-rings were used, as well as 3D printing the entrainer

valve in highly accurate resin, a more ductile material should be investigated to provide a compression fit in attempt to limit leakages.

o *Pressure regulation:* Due to the large pressure drop requirements needed to reach desirable high flow at high FiO_2 percentages, pressures must be regulated to prevent excessively exceeding output target total flow rates. It was found that a maximum of 40 l/min requires 2.2 bar gauge pressure input for the given Venturi needle diameter. On the other extreme, a 1 bar pressure input is required to reach the 60 l/min target total flow rates for Setting 5.

ii.   Heating and humidification unit

Initial tests showed that it was beneficial to allow the water chamber to heat up before applying flow rates. The temperature read from the chamber temperature sensor displayed to settle at the point flow was introduced to the system. Therefore, preliminary tests at intermittent 30 l/min total flow were introduced throughout the entire device. The results are shown in Figure 4 with the following aspects to be discussed:

o *Water chamber:* The heater element can reach 85°C as a maximum temperature after a warm-up cycle. The element is concealed well within a heat exchanger to transfer heat to the water chamber. When flow was off, relative humidity values reached just over 90°C. However, there is minimal transfer of heat from the water chamber to the inspiratory gas, only slowly reaching 22°C at the end of the test. With flow rate turned on, relative humidity drops to approximately 55%.

o *Heated circuit:* The circuit regulates humidity and temperatures inversely, as shown by the patient-end humidity and temperature measurements. When flow is turned off, humidity is stable at 42% whereas temperature is poorly transmitted to the gas and across the sensors, reaching approximately 26°C. In contrast, when the flow is turned on, the relative humidity drops to 30% and the temperature reaches 40°C. The results show that flow is important for heat transfer to inspiratory gases, but the prototype needs a more sophisticated control method to increase relative humidity at desired gas temperatures.
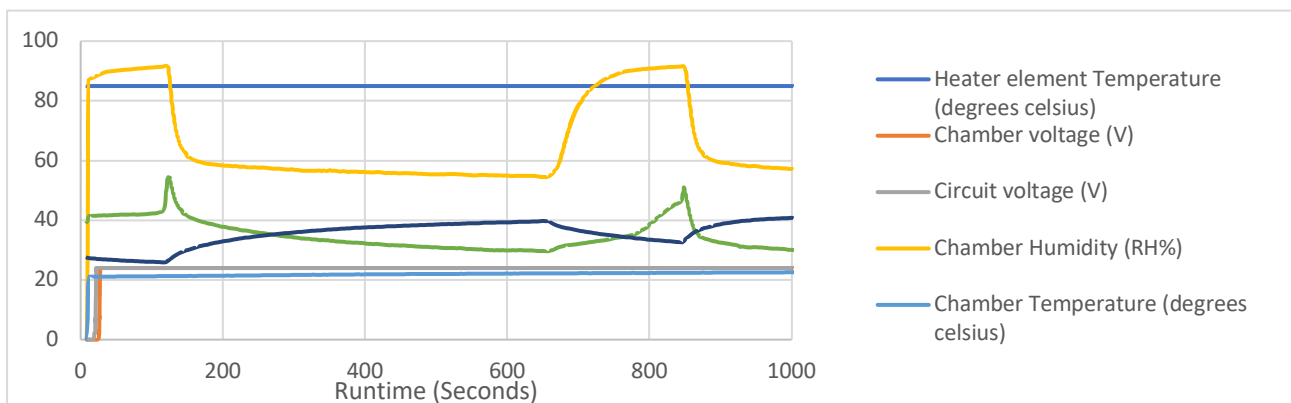

Figure 4: Results showing measurement responses from temperature and humidity sensors for intermittent 30 l/min total flow rates.

iii.   Patient interface

The patient interface is demonstrated in Figure 5, depicting the fitment onto the patient's face, as well as the position and connections of all components relative to the patient.
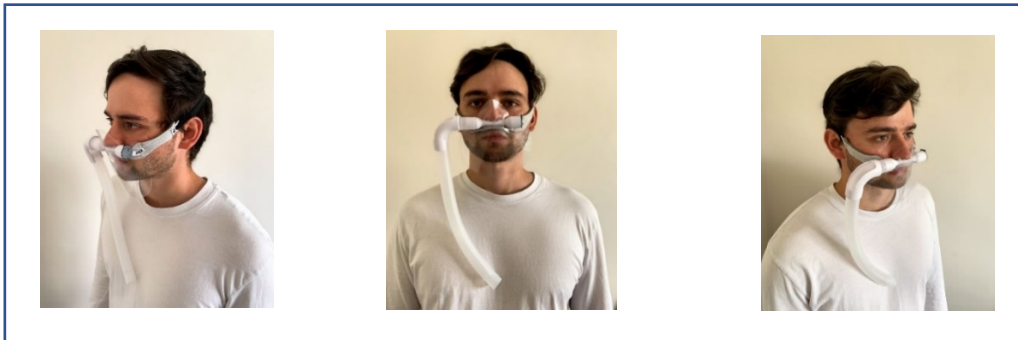

Figure 5: Demonstration of patient fitment and components of the patient interface.

iv.   Validation discussion

The general technical specifications for the target Proof of Concept (based on WHO technical specifications and similar device specifications) and the tested prototype is presented in Table 1.

Table 1: Technical specifications and comparison between Proof of Concept and initial final concept.

Unit	Specification	Test condition	Prototype Value	Concept Target	Unit
Oxygen regulation and mixing	Minimum total flow output	@2.2 Bar	10	5	L/min
	Maximum total flow output	@2.2 Bar Entrainer setting 5	105	60	L/min
	Maximum Oxygen concentration	@2.2 Bar Entrainer setting 0	99	100	%
	Minimum oxygen concentration (FiO2)	Total VFR > 20 l/min	40	40	%
Humidification and heating	Max Patient end Temperature	@ 30 l/min	40	37	ºC
	Max Patient end humidity	@ 0 l/min, 28 ºC	55	100	%
		@ 30 l/min, 22 ºC	48		

The prototype may be validated to the intended use of the device as well as the top needs defined. This is summarized in Table 2.

Table 2: Validation methods used for the overall outputs of intended use and needs of the Proof of Concept.

Criteria	Description	Validation
Intended use	Oxygenation effect to patient	Device can provide suitable ranges similar to predicate devices. WHO technical specifications for non-invasive ventilation (WHO, 2021).
	Flow rate outputs to patient	
	Heating and humidification active components	Mechanisms of benefits associated with HFNO active patient comfort provision.
Top Needs	Low cost and affordable treatment	Bill of materials approximately R8100.00. Manual control reduces overall costs but is technically limited.
	Components should not inhibit patient comfort in any reasonable physical manner.	Comfortable and adjustable nasal patient interface to deliver treatments minimally and directly. (Similar to predicate devices)
	Manual control of oxygen regulation.	Manually controlled safety valve, oxygen flow rate valve, and air entrainer control valve.
	A safe and reliable solution.	Additional risk management processes (ISO 14971)

CONCLUSION

The project in its current state of development was able to show the feasibility of a low-cost and affordable High Flow Nasal Oxygen solution, both quantitatively and qualitatively. It is well equipped to meet the current requirements and needs of a resource-constrained setting, using a combination of manual analog and digital control. Further design and development processes should be considered to improve the solution's performance in terms of accuracy, usability, safety, and general quality management. Verification in terms of ISO 80601-2-90:2021 should be considered to achieve basic safety and performance (ISO, 2021). Further optimisation and refinement with standardised testing in the laboratory and clinical settings will be conducted.

ACKNOWLEDGEMENTS

The authors would like to acknowledge all enablers involved in collaboration, manufacturing processes, and testing equipment, particularly the UCT Mechanical Engineering technical staff, UCT MDL colleagues, and the UCT Private Hospital Technologists and Pulmonologists.

REFERENCES

Bice, T., Cox, C., & Carson, S. (2013). Cost and Health Care Utilization in ARDS—Different from Other Critical Illness? *Seminars in Respiratory and Critical Care Medicine*, *34*(04), 529-536. doi: 10.1055/s-0033-1351125

Calligaro, G. L., Lalla, U., Audley, G., Gina, P., Miller, M. G., Mendelson, M., Dlamini, S., Wasserman, S., Meintjes, G., Peter, J., Levin, D., Dave, J. A., Ntusi, N., Meier, S., Little, F., Moodley, D. L., Louw, E. H., Nortje, A., Parker, A., . . . Koegelenberg, C. F. N. (2020). The utility of high-flow nasal oxygen for severe COVID-19 pneumonia in a resource-constrained setting: A multi-centre prospective observational study. *EClinicalMedicine*, *28*, 100570. doi: 10.1016/j.eclinm.2020.100570

Cerpa, F., Cáceres, D., Romero-Dapueto, C., Giugliano-Jaramillo, C., Pérez, R., Budini, H., Hidalgo, V., Gutiérrez, T., Molina, J., & Keymer, J. (2015). Humidification on Ventilated Patients: Heated Humidifications or Heat and Moisture Exchangers? *The Open Respiratory Medicine Journal*, *9*(1), 104-111. doi: 10.2174/1874306401509010104

Hardavella, G., Karampinis, I., Frille, A., Sreter, K., & Rousalova, I. (2019). Oxygen devices and delivery systems. *Breathe*, *15*(3), e108-e116. doi: 10.1183/20734735.0204-2019

High-Flow Nasal Cannula Oxygen COVID-19 cases. (2020). https://fcmedical.co.za/wp-content/uploads/2021/01/High-Flow-Nasal-Cannula-Oxygen-Advisory-.pdf

ISO. (2021). *ISO 80601-2-90:2021, Medical electrical equipment, Part 2-90: Particular requirements for basic safety and essential performance of respiratory high-flow therapy equipment*. International Organization for Standardization. Retrieved 8 March from https://www.iso.org/standard/80858.html

Kedzierewicz, R., Derkenne, C., Fraudin, A., Vanhaecke, P., Jouffroy, R., Jost, D., & Prunet, B. (2021). Logistical Challenge With Prehospital Use of High-Flow Nasal Oxygen Therapy in COVID-19-Induced Respiratory Distress: A Case Report. *The Journal of Emergency Medicine*, *61*(1), 37-40. doi: 10.1016/j.jemermed.2021.03.006

Li, J., Fink, J. B., & Ehrmann, S. (2020). High-flow nasal cannula for COVID-19 patients: low risk of bio-aerosol dispersion. *European Respiratory Journal*, *55*(5), 2000892. doi: 10.1183/13993003.00892-2020

Liu, X., Wu, R., Lai, L., & Lin, J. (2021). Clinical application of High-flow nasal cannula oxygen therapy in acute heart failure. *Food Science and Technology*. doi: 10.1590/fst.40020

Nishimura, M. (2019). High-Flow Nasal Cannula Oxygen Therapy Devices. *Respiratory Care*, *64*(6), 735-742. doi: 10.4187/respcare.06718

ResMed. (2021). *Home high-flow therapy*. Retrieved 8 December from https://www.resmed.co.uk/healthcare-professional/respiratory-care/respiratory-therapy/home-high-flow-therapy/

SARAO. (2020). UCL-Ventura CPAP System Clinical Guidance https://www.sarao.ac.za/wp-content/uploads/2020/06/NVP-cpap_devices-information-sheet.pdf

Slain, K. N., Shein, S. L., & Rotta, A. T. (2017). The use of high-flow nasal cannula in the pediatric emergency department. *Jornal de Pediatria*, *93*, 36-45. doi: 10.1016/j.jped.2017.06.006

Vega, M. L., & Pisani, L. (2021). Nasal high flow oxygen in acute respiratory failure. *Pulmonology.*, *27*(3), 240-247. doi: 10.1016/j.pulmoe.2021.01.005

WHO. (2021). *Technical specifications for invasive and non-invasive ventilators for COVID-19: Interim guidance, 15 April 2020*. World Health Organization. Retrieved 9 December from https://apps.who.int/iris/handle/10665/331792

CHAPTER 19
SYSTEMS INTEGRATION OF A SMART IOT-BASED TELEMONITORING SYSTEM

Pragesh Govender, Riaan Stopforth
ORCID ID: 0000-0001-5173-4379,0000-0002-8878-2232
Stopforth Mechatronics
Robotics and Research Lab
University of KwaZulu-Natal Durban
South Africa

Sudesh Sivarasu
ORCID ID: 0000-0002-0812-568X
Division of Biomedical Engineering
Division of Human Biology
University of Cape Town
Western Cape
South Africa

Elisha Didam Markus
ORCID ID: 0000-0001-6778-4004
Faculty of Engineering
Built Environment and Information Technology
Central University of Technology
Free State
South Africa

Clive Hands
ORCID ID: 0000-0003-2590-6055
Mechanical Engineering Department
Advanced Engineering Design Group
Nelson Mandela University
South Africa

ABSTRACT

Due to the overburden on healthcare resources, there is a need to invest in Internet of Things (IoT) based telemonitoring devices that can remotely monitor and diagnose patients without constant supervision by health practitioners. Current commercial and research initiatives in this area fail to create a comprehensive IoT-based system with deficits in the sensing layer and model consumption phase being

an underlying concern. This gap was closed through the development of an IoT-based system consisting of a multi-faceted wireless body access network (WBAN), cloud integration and two application layers (mobile and web-based). Global Positioning System (GPS) tracking on the patient's phone was used to allow doctors to track and dispense ambulatory services in cases of emergencies. Overall, the developed system was able to possess around 15 of the features common in most wearable health device systems at a reduced cost, thereby successfully achieving the desired outcomes of this research.

Keywords: IoT, telemonitoring

INTRODUCTION

IoT can be defined as an emerging technology which enables devices containing sensors, processors, and communication hardware to connect to the internet by means of a wired or wireless connection (Chandini & Kumar, 2018), (Patel & Salazar, 2016). With nearly two-thirds of the global population expected to have Internet access by the year 2023, the attractiveness of using IoT within an array of industry sectors becomes highly plausible. One such industry which can benefit from the usefulness of IoT is the medical sector, which is expected to have an annual compound growth rate increase of 19% for the period 2019 - 2025 (Grand View Research, 2019). By using telemonitoring systems, patient care can be improved without overburdening health care resources (Christensen, 2018).

Utilising an IoT framework with powerful cloud platforms, predictive modelling, and application layers (mobile and web-based) can assist with health care management of patients (CDC,2020) while also assisting, rather than eliminating, health care professionals (Sarker, 2021). Such a healthcare system will allow for remote monitoring and tracking of patients both in real time and historically, thereby preventing the late detection of communicable and non-communicable diseases (World Health Organization, 2021). This data and tracking can be an invaluable means of proactively managing patients' health conditions before a medical issue escalates (J. Mathew, 2018). Furthermore, according to a WHO report, 46% of the population live in rural areas, yet only 12% of doctors and 19% of nurses work there (World Health Organization, 2010). This indicates a genuine need to utilise such an IoT system for knowledge sharing and bridging the gaps in global healthcare. Since the diagnostic models built within the IoT system will be developed using the intuitive knowledge of experienced doctors as well as a rich information database – rural doctors can stand to benefit from not only better diagnostic tools but also reduced strain because of automatic diagnostics and monitoring. GPRS can be used to facilitate the use of the IoT system within rural areas to replace other more complex protocols such as Wi-Fi, which has not been established in these areas. These simple systems therefore reduce connectivity issues and maintenance costs which are major challenges for technology roll-out in rural areas (Dimitrievski et al., 2021). The transmission of critical patient physiological data directly to caregivers can then be achieved via a mobile application (MA) or web application (WA) interface (G.F. Gensini, 2017).

This research aims to develop such a system which can serve as a fundamental tool within the healthcare sector. Figure 1 displays a high-level overview of the developed system with the MA serving as an IoT gateway (Hulft, 2018). The following contributions will be addressed in this research:

- o The development of a multi-sensory WBAN with IoT connectivity.
- o A holistic telemonitoring system with a feature-rich offering at a reduced cost.
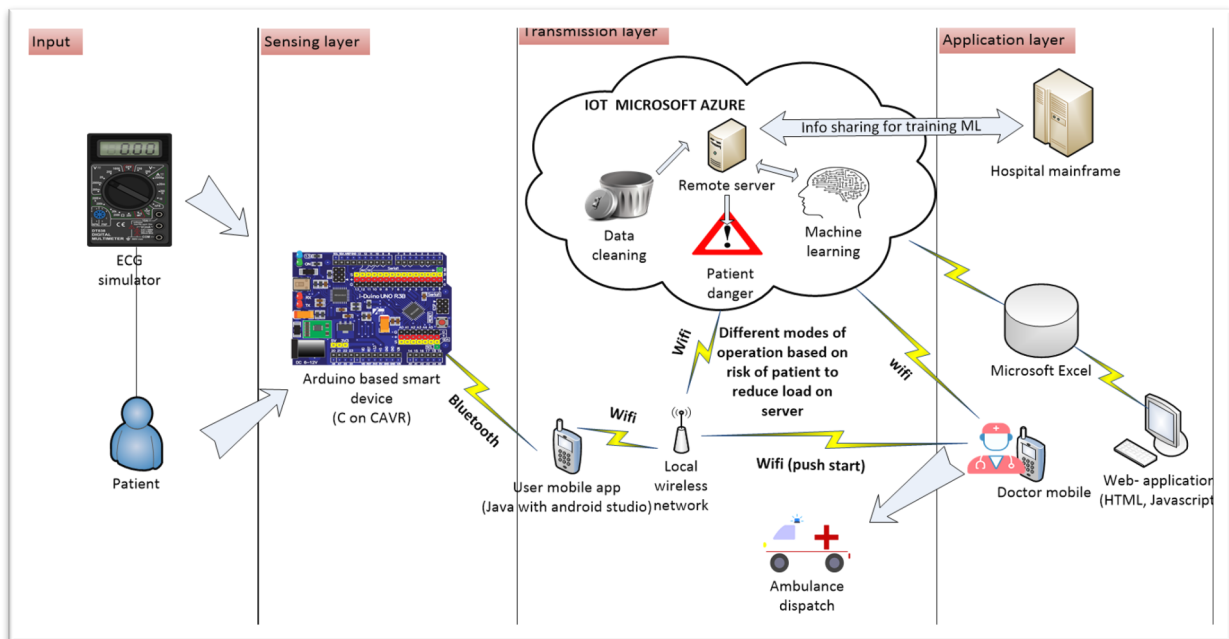

Figure 1: High-level overview of the developed system

MATERIALS AND METHODS

The following material and methods were utilised for the developed IoT system.

i. Materials

The WBAN was developed using various commercial sensors to measure Infrared light, pulse rate, electromyography, electrocardiography, body temperature and humidity. These sensors were read using an Arduino Nano Microcontroller unit (MCU). A 7.4V lithium battery was used with voltage regulators to control the input voltage to the various sensors. Haptic feedback was made possible with a LED and vibration module while short range communication was achieved using a Bluetooth module. A Veroboard was used for creating connections and the electronics were enclosed in a COTS enclosure with a Velcro strap holding the enclosure firmly to the wrist. Figure 2 illustrates this fitting.

Figure 2: Fitting of WBAN on patient

The LM35 temperature sensor was utilised for measuring body temperature. The LM35 is low cost (due to wafer-level trimming), compact (20 mm ×5 mm), low energy (<60 µA) and easily accessible with analogue output capabilities. It also operates in the range of -55°C to 50°C which is sufficient for body temperature measurement (EJ Projects, 2021). A HC-06 Module was selected for Bluetooth since it is a common off-the-shelf (COTS) product and can operate in a range of two meters (being a class 2 device) which is sufficient for wearable-to-smartphone communication (etechnophiles, 2022). The Keystudio AD8232 ECG sensor was used for electrocardiography readings due to its low power requirement (170µA) and low supply voltage of 3.3V (Keyestudio, 2021). In addition, the Myoware EMG sensor was chosen for electromyography readings due to its accuracy and because electro pads are placed directly on the sensor which prevents noise in terms of motion artefacts (Sparkfun, 2021). Lastly, the HIH-4000 humidity sensor was used since it required a low voltage supply 4V- 5.8V, had a less than 200µA current requirement, and has a three-layered design to protect against dirt and dust (Honeywell, 2021).

ii.   Method

The WBAN was developed by soldering the various sensors onto the Veroboard. Each component was powered by a lithium battery to reduce the strain on the MCU. Voltage reductions were done using voltage regulators. The completed electronics for the WBAN was then placed within the purchased enclosure with holes allowing external components to be placed outside of the enclosure. A Velcro strap was then used to secure the enclosure to the wrist.

The mobile application (MA) was developed using Java on Android Studio. It consisted of two interfaces: one for the doctor and one for the patient. The MA was integrated with Firebase using an application programming interface (API) to allow

storage and user authentication during the login and registration. The MCU was programmed using C on CVAVR. The code utilised delimiters to allow for splitting of data on the MA. The MA used broadcast receivers to collect data from the Bluetooth module. The MA was then programmed to split the data and store it on a SQLite database.

A Java database connection (JDBC) was established between the MA and SQL database within the MS Azure Cloud platform. This enabled the transfer of data to the cloud from the patient's phone and subsequent reading of data from the cloud to the doctor's phone. Reading data on the WA was also possible through POST requests using the embedded Javascript template (EJS) engine.

GPS tracking was enabled on the MA using the phone's built-in GPS tracking mechanism. This data was retrieved and uploaded onto Firebase for viewing by health practitioners.

RESULTS AND DISCUSSION

Table 1 shows that the developed IoT telemonitoring system was able to achieve 15 of the typical features present in wearable devices. This included GPS location, interfacing with doctors, and a multi-sensory layer. In terms of sensory inputs, the developed WBAN was able to obtain readings for ECG, EMG, pulse rate, IR, body temperature and humidity while other systems occupied just a few of these sensors. The developed IoT system was also able to consume FL- and ML-based models which many of the systems did not have the capability and infrastructure to do. The developed system was also able to calculate the patient BMI and MEWS rating (an accepted measure of a patient's health). Another improvement of the current system was the use of two application layers via a WA and MA interface which was not present in any of the compared devices.

Figure 3 shows the developed system was also cost effective considering the array of features at its disposal. The system employed had a price tag of US$70.9 which is considerably lower than most of the devices it was compared to. This takes material costs into consideration, but not manufacturing costs. The addition of best practices and large-scale production could potentially reduce the price further through standardisation, buyer negotiations and outsourcing. The Apple Watch Series 3 was the most expensive at US$251 followed by the Samsung Galaxy Fit 2 and Polaroid at US$87.8 and US$34.5 respectively (Game, 2021). The Polaroid is much cheaper but also has a feature reduction of 40% in comparison to the designed system.
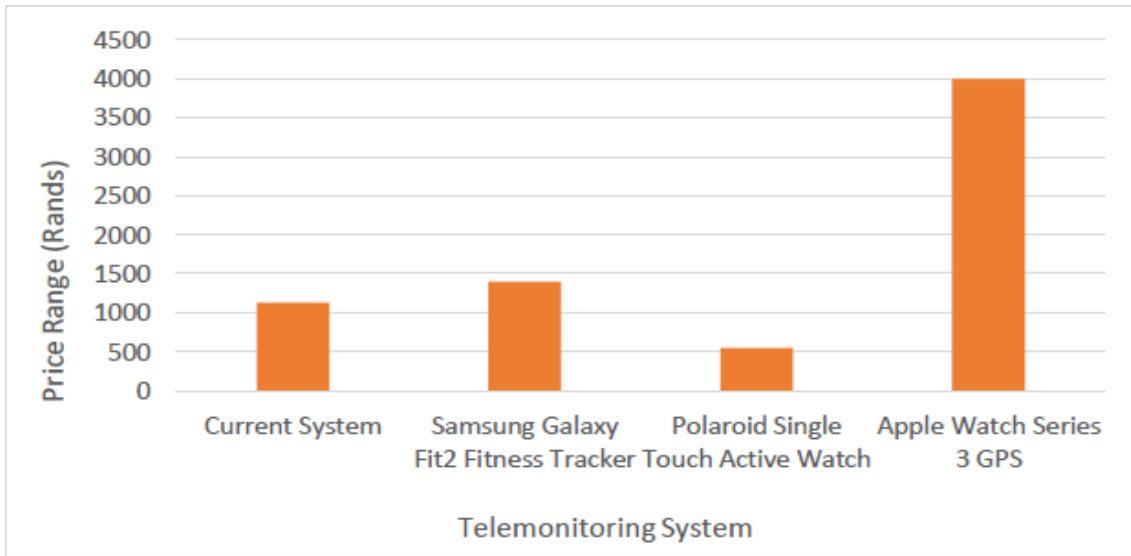
Figure 3: Cost comparison of developed system relative to other commercial products

Table 1: Table showing features of current system compared to commercial and literature products

Feature	Current System	Samsung Galaxy Fit2 Fitness Tracker	Polaroid Single Touch Active Watch	Apple Watch Series 3 GPS	(Simeone et al., 2021) (Literature)	(Hameed et al., 2020) (Literature)
ECG	×			×		
EMG	×					
Pulse Rate	×	×	×	×	×	×
Body Temp	×				×	×
Blood Pressure			×		×	×
Pedometer			×			
Sleep Tracker		×				
Humidity	×				×	
Stress Tracker		×				
Accelerometer			×	×		
Barometer				×		
BMI	×					
MEWS Rating	×					
FES	×				×	×
ML	×				×	×
GPS	×			×	×	
MA GUI	×	×	×	×	×	×
WA GUI	×					
Cloud Integration/IoT	×	×		×	×	×
Doctor Interfacing	×				×	
Alerts	×	×	×	×	×	×
Total	15	6	6	8	11	8

CONCLUSION

This research was able to successfully deliver an IoT system which enabled remote monitoring of patients by health practitioners. The developed system utilised a wide array of sensory inputs to gauge patient health via the development of predictive ML- and FL-based models. In accordance with the above-mentioned contributions, the following was achieved in this research:

- o A WBAN consisting of multiple sensors which was integrated with an IoT framework was developed.
- o This system was developed at a reduced cost while not compromising on a feature-rich experience.
- o The consumption of FL- and ML-based models were achieved.

ACKNOWLEDGEMENTS

REFERENCES

Al-Dmour, J. A., Sagahyroon, A., Al-Ali, A., & Abusnana, S. (2019). A fuzzy logic-based warning system for patients classification. *Health Informatics Journal, 25*(3), 1004-1024. doi: 10.1177/1460458217735674

CDC. (2020, June 10 2020). *Using Telehealth to Expand Access to Essential Health Services during the COVID-19 Pandemic*. Retrieved from Centers for disease control and prevention: https://www.cdc.gov/coronavirus/2019-ncov/hcp/telehealth.html

Chandini, H. P., & Kumar, M. S. (2018). ECG Telemetry System for IOT Using Rasberry Pi. *International Journal of Engineering Research & Technology (IJERT), 6*(13), 1-4.

Christensen, J. (2018). The Emergence and Unfolding of Telemonitoring Practices in Different Healthcare Organizations. *International journal of environmental research and public health, 15*(1), 16. Doi: 10.3390/ijerph15010061

Dimitrievski , A., Filiposka , S., Francisco , J., Eftim , Z., Petre , L., Pires , I. M., . . . Trajkovik , V. (2021). Rural Healthcare IoT Architecture Based on Low-Energy LoRa. *International Journal of Environmental Research and Public Health*, 18(14), 7660. doi: 10.3390/ijerph18147660

EJ Projects. (2021, 5 9). *LM35 Temperature Sensor Pin out, Interfacing guide, Circuit Construction and Working Principals*. Retrieved from Engineers Garage: https://www.engineersgarage.com/lm35-description-and-working-principal/#:~:text=LM35%20is%20a%20temperature%20sensor,not%20require%20any%20external%20calibration.

eTechnophiles. (2022). *HC-06 Pinout, specifications, datasheet and Arduino connection*. Retrieved from etechnophiles.com: https://www.etechnophiles.com/hc06-pinout-specifications-datasheet/

G.F. Gensini, C. A. (2017). Value of Telemonitoring and Telemedicine in Heart Failure Management. *Cardiac failure review, 3*(2), 116-121. doi: 10.15420/cfr.2017:6:2

Game. (2021, November 15). *Electronics & Entertainment*. Retrieved from Game: https://www.game.co.za/game- za/en/All-Game-Categories/Electronics-%26-Entertainment/c/G002

Grand View Research. (2019). *Internet of Things in Healthcare Market Size, Share & Trends Analysis Report By Component (Service, System & Software), By Connectivity Technology (Satellite, Cellular), By End Use (CRO, Hospital & Clinic), By Application, And Segment Forecasts, 2019 - 20.* Grand View Research.

Honeywell. (2021). *Humidity with temperature sensors*. Retrieved from Honeywell: https://www.mouser.co.za/ProductDetail/Honeywell/HIH-4000-004?qs=yJVtgANCw00aQBCIf2C1DQ%3D%3D

Hulft. (2018). *IoT Architecture 101*. Retrieved September 15, 2021, from https://medium.com/enterprise- strategist/iot-architecture-basics-guide-ff4bcf8e6859

J. Mathew, J. L. (2018). *Heart Failure in the Child and Young Adult* (illustrated ed.). Elsevier Science. Keyestudio. (2021). *Keyestudio.com*. Retrieved from Keyestudio AD8232 ECG Measurement Heart Monitor Sensor Module for Arduino UNO R3: https://www.keyestudio.com/products/keyestudio-ad8232-ecg-measurement-heart-monitor-sensor-module-for-arduino-uno-r3

Patel, S., & Salazar, C. (2016). Internet of Things-IOT: Definition, Characteristics, Architecture, Enabling Technologies, Application & Future Challenges. *IJESC*, 6122-6131. doi: 10.4010/2016.1482

Sarker, I. H. (2021). Machine Learning: Algorithms, Real-World Applications and Research Directions. *SN computer science, 2*(160), 1-28. doi: 10.1007/s42979-021-00592-x

Sparkfun. (2021). *MyoWare Muscle Sensor*. Retrieved from Sparkfun.com: https://www.sparkfun.com/products/13723

World Health Organization. (2010). *Increasing access to health workers.* Switzerland: WHO Press.

World Health Organization. (2021). *Cardiovascular diseases (CVDs)*. Retrieved September 13, 2021, from https://www.who.int/news-room/fact-sheets/detail/cardiovascular-diseases-(cvds)

Medical device engineering and innovation are en route to being the most sophisticated and celebrated discipline in future!

This book is the proceedings from the MediVentors Consortium funded by the Manufacturing, Engineering and Related Services SETA (MerSETA) and hosted by the University of Cape Town's Division of Biomedical Engineering within the Department of Human Biology, Faculty of Health Sciences.

Over 30 students from 4 universities (UCT, CPUT, UKZN and WITS) participated and were trained in this Integrated Skills Development Programme (ISDP) around medical device industrialisation. This book compilation summarises key outcomes from select innovations from our future medical device manufacturing industry leaders.

Come, let us start a new industrial revolution in the Medical Device Industry!